

Towards an artificial cell: Development of a system which self-regenerates the protein components of the PURE system in microfluidic reactors

Présentée le 22 octobre 2021

Faculté des sciences et techniques de l'ingénieur
Laboratoire de caractérisation du réseau biologique
Programme doctoral en biotechnologie et génie biologique

pour l'obtention du grade de Docteur ès Sciences

par

Barbora LAVICKOVA

Acceptée sur proposition du jury

Prof. A. Radenovic, présidente du jury
Prof. S. Maerkl, directeur de thèse
Prof. Y. Shimizu, rapporteur
Prof. F. Simmel, rapporteur
Prof. B. Correia, rapporteur

Acknowledgements

First of all, I would like to thank my advisor, Professor Sebastian Maerkl, for giving me the opportunity to work in his lab, for always being of fundamental support with his ideas, suggestions, and passion for science, and for his honest and encouraging personality.

I want to thank the members of my thesis committee: Professor Yoshihiro Shimizu and Professor Friedrich Simmel for being part of the examination jury and for evaluating my Ph.D. work; Professor Bruno Correia for being part of my thesis as well as candidacy jury; Professor Aleksandra Radenovic for being president of my jury and being a great Professor at the neighboring LBEN lab.

I am thankful to have had a great mentor in Professor Suliana Manley, who took the time to talk to me, encourage me, and give me wonderful pieces of advice which were of great benefit to me. I am also thankful to have met Professor Carlotta Guiducci, who always brings her cheerful nature to any encounter and inspires me greatly. My sincere thanks go to Jan Grégr for igniting my passion for science and introducing me to the laboratory environment I fell in love with, and Veronika Máková for being a fantastic supervisor during my Bachelor studies, thereby inspiring me to do a Ph.D.

Thank you to all past and current LBNC members. Special thanks to Nadanai for being an excellent colleague, mentor, and friend; thank you for our collaboration and for making me a better scientist. I am thankful to Francesca, Ekaterina, and Zoe for teaching me most of the laboratory skills I needed to succeed in my Ph.D. and being friendly since the first day, and making my experience at EPFL wonderful and full of great memories. Thank you to my crazy and sometimes lovely friends Laura, Fabien, and Michael for extending my life by at least 100 years with all the laughs and fun we had together in and outside the lab. I am delighted to have met Julia, who is always uplifting and encouraging to everyone around. I am also thankful for Evan, Greg, Ming, Fatemeh, Moustafa, Daniel and all other current and past LBNC members. Lastly, I would like to thank Martine and Helen for being the best administrative support LBNC could ask for. I must also express my gratitude to Carolina for being an outstanding student and the iGEM 2017 and 2018 teams for the pleasant experience of supervising them. Mainly I want to thank Lena, who became one of my dearest friends.

Outside LBNC, I would like to thank all the other people I had the pleasure to meet or collaborate with: the members of our neighboring lab LBEN and members of CLSE and BIOS, especially Martina, Pierre, Kseniia, and Jihye. Thanks also to Jan Krizek and Saurabh Tomar for allowing me

Acknowledgements

to collaborate on their exciting projects.

I would like to thank people who were not part of my research but were fundamental to my Ph.D. life, primarily to my yoga team, among others Joelle, Edgar, Sena, and Isinsu. My friends from Czech Republic Kát'a, Michal, and Šárka. Thanks to Aurélian for his support during my master's studies and Ph.D., for endlessly listening to my stories, motivating me to become a yoga teacher, and all the fun times we had skiing, cycling, and windsurfing. Many thanks to Amandine and Caroline for welcoming me to their family and for their support.

I want to thank my family: my grandparents Jana and František for being an amazing inspiration to life, my other grandparents Marie and Miroslav for always taking care of me, my cousins Andrea and Gábina for being great friends and motivations in life, and my brother Jan for just being him. Lastly, all the love and gratitude to my amazing parents for being there from the first moment till now, and at any time I needed them; my mum for all the times helping me to study and encouraging me to be better, and my dad for always supporting me and motivating me to try and fight for what I want.

Lausanne, September 2021

Barbora Lavickova

Abstract

Thanks to recent advancements in synthetic biology, the dream of creating a synthetic cell has become feasible. However, due to its inherent complexity, one of the fundamental functions of all living systems, i.e., self-replication, remains to be introduced. The development of a system capable of self-regeneration faces several challenges, as the system needs to be able to functionally synthesize all of its components at sufficient capacity in an environment that allows continuous and sustained regeneration. In this work, we have developed a system coupling a microfluidic platform with cell-free systems, which provides a viable approach for developing and optimizing self-regeneration at non-equilibrium conditions.

Reconstituted transcription-translation systems are a viable starting point for achieving a self-regeneration system. Therefore, in this work, we begin by presenting a simple, robust, and low-cost production method for the cell-free system called protein synthesis using recombinant elements (PURE). Our approach relies on streamlining protein purification by coculturing and co-purification. We show that our "OnePot" method allows for minimizing time and labor requirements while preserving the versatility and purity of the system. Moreover, we demonstrate that the OnePot PURE system can achieve a similar protein synthesis yield to a commercial PURE system, which leads to a 14-fold improvement in cost-normalized protein synthesis yield over existing PURE systems with similar composition.

Living organisms continuously exchange energy and matter with their environment. Similarly, one of the requirements of continuous and sustained regeneration is a life-like non-equilibrium environment. Therefore, we developed an improved microfluidic chemostat with fluidically hard-coded dilution fractions defined by the reactor geometry, which enable long-term steady-state reactions. We employed the introduced microfluidic platform in combination with the PURE systems to study self-regeneration. We demonstrated that the system can regenerate proteins essential for transcription and translation from DNA templates and that simultaneous self-regeneration of multiple proteins is sustainable in the system. Moreover, in combination with computational modeling, we showed that minimizing resource competition and optimizing resource allocation is critically important for achieving robust system functions.

Lastly, we developed a microfluidic platform with an integrated hydrogel membrane with adjustable permeability. The integrated membranes separate transcription-translation machinery from the feeding solution of small molecular components, which can diffuse into the reactor through the membranes without diluting the machinery. Utilizing the dialysis-based continuous-

Abstract

exchange reaction, we extended the protein synthesis beyond traditional batch conditions.

Keywords: synthetic cell, self-replication, synthetic biology, protein expression, cell-free transcription and translation

Résumé

Grâce aux récents progrès de la biologie synthétique, le rêve de créer une cellule synthétique est devenu réalisable. Cependant, en raison de sa complexité inhérente, l'une des fonctions fondamentales de tous les systèmes vivants, à savoir l'autoréplication, reste à réaliser. Le développement d'un système capable de s'auto-régénérer fait face à plusieurs défis, car le système doit être capable de synthétiser fonctionnellement tous ses composants à concentrations suffisantes dans un environnement qui permet une régénération continue et soutenue. Dans cette thèse, nous avons développé un système couplant une plate-forme microfluidique avec des systèmes acellulaires qui fournit une approche viable pour développer et optimiser l'auto-régénération dans des conditions de non-équilibre.

Les systèmes de transcription-traduction reconstitués sont un point de départ viable pour réaliser un système d'auto-régénération. Par conséquent, dans ce travail, nous commençons par présenter une méthode de production simple, robuste et peu coûteuse pour le système acellulaire appelé synthèse de protéines à l'aide d'éléments recombinants (PURE). Notre approche repose sur la rationalisation de la purification des protéines par co-culture et co-purification. Nous montrons que notre méthode "OnePot" permet de minimiser les besoins en temps et en main-d'œuvre tout en préservant la polyvalence et la pureté du système. De plus, nous démontrons que le système OnePot PURE peut atteindre un rendement de synthèse protéique similaire à un système PURE commercial. Cela conduit à une amélioration du rendement de synthèse protéique à coût normalisé 14 fois supérieure par rapport aux systèmes PURE existants avec une composition similaire.

Les organismes vivants échangent continuellement de l'énergie et de la matière avec leur environnement. De même, l'une des exigences d'une régénération continue et soutenue est un environnement de non-équilibre similaire au vivant. Par conséquent, nous avons développé un chémostat microfluidique amélioré, avec des fractions de dilution définies par la géométrie du réacteur, qui permettent des réactions à long terme en régime permanent. Nous avons utilisé cette nouvelle plate-forme microfluidique en combinaison avec les systèmes PURE pour étudier l'auto-régénération. Nous avons démontré que le système peut régénérer des protéines essentielles à la transcription et à la traduction à partir de matrices d'ADN et que l'auto-régénération simultanée de plusieurs protéines est durable dans le système. De plus, en combinaison avec la modélisation informatique, nous avons montré que la minimisation de la concurrence des ressources et l'optimisation de l'allocation des ressources sont d'une importance cruciale pour

Résumé

obtenir des fonctions robustes du système.

Enfin, nous avons développé une plate-forme microfluidique avec une membrane hydrogel intégrée à perméabilité réglable. Les membranes intégrées séparent la machinerie de transcription-traduction de la solution d'alimentation de petits composants moléculaires, qui peuvent diffuser dans le réacteur à travers les membranes sans diluer la machinerie. En utilisant la réaction d'échange continu basée sur la dialyse, nous avons étendu la synthèse des protéines au-delà des conditions traditionnelles par lots.

Mots clefs : cellule synthétique, machine autorépliquative, biologie synthétique, expression des protéines, transcription et traduction sans cellule

Contents

Acknowledgements	i
Abstract	iii
Résumé	vi
List of figures	xi
List of tables	xiii
1 Introduction	1
1.1 Synthetic cell	2
1.2 Self-reproduction	4
1.2.1 Self-replication of instruction set	4
1.2.2 The core constructor self-regeneration	4
1.2.3 Regulation in artificial cell	6
1.3 Cell-free synthetic biology	7
1.3.1 Recombinant systems	7
1.4 Microfluidic platforms	11
1.4.1 Steady-State cell-free reactions	11
1.5 Overview and objective of this work	13
2 A simple, robust, and low-cost method to produce the PURE cell-free system	15
2.1 Abstract	16
2.2 Introduction	16
2.3 Results and discussion	17
2.4 Methods	23
2.4.1 <i>Escherichia coli</i> strains, plasmids, and linear DNA templates	23
2.4.2 Buffers used for protein and ribosome purification	23
2.4.3 OnePot protein preparation	23
2.4.4 HomeMade PURE protein preparation	24
2.4.5 Ni-NTA resin preparation and regeneration	24
2.4.6 OD600 measurement	25
2.4.7 Ribosome purification	25
2.4.8 SDS-PAGE gels	26

Contents

2.4.9	Mass spectrometry	26
2.4.10	Energy solution preparation	27
2.4.11	<i>In vitro</i> protein expression and functional assays	27
2.4.12	Cost calculations	28
2.4.13	Important details and tips	29
2.5	Supplementary information	30
2.5.1	Supplementary figures	30
2.5.2	Supplementary tables	39
3	Steady-state cell-free gene expression with microfluidic chemostats	49
3.1	Abstract	50
3.2	Introduction	50
3.3	Materials	52
3.4	Methods	54
3.4.1	Design of microfluidic devices	54
3.4.2	Photolithography for mask and wafer fabrication	55
3.4.3	Soft lithography for device fabrication	57
3.4.4	Hardware setup	58
3.4.5	Device operation	59
3.4.6	Notes	61
4	A partially self-regenerating synthetic cell	65
4.1	Abstract	66
4.2	Introduction	66
4.3	Results	68
4.3.1	Experimental design	68
4.3.2	Aminoacyl-tRNA synthetase regeneration	70
4.3.3	T7 RNAP regeneration	72
4.3.4	Regeneration of multiple components	75
4.4	Discussion	78
4.5	Methods	80
4.5.1	Materials	80
4.5.2	Ribosome purification	80
4.5.3	PURE system preparation	81
4.5.4	Ni-NTA resin preparation and regeneration for ribosome purification	81
4.5.5	Energy solution preparation	82
4.5.6	Batch <i>in vitro</i> protein expression experiments	82
4.5.7	SDS-PAGE gels	82
4.5.8	Fabrication and design of the microfluidic device	82
4.5.9	Device setup	83
4.5.10	Data acquisition and analysis	83
4.6	Modeling	84
4.6.1	Minimal resource-dependent TX-TL model	84

4.6.2	Chemostat simulation	85
4.6.3	Model design and parameters	85
4.6.4	Elucidation of model behaviour	86
4.6.5	Sufficiency of model mechanism	87
4.7	Supplementary information	89
4.7.1	Supplementary figures	89
4.7.2	Supplementary tables	107
5	Continuous-exchange cell-free expression in microfluidic chemostats with hydrogel membranes	113
5.1	Introduction	114
5.2	Results	115
5.2.1	Prevention of evaporation in microfluidic chip	115
5.2.2	Formation of PEG-DA hydrogel	117
5.2.3	Cell-free expression	119
5.3	Conclusion	120
5.4	Methods	121
5.4.1	Microfluidic chip fabrication	121
5.4.2	Chip silanisation and formation of PEG-DA hydro-gel membrane	121
5.4.3	Solute diffusion through the membrane	122
5.4.4	PURE system and energy solution preparation	122
5.4.5	Device setup for cell-free expression	122
5.4.6	Data acquisition and analysis	123
6	Conclusion and outlook	125
	Bibliography	129
	Curriculum Vitae	143

List of Figures

1.1	Bottom-up synthetic cell	3
1.2	Recombinant cell-free systems	8
1.3	Continuous cell-free reaction platforms	11
2.1	OnePot PURE preparation and optimization	18
2.2	OnePot PURE comparison to existing PURE systems.	21
2.3	Schematics depicting all steps of the OnePot PURE production	30
2.4	Comparison of eGFP expression levels	31
2.5	Coomassie blue stained SDS-PAGE gels of the four OnePot PURE formulations	31
2.6	EF-Tu analysis	32
2.7	OD600 measurement of overnight cultures	33
2.8	Mass spectrometry analysis of the PURE systems	34
2.9	Protein concentration calibrations and adjustments	35
2.10	SDS-PAGE gel of proteins synthesized in PURExpress or OnePot	35
2.11	Activities of different proteins, expressed in PURExpress and OnePot	36
2.12	Comparison of ribosomes	37
2.13	Standard calibration curve for EF-Tu protein concentration	37
2.14	Standard calibration curve for eGFP	38
3.1	A two-layer microchemostat design	54
3.2	Pneumatic connections for the setup	59
3.3	Basic operations and characterisation of the chip	60
3.4	Typical experimental operation of the chip	62
4.1	Experimental design for a self-regenerating synthetic cell	69
4.2	Aminoacyl-tRNA synthetase regeneration	71
4.3	T7 RNAP regeneration	73
4.4	Multi-component regeneration	76
4.5	Microfluidic device design	89
4.6	Comparison of eGFP expression at different temperatures in batch reactions	90
4.7	<i>In vitro</i> expression of different self-regenerated proteins	90
4.8	Comparison of eGFP expression rates in batch reactions at different components concentrations	91

List of Figures

4.9	Comparison of eGFP expression rates in batch reactions at different DNA template concentrations	91
4.10	Aminoacyl-tRNA synthetase regeneration	92
4.11	Synthesis rate for single component expression	93
4.12	T7 RNAP regeneration	94
4.13	Chemostat simulations	95
4.14	Simulation results for mRNA, protein and resource concentration	95
4.15	Derivatives can be directly calculated in the model, yielding rates of transcription and translation	96
4.16	Parameter variations for the resource-dependent model	96
4.17	Varying resource allocation over the course of the simulation	97
4.18	Parameter variations for the resource-dependent model	98
4.19	The effect of varying eGFP DNA on the SR/PC ratio	99
4.20	Comparison of different models	99
4.21	Parameter variations for the resource-independent model	100
4.22	Parameter variations for the combined model	101
4.23	Schematic description of the concepts of resource loading and resource allocation .	102
4.24	Multi-component regeneration	103
4.25	Multiple aaRSs protein regeneration	104
4.26	Synthesis rate for single components in multi-component expression	104
4.27	PURE system composition and synthesis rates	105
4.28	Calibration curve for eGFP	106
5.1	Design of microfluidic device with hydrogel membranes	116
5.2	Hydrogel membranes formation:	117
5.3	Solute diffusion through the membrane	118
5.4	Cell-free expression in microfluidic device with hydrogel membranes	119

List of Tables

2.1	OnePot protocol cost and time estimate	39
2.2	Ribosome protocol cost and time estimate	39
2.3	Energy solution cost estimates	40
2.4	OnePot inoculation culture volumes	41
2.5	HomeMade PURE protein concentrations	42
2.6	HomeMade protocol cost estimates	43
2.7	Energy solution and ribosome cost estimates for TraMOS	44
2.8	DNA sequences of primers used for CPEC	44
2.9	PURE protein list	45
2.10	DNA sequences for linear templates with T7 RNAP promoter	46
2.11	DNA sequences for linear templates with <i>E. coli</i> RNAP promoter	47
2.12	Buffers and energy solution	47
4.1	Microfluidic chip operations for self-regeneration experiments, including positive, and negative controls	107
4.2	Microfluidic chip operations with four self-regeneration experiments	107
4.3	PURE system formulations used	108
4.4	Calculated dilution rates based on concentrations in Table 4.3	109
4.5	Replenishing schedule for modeling the three-stage experiment	110
4.6	DNA sequences	110
4.7	Primer sequences	110
4.8	Buffers and energy solution	111
5.1	PURE system formulations used	123

1 Introduction

Parts of section 1.3 and 1.4 have been adapted from a recent review published in *Frontiers in bioengineering and biotechnology*, 2020.

Authors: Nadanai Laohakunakorn, Laura Grasemann, Barbora Lavickova, Grégoire Michielin, Amir Shahein, Zoe Swank, Sebastian J Maerkl

Reference: Laohakunakorn, Nadanai, et al. "Bottom-up construction of complex biomolecular systems with cell-free synthetic biology." *Frontiers in bioengineering and biotechnology* 8 (2020): 213.

1.1 Synthetic cell

How did life originate? This question that lurks in the minds of many has led to the start of a field that can change how we think about life. This field aims to build an artificial or synthetic cell, and achieving this holy grail does not seem to be so far away anymore. Although the initial question of the origin of life remains, the application and motivation to construct synthetic cells evolved toward understanding and controlling biological systems throughout the decades [1]. As even the simplest known organisms and mechanisms they rely on are complex and remain to be understood. There are two main approaches to creating artificial and "simplified" biological systems, with different levels of engineering involved: top-down and bottom-up [2, 3].

As can be derived from the name top-down, the approach derives the synthetic cell from a biological one by modifying the existing genome or replacing it with a synthetic one, focusing mainly on the creation of a minimal cell [2, 4]. A minimal cell is a theoretical cell created by reducing or simplifying the genome to a minimum number of genes for the cell to survive. Tremendous advances in the top-down approach were recently accomplished, such as the creation of an artificial chromosome [5], and minimal bacterial genome [6]. Nevertheless, we still do not know the functions of all of these essential genes and might be even further from understanding the whole picture of how this symphony of life works [7, 8]. Moreover, the minimality of the genome remains questionable [8]. In comparison, the bottom-up approach is a pure engineering approach, pursuing assembly of synthetic cells from non-living matter [3, 4]. While this is much more challenging, generating cells with defined compositions from basic elements can bring us a complete understanding of the processes behind life. The synthetic cell field is vast, regrouping different motivations for the construction of a synthetic cell, and various experimental and theoretical methods related to the approaches mentioned above [2, 3]. The work presented in this thesis is focused purely on the bottom-up approach.

All-natural cells have common characteristics and materials they are composed of. In contrast, when building synthetic cells, there are fewer constraints, and natural or *de-novo* materials can be used (Figure 1.1a). For example, self-replicating systems including autocatalytic peptides, ribozyme replication, or RNA replicators have been established in the past [9], and artificial cell mimics have been built on microfluidic chips [10] or from inorganic membranes [11, 12]. However, currently, an RNA-based or completely *de-novo* synthetic cell seems far more complicated to build than a DNA cell, which mimics the natural cell [4, 13]. Although it might seem easy to assemble the different natural materials to create a synthetic cell, putting this biological puzzle together is immensely complex. This complexity is due to the endless possible combinations of puzzle pieces that must work together efficiently in a perfect symphony. Consequently, combining the use of native biological parts with a *de-novo* approach is the most advantageous [14, 15].

However, the different approaches and the use of various components brought up fundamental questions to which we still lack universally accepted answers, i.e., how do we define synthetic and minimal cells and their lifelikeness, and when do they become alive [16–19]? These questions become even more complicated when we consider different motivations and applications for

creating synthetic cells. Most likely, there will not be one synthetic cell, but many with various core and adaptive abilities [7, 20], i.e., maintenance of non-equilibrium conditions [13], self-replication [3, 13, 21], regulation [22, 23], informational storage [24], self-organization [13, 19, 25], metabolic pathways [14, 26], motility [14, 26], communication [3, 27, 28], compartment [29–31], sensing [28, 32], growth, division [14], and evolution [33]. Let's consider the example of metabolic pathways. With respect to the environment the cell will be exposed to, the presence and the complexity of the metabolic pathways will significantly vary, e.g., if specific small molecules are constantly supplied to the system, no extensive metabolism is required [13, 24, 34, 35]. In recent years, there has been rapid growth in the technologies involved in creating synthetic cells, e.g., compartments [29–31], cell-free transcription-translation systems (Chapter 1.3) [23, 36], numerical modeling [37, 38], and microfluidics (Chapter 1.4) [31, 39, 40]. Despite allowing the development of simpler non-living artificial cells and different subparts, which mimic specific properties of the cells [2, 19], these technologies did not yet enable fully sustainable artificial life.

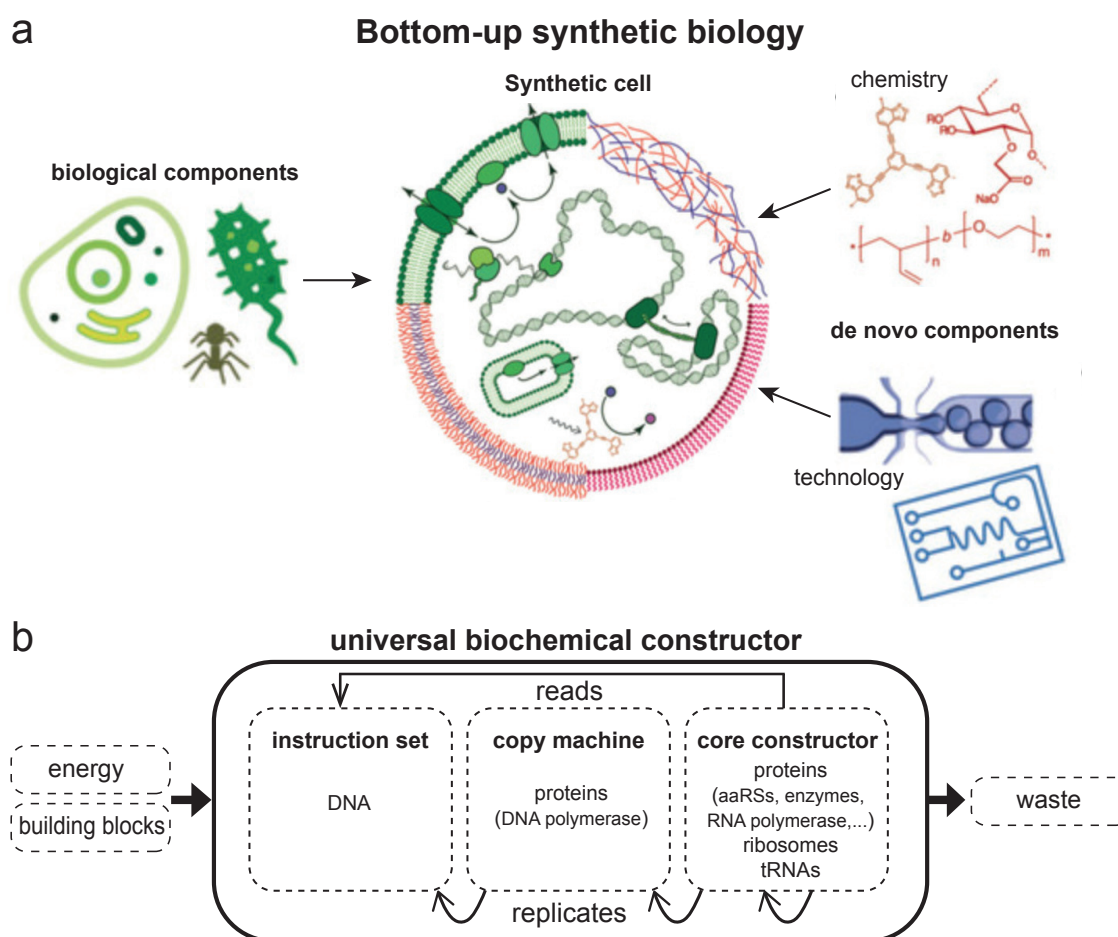


Figure 1.1: **Bottom-up synthetic cell:** (a) Schematic depiction of synthetic cell assembly from biological and *de-novo* building blocks. Adapted from Ref. [41] Copyright 2019, John Wiley & Sons, Inc. (b) Diagram of the universal biochemical constructor concept.

1.2 Self-reproduction

As stated above, the definition of lifelikeness of synthetic cells is not universally agreed upon, and the defining core and adaptive abilities depend on the artificial cell application. However, reproduction is recognized as a crucial component in any autonomous, self-sustaining system. Von Neumann's self-reproducing automata [42] is conceptually analogous to self-replicating biological systems like synthetic cells [3, 13, 43], and provide us with a guideline to understand the parts that compose the system (Figure 1.1b). The hardware of the automata consists of a copy machine, a universal constructor, and a controller. During replication, a universal constructor reconstructs the whole hardware according to the instruction set, or DNA genome, which is copied by the copy machine, or DNA replication machinery, and the whole process is controlled by regulation. In comparison to biological systems, in the model, the idea of a compartment is somewhat simplified and does not include encapsulation of the different parts of the constructor [13].

1.2.1 Self-replication of instruction set

In recent years, the decreasing cost of chemical gene synthesis [19] and the advent of high-throughput DNA assembly [44–47], allowed for the de novo design and synthesis of DNA to become a routine tool in synthetic biology, and led to the construction of the first artificial bacterial chromosome [5, 48]. Besides the advancements in the generation of an artificial genome, major progress was also achieved in DNA replication [23]. An artificial gene circuit was replicated *in vitro* by *E. coli* the DNA replication machinery [49]. However, the *E. coli* DNA replication machinery requires thirteen proteins and an intricate assembly process. In comparison, DNA polymerases from phages, such as Phi29, require only a single protein, and are therefore promising candidates for genome replication [24] in synthetic cells. Plasmid DNA replication by Phi29 rolling circle amplification coupled with transcription and translation was demonstrated under optimized conditions without any enzymatic post-processing [50–52]. However, a significant shortcoming of this system is that the product is a long linear concatemer, which limits the system recursion. Therefore, implementation of re-circulation by recombination [53] will most probably be a prerequisite for a self-sustainable DNA replication system based on rolling circle amplification. Although replication of linear DNA with proteins from phi29 bacteriophage was recently also reported [54], continuous multi-round replication in synthetic cell models remains to be demonstrated.

1.2.2 The core constructor self-regeneration

Due to its minimal, defined, and adjustable composition, the reconstituted translation system is a viable option to act as the core constructor. The ability of the core constructor to sustainably construct all of its components is essential to achieve full self-replication. Despite its minimal nature, the PURE system is an elaborate apparatus, and it is still unknown if it can fulfill this requirement and at which composition. Therefore, the current research focuses on the PURE system's ability to regenerate its different subgroups: transcription enzymes and translation factors, ribosomes, and tRNA.

As specified in Chapter 1.3.1, the PURE system comprises only purified recombinant proteins deemed essential to the system. Therefore, the system does not contain any chaperones or post-translational modification proteins. Although it was proposed that specific chaperones and post-translational modification enzymes will be required to achieve self-replication, the requirement of those proteins remains ambivalent [24]. For example, Niwa et al. [55] showed that the PURE system could synthesize 70% of all *Escherichia coli* proteins. The same group [56] established that the translation-associated proteins, which are cytosolic, generally have a high solubility and low precipitation, even without any chaperones facilitating their folding. Moreover, recent studies synthesized the proteins of the reconstituted translation system in a single reaction. However, the results and the number of proteins expressed at levels matching the input concentrations varied significantly for different compositions of the PURE system and various reaction conditions [47, 51, 57]. Although these studies are highly encouraging and expand our knowledge of the system, the findings also highlight the high per-codon ribosome processivity loss and varying yields of the synthesized proteins [57, 58], and therefore emphasize the need to incorporate direct functional feedback of the synthesized proteins.

One of the earliest works directly focusing on the functionality of the synthesized translation machinery showed that all aaRSs, except for PheRS, retain their aminoacylation activity when synthesized in the PURE system supplemented with molecular chaperone trigger factor, without any other chaperones or enzymes required for post-translational modification [59]. Likewise, recent work from Wei et al. [60] exploring the functionality of the reconstituted translation system, supplemented with proteins expressed and purified from the PURE system instead of *E. coli*, showed that the system is able to synthesize active elongation factors, energy recycling enzymes, IF3, and a subset of aaRSs. Besides, this work emphasized the importance of studying the essentiality of the individual proteins of the system and the potential contamination problems due to the co-purification of native enzymes, which might impact the findings of these drop-out studies. Although the studies summarised above brought crucial insights for using the PURE system as the chassis of a self-replicating system, these studies were not able to answer if the system can regenerate its components and maintain protein synthesis. Libicher et al. [61] demonstrated self-maintenance of several individual PURE proteins and explored co-regeneration of multiple proteins by employing a serial transfer strategy. Despite being a valuable approach for probing self-regeneration in a cell-free environment, this batch-based method has its limitations, i.e., it requires small volume transfers over an extended period of time, limiting the number and volume of the serial transfers.

Integrated ribosome synthesis, assembly, and translation will be indispensable to a self-replicating machine derived from the reconstituted translation system because ribosomes are required to translate genetic information into proteins. These unique machines are composed of dozens of ribosomal proteins (r-proteins) and RNAs (rRNAs) assembled in a sophisticated stepwise process. In 2013 Jewett et al. [62] developed integrated synthesis, assembly, and translation (iSAT) technology that allowed for one-step rRNA transcription and assembly of native ribosomal proteins of both ribosome subunits in *E. coli* lysate. The same group later showed the reconstruction of an active small ribosome subunit from r-proteins synthesized and purified from the PURE system

[63]. Besides, they demonstrated coexpression of all the r-proteins of the small ribosomal subunit and 29 out of 33 r-proteins of the large ribosomal subunit. In the past year, key progress in the self-regeneration of ribosomes has been made. Shimojo et al. [64] developed a recombinant-based integrated synthesis, assembly, and translation (R-iSAT) method for the small ribosomal subunit assembly coupled with 16S rRNA synthesis and ribosomal protein synthesis. Levy et al. [65] were able to assemble the small ribosomal subunit from in vitro synthesized 16S rRNAs and r-proteins, showing the importance of high local concentration and the timeline for an efficient assembly process. However, it remains to be established if the synthesized ribosome is capable of expressing proteins.

The key to the genetic information translation is carried by the transfer RNA (tRNA). Despite tRNAs being only transcribed, their requirement for proper folding and modification of specific nucleotides in the tRNA sequence, essential for decoding specific codons and efficient aminoacylation, makes tRNA regeneration in vitro a challenge. Fortunately, amino acids are encoded by multiple codons, this redundancy in the tRNA coding allows us to reduce the set of tRNAs and ensure the use of tRNAs that do not require modified nucleotides [66]. Recent works on tRNA demonstrated that in vitro expressions can be achieved with semisynthetic tRNAs [67], chemically synthesized tRNAs [68], and in vitro transcribed minimal sets of tRNAs [69]. However, these tRNAs were synthesized separately and purified before their addition to the reaction. Accordingly, direct synthesis of tRNAs has yet to be demonstrated within a PURE system.

1.2.3 Regulation in artificial cell

A complex regulatory behavior, driven by underlying gene regulatory circuits, is found in microorganisms [70]. Currently, cell-free synthesis can be optimized by varying individual DNA input concentrations to adjust protein synthesis [71]. Tuning the genes' expression strength will be required in the future when all genes will be encoded on a single genome [24]. Protein expression can be controlled on the transcription level by promoter strength [22], synthetic terminators [72] or transcription factors [73], or on the translation level by ribosome binding sites [74]. Although it was recently reported that the transcriptional promoter strength is more effective in the control of RNA synthesis than protein synthesis in cell-free systems utilizing the phage RNAP system [75], it remains to be seen if finer control can be obtained by fine-tuning the polymerase concentrations. Moreover, strong control of translation was demonstrated for different ribosome binding sites [74] and gene positions in open reading frames [75]. Autonomous artificial cells will require regulatory networks to gather information and make decisions [76]. Fortunately, advancements in molecular component standardization, characterization, and engineering allows for the development of new regulatory networks [23].

1.3 Cell-free synthetic biology

Cell-free synthetic biology has evolved from a research tool used to advance our understanding of transcription and translation to a commonly used technological platform in many research fields, including synthetic cell systems. Cell-free systems are created by extracting cellular machinery and combining it with energetic substrates and cofactors to replicate central biological processes such as transcription and translation *in vitro*. Early pioneers of cell-free investigations took advantage of two important properties of the system: its simplified biochemical nature and its open reaction environment. Preparing a cell-free extract strips away much of the complexity of cellular regulation, homeostasis, and growth, thereby revealing the isolated, underlying biochemical mechanisms.

In recent years the number of cell-free transcription-translation (TX-TL) systems from different organisms has grown rapidly [77–79]. The most common lysate systems include *E. coli*, insect, yeast, Chinese hamster ovary, rabbit reticulocyte, wheat germ, and human HeLa cells. Many of these lysate systems are currently commercially available. Concurrent with the expanding set of available lysate systems, there has also been a resurgence of interest in reconstituted recombinant systems, which are composed of mixtures of purified enzyme components, especially in conjunction with synthetic cell explorations.

1.3.1 Recombinant systems

Lysate systems contain essentially all cytoplasmic components, which is advantageous for recapitulating cellular processes. However, this makes their composition ill-defined, leading to challenges in basic science and engineering. To address these difficulties, efforts were made to generate fully recombinant cell-free systems from a small number of purified enzyme components, whose composition can be defined exactly. Such defined systems are especially important for bottom-up synthetic biology for three main reasons. The first is that their use supports research into minimal cellular systems, as ‘minimality’ of components and pathways can be directly tested. Secondly, the composition of the recombinant system is known much more precisely than for extract-based systems. This property is highly beneficial for modeling, optimization, troubleshooting, and mechanistic understanding of engineered pathways. Thirdly, the use of recombinant cell-free systems presents a viable approach towards the development of *de-novo* constructed synthetic cells.

Almost half a century ago, Weissbach’s group developed the first such systems from recombinant *E. coli* proteins [80], but observed very low protein yield. About 25 years later, thanks to the advent of His-tag purification as well as the addition of a creatine-phosphate-based energy regeneration system, Shimizu *et al.* [81] developed a very similar system called PURE (protein synthesis using recombinant elements) but with markedly higher protein synthesis yield (Figure 1.2A, B). Currently, there are three commercially available versions of this system: PUREfrex 2.0 (GeneFrontier), PURExpress (NEB) [82], and Magic PURE system (Creative Biolabs). Although highly popular, these systems are more expensive (\$0.6–\$2/ μ L) than lysate systems (\$0.3–\$0.5/ μ L). Moreover, despite the fact that the commercial systems are all based on the original PURE system, their exact composition is proprietary, and functional differences can be observed between them in terms of

batch to batch variability, system yield, translation rate, lifespan of the reaction, and shelf-life [83].

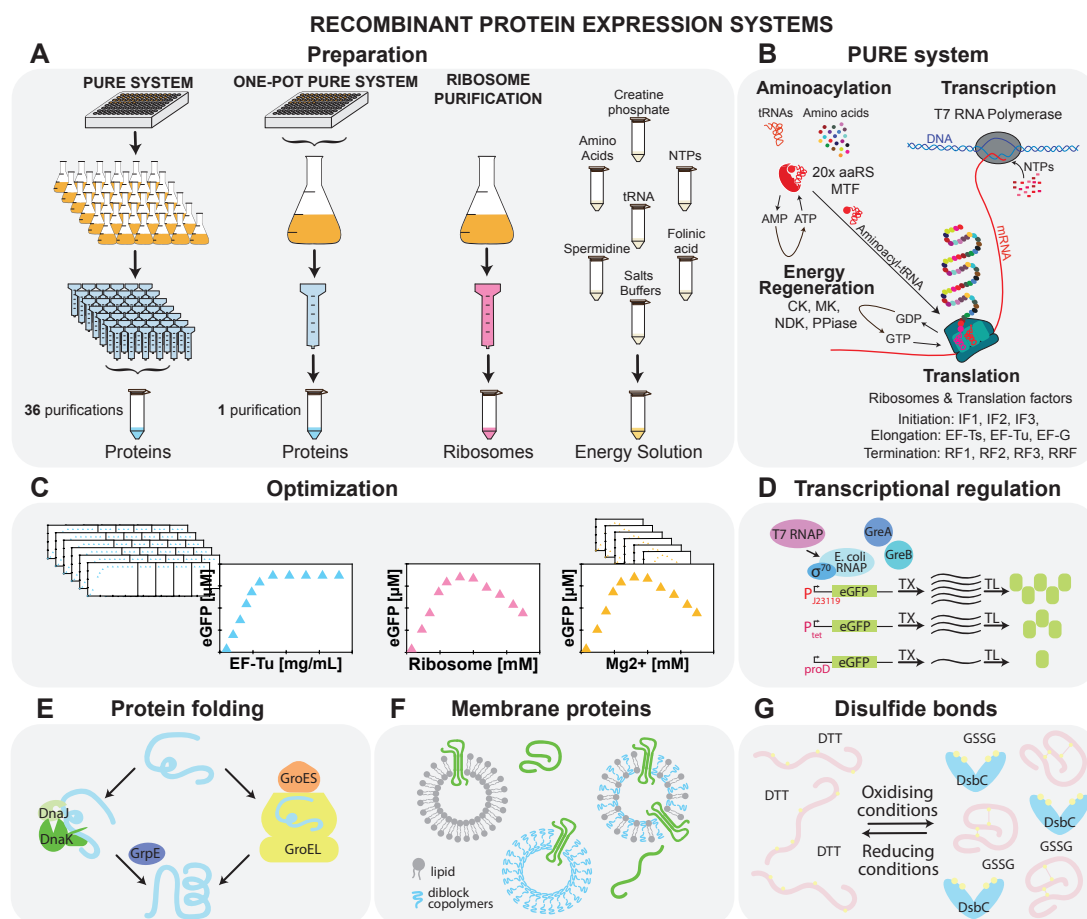


Figure 1.2: Recombinant cell-free systems: (A) Schematic of the preparation of the three elements constituting the PURE system: proteins, ribosomes, and energy solution. (B) The four major reactions, aminoacylation, transcription, translation, and energy regeneration occurring during cell-free protein synthesis in the PURE system are shown along with a list of the components involved. (C) Optimization of the system can be carried out by adjusting both protein and energy solution components. Potential system modifications are shown: (D) supplementation with *E. coli* RNAP allows for more complex transcription regulation [84]; (E) addition of chaperones aids protein folding [56]; (F) vesicles enable membrane protein folding and assembly [85–87]; and (G) oxidising conditions allow for disulfide bond formation [88].

Cost-effective and modular PURE systems with user-defined compositions can be prepared in the laboratory [89, 90], but the labour-intensive protocol requires ~36 medium to large scale His-tag and ribosome purification steps (Figure 1.2A). Thus, different approaches to simplify the protocol have been developed, including His-tagging of *in vivo* enzyme pathways [91], microbial consortia [92], and bacterial artificial chromosomes [47]. The first two systems achieved a 10–20% protein yield compared to the commercial PURExpress (NEB). Although the third approach reached protein synthesis levels comparable to PURExpress, in all three of these approaches it is

not possible to rapidly modify protein levels or omit proteins. We recently demonstrated that all proteins, except ribosomes, can be prepared from individual strains in a single co-culture and purification step called the OnePot PURE system, which achieves a similar protein synthesis yield as commercial PURExpress [93] (Figure 1.2A).

Much work has been carried out to improve existing recombinant systems, particularly focusing on the protein expression yield: in addition to increasing the versatility of the system, this has also resulted in a better understanding of the system itself. Improved yield, lower cost, and the ability to adjust the system composition opens up many possibilities for applications such as the development of defined artificial cells, gene network engineering, biosensors, and protein engineering. Here we separated the various approaches into two distinct types: the first includes experimental and theoretical approaches which aim to find an optimal composition of the system, while the second involves supplementing the existing system with factors that augment its behaviour.

One direction for optimizing recombinant systems for protein synthesis yield is focused on finding optimal concentrations of the basic system components such as proteins, energy sources, small molecules, and salts [58, 83, 94, 95] (Figure 1.2C). Important work to improve our understanding of the system was done by Matsuura *et al.*, who performed titrations of all protein components [96]. These studies showed that although the system is composed of a relatively small number of components, its behaviour is complex, and its analysis requires multivariate optimisation. One of the most important parameters in the system is the magnesium ion concentration, which influences ribosome function. It is difficult to control the concentration of magnesium ions as they can be chelated by negatively charged molecules such as NTPs, creatine phosphates, and pyrophosphates [58, 94]. Studies focused on protein component concentrations showed that the performance of the system is mostly influenced by the concentration of ribosomes and translation factors. Increased yield depended strongly on high concentrations of EF-Tu, which often forms more than 50% of the non-ribosomal protein content *in vivo*. Moreover, finding optimal concentrations is essential for release factors and initiation factors, as an inhibitory effect was shown for these components when higher-than-optimal concentrations were used [94–96]. Finally, the optimal composition of the system will vary depending on the application. As an example, high concentrations of components such as NTPs enhance transcription and translation, while inhibiting DNA replication [50].

To better understand the system behaviour and to identify limiting factors, computational models of the PURE system have been developed. This includes coarse-grained ordinary differential equation (ODE) models containing effective lumped parameters and a small number of reactions [83, 97, 98], as well as more complex models based on modelling of a large number of elementary reactions, which can provide more detailed mechanistic insights but whose connection to experimental data as well as parameter inference is challenging [99, 100]. These models show that a number of steps involving ribosomes could potentially become rate-limiting: these include slow elongation rates, peptide release, and ribosome dissociation; qualitatively similar results were observed experimentally [58, 83, 101].

A second approach is based on augmenting the system with additional components such as proteins [102], crowding agents, and liposomes. For example, yields can be slightly increased by adding proteins such as EF-4 [94], EF-P [58], Pth [95], and HrpA [102]. Recently, an energy regeneration system originally based on three kinases was replaced by one featuring a single polyphosphate kinase. This improvement lowers the price of the energy source and simplifies the energy regeneration process [103]. While the original PURE system only contains T7 RNA polymerase, with its limited capability for transcriptional regulation, *E. coli* σ -factor based transcription has been successfully demonstrated, albeit with low efficiency with certain promoters, which can be enhanced by adding purified *E. coli* polymerase alone or in combination with transcription elongation factors [84] (Figure 1.2D).

Protein folding can be improved by incorporating chaperones such as a trigger factor, DnaK / DnaJ / GrpE, and chaperonin GroEL / GroES (Figure 1.2E). Likewise, Niwa *et al.* showed that the solubility of 800 aggregation-prone *E. coli* cytoplasmic proteins can be enhanced if chaperones are added [56]. Furthermore, an oxidising environment and a disulfide bond isomerase are essential for the expression of proteins containing disulfide bonds [88] (Figure 1.2G). The addition of liposomes [85, 86] together with diblock copolymers [87] is important for membrane-protein synthesis (Figure 1.2F). Finally, the concentration of components in the cell-free system is up to 100 times lower than the native *E. coli* cytoplasm. Crowding agents such as bovine serum albumin (BSA) [94], Ficoll [104], polyethylene glycol (PEG) [94, 104], or osmolites [105] can help mimic the *E. coli* cytosol [104], but they affect both transcription, translation [106], and the final synthesised proteins [107] in a complex way. Further studies will be needed to decipher the various physico-chemical effects of crowding on gene expression. Lastly, it was shown that temperature optimization is a key factor for chaperone-free assembly of protein complexes such as DNA polymerase [49].

1.4 Microfluidic platforms

While cell-free reactions can be carried out successfully in a simple test tube, the complexity and sophistication of experiments can be dramatically augmented by coupling them to the appropriate technological platform. There have been numerous technological advancements with respect to cell-free gene expression over the past few decades, leveraging advances in microarraying, automation, and in particular, microfluidics. In recent years microfluidic technology has offered tremendous improvements in control and throughput of cell-free reactions [108, 109]. High-throughput methods of spatially confined cell-free batch reactions were applied to the generation of protein arrays [110–113], enabled the exploration of larger design spaces at faster time scales [22, 114], and allowed for introduction of spatial organization [115–119].

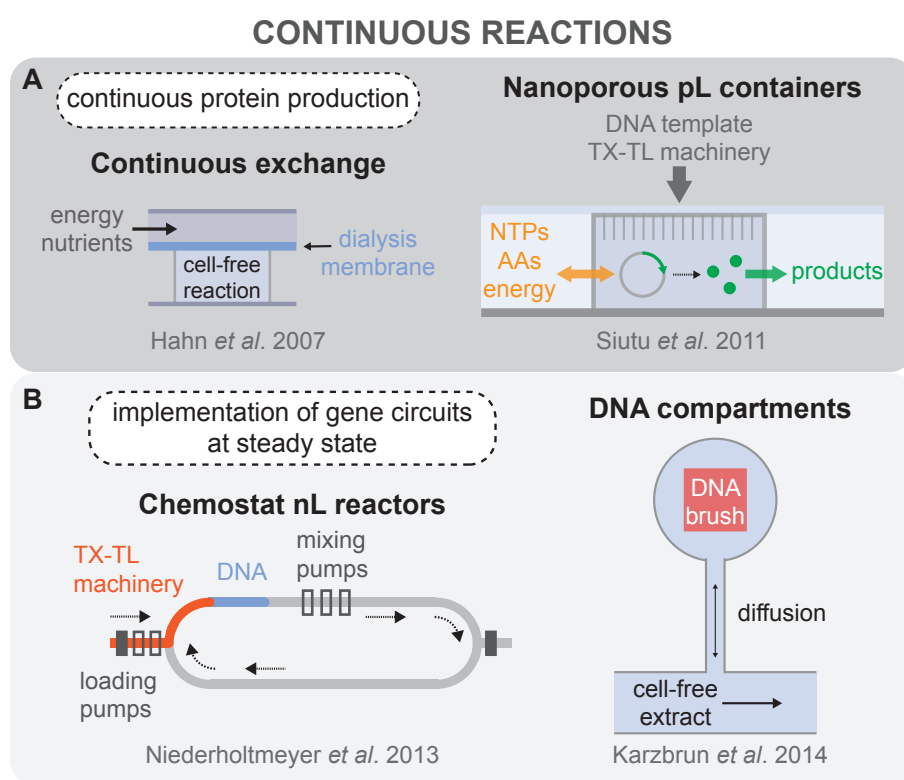


Figure 1.3: **Continuous cell-free reaction platforms.** Devices developed for continuous cell-free reactions, separated into two categories: continuous protein production, and steady-state reactors that enabled the implementation of genetic oscillatory circuits.

1.4.1 Steady-State cell-free reactions

Main constrain of cell-free batch reactions is that they quickly reach chemical equilibrium, due to byproduct or cofactor accumulation and subsequent drift from the initial reaction composition (e.g. inorganic phosphate, Mg^{+2} , H^{+}); denaturation or degradation of reaction components; and simple exhaustion of substrate molecules. This is opposed to living organisms which continuously

exchange energy and matter with the environment. Cell-free TX-TL reactions were successfully prolonged by providing a continuous flow of amino acids and energy sources to a reaction chamber from which synthesized proteins and by-products could be removed across an ultrafiltration membrane [120] or by using a dialysis membrane to separate the reaction from the feeding solution of amino acids and energy sources, leading to a semi-continuous reaction [95, 121, 122]. This idea was then extended to be compatible with standard micro-well plate systems [123–127] and a passive PDMS microreactor, enabling protein synthesis for up to 15 hours [128] (Figure 1.3A).

Continuous-flow and continuous-exchange formats allow small molecule exchange with the environment but lack efficient protein turnover, limiting their use for dynamical systems such as oscillators or self-replicating systems. Recently these limits have been overcome. Continuous protein synthesis was demonstrated for example in an array of cell-sized nanoporous silicon containers [129] (Figure 1.3A). Moreover, in 2013, Niederholtmeyer *et al.* reported a two-layer PDMS device with 8 independent nano-reactors that utilise a peristaltic pump for active reagents exchange. Using this approach dilution rates similar to those of growing bacteria can be achieved, allowing to maintain steady-state TX-TL reactions up to 30 hours, and enabling the first *in vitro* implementation of genetic oscillator circuits [130, 131] (Figure 1.3B). In 2014, Karzbrun *et al.* demonstrated two-dimensional DNA compartments capable of creating oscillating protein expression patterns and protein gradients. Each DNA compartment was linked to a supply channel by a small capillary channel for continuous diffusion of nutrients and products into and out of the compartment [132] (Figure 1.3B). The geometry of the compartments determined the dilution rate of the reaction, giving rise to different observed reaction kinetics. Recently, Swank *et al.* demonstrated automated microfluidic cell-free processing unit contains 280 chemostats, based on the design geometries by [132]. The chemostats periodically supplied with cell-free reagents giving rise to long-term steady-state condition.

1.5 Overview and objective of this work

As outlined in the previous sections, due to its well-defined and straightforward nature, a recombinant cell-free system is an ideal choice as a chassis for a synthetic cell. However, whether or not the PURE system can regenerate itself and drive the self-replication of an artificial cell remains to be demonstrated. Consequently, we set out to couple the PURE system with a microfluidic device to study the regeneration of the protein components essential to transcription and translation.

Given the task at hand, a highly modifiable PURE system, where different components can be adjusted or omitted, was imperative. Hence, we decided to prepare the PURE system in-house to have the most control over the system. However, as stated above, this is time-consuming and tedious (Chapter 1.3.1). Therefore, as part of the preparation process, we also developed a novel "OnePot" preparation method for the PURE system, which significantly simplifies the preparation. Chapter 2 is dedicated to this coculturing and co-purification method for preparing the protein components of the PURE system. By utilizing this method, we were able to cut down the preparation time of the PURE system from weeks to days while ensuring comparable expression levels to the commercial system and preserving system versatility. We anticipate that this method will make this powerful platform accessible to more laboratories worldwide, further expanding the applications of cell-free synthetic biology.

As outlined in Chapter 2, a cell-free reaction can easily be performed in a batch mode. However, to successfully realize prolonged self-regeneration, a biologically more relevant steady-state is required. Chapter 3 outlines the protocol for preparing a microfluidic chemostat that allows regular replenishment and dilution of cell-free TX-TL reactions and, therefore, enables steady-state implementation. We designed a nanoliter microfluidic chemostat with fluidically hard-coded dilutions defined by reactor geometry. Contrary to the peristaltic pump-based dilutions used previously, the hard-coded dilutions are not affected by solution viscosity. This allowed us to separate the energy and protein components of the TX-TL reaction, thereby enabling a vaster experimental versatility and storage of components without cooling.

In Chapter 4, we applied the microfluidic platform developed in Chapter 3 to the TX-TL self-regeneration of proteins. By implementing the kick-start method to boot-up regeneration, we demonstrated that our platform could facilitate the long-term regeneration of essential protein components from DNA templates. Moreover, by coupling our experimental results with computational modelling, we highlight the importance of minimizing resource competition and optimizing resource allocation to achieve robust system function. Lastly, we demonstrated the system's capability to regenerate multiple protein components and showed that the optimal system is surprisingly similar to fitness landscapes observed in living systems.

Self-regeneration of multiple components in Chapter 4 emphasized the significant challenges for achieving a fully self-regenerating system related to a low synthesis rate relative to the fully self-regenerating system requirements. As summarised in Chapter 1.4, synthesis rates and yields can be significantly improved using non-equilibrium systems, e.g., semi-continuous reactions, where the small molecule components are separated from the TX-TL reaction and supplied through diffusion.

Chapter 5 outlines the progress towards microfluidic devices, which enable semi-continuous and continuous cell-free systems on a single device. We demonstrate the incorporation of PEG-DA hydrogel into the device, where the hydrogel acts as a cut-off membrane. This allows for the diffusion of small molecules to the microfluidic reactor while retaining other reaction components.

Finally, the results, limitations, and future work outlook are briefly summarized and discussed in chapter 6.

2 A simple, robust, and low-cost method to produce the PURE cell-free system

This work has been published in ACS Synthetic Biology, 2019.

Authors: Barbora Lavickova and Sebastian J. Maerkl

Contribution: B.L. performed experiments designed experiments, analyzed data, and wrote the manuscript.

Reference: Lavickova, Barbora, and Sebastian J. Maerkl. "A simple, robust, and low-cost method to produce the PURE cell-free system." ACS synthetic biology 8.2 (2019): 455-462.

Permission to reproduce the article is granted by American Chemical Society.

2.1 Abstract

We demonstrate a simple, robust, and low-cost method for producing the PURE cell-free transcription-translation system. Our OnePot PURE system achieved a protein synthesis yield of 156 $\mu\text{g}/\text{mL}$ at a cost of 0.09 USD/ μL , leading to a 14-fold improvement in cost normalized protein synthesis yield over existing PURE systems. The OnePot method makes the PURE system easy to generate and allows it to be readily optimized and modified.

2.2 Introduction

Cell-free transcription-translation systems have become popular for molecular engineering [73, 132–136]. Cell-free systems can be categorized into two main classes: cell extract and recombinant systems. Cell extracts are highly functional but complex and undefined cell-free systems. In 2001, Shimizu *et al.* demonstrated that a defined cell-free system called the “PURE” system (protein synthesis using recombinant elements) could be reconstituted from purified recombinant components [81]. Because of its defined and minimal nature, PURE is an appealing choice for biological systems engineering. The PURE system has been used for genetic network engineering [134], recombinant DNA replication [137], molecular diagnostics [138], therapeutics [139], and educational kits [140]. The PURE system also represents a viable starting point for generation of an artificial cell [14, 24] and its composition has been optimized [94, 141] and extended [84] to achieve higher functionality.

Unfortunately, producing PURE is an arduous and costly process, requiring 36 individual medium to large-scale protein purifications. PURE is now commercially available (PURExpress, New England Biolabs (NEB)), but the high-cost of the commercial system at 1.36 USD/ μL still limits its use. Although NEB provides a few different formulations of the PURE system, the commercial system can’t be customized or optimized by the user, and the precise formulation of the commercial PURE system is not publicly available. It was recently demonstrated that the PURE system could be produced using synthetic microbial “consortia” (TraMOS PURE) [92], which simplified the process of making PURE by co-expressing multiple protein components in a single *E. coli* clone combined with co-culturing of multiple strains. TraMOS PURE achieved only a ~20% protein yield compared to the commercial PURExpress and production cost was reduced from 1.36 USD/ μL to 0.96 USD/ μL . An earlier approach used MAGE to His-tag most PURE protein components in their endogenous locus and co-purified them from 6 strains to generate an ensemble PURE system (ePURE) [91]. The approach led initially to only minimal protein synthesis activity, and an optimized ePURE system ultimately reached a 11% protein yield compared to the original PURE system [81]. Shephard *et al.* cloned 30 PURE protein components onto 3 separate plasmids for simplified and low-cost generation of the PURE system [47]. Upon optimization, this PURE 3.0 system reached protein synthesis levels comparable to the commercial PUREfrex kit (GeneFrontier, Chiba, Japan). As multiple proteins are being expressed and purified from a single *E. coli* clone in all three of these approaches it is not possible to rapidly modify protein levels or omit proteins from the PURE system, which is a critical feature for further PURE system development and optimization.

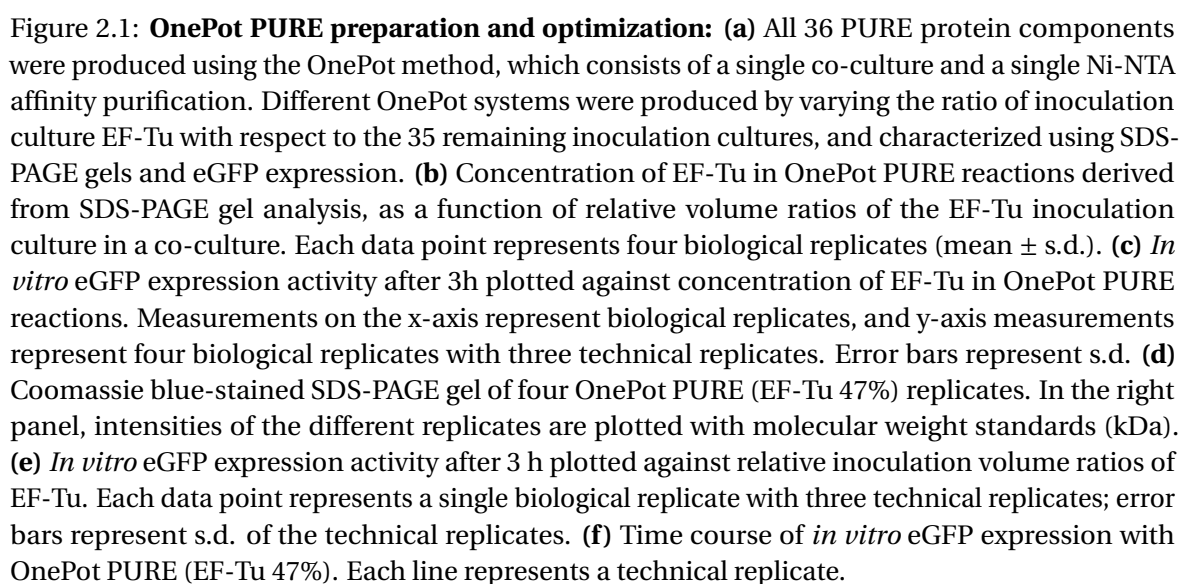
Here we present a simple, robust, and low-cost method for producing the PURE system. Our method co-cultures [142] and induces all 36 protein producing *E. coli* clones in a single flask followed by a single Ni-NTA purification. Our “OnePot” method produces PURE at a cost of 0.09 USD/ μ L and a protein synthesis capacity of 156 μ g/mL, which is as high as the commercial PURE system. OnePot PURE production reduces the cost per microliter to 6% compared to the commercially available PURExpress from NEB (1.36 USD/ μ L). A single batch prepares enough proteins for a total of 15 mL of PURE which is sufficient material for $\sim 1,500$ 10 μ L reactions and can be generated together with ribosomes in 4 days. The method produces consistent PURE across different batches and allows the rapid optimization of individual PURE protein components.

2.3 Results and discussion

The PURE system consists of several different components [81], that can be separated into three main categories: proteins (transcription, translation, and energy regeneration), ribosomes, and small molecule components (salts, buffers, NTPs, creatine phosphate, and folinic acid). In this work, we developed a “OnePot” method for the preparation of all 36 protein components using a single mixed co-culture and Ni-NTA affinity purification step to simplify the process and decrease the cost of the PURE system. All 36 *E. coli* expression clones are cultured individually in small volumes overnight, which are then combined to inoculate a single 500 mL culture. The mixed culture is allowed to outgrow and is induced, followed by pelleting, lysis and loading of the lysate onto a Ni-NTA column for protein purification. To keep the final cost of the PURE system as low as possible, we also prepared ribosome and energy solutions (Figure 2.1a, Supplementary Figure 2.3, 2.4). The entire process of OnePot PURE system preparation, including protein and ribosome purification and energy solution preparation, requires 4 days with 20 hours of hands-on time (Supplementary Table 2.1, 2.2, 2.3). To date no method has been presented in which all non-ribosomal PURE proteins were prepared using a single co-culture and purification step [91, 92]. Moreover, other simplified protocols resulted in low protein synthesis activity as compared to the original PURE system [92].

We explored whether it is possible to adjust the protein component ratios in the OnePot PURE system simply by varying the ratios of the inoculation culture volumes added to the mixed co-culture (Supplementary Table 2.4). Besides ribosomal proteins, elongation factor thermo unstable (EF-Tu) is one of the most abundant proteins in rapidly growing *E. coli* [143] and it was shown to be one of the key factors for *in vitro* protein synthesis [94]. Previous work showed that PURE is otherwise relatively robust to changes in protein concentrations as demonstrated by experimental work where PURE protein components were titrated [94, 96] and computational modeling [99]. Additionally, over 50% of the HomeMade PURE protein components consist of EF-Tu (Supplementary Table 2.5). Hence, we decided to optimize our OnePot PURE system with a particular focus on this translation factor.

We varied the relative volume of the EF-Tu inoculating culture with respect to the 35 remaining inoculation cultures to generate ratios of 3%, 17%, 38%, and 47%. The 3% ratio corresponds



to 100 μ L of all 36 inoculation cultures, including EF-Tu, being added to the mixed co-culture (Supplementary Table 2.4). As can be seen from gels and corresponding analysis, larger percentages of the EF-Tu strain in the co-culture led to higher absolute levels of EF-Tu in the OnePot protein system (Fig. 2.1b, Supplementary Fig. 2.5, 2.6). Increased concentrations of EF-Tu also gave rise to higher protein expression yields (Fig. 2.1c). We could therefore show that it is possible to modify the ratio of an individual PURE protein component simply by varying the initial inoculation ratio of the corresponding strain, and that the OnePot PURE system gave rise to high protein expression yields.

It has been thought that precise control over the PURE system composition is required to achieve reproducible, and high protein expression yields and it has been suggested that a simple one-pot method would not be a viable option for robustly generating the PURE system [92]. However, we observed that variations in overnight culture densities (Supplementary Fig. 2.7) did not lead to substantial differences in OnePot PURE protein content (Fig. 2.1d, Supplementary Fig. 2.5, 2.8c-e). We observed high protein expression robustness across four biological replicates, especially for the 38% and 47% EF-Tu formulations, with coefficients of variation (CV) of 8% and 12%, respectively (Fig. 2.1e, f). In comparison, the CV for a technical replicate of PURExpress and HomeMade PURE were 5% and 12%, respectively. To avoid significant total protein concentration differences across replicates, we adjusted the concentration of the protein mixture to 1.6 mg/mL in the final reaction. This optimal concentration was chosen based on titrations of OnePot PURE (47% EF-Tu) replicate A (Supplementary Fig. 2.9).

We compared the protein composition of our OnePot PURE system to the commercially available PURExpress (NEB) and our HomeMade PURE system prepared based on the Shimizu protocol with minor adjustments [81]. From gels and mass spectrometry (MS) we determined that the overall composition of the PURExpress and HomeMade PURE systems were quite similar to one another as expected (Fig. 2.2a, Supplementary Fig. 2.8d). Both PURExpress and HomeMade PURE had a higher relative percentage of EF-Tu and a lower total protein concentration (1 mg/mL for HomeMade PURE) than OnePot PURE. The relative intensities of individual proteins in the OnePot PURE deviated from the PURExpress and HomeMade PURE standards although the protein expression yield of the OnePot PURE system (47% EF-Tu) was similar to PURExpress, 1.6 times higher than our HomeMade PURE and 5 times higher than TraMOS (Fig. 2.2b).

Moreover, we compared expression levels of different proteins in PURExpress and OnePot PURE (47% EF-Tu). Based on SDS-PAGE gels of proteins labeled with FluoroTect GreenLys tRNA, we reached similar levels of expression in PURExpress and OnePot PURE for eGFP (26.9 kDa), T3 RNAP (98.8 kDa), β -galactosidase (116.5 kDa) and trehalase (63.7 kDa) (Supplementary Fig. 2.10). We were not able to separate bands for DHFR (18 kDa) as it co-migrated with FluoroTect GreenLys tRNA bands. However, we were able to distinguish the expected bands for all four proteins on a Coomassie-stained gel (Supplementary Fig. 2.10b). Activity assays for β -galactosidase and trehalase (Supplementary Fig. 2.11) showed that the synthesized proteins were functional. We also synthesized a zinc-finger transcription factor demonstrating functional repression of deGFP [22, 113], and achieved comparable fold-repression levels in PURExpress and OnePot PURE supplemented

with *E. coli* RNA polymerase and $\sigma 70$ factor (Supplementary Fig. 2.11).

Since PURE systems are prepared by affinity chromatography, a certain amount of contaminants can be expected in the systems. To approximate the amount of protein contamination present we analyzed PURExpress, HomeMade PURE and OnePot PURE by LC-MS/MS. The percentage of contaminants was estimated based on total independent spectral counts, which correlated with the amount of protein present in the sample (Supplementary Fig. 2.8a, b). Our OnePot method gave rise to a similar amount of contamination as in-house prepared HomeMade PURE (Supplementary Fig. 2.8e). The amount of contamination across all OnePot PURE (EF-Tu 47%) replicates was $12.6 \pm 1.5\%$ and for the HomeMade PURE 11.3%. PURExpress had a lower level of contamination of 4.5%. Moreover, the contaminants present across the different PURE systems are similar; more than 50% of contaminants present in OnePot PURE are present in HomeMade PURE as well (Supplementary Excel file for LC-MS/MS). Moreover, many of these contaminants are well-known His-tag based purification contaminants [144]. The main difference is the presence of ribosomal proteins (Supplementary Fig. 2.8f, Supplementary Excel file for LC-MS/MS), these represent around 40% of the contaminating proteins present in OnePot PURE only. This observation is in agreement with results obtained for TraMOS [92]. Based on these results the OnePot PURE system achieved similar levels of purity as PURE produced in-house using the standard method.

One of the main factors limiting the use of the PURE system is its high cost. We performed a detailed cost analysis of different PURE systems: two systems prepared from individually purified protein components (PURExpress and HomeMade PURE), as well as two systems prepared from batch cultures and pooled purifications (OnePot and TraMOS) (Fig. 2.2c, Supplementary Table 2.1, 2.2, 2.3, Supplementary Table 2.6, 2.7). The commercial PURExpress is the most expensive at a cost of 1.36 USD/ μ L followed by TraMOS (0.96 USD/ μ L), HomeMade PURE (0.36 USD/ μ L), and OnePot PURE (0.09 USD/ μ L). For the HomeMade PURE and TraMOS preparations, cost originates primarily from protein components and ribosomes. The OnePot approach reduces the cost of the non-ribosomal protein components to negligible levels and relies on ribosome purification to further reduce cost. Combining in-house ribosome purification with bulk purification of non-ribosomal proteins is thus a general strategy to reduce cost. In-house ribosome purification does not only reduce the price by almost 16-fold as compared to using commercial ribosomes, but also allows for higher ribosome concentrations in the PURE system. The standard ribosome purification protocol used in this work is simple and robust. We compared a total of six ribosome preparations purified over a period of 11 months (Supplementary Fig. 2.12a) showing similar expression levels in OnePot PURE for all batches, demonstrating the robustness of the purification process as well as long-term stability of the purified ribosomes (Supplementary Fig. 2.12b). Moreover, in case ultracentrifugation is not accessible, His-tag purification of ribosomes could be a viable alternative [91, 145]. OnePot PURE substantially outperformed all other systems when directly comparing protein synthesis yield and cost per microliter (Fig. 2.2d), achieving a cost normalized protein yield of 1.70 μ g/USD compared to 0.27 μ g/USD for HomeMade PURE, 0.12 μ g/USD for PURExpress, and 0.03 μ g/USD for TraMOS (Fig. 2.2e).

We demonstrated that it is possible to robustly produce a highly functional PURE system at low

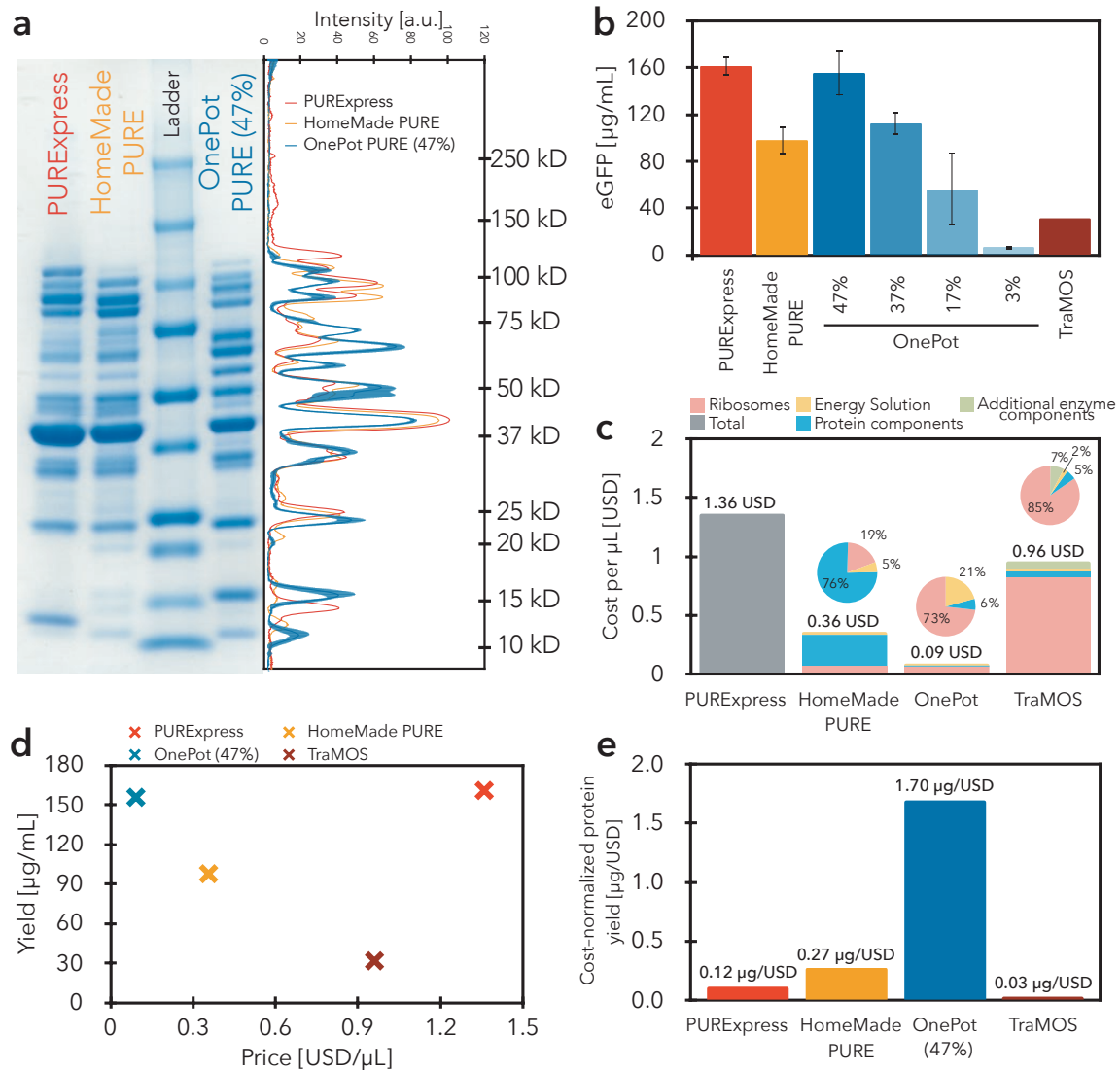


Figure 2.2: OnePot PURE comparison to existing PURE systems: (a) SDS-PAGE gel of PURExpress, HomeMadePURE, OnePot PURE (EF-Tu 47%, replicate A). In the right panel, intensities of different replicates are plotted with molecular weight standards (kDa). (b) Comparison of eGFP expression activity (after 3 h) of different PURE systems. The different systems were tested in the same conditions except for TraMOS where the reported value was used [92]. (c) Price comparison of the different PURE systems. Calculations are detailed in Supplementary Tables 2.1, 2.2, 2.3, Supplementary Table 2.6, 2.7. (d) Yield of the different PURE systems plotted against their price per μL . Mean values of the eGFP expression yield were plotted. (e) Cost-normalized yield of the different PURE systems. The mean value of the eGFP expression yield was used for the calculations.

cost using a practical single batch culture and purification approach. Previous approaches such as ePURE, TraMOS, and PURE 3.0 all expressed multiple proteins within a single host to simplify downstream purification. TraMOS further combined this concept with co-culturing of multiple strains but failed to produce highly functional PURE from a 34 strain co-culture in which each strain expressed a single protein. Here we show that 36 strains can be successfully co-cultured, eliminating the need to co-express multiple proteins in a single host. This in turn makes it possible to rapidly adjust the formulation of the resulting PURE mix which would require tedious and time-consuming cloning steps with the previous methods. The OnePot PURE system described here achieved a protein synthesis yield of 156 $\mu\text{g}/\text{mL}$ at a cost of 0.09 USD/ μL . At 1.7 $\mu\text{g}/\text{USD}$ the cost normalized protein synthesis yield is over a magnitude higher than the commercial PURE system and substantially higher than TraMOS. We also showed that it is possible to adjust and optimize the OnePot PURE system by varying the inoculation fraction of an individual strain. This simple, low-cost, and robust protocol for producing the PURE system should broaden access to the technology and enable new applications which hitherto were not feasible due to the high cost and complexity of producing the PURE system.

2.4 Methods

2.4.1 *Escherichia coli* strains, plasmids, and linear DNA templates

E. coli BL21(DE3) and M15 strains were used for protein expression. All plasmids encoding PURE proteins used in this work were originally obtained from Y. Shimizu (RIKEN Quantitative Biology Center, Japan). Genes coding for MK and PPIase were originally cloned in pET29b vectors with kanamycin resistance. To establish a OnePot system, we used CPEC assembly (Circular Polymerase Extension Cloning) [45] to clone a DNA fragment amplified from pET29b vectors containing MK and PPIase genes as well as the T7 promoter, RBS, and T7 terminator, into a pET21a vector containing ampicillin resistance. The primer sequences used are listed in Supplementary Table 2.8. A list of the PURE proteins with their corresponding gene, vector and reference number are given in Supplementary Table 2.9. *E. coli* A19 (Coli Genetic Stock Center, CGSC#: 5997) was used for ribosome purification.

Linear template DNA for *in vitro* eGFP synthesis was initially prepared by extension PCR from a pKT127 plasmid as described [134] and cloned into a pSBlue-1 plasmid. The DNA fragment used for PURE system characterization was amplified from this plasmid by PCR. DNA templates coding for trehalase, β -galactosidase and T3 RNA polymerase were amplified from *E. coli* MG1655Z1 genome, ZIKV_Sensor_27B_LacZ (Addgene plasmid # 75006) [138] and BBa_K346000 (Registry of Standard Biological Parts), respectively, by extension PCR. Primer sequences are listed in Supplementary Table 2.10. For DHFR expression the control template supplied with PURExpress was used. DNA templates for Zinc-fingers (Supplementary Table 2.11) were prepared as described [22]. DNA fragments were purified using DNA Clean and Concentrator-25 (Zymo Research). DNA was eluted in nuclease-free water instead of elution buffer.

2.4.2 Buffers used for protein and ribosome purification

All buffers used in this work are listed in Supplementary Table 2.12. All buffers were filtered (Flow Bottle Top Filters, 0.45 μ m aPES membrane) and stored at 4°C. 2-mercaptoethanol was added immediately before use.

2.4.3 OnePot protein preparation

Lysogeny broth (LB) used for OnePot protein component preparation was supplemented with 100 μ g/mL ampicillin and all cultures were grown at 37°C, 260 RPM. To allow for fast and easy inoculation, the different strains were stored as a glycerol stock in a single 96 well microplate. All overnight cultures were inoculated by a 96-well replicator (VP 408FS2AS, V & P Scientific), except for the EF-Tu strain, and grown in 0.3 mL of LB in a deep-well microplate (96 wells, void volume 1.5 mL). The strain expressing EF-Tu was grown in 3 mL of LB in a standard 14 mL culture tube. Overnight cultures (in total 3.6 mL) were used to inoculate 500 mL of LB media in a 1 L baffled flask. The exact composition of the inoculation cultures for different OnePot systems are given in

Supplementary Table 2.4. Cells were grown 2 h before induction with 0.1 mM IPTG for 3 h, then harvested by centrifugation (4,000 RPM, 10 min, 4°C) and stored at –80°C overnight. Cells were resuspended in 7.5 mL buffer A and lysed by sonication on ice (Vibra cell 75186 and probe tip diameter: 6 mm, 4 × 20s:20s pulse, 70% amplitude). Cell debris was removed by centrifugation (15,000 RPM, 20 min, 4°C). The supernatant was mixed with 2 mL of equilibrated resin, prepared as described below, and incubated for 3 h, at 4°C. After the incubation, unbound lysate was allowed to flow through the column. The column was washed with 25 mL of a wash buffer (95% buffer A, 5% buffer B) and eluted with 5 mL of elution buffer (10% buffer A, 90% buffer B). Instead of dialysis, buffer exchange was done using a 15 mL Amicon Ultra filter unit with a 3 kDa molecular weight cutoff (Merck). All centrifugation steps were performed at 4,000 RPM and 4°C. The elution fraction was diluted with 25 mL of HT buffer and concentrated to 1 mL (2 × 60 min). The concentrated sample was then diluted with 10 mL of HT buffer, concentrated to 1.5 mL (60 min), and mixed with 1.5 mL of stock buffer B. The protein solution was then concentrated (14,000 RPM, 30 min, 4°C) using a 0.5 mL Amicon Ultra filter unit with a 3 kDa molecular weight cutoff (Merck) and stored at –80°C. Total protein concentration in the OnePot protein mixture was determined using a microplate Bradford protein assay with bovine gamma-globulin as a standard (Bio-Rad). Samples were diluted 1:25 and 5 µL of the diluted sample was mixed with 250 µL of Bradford reagent. Absorbance at 595 nm was measured using a SynergyMX platereader (BioTek). The OnePot protein mixture was then adjusted to a concentration of 12.25 mg/mL.

2.4.4 HomeMade PURE protein preparation

Proteins were prepared by Ni-NTA gravity-flow chromatography. The LB medium used was supplemented with 100 µg/mL of ampicillin and/or 50 µg/mL of kanamycin (Supplementary Table 2.5), and all cultures were grown at 37°C, 250 RPM. Overnight cultures were grown in 3 mL of LB. Each strain was then individually inoculated in a flask with 2 L of LB. Cells were grown 2 h before induction with 0.1 mM of IPTG for 3 h, then harvested by centrifugation and stored at –80°C overnight. The cells were resuspended in 30 mL of buffer A and lysed by sonication on ice (Vibra cell 75186 and probe tip diameter: 6 mm, 8 × 20s:20s pulse, 70% amplitude). Cell debris was removed by centrifugation (25,000 RCF, 20 min, 4°C). The supernatant was mixed with 2-3 mL of equilibrated resin (described below), and incubated for 1-2 h, at 4°C. After the incubation, unbound lysate was allowed to flow through the column. The column was washed with 30 mL of a wash buffer (95% buffer A, 5% buffer B) and eluted with 15 mL of an elution buffer (10% buffer A, 90% buffer B). The elution fraction was dialysed against HT buffer (2×) and stock buffer and stored at –80°C. Protein concentrations were estimated by absorbance at 280 nm and calculated protein extinction coefficients. When a higher protein concentration was required, the protein solution was concentrated using a 0.5 mL Amicon Ultra filter unit (Merck).

2.4.5 Ni-NTA resin preparation and regeneration

2 mL IMAC Sepharose 6 FF (GE Healthcare) was pipetted into Econo-Pac chromatography columns (Bio-Rad), and charged with 15 mL of 100 mM nickel sulfate solution. The charged column

was washed with 50 mL of DEMI water and equilibrated with 35 mL of buffer A. After protein purification, columns were regenerated with 10 mL of buffer containing 0.2 M EDTA and 0.5 M NaCl, and washed with 30 mL of 0.5 M NaCl, followed by 30 mL of demineralized water, and stored in 20% ethanol at 4°C.

2.4.6 OD600 measurement

OD600 measurements of over-night cultures were measured on a 96-well plate with tenfold dilutions (20 μ L of over-night culture in 180 μ L of LB) using a SynergyMX platereader (BioTek). The background (OD600 of 200 μ L of LB) was subtracted from all samples.

2.4.7 Ribosome purification

Ribosomes were prepared from *E. coli* A19 by hydrophobic interaction chromatography (HIC) and sucrose cushion buffer ultracentrifugation as described previously with slight modifications [89, 146]. *E. coli* A19 strain was grown overnight in 100 mL of LB media at 37°C. 2 \times 30 mL of the overnight cultures was used to inoculate 2 \times 2 L of LB. Cells were grown at 37°C, 250 RPM to exponential phase (3-4 h, OD600 = 0.6-0.8), harvested by centrifugation (4,000 RCF, 20 min, at 4°C), resuspended in 50 mL suspension buffer and stored at -80°C. The resuspended cells were lysed by sonication on ice (Vibra cell 75186 and probe tip diameter: 6 mm, 12 \times 20s:20s pulse, 70% amplitude). The cell debris was removed by centrifugation (20,000 RCF, 20 min, at 4°C). The recovered fraction was mixed with the same amount of high salt suspension buffer. The precipitate was removed by centrifugation (20,000 RCF, 20 min, at 4°C) and the supernatant was filtrated with a GD/X syringe filter membrane (0.45 mm, PVDF, Whatman).

Ribosomes were purified using a 15 mL (3 \times 5 mL HiTrap Butyl HP column (GE Healthcare) on Akta Purifier FPLC (GE Healthcare) at 4°C. After the column was equilibrated with 60 mL of buffer C, the prepared lysate solution was loaded onto the column and washed with 45 mL of wash buffer 1 (100% buffer C) followed by 75 mL of wash buffer 2 (80% buffer C, 20% buffer D). Ribosomes were eluted with 60 mL of ribosome elution buffer (50% buffer C, 50% buffer D) followed by 60 mL of final elution buffer (100% buffer D) at a flow rate of 4 mL per minute. All fractions containing ribosomes (absorbance peak at 280 nm during elution with ribosome elution buffer) were pooled together (around 55 mL). The column was recovered by washing with NaOH (1 M) and acetic acid (0.1 M), and stored in 20% ethanol.

14 mL of recovered fraction was overlaid onto 15 mL of cushion buffer in four polycarbonate tubes (void volume: 32 mL). The ribosomes were pelleted by ultracentrifugation (Beckman type SW 32 Ti rotor, 100,000 RCF, 16 h, 4°C). Each transparent ribosome pellet was washed two times with 0.5 mL ribosome buffer and resuspended with a magnetic stirrer in 100 μ M of ribosome buffer. To ensure that all the ribosomes are recovered every tube was washed with 100 μ M ribosome buffer. The recovered solution was concentrated using a 0.5 mL Amicon Ultra filter unit with a 3 kDa molecular weight cutoff (Merck) by centrifugation (14,000 RCF, 10 min, at 4°C). Ribosome concentrations

were determined by measuring absorbance at 260 nm of a 1:100 dilution. An absorbance of 10 for the diluted solution corresponded to a 23 μM concentration of undiluted ribosome solution. Final ribosome solution used for *in vitro* protein synthesis was prepared by diluting the sample to 10 μM . The usual yield is above 0.75 mL of 10 μM ribosome solution.

2.4.8 SDS-PAGE gels

Proteins were separated by SDS-PAGE using 15-well 4-20% Mini-PROTEAN TGX Precast Protein Gels (Bio-Rad). Gels were stained using Bio-Safe Coomassie stain (Bio-Rad), scanned using an EPSON Perfection V10 scanner and analyzed with ImageJ. In case of all gels containing PURE proteins a mixture 0.625 μL of the adjusted solution was loaded. Concentration of EF-Tu in different PURE systems was determined based on SDS-PAGE gels of EF-Tu with known concentrations (Supplementary Fig. 2.13). PURE reactions (5 μL) labeled with FluoroTect GreenLys (Promega) were analyzed by SDS-PAGE using 15-well 4-20% Mini-PROTEAN TGX Precast Protein Gels (Bio-Rad) scanned (AlexaFluor 488 settings, excitation: Spectra blue 470nm, emission: F-535 Y2 filter) at Fusion FX7 (Vilber).

2.4.9 Mass spectrometry

Prior the MS analysis, 15 μL of PURE proteins was subjected to buffer exchange. The samples were diluted to 500 μL in 100 mM ammonium bicarbonate buffer and concentrated by 0.5 mL Amicon Ultra 3 kDa filter unit by centrifugation (14,000 RCF, at 4°C) to 100 μL . This process was repeated three times, with 100 μL of the sample prepared for tryptic digestion and LC-MS/MS analysis. Samples were submitted to tryptic digestion as follows. First, 90 μL of each sample were denaturated by heating for 10 min at 95°C. Then, disulfide bridges were reduced by incubation with tris(2-carboxyethyl)phosphine at 15 mM final concentration for 1 h at 30°C. Cysteine residues were subsequently alkylated for 30 min with iodoacetamide at 20 mM final concentration at room temperature in the dark. Afterwards trypsin was added to the reaction mixture in the ratio 1:50 for overnight digestion. Reaction was quenched by addition of trifluoroacetic acid to 1% final concentration.

Digested samples containing proteolytic peptides were analyzed by LC-MS/MS. 5 μL of each sample were loaded onto a Zorbax Eclipse Plus C18 (1.8 μm , 2.1 x 150 mm) analytical column from Agilent Technology for separation using analytical Dionex Ultimate 3000 RSLC system from Thermo Scientific. The separation was performed with a flow rate of 250 $\mu\text{L}/\text{min}$ by applying an effective gradient of solvent B from 5 to 35% in 60 min, followed by column washing and re-equilibration steps. Solvent A was composed of water with 0.1% formic acid, while solvent B consisted of acetonitrile with 0.1% formic acid. The outlet of the chromatographic column was coupled online with the conventional HESI source from Thermo Scientific and eluting peptides were analyzed by high resolution QExactive HF-HT-Orbitrap-FT-MS benchtop mass spectrometer from Thermo Scientific. Analysis was performed in data-dependent manner with 60000 resolution and AGC (automatic gain control) of 3e6 for MS1 scan. MS2 scans were realized in Top10 mode

with dynamic exclusion of 30 sec, 15000 resolution, 2 scans, AGC of 1e5, precursor isolation window of 2 m/z and NCE (normalized collision energy) of 27% for HCD (higher energy collisional dissociation) fragmentation.

Obtained shotgun bottom-up proteomic data were processed with open source Trans-Proteomic Pipeline software (Institute for System Biology, Seattle Proteome Center) using X! search engine. Peptides were searched against custom database containing all *E.coli* proteins from SwissProt database (Uniprot) together with creatine kinase and adenylate kinase from *Gallus gallus*, inorganic pyrophosphatase from *S. cerevisiae*, T7 RNA polymerase from enterobacteria phage T7 and cationic trypsin from *Bos taurus*. The precursor ion mass tolerance was set to 10 ppm with product ion tolerance of 0.02 Da. Cysteine carbamidomethylation was set as fixed modification, while methionine oxidation, asparagine/glutamine deamidation and N-terminal acetylation were specified as dynamic modifications. The cleavage specificity was set to trypsin with two allowed missed cleavages. 1% false discovery rate (FDR) was allowed with minimum peptide length of 7 amino acids and minimum 2 peptides per protein.

2.4.10 Energy solution preparation

Energy solution was prepared as described previously with slight modifications [89]. 2.5× energy solution contained 0.75 mM of each amino acid, 29.5 mM of magnesium acetate, 250 mM of potassium glutamate, 5 mM of ATP and GTP, 2.5 mM CTP, UTP, and DTT (Dithiothreitol), 130 U_{A260}/mL of tRNA, 50 mM of creatine phosphate, 0.05 mM of folinic acid, 5 mM of spermidine, and 125 mM of HEPES.

2.4.11 *In vitro* protein expression and functional assays

HomeMade or OnePot PURE reactions (5 μ L) were established by mixing 2 μ L of 2.5x energy solution, 0.9 μ L of 10 μ M ribosomes (final concentration: 1.8 μ M), 0.65 μ L of PURE proteins (HomeMade or OnePot solution), DNA template and brought to a final volume of 5 μ L with addition of water. PURExpress reactions (5 μ L) were established by mixing 2 μ L of solution A, 1.5 μ L of solution B, DNA template and brought to 5 μ L with water.

All reactions measuring eGFP expression levels were prepared as described above with eGFP linear template at a final concentration of 5 nM and incubated at 37°C at constant shaking for 3 h, and measured (excitation: 488 nm, emission: 507 nm) on a SynergyMX platereader (BioTek). Absolute eGFP concentrations were determined from a standard curve (Supplementary Fig. 2.14).

Reactions expressing other proteins were prepared as described above and supplemented with 0.2 μ L FluoroTect GreenLys (Promega). DNA templates at a final concentration of 5 nM, except DHFR which was supplied at a concentration of 10 ng/ μ L, were used. The reactions were incubated at 37°C for 3 h.

β -galactosidase expression reactions was prepared as described above with 5 nM of DNA coding

for β -galactosidase and incubated at 37°C for 3 h. The reaction was then diluted 50x in PBS and 2 μ L of the diluted solution was mixed with 20 μ L of chlorophenol red- β -D-galactopyranoside (1 mg/mL, Sigma) and measured (absorbance: 580 nm) on a SynergyMX platereader (BioTek).

Trehalase expression reaction was prepared as described above with 5 nM of DNA coding for trehalase and incubated at 37°C for 3 h, 2.5 μ L of the PURE reaction was mixed with 2.5 μ L trehalose (500mM) and incubated for 15 min at room temperature. After incubation, 5 μ L of DNS reagent was added, the final solution was incubated for 10 min at 99°C and 5 μ L was measured (absorbance: 540 nm) on a SynergyMX platereader (BioTek). DNS reagent was prepared by dissolving 5 mg of dinitrosalicylic acid (Acros Organics) in 250 μ L of water at 80°C. When this solution reaches room temperature, 100 μ L of NaOH, 2 N (Sigma) and 150 mg of potassium sodium tartrate-4-hydrate (Merck) were added and the volume is brought to a volume of 500 μ L with distilled water.

Repression of deGFP expression with zinc-finger transcription factors was measured in the reaction set-up as described above and supplemented with 800 nM of *E. coli* core RNAP and 4 μ M of σ 70 factor, which were prepared as described previously [84]. 1 nM of linear DNA template coding for deGFP and 1 nM of linear DNA template coding for ADD or CBD zinc-finger were used. The reaction was incubated at 37°C at constant shaking for 3 h, and measured (excitation: 488 nm, emission: 507 nm) on a SynergyMX platereader (BioTek).

2.4.12 Cost calculations

To estimate the cost of PURE systems, we analyzed in detail the costs of the different subsets: protein components, ribosomes, and energy solution. The calculation for protein subset costs varies with the type of the system. For the TraMOS system, the reported cost of 0.052 USD/ μ L was used [92]. For our OnePot system, the cost was estimated based on the calculations given in Supplementary Table 2.1, with the assumptions that some of the materials can be reused and that four purifications can be done simultaneously in one working day. In the case of the HomeMade PURE system (Supplementary Table 2.6), our estimate was based on the price charged by the EPFL protein expression core facility: 300 USD per 2 L expression culture, which corresponds to our calculation for OnePot PURE of 83 USD per 0.5 L culture (332 USD for 2 L, Supplementary Table 2.1). Although the total price of this PURE system is high, the total amount of proteins purified is higher as well which can generate at least 40 mL of PURE HomeMade system (based on the volume of the protein limiting the preparation, in our case EF-Tu). Therefore, the price per μ L of HomeMade protein components is 0.27 USD.

Two different possibilities were taken into account in the case of the ribosome subset. In the first system, commercial ribosomes (Supplementary Table 2.7) were used for the PURE reactions (TraMOS). In the second system, purified ribosomes were used (HomeMade and OnePot PURE). The cost calculations for purified ribosomes are given in Supplementary Table 2.2, with the assumptions that some of the materials can be reused and that hands-on time for one purification is a single working day.

The cost calculation for the OnePot energy solution is described in Supplementary Table 2.3, with the assumption that half a day is necessary for the preparation of 20 mL of energy solution. For the TraMOS energy solution and the additional protein components, the costs were recalculated based on the component's price that would apply for the preparation of the given solutions (Supplementary Table 2.7). For some of the additional protein components, we were not able to determine the exact protein which was purchased and its amount used, mostly due to a difference in the type of units reported in the paper as compared to the units specified by the supplier. However, we arrived at a very similar cost estimate as given in the original calculation. Furthermore, we assumed that the work required for the solution preparation is taken into account in the purification cost calculation, so we did not consider it.

In the case of PURExpress, the total cost was based on the commercial price. The values used in the cost calculation were derived from experience with the actual experiments while preparing the different subsets. All costs for the different components were based on the prices given in our internal EPFL system when performing the calculation; no delivery costs were taken into account.

2.4.13 Important details and tips

1. The optimal concentration of Mg^{2+} in the energy solution is essential to high expression levels. If low expression levels are observed with an in-house prepared energy solution, we recommend to perform a Mg^{2+} titration.
2. tRNAs should not be weighed, but should be diluted directly in the flask, to avoid RNAase contamination [89].
3. All buffers should be sterile filtered to avoid bacterial contamination.
4. 2-mercaptoethanol should be added to the solutions immediately before use, buffers without 2-mercaptoethanol can be stored for an extended period in the fridge.
5. The overnight cultures should be shaken at 260 rpm, and well mixed prior to culture inoculation.
6. The expression cultures should be performed in a baffled flask to ensure proper oxygenation.

2.5 Supplementary information

2.5.1 Supplementary figures

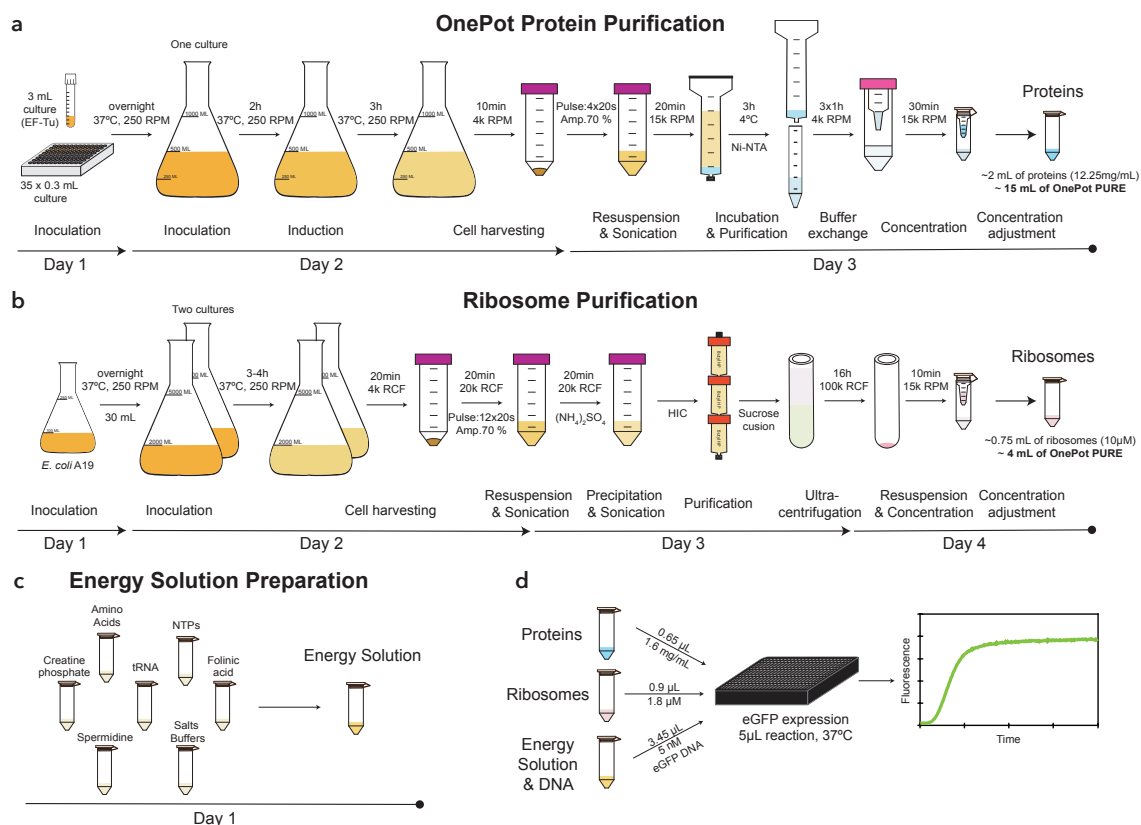


Figure 2.3: Schematics depicting all steps of the OnePot PURE production: (a) Protein purification, (b) ribosome purification, and (c) energy solution preparation steps. The description of the different steps as well as the day on which they are performed are indicated below the schematics. (d) Composition of the OnePot PURE reaction. Two numbers are given for each subset, the volume required for a 5 μ L reaction and the component concentration in the reaction.

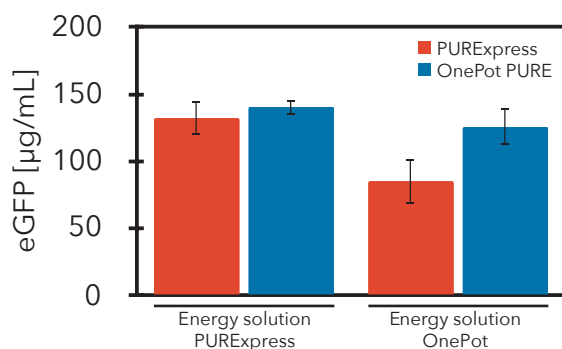


Figure 2.4: Comparison of eGFP expression levels: Comparison of eGFP expression levels in PURExpress (Solution B) and OnePot PURE (EF-Tu 47%, replicate A) supplied with commercial energy solution (Solution A, PURExpress) and the OnePot energy solution used in this study. Each data point represents at least five technical replicates (mean \pm s.d.)

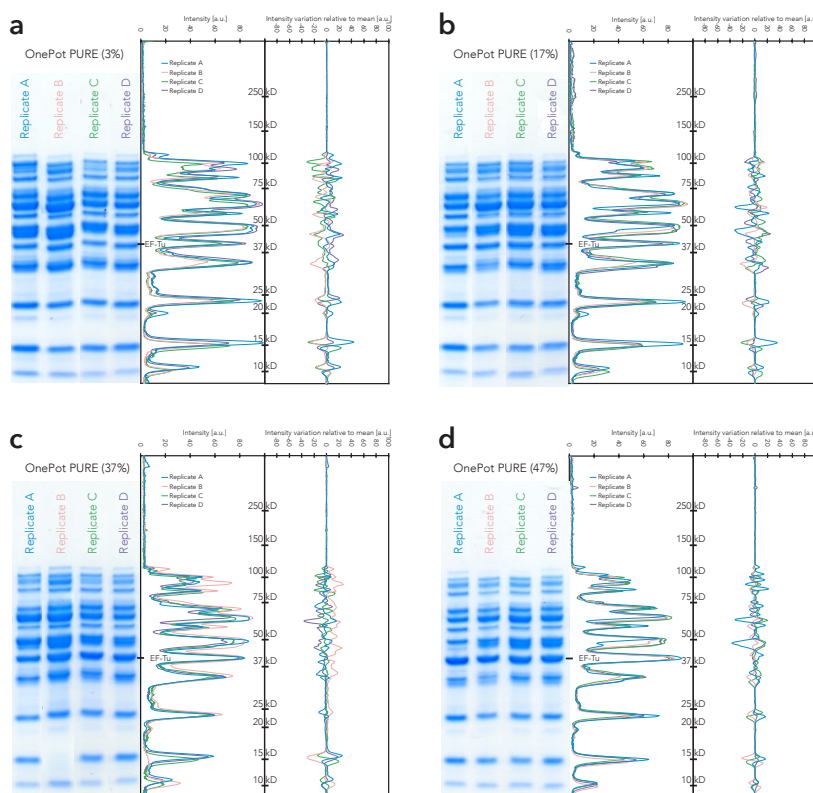


Figure 2.5: Coomassie blue stained SDS-PAGE gels of the four OnePot PURE formulations: (a) 3% EF-Tu, (b) 17% EF-Tu, (c) 37% EF-Tu, and (d) 47% EF-Tu. In the panels to the left of the gels, intensities of the different replicates are plotted with molecular weight standards (kDa). On the right the intensity variations relative to the inter-replicate mean is shown.

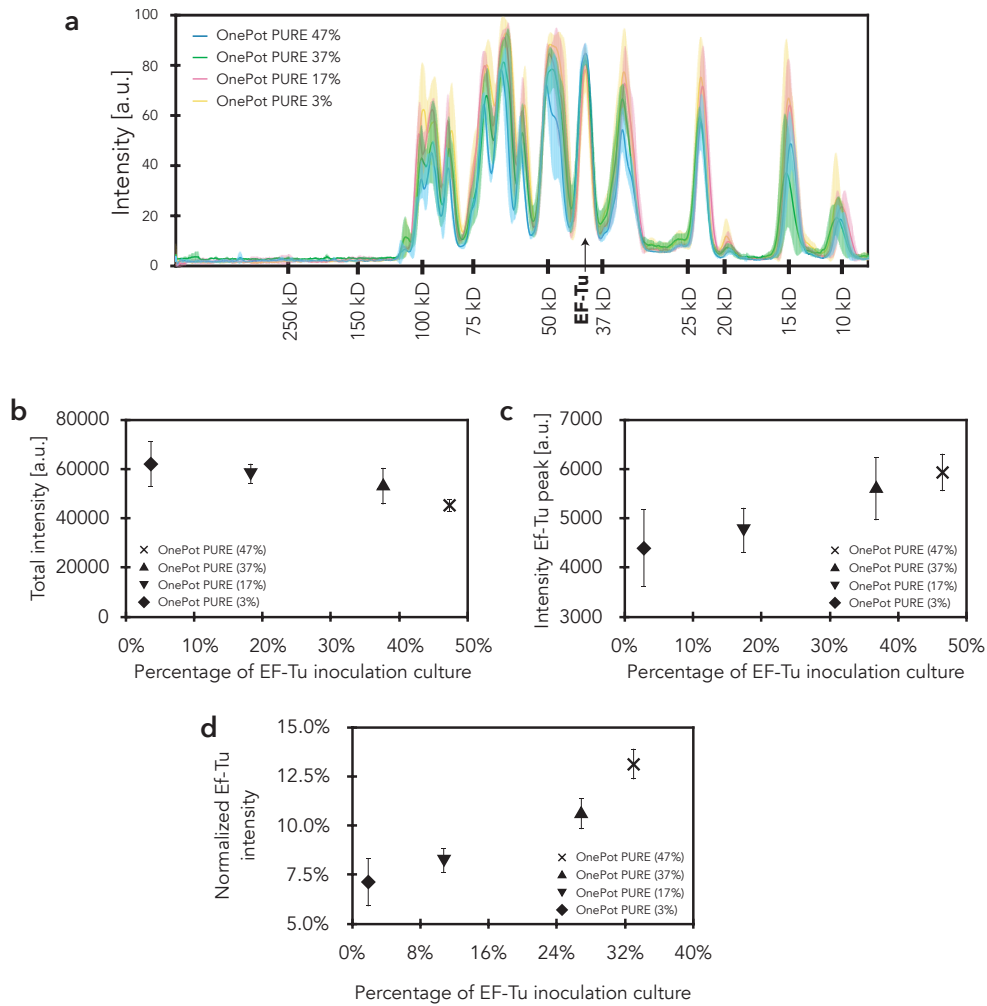


Figure 2.6: EF-Tu analysis: (a) Mean intensities of the different OnePot systems are plotted against molecular weight standards (kDa); the shaded regions represent the s.d. of the four biological replicates. (b) Total intensity of all protein bands as a function of EF-Tu clone inoculation percentage. (c) The integrated intensity of the EF-Tu peak from SDS-PAGE gel analysis as a function of EF-Tu clone inoculation percentage. (d) The normalised EF-Tu intensity (integrated EF-Tu peak intensity / total protein intensity) as a function of EF-Tu clone inoculation percentage. (b) - (d) Each data point represents four biological replicates (mean \pm s.d.)

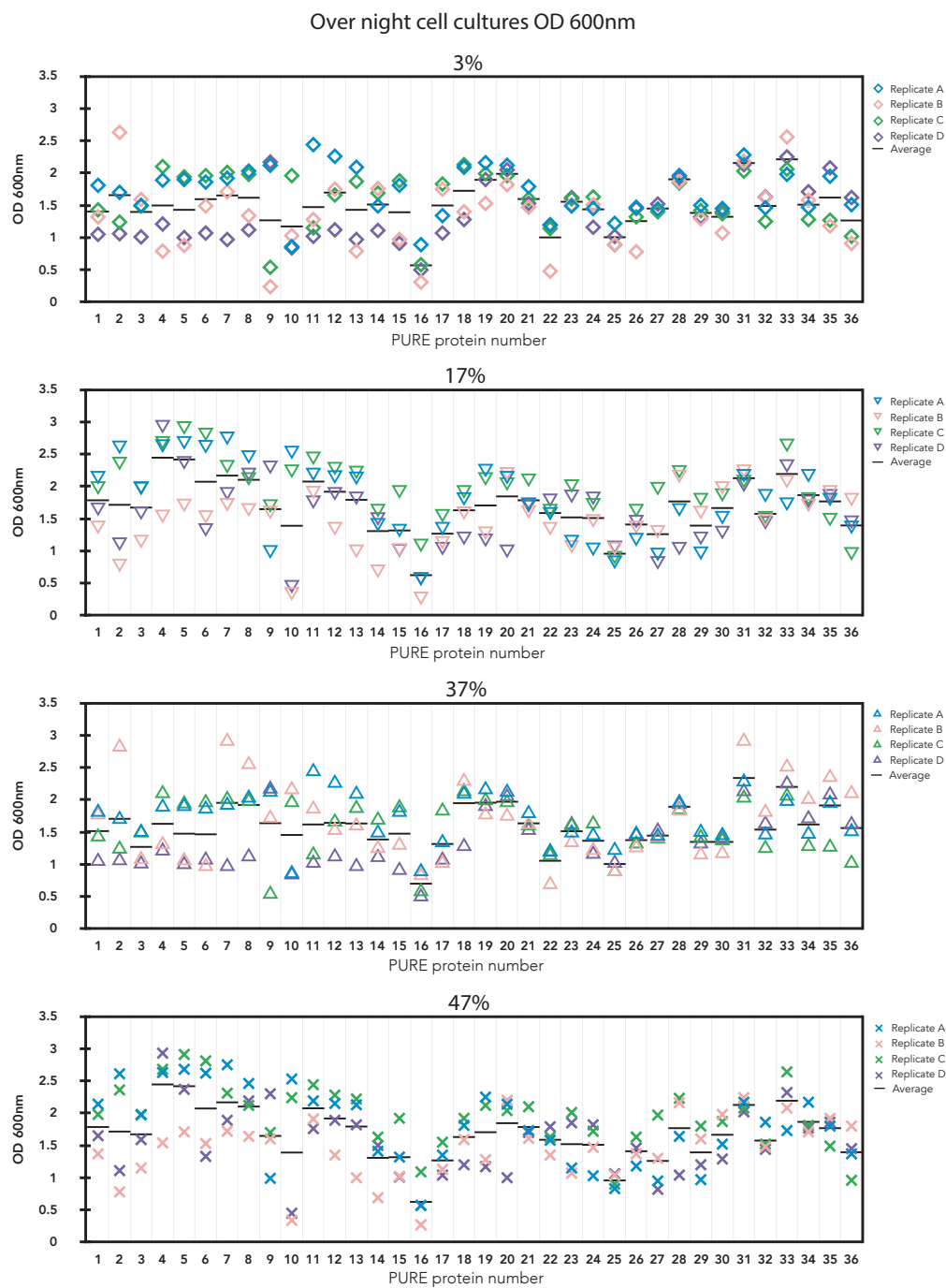


Figure 2.7: OD600 measurement of overnight cultures used for inoculation of the mixed culture.

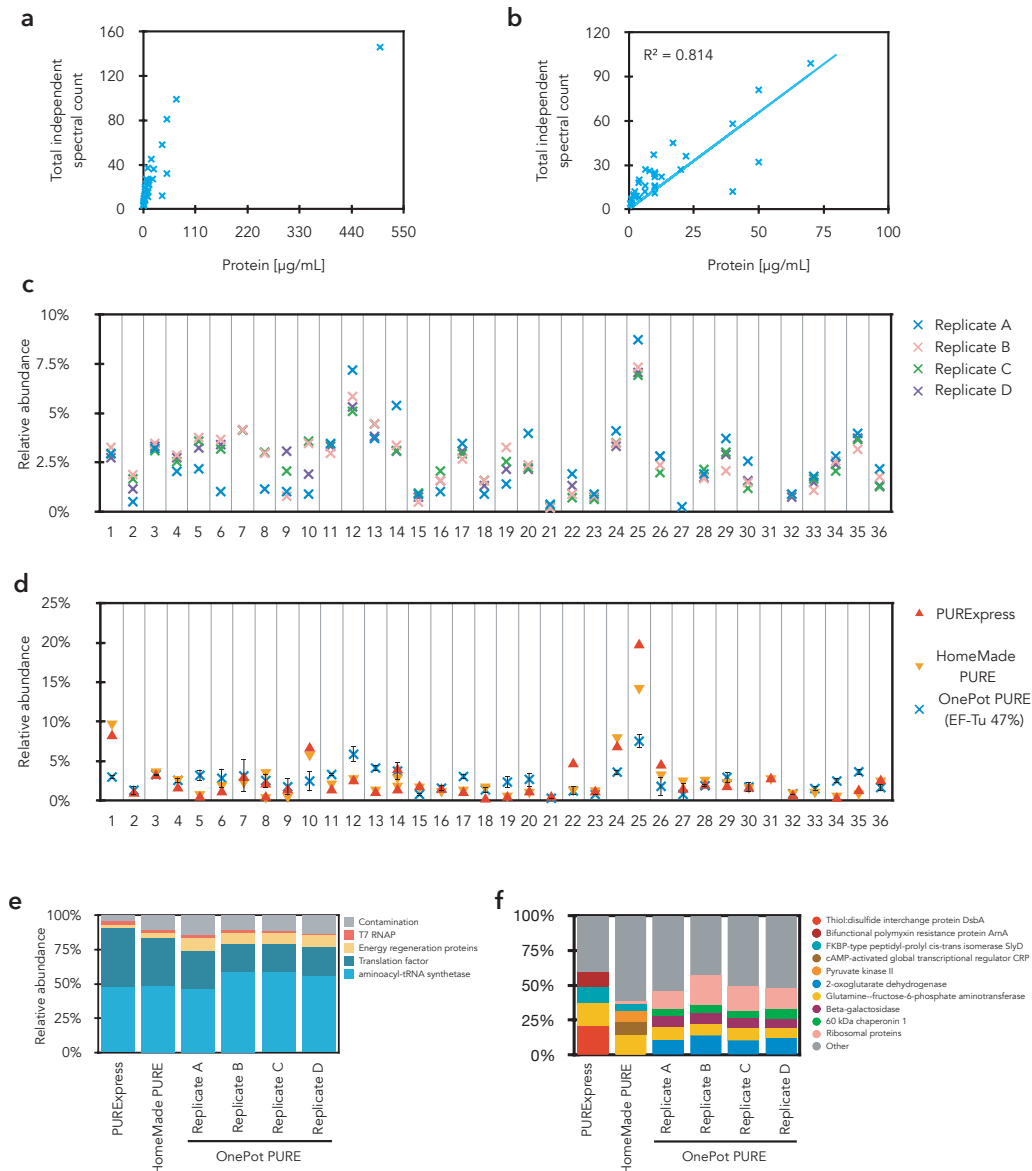


Figure 2.8: Mass spectrometry analysis of the PURE systems: (a) Total independent spectral count from MS analysis of HomeMade PURE system vs protein concentration based on A280 in the HomeMade PURE system (b) Correlation of total independent spectral count and protein concentration (excluded EF-Tu). (c) Relative abundance of OnePot (EF-Tu 47%) system components normalized to total protein content based on total independent spectral count. (d) Relative abundance of PUREExpress, HomeMade PURE, OnePot (EF-Tu 47%) system components normalized to total protein content based on total independent spectral count. (e) Normalized composition of different PURE systems based on total independent spectral count. (f) Detailed description of contamination in the different PURE systems. Relative abundance of the four highest contaminant and ribosomal proteins are shown.

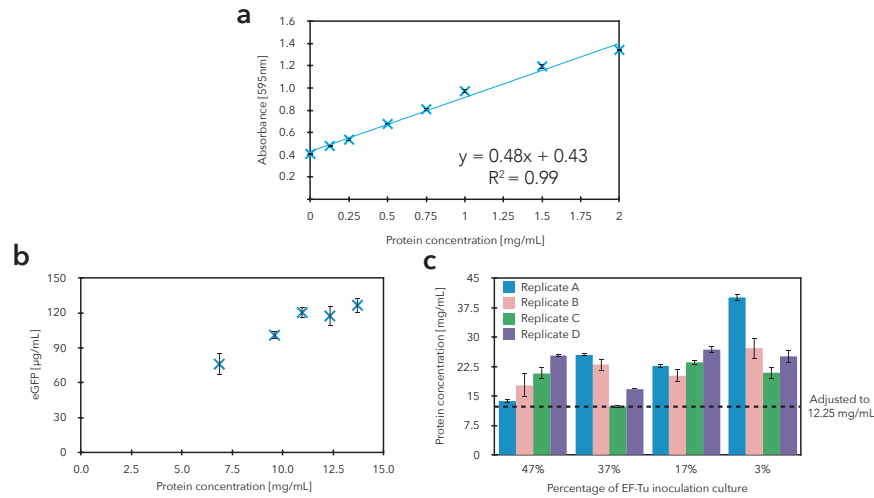


Figure 2.9: Protein concentration calibrations and adjustment: (a) Bradford assay standard calibration curve for protein concentration. The standard curve was produced by measuring the absorbance at 595 nm of prediluted bovine γ -globulin standards. Data are shown as mean \pm s.d. ($n = 3$). Linear fit errors were not propagated as they were negligible compared to experimental errors. (b) eGFP expression as a function of protein concentrations in the protein subset of OnePot PURE (47%) replicate A (7.7 \times concentration in the final reaction). Each point represents at least two replicates; data are shown as mean \pm s.d. (c) The concentrations of all OnePot protein subsets and their replicates after purification. Each bar represents two independent measurements in technical duplicate. Data are shown as mean \pm s.d. The dotted line represents concentration (12.25 mg/mL, which is equal to 1.6 mg/mL in the final PURE reaction) to which all reactions were adjusted to.

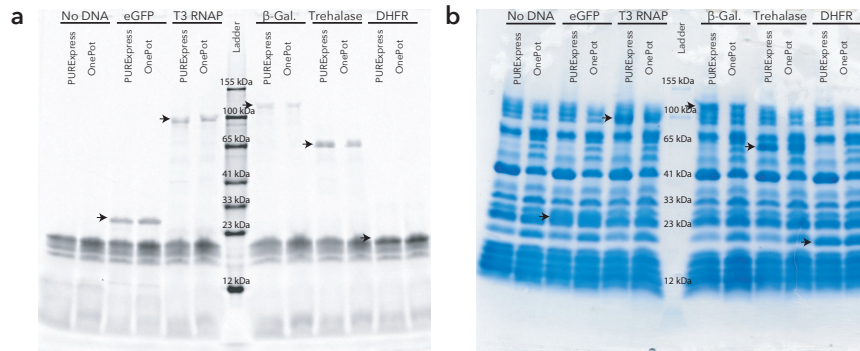


Figure 2.10: SDS-PAGE gel of proteins synthesized in PURExpress or OnePot (EF-Tu 47%, replicate A): (a) labeled with FluoroTect GreenLys, (b) Coomassie blue stained. Black arrows indicate the expected bands of synthesized proteins, GFP (26.9 kDa) T3 RNAP (98.8 kDa), β -galactosidase (116.5 kDa) and trehalase (63.7 kDa), DHFR (18 kDa)

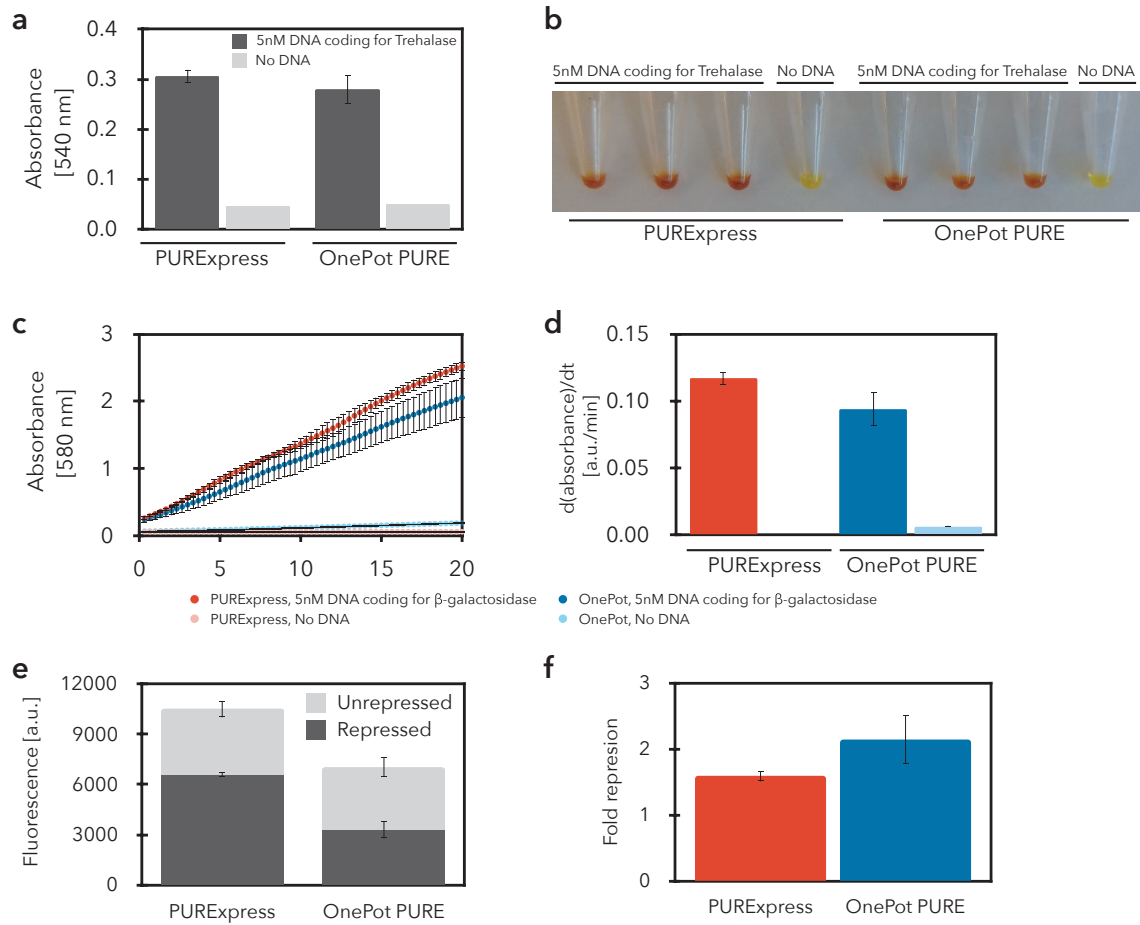


Figure 2.11: **Activities of different proteins, expressed in PURExpress and OnePot (EF-Tu 47%, replicate A):** Trehalase assay: **(a)** Absorbance change at 540 nm and **(b)** image of resulting color change due to the presence of trehalase in the reaction. Three reactions were measured for positive samples. Error bars represent standard deviation. β -galactosidase assay: **(c)** absorbance (580 nm) increase over time due to substrate cleavage, **(d)** slope of absorbance. Three and one OnePot PURE reactions were measured for positive and negative samples, respectively. Each reaction was measured in triplicate. Error bars represent standard deviation. Zinc-finger (ZF) repression: **(e)** Down-regulation of deGFP expression, due to binding of ZF to the target promoter. deGFP containing lambda PR promoter containing double ADD ZF binding sites was used as a reporter. The ADD ZF was co-expressed with deGFP (repressed state), and the CBD ZF was co-expressed as a negative control (unrepressed state). **(f)** Fold-repression, the ratio of unrepressed to repressed expression levels. Each data point represents three technical replicates (mean \pm s.d.)

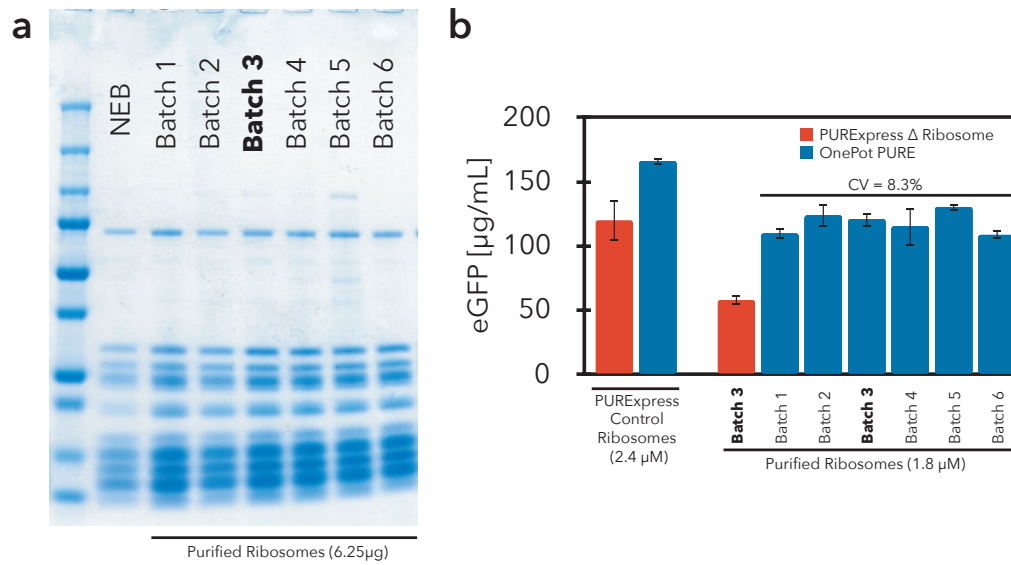


Figure 2.12: **Comparison of ribosomes:** Comparison of commercial ribosomes (ribosomes from PURExpress Δ ribosome kit, NEB) and different batches of ribosomes purified in our laboratory. Batch 3 was used throughout this study. **(a)** Coomassie blue stained SDS-PAGE gels of different ribosomes. The amounts loaded onto the gel were 6.24 μg for NEB ribosomes and 6.25 μg in the case of purified ribosomes. **(b)** Comparison of expression levels in PURExpress Δ ribosome kit and OnePot PURE (EF-Tu 47%, replicate A) supplied with PURExpress control ribosomes (2.4 μM) and purified ribosomes (1.8 μM). Each data point represents two technical replicates (mean ± s.d.)

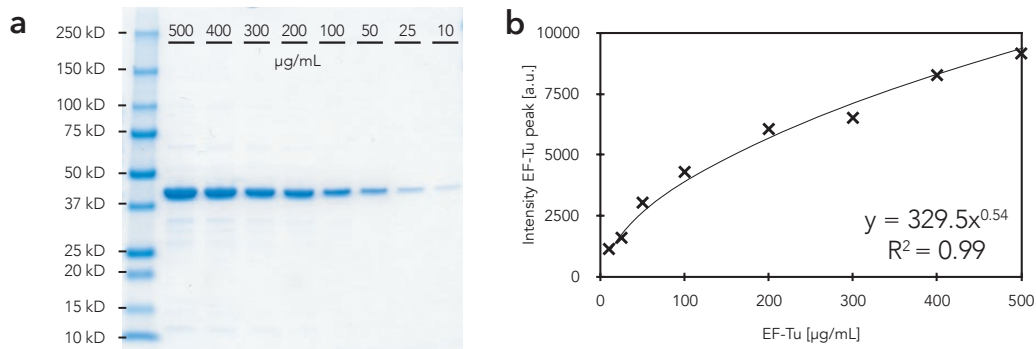


Figure 2.13: **Standard calibration curve for EF-Tu protein concentration:** **(a)** Coomassie blue stained SDS-PAGE gels of different concentrations of EF-Tu. **(b)** The standard curve was produced by measuring the integrated intensity of the EF-Tu peak at different EF-Tu concentrations. The reference EF-Tu concentration was determined by absorbance measurement at 280 nm.

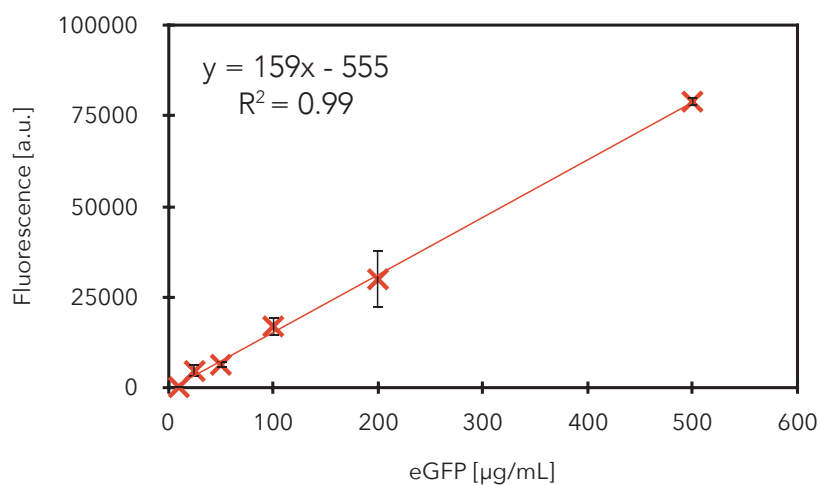


Figure 2.14: **Standard calibration curve for eGFP:** The standard curve was produced by measuring the fluorescence over 60 min for different eGFP (TP790050, AMS Biotechnology) concentrations in PBS on a plate reader with the same settings as for *in vitro* expression. Excitation and emission wavelengths were 488 nm and 507 nm, respectively. Experiments were performed in triplicates. Fluorescence measurements for the first 20 min were not considered. Data are shown as mean \pm s.d. ($n = 3$). Linear fit errors were not propagated as they were negligible compared to experimental errors.

2.5.2 Supplementary tables

Table 2.1: OnePot protocol cost and time estimate

OnePot Protein Purification

Description	Catalog Number	Company	Amount	Price [USD]	Amount per purification	Price per purification [USD]	Note
LB media	A0954	PanReac AppliChem	2,500 g	163	15 g	0.98	
IMAC Sepharose® 6 Fast Flow	17-0921-07	GE Healthcare	25 mL	208	0.5 mL	4.17	2 mL per purification (reused at least for 4 purifications)
Econo-Pac Chromatography Columns	7321010	Bio-Rad Laboratories	50 pcs	382	0.25 pcs	1.91	1 per purification (reused at least for 4 purifications)
Nickel Sulfate	15414469	Alfa Aesar	100 mL	47	3 mL	1.41	
Buffers						4.30	
AMICON ULTRA 15ML - 3 KDa	UFC900324	Merck Millipore	24 pcs	248	1 pcs	10.33	
AMICON ULTRA 0.5ML - 3 KDa	UFC500324	Merck Millipore	24 pcs	112	1 pcs	4.69	
Additional Lab supplies (pipets, tubes)						5.00	
Work			1	200	0.25	50.00	4 purifications can be done at the same time
				Total price per one purification		82.8	
Amount of PURE from single purification			15 mL	Price per 1µL		0.006	

Protein Purification	Total time	Active time
Day 1	14h	2h 30m
Inoculation + Cell Growth	12h	30m
Preparation of media and buffers	2h	2h
Day 2	6h 30m	1h 30m
Inoculation + Cell Growth	2h 20m	20m
Induction + Cell Growth	3h 10m	10m
Centrifugation	1h	1h
Day 3	9h	4h
Preparation of columns	40m	40m
Cell sonication and centrifugation	40m	40m
Purification	3h 30m	1h
Buffer exchange	3h 30m	1h
Concentration	40m	40m
Total	29h 30m	8h

Table 2.2: Ribosome protocol cost and time estimate

Ribosomes Purification

Description	Catalog Number	Company	Amount	Price [USD]	Amount per purification	Price per purification [USD]	Note
LB media	A0954	PanReac AppliChem	2500 g	163	100 g	6.53	
HiTrap Butyl HP Column	28411005	GE Healthcare	5 pcs	323	0.2 pcs	12.91	2-3 per purification (reused for multiple purifications)
Thickwall Polycarbonate Tube	355631	Beckman	25 pcs	275	1 pcs	10.99	reused for multiple purifications
Whatman® GD/X syringe filters	WHA68722504	GE Whatman	50 pcs	304	1 pcs	6.07	
Buffers						22.63	
AMICON ULTRA 0.5ML - 3 KDa	UFC500324	Merck Millipore	24 pcs	112	1 pcs	4.69	
Additional Lab supplies (pipets, tubes)						5.00	
Work			1	200	1	200.00	
				Total price per one purification		268.8	
Amount of PURE from single purification			4 mL	Price per 1µL		0.07	

Ribosome Purification	Total time	Active time
Day 1	14h	2h 10m
Inoculation + Cell Growth	12h	10m
Preparation of media and buffers	2h	2h
Day 2	5h	1h 10m
Inoculation + Cell Growth	4h	10m
Centrifugation	1h	1h
Day 3	21h	3h 40m
Preparation and cleaning of columns	2h	1h
Cell sonication and centrifugation	1h 30m	40m
Purification	1h 30m	1h 30m
Ultracentrifugation	16h	30m
Day 3	1h	1h
Resuspension, Concentration	1h	1h
Total	41h	8h

Table 2.3: Energy solution cost estimates

OnePot Energy Solution

Compound	Catalog Number	Company	Amount	Price [USD]	Amount per 1 μ L reaction	Price per 1 μ L reaction [USD]
Amino acids	LAA21-1KT	Sigma-Aldrich	1 g	464	0.04 μ g	0.000020
Magnesium acetate	M0631	Sigma-Aldrich	100 g	20	2.5 μ g	0.000001
Potassium glutamate	49601	Sigma-Aldrich	500 g	120	20 μ g	0.000005
DTT	sc-29089B	SantaCruz Biotech	10 g	139	0.15 μ g	0.000002
ATP	R0481	ThermoFisher	250 μ L	36	20 nL	0.002844
GTP	R0481	ThermoFisher	250 μ L	36	20 nL	0.002844
CTP	R0481	ThermoFisher	250 μ L	36	10 nL	0.001422
UTP	R0481	ThermoFisher	250 μ L	36	10 nL	0.001422
tRNA	10109541001	Roche	500 μ L	244	17 nL	0.008186
Creatine phosphate	27920	Sigma-Aldrich	1 g	38	7 μ g	0.000248
Folinic acid	PHR1541	Sigma-Aldrich	1 g	55	0.01 μ g	0.000000
Spermidine	S2626	Sigma-Aldrich	1 g	34	0.29 μ g	0.000010
HEPES	H0887-100ML	Sigma-Aldrich	100 mL	39	50 nL	0.000020
Work			20 mL	100	0.4 μ L	0.002000
Total Price per 1 μ L						0.019

Table 2.4: OnePot inoculation culture volumes

Number	Protein	Vector	Strain	OnePot (3%)		OnePot (17%)		OnePot (37%)		OnePot (47%)	
Amount of inoculation culture				μL	%	μL	%	μL	%	μL	%
1	AlaRS	pQE30	M15	100	2.8%	85	2.4%	65	1.8%	55	1.5%
2	ArgRS	pET16b	BL21(DE3)	100	2.8%	85	2.4%	65	1.8%	55	1.5%
3	AsnRS	pQE30	M15	100	2.8%	85	2.4%	65	1.8%	55	1.5%
4	AspRS	pET21a	BL21(DE3)	100	2.8%	85	2.4%	65	1.8%	55	1.5%
5	CysRS	pET21a	BL21(DE3)	100	2.8%	85	2.4%	65	1.8%	55	1.5%
6	GlnRS	pET21a	BL21(DE3)	100	2.8%	85	2.4%	65	1.8%	55	1.5%
7	GluRS	pET21a	BL21(DE3)	100	2.8%	85	2.4%	65	1.8%	55	1.5%
8	GlyRS	pET21a	BL21(DE3)	100	2.8%	85	2.4%	65	1.8%	55	1.5%
9	HisRS	pET21a	BL21(DE3)	100	2.8%	85	2.4%	65	1.8%	55	1.5%
10	IleRS	pET21a	BL21(DE3)	100	2.8%	85	2.4%	65	1.8%	55	1.5%
11	LeuRS	pET21a	BL21(DE3)	100	2.8%	85	2.4%	65	1.8%	55	1.5%
12	LysRS	pET21a	BL21(DE3)	100	2.8%	85	2.4%	65	1.8%	55	1.5%
13	MetRS	pET21a	BL21(DE3)	100	2.8%	85	2.4%	65	1.8%	55	1.5%
14	PheRS	pQE30	M15	100	2.8%	85	2.4%	65	1.8%	55	1.5%
15	ProRS	pET21a	BL21(DE3)	100	2.8%	85	2.4%	65	1.8%	55	1.5%
16	SerRS	pET21a	BL21(DE3)	100	2.8%	85	2.4%	65	1.8%	55	1.5%
17	ThrRS	pQE30	M15	100	2.8%	85	2.4%	65	1.8%	55	1.5%
18	TrpRS	pET21a	BL21(DE3)	100	2.8%	85	2.4%	65	1.8%	55	1.5%
19	TyrRS	pET21a	BL21(DE3)	100	2.8%	85	2.4%	65	1.8%	55	1.5%
20	ValRS	pET21a	BL21(DE3)	100	2.8%	85	2.4%	65	1.8%	55	1.5%
21	IF1	pQE30	M15	100	2.8%	85	2.4%	65	1.8%	55	1.5%
22	IF2	pQE30	M15	100	2.8%	85	2.4%	65	1.8%	55	1.5%
23	IF3	pQE30	M15	100	2.8%	85	2.4%	65	1.8%	55	1.5%
24	EF-G	pQE60	M15	100	2.8%	85	2.4%	65	1.8%	55	1.5%
25	EF-Tu	pQE60	M15	100	2.8%	625	17.4%	1325	36.8%	1675	46.5%
26	EF-Ts	pQE60	M15	100	2.8%	85	2.4%	65	1.8%	55	1.5%
27	RF1	pQE30	M15	100	2.8%	85	2.4%	65	1.8%	55	1.5%
28	RF2	pET15b	BL21(DE3)	100	2.8%	85	2.4%	65	1.8%	55	1.5%
29	RF3	pQE30	M15	100	2.8%	85	2.4%	65	1.8%	55	1.5%
30	RRF	pQE60	M15	100	2.8%	85	2.4%	65	1.8%	55	1.5%
31	MTF	pET21a	BL21(DE3)	100	2.8%	85	2.4%	65	1.8%	55	1.5%
32	CK	pQE30	M15	100	2.8%	85	2.4%	65	1.8%	55	1.5%
33	MK	pET21a	BL21(DE3)	100	2.8%	85	2.4%	65	1.8%	55	1.5%
34	NDK	pQE30	M15	100	2.8%	85	2.4%	65	1.8%	55	1.5%
35	PPiase	pET21a	BL21(DE3)	100	2.8%	85	2.4%	65	1.8%	55	1.5%
36	T7 RNAP	pQE30	M15	100	2.8%	85	2.4%	65	1.8%	55	1.5%
Total amount of inoculation culture				3600	100%	3600	100%	3600	100%	3600	100%

Table 2.5: HomeMade PURE protein concentrations

Number	Protein	Vector	Antibiotic	Strain	HomeMade PURE	
					Final Concentration in reaction [µg/mL]	Concentration in PURE protein solution [µg/mL]
1	AlaRS	pQE30	Amp, Kan	M15	70	538
2	ArgRS	pET16b	Amp	BL21(DE3)	2	15
3	AsnRS	pQE30	Amp, Kan	M15	22	169
4	AspRS	pET21a	Amp	BL21(DE3)	8	62
5	CysRS	pET21a	Amp	BL21(DE3)	1	9
6	GlnRS	pET21a	Amp	BL21(DE3)	4	29
7	GluRS	pET21a	Amp	BL21(DE3)	13	97
8	GlyRS	pET21a	Amp	BL21(DE3)	10	74
9	HisRS	pET21a	Amp	BL21(DE3)	1	6
10	IleRS	pET21a	Amp	BL21(DE3)	40	308
11	LeuRS	pET21a	Amp	BL21(DE3)	4	31
12	LysRS	pET21a	Amp	BL21(DE3)	6	49
13	MetRS	pET21a	Amp	BL21(DE3)	2	18
14	PheRS	pQE30	Amp, Kan	M15	17	131
15	ProRS	pET21a	Amp	BL21(DE3)	10	77
16	SerRS	pET21a	Amp	BL21(DE3)	2	15
17	ThrRS	pQE30	Amp, Kan	M15	6	48
18	TrpRS	pET21a	Amp	BL21(DE3)	6	48
19	TyrRS	pET21a	Amp	BL21(DE3)	1	5
20	ValRS	pET21a	Amp	BL21(DE3)	2	14
21	IF1	pQE30	Amp, Kan	M15	10	77
22	IF2	pQE30	Amp, Kan	M15	40	308
23	IF3	pQE30	Amp, Kan	M15	10	77
24	EF-G	pQE60	Amp, Kan	M15	50	385
25	EF-Tu	pQE60	Amp, Kan	M15	500	3846
26	EF-Ts	pQE60	Amp, Kan	M15	50	385
27	RF1	pQE30	Amp, Kan	M15	10	77
28	RF2	pET15b	Amp	BL21(DE3)	10	77
29	RF3	pQE30	Amp, Kan	M15	10	77
30	RRF	pQE60	Amp, Kan	M15	10	77
31	MTF	pET21a	Amp	BL21(DE3)	20	154
32	CK	pQE30	Amp, Kan	M15	4	31
33	MK	pET29b	Kan	BL21(DE3)	3	23
34	NDK	pQE30	Amp, Kan	M15	1	8
35	PPIase	pET29b	Kan	BL21(DE3)	1	8
36	T7 RNAP	pQE30	Amp, Kan	M15	10	77
Total protein concentration [µg/mL]					966	7428

Table 2.6: HomeMade protocol cost estimates

Description	Catalog Number	Amount per 1 μ L reaction	Amount per purification	Price per purification [USD]
1	AlaRS	70 ng	49 mg	300
2	ArgRS	2 ng	6 mg	300
3	AsnRS	8 ng	93 mg	300
4	AspRS	1 ng	34 mg	300
5	CysRS	4 ng	48 mg	300
6	GlnRS	10 ng	38 mg	300
7	GluRS	2 ng	69 mg	300
8	GlyRS	17 ng	20 mg	300
9	HisRS	10 ng	85 mg	300
10	IleRS	6 ng	26 mg	300
11	LeuRS	22 ng	33 mg	300
12	LysRS	13 ng	112 mg	300
13	MetRS	1 ng	39 mg	300
14	PheRS	40 ng	27 mg	300
15	ProRS	4 ng	16 mg	300
16	SerRS	6 ng	42 mg	300
17	ThrRS	2 ng	67 mg	300
18	TrpRS	6 ng	64 mg	300
19	TyrRS	1 ng	56 mg	300
20	ValRS	2 ng	26 mg	300
21	IF1	10 ng	14 mg	300
22	IF2	40 ng	16 mg	300
23	IF3	10 ng	36 mg	300
24	EF-G	50 ng	56 mg	300
25	EF-Tu	500 ng	20 mg	300
26	EF-Ts	50 ng	36 mg	300
27	RF1	10 ng	37 mg	300
28	RF2	10 ng	16 mg	300
29	RF3	10 ng	66 mg	300
30	RRF	10 ng	8 mg	300
31	MTF	20 ng	36 mg	300
32	CK	4 ng	12 mg	300
33	MK	3 ng	41 mg	300
34	NDK	1 ng	119 mg	300
35	PPiase	1 ng	149 mg	300
36	T7 pol.	10 ng	20.8 mg	300
Total price per purifications				10800
Amount of PURE from single run of purifications (based on EF-Tu)		40 mL	Price per 1 μ L	0.27

Table 2.7: Energy solution and ribosome cost estimates for TraMOS

TraMOS Energy Solution

Compound	Catalog Number	Company	Amount	Price [USD]	Amount per 1uL reaction	Price per 1uL reaction [USD]
Amino acids	LAA21-1KT	Sigma-Aldrich	1 g	464	0.39 µg	0.000181
Magnesium acetate	M0631	Sigma-Aldrich	100 g	20	3.9 µg	0.000001
Potassium glutamate	49601	Sigma-Aldrich	500 g	120	71 µg	0.000017
DTT	sc-29089B	SantaCruz Biotech	10 g	139	0.77 µg	0.000011
ATP	R0481	ThermoFisher	250 uL	36	38 nL	0.005333
GTP	R0481	ThermoFisher	250 uL	36	25 nL	0.003555
CTP	R0481	ThermoFisher	250 uL	36	13 nL	0.001778
UTP	R0481	ThermoFisher	250 uL	36	13 nL	0.001778
tRNA	10109541001	Roche	500 uL	244	17 nL	0.008501
Creatine phosphate	27920	Sigma-Aldrich	1 g	38	16 µg	0.000620
Folinic acid	PHR1541	Sigma-Aldrich	1 g	55	0.03 µg	0.000002
Spermidine	S2626	Sigma-Aldrich	1 g	34	0.15 µg	0.000005
HEPES	H0887-100ML	Sigma-Aldrich	100 mL	39	50 nL	0.000020
Total Price per 1µL						0.022

TraMOS Additional Enzymes

Compound	Catalog Number	Company	Amount	Price [USD]	Amount per 1uL reaction	Price per 1uL reaction [USD]
BSA	A3912	Sigma-Aldrich	100 g	229	1 µg	0.000002
Creatine kinase	10127566001	Roche	100 mg	142	81 ng	0.000115
Myokinase	M3003	Sigma-Aldrich	0.3 mg	63	50 ng	0.010425
Diphosphonucleotide kinase	N2635	Sigma-Aldrich	0.1 mg	233	4.1 ng	0.009517
T7 RNAP	M0251S	New England Biolabs	100 uL	96	40 nL	0.038360
RNAse inhibitor	M0314S	New England Biolabs	75 uL	101	10 nL	0.013413
Total Price per 1µL						0.072

Ribosomes

Compound	Catalog Number	Company	Amount	Price [USD]	Amount per 1uL reaction	Price per 1uL reaction [USD]
Ribosomes	M0314S	New England Biolabs	1 mg	250	3 µg	0.815163
Total Price per 1µL						0.815

Table 2.8: DNA sequences of primers used for CPEC

	Forward primers	Reverse primers
Primers used for amplification DNA fragment from pET29b vectors	5'-GCGTCCCATTCGCAATC-3'	5'-GCGTCCCATTCGCAATC-3'
Primers used for amplification DNA fragment from pET21a vectors	5'-CCATTCCTTGCGGCGG-3'	5'-CTGAAAGGAGGAACATATATCCGATTGG-3'

Table 2.9: PURE protein list

Number	Protein	Protein name	Gene	Organism	Vector used for Home Made PURE	Vector used for OnePot PURE	Expression Strain
1	AlaRS	Alanyl-tRNA synthetase	alaS	E. coli	pQE30	pQE30	M15
2	ArgRS	Arginyl-tRNA synthetase	argS	E. coli	pET16b	pET16b	BL21(DE3)
3	AsnRS	Asparaginyl-tRNA synthetase	asnS	E. coli	pQE30	pQE30	M15
4	AspRS	Aspartate-tRNA synthetase	aspS	E. coli	pET21a	pET21a	BL21(DE3)
5	CysRS	Cysteinyl-tRNA synthetase	cysS	E. coli	pET21a	pET21a	BL21(DE3)
6	GlnRS	Glutaminyl-tRNA synthetase	glnS	E. coli	pET21a	pET21a	BL21(DE3)
7	GluRS	Glutamyl-tRNA synthetase	gltX	E. coli	pET21a	pET21a	BL21(DE3)
8	GlyRS	Glycyl-tRNA synthetase	glyQ & glyS	E. coli	pET21a	pET21a	BL21(DE3)
9	HisRS	Histidyl-tRNA synthetase	hisS	E. coli	pET21a	pET21a	BL21(DE3)
10	IleRS	Isoleucyl-tRNA synthetase	ileS	E. coli	pET21a	pET21a	BL21(DE3)
11	LeuRS	Leucyl-tRNA synthetase	leuS	E. coli	pET21a	pET21a	BL21(DE3)
12	LysRS	Lysyl-tRNA synthetase	lysS	E. coli	pET21a	pET21a	BL21(DE3)
13	MetRS	Methionine-tRNA ligase	metG	E. coli	pET21a	pET21a	BL21(DE3)
14	PheRS	Phenylalanyl-tRNA synthetase	pheT & pheS	E. coli	pQE30	pQE30	M15
15	ProRS	Prolyl-tRNA synthetase	proS	E. coli	pET21a	pET21a	BL21(DE3)
16	SerRS	Seryl-tRNA synthetase	serS	E. coli	pET21a	pET21a	BL21(DE3)
17	ThrRS	Threonyl-tRNA synthetase	thrS	E. coli	pQE30	pQE30	M15
18	TrpRS	Tryptophanyl-tRNA synthetase	trpS	E. coli	pET21a	pET21a	BL21(DE3)
19	TyrRS	Tyrosyl-tRNA synthetase	tyrS	E. coli	pET21a	pET21a	BL21(DE3)
20	ValRS	Valyl-tRNA synthetase	valS	E. coli	pET21a	pET21a	BL21(DE3)
21	IF1	Initiation factor 1	infA	E. coli	pQE30	pQE30	M15
22	IF2	Initiation factor 2	infB	E. coli	pQE30	pQE30	M15
23	IF3	Initiation factor 3	infC	E. coli	pQE30	pQE30	M15
24	EF-G	Elongation factor G	fusA	E. coli	pQE60	pQE60	M15
25	EF-Tu	Elongation factor Tu	tufB	E. coli	pQE60	pQE60	M15
26	EF-Ts	Elongation factor Ts	tsf	E. coli	pQE60	pQE60	M15
27	RF1	Release factor 1	prfA	E. coli	pQE30	pQE30	M15
28	RF2	Release factor 2	prfB	E. coli	pET15b	pET15b	BL21(DE3)
29	RF3	Release factor 3	prfC	E. coli	pQE30	pQE30	M15
30	RRF	Ribosome recycling factor	frr	E. coli	pQE60	pQE60	M15
31	MTF	Methionyl-tRNA formyltransferase	fnt	E. coli	pET21a	pET21a	BL21(DE3)
32	CK	Creatine kinase	CKM	Chicken	pQE30	pQE30	M15
33	MK	Adenylate kinase (Myokinase)	AK1	Chicken	pET29b	pET21a	BL21(DE3)
34	NDK	Nucleotide diphosphate kinase	ndk	E. coli	pQE30	pQE30	M15
35	PPiase	Inorganic pyrophosphatase	IPP1	Saccharomyces cerevisiae	pET29b	pET21a	BL21(DE3)
36	T7 RNAP	T7 RNA polymerase	1	Enterobacteria phage T7	pQE30	pQE30	M15

Chapter 2

A simple, robust, and low-cost method to produce the PURE cell-free system

Table 2.10: DNA sequences for linear templates with T7 RNAP promoter

[illegible]

	DNA sequence
deGFP linear DNA fragment	ccagccagaagacgactcttcttggtgaaccggatgtgcattacagcggcgacagtcgaagtcggggacagcagaagctgaccgcgcagatgtgatgttgacatgtggaagactctgcaccatcagccagaagaaacgaatttctgggtgggttcac-gatatccgcgtgatgcgtgaacgtgacggagctgaaccacgcgcagatgtgtctgtcttcggtcgatgtgagctaacAGCGGATGGAggtTgacaaGCGGATGAGAgggccgtgtataagttgttgacatagacaataatttggtaaacttaagaggagataaccATGGAGCTTCTTCACTGGCGTTGTTCCATCTCGTGTCGAGCTTGGACGGCGACGTAAACGGCCACAAGTTCCAGCTGTCTCGCGGAGGGCGAGGGCGATGCCACATCAGCGCAAGCTGACCTGAAGTTCATCTGCACCCAGCGGACAGCTGCCGTGCCCTGCGCCACCCTCTGTGACCACCTTGACCTACGGCGTGCAGTGTCTTCAGCCGCTACCCGACCATGAAGCAGCAGCTTCTTCAAAGTCCGGCATCCGGCAAGGTACGTCTCGAGGAGCGGCACATCTTCTTCAAGGACGACGCAACTATAGAACGCGCCGAGGTGAAGTTGCAGGGGGACACCTTGTTGAAGCCAGCTGAGAGCTGAAGGCGATCATTAAGGAAGCGGCGCAACATCTGGGGACCAAGCTGTGAGTACAACTACAACAGCCACAAGCTCTATATCATGTGCGCGAGAGAGAAGCGCATCAAGTGAATGATCTCAAGATCGGCCACAACATCAGAGCGGCGAGCTGCGCGACCATCAGCAGAAACACCCCTCATCGGGCAGCGGCCCGCTGTGCTGCGCCGACAACTACATCTTGAGCAACCAAGTTCGCCCTTGAGCAAGACCCCAACAGGAGAAGCGGCATCATGATGTCTCTGTGGAGTTGGTAGCCCGCGCGGGGATCTAAAGTgcgaagccgcggaagcggggtttctatgtgtcgacagtgatgcgttgagagcttaccacagctctcttcggtggggggggcgactgactatgtgcgcagctatgactgtcttcttatgcgaactgcaggacaggtgcgcgagcgtcttcgctctcgtcgtcaactgactcgtcgtcgttcggttcggtgcgcgagcggttatcagctactcaaaagcggttaacggtttaccacgaatcagggtgaacgcaggaaga
ZF _{ADD} linear DNA fragment	gacatggtgaagactatccacattcagccagaagaaacgaatttctgtgggttcacgatctgcctgatgcgtgaacgtgacggcagcagtcgcgcagatgtgtgtctgtccgtgggatcgtgagctaacacgctggtgtgacaaattttactctcgccgtgataaagtggttcagctagcgcataatttttttgaagaggagataaccATGCAGCTCGTATGCTTTCGACAAACCAAACTCGCTGTTTCATATAGAAATCTACTGTGACAAAAACCATTCCTCAATGTAGAATTGTATGAGAAATTTCTCTGTTGCTGCACAACTGACCCGTACATCTCGTACCACACCGGTGAAAAACCGTTCGCTTGCGCACATCTCGCGTGTAAATTCGCTGTCTGACGAACGTAAACGTACACCAAAATCACCTGCGTCGCTCAGGGCAGCGGACGTGAAGAAGAGCTGTGTTAATAAgaatcagggtgaacgcaggaaga
ZF _{CBD} linear DNA fragment	gacatggtgaagactatccacattcagccagaagaaacgaatttctgtgggttcacgatctgcctgatgcgtgaacgtgacggcagcagtcgcgcagatgtgtgtctgtccgtgggatcgtgagctaacacgctggtgtgacaaattttactctcgccgtgataaagtggttcagctagcgcataatttttttgaagaggagataaccATGCAGCTCGTATGCTTTCGACAAACCAAACTCGCTGTTTCATATAGAAATCTACTGTGACAAAAACCATTCCTCAATGTAGAATTGTATGAGAAATTTCTTGACCGTGTAACTCGCTGCTGCATCTGCACCTACACACCGGTGAAAAACCGTTCGCTTGCGCACATCTCGCGTGTAAATTCGCTGAACGTGTGATGCTGACCCGTACCCCAAAATCACCTGCGTCGCTGACGAGCGCGCTGAAGAAGAGCTGTGTTAATAAgaatcagggtgaacgcaggaaga
Blue	E. coli RNAP
Red	RBS
Green	Gene coding for protein
Bold	T500 terminator

Bufferes for protein purification

Compound	Catalog number	Company	Buffer A	Buffer B	Buffer HT	Stock buffer	Stock buffer B	Note
			mM	mM	mM	mM	mM	
HEPES	H0887-100ML	Sigma-Aldrich	50	50	50	50	50	pH = 7.6, KOH
Ammonium chloride	09718-250G	Sigma-Aldrich	1000					
Magnesium chloride	63020-1L	Honeywell Fluka	10	10	10	10	10	
Potassium chloride	P5405-1KG	Sigma-Aldrich		100	100	100	100	
Indisadol	I2399	Sigma-Aldrich		500				pH = 7.6, KOH
Glycerol	G7757-1L	Sigma-Aldrich				30%	60%	
β-mercaptoethanol	M6250-100ML	Sigma-Aldrich	7	7	7	7	7	

Compound	Catalog number	Company	Suspension buffer	Suspension buffer high salt	Buffer C	Buffer D	Cusion buffer	Ribosome buffer	Note
			mM	mM	mM	mM	mM	mM	
HEPES	H0887-100ML	Sigma-Aldrich	10	10	20	20	20	20	pH = 7.6, KOH
Magnesium acetate	M0631	Sigma-Aldrich	10	10	10	10	10	6	
Potassium chloride	P5405-1KG	Sigma-Aldrich	50	50				30	
Ammonium chloride	09718-250G	Sigma-Aldrich					30		
Ammonium sulfate	A4418	Sigma-Aldrich		3000	1500				pH = 7.6, KOH
Sucrose	84097	Sigma-Aldrich					30%		
β -mercaptoethanol	M6250-100ML	Sigma-Aldrich	7	7	7	7	7	7	

Compound	Catalog number	Company	Concentration in reaction	Concentration in subset (2.5x)	Units
Amino acids	LAA21-1KT	Sigma-Aldrich	0.3	0.75	mM
Magnesium acetate	M0631	Sigma-Aldrich	11.8	29.5	mM
Potassium glutamate	49601	Sigma-Aldrich	100	250	mM
DTT	sc-29089B	SantaCruz Biotech	1	2.5	mM
ATP	R0481	ThermoFisher	2	5	mM
GTP	R0481	ThermoFisher	2	5	mM
CTP	R0481	ThermoFisher	1	2.5	mM
UTP	R0481	ThermoFisher	1	2.5	mM
tRNA	10109541001	Roche	52	130	U ₂₆₀ /mL
Creatine phosphate	27920	Sigma-Aldrich	20	50	mM
Folic acid	PHR1541	Sigma-Aldrich	0.02	0.05	mM
Spermidine	S2626	Sigma-Aldrich	2	5	mM
HEPES	H0887-100ML	Sigma-Aldrich	50	125	mM

3 Steady-state cell-free gene expression with microfluidic chemostats

This work has been published in Synthetic Gene Circuits, 2021.

Authors: Nadanai Laohakunakorn, Barbora Lavickova, Zoe Swank, Julie Laurent, Sebastian J. Maerkl

Contribution: B.L. performed and designed experiments, analyzed data.

Reference: Laohakunakorn, Nadanai, et al. "Steady-state cell-free gene expression with microfluidic chemostats." Synthetic Gene Circuits. Humana, New York, NY, 2021. 189-203.

Permission to reproduce the article is granted by Springer Nature.

3.1 Abstract

Cell-free synthetic biology offers an approach to building and testing gene circuits in a simplified environment free from the complexity of a living cell. Recent advances in microfluidic devices allowed cell-free reactions to run under non-equilibrium, steady state conditions enabling the implementation of dynamic gene regulatory circuits *in vitro*. In this chapter we present a detailed protocol to fabricate a microfluidic chemostat device which enables such an operation, detailing essential steps in photolithography, soft lithography, and hardware setup.

3.2 Introduction

One of the enduring challenges in synthetic biology today is the overwhelming difficulty of predictive forward-engineering, despite major efforts to characterise, standardise, and mathematically model synthetic biological parts and systems [147]. Even if parts such as promoters and regulators are initially well-characterised, combining them together into larger subsystems typically changes the context of the parts as well as the host cell, resulting in diminished predictive accuracy and in some cases a loss of the original function altogether. Functional designs are therefore usually developed not in a purely rational manner, but require rounds of empirical design-build-test cycles. While this approach can certainly yield functional designs, it is preferable to ultimately develop more efficient and rational ways of engineering gene circuits.

Within synthetic biology, the adoption of cell-free systems has become increasingly widespread [148]. From an engineering perspective, they behave as a very simplified ‘host cell’, providing a constant and controllable environment in which to build synthetic gene networks. Cell-free systems are thus well-suited for rational, bottom-up engineering of biomolecular systems [79, 149]. Furthermore, the functionality of cell-free systems can be expanded by inclusion of additional components [84], and provide a system for quantitative analysis including mRNA and protein concentrations [130, 150]. A second key benefit is that their ease of preparation and scalability also accelerates design-build-test cycles, resulting in their adoption as an efficient rapid prototyping platform. Both lysate [151, 152] and recombinant [93] cell-free reaction systems can now be readily generated using standard laboratory equipment at reasonably low costs. Microfluidics have allowed these benefits of cell-free synthetic biology to be more fully realised [109]. By increasing the throughput, lowering reagent consumption, and providing control and quantitative monitoring of thousands of reactions in parallel, they have enabled precise characterisation of cell-free gene circuits both in integrated chips [153] as well as in encapsulated droplets [114, 154].

Batch cell-free reactions typically run to chemical equilibrium as substrates are exhausted, reaction products accumulate, and enzymatic machinery degrades. To maintain a more life-like non-equilibrium steady state, large-scale continuous exchange or continuous flow reactors have been used to feed the reaction with small molecules and wash away products through ultrafiltration membranes [120]. At the microfluidic level, microchemostat devices have been developed which replenish not only substrates but also the enzymatic machinery, while at the same time diluting

away reaction products [134]. These microchemostats enable long-term steady state reactions, and also allow for the investigation of biologically-relevant dynamical behaviours such as oscillations [132, 134] and pattern formation [155].

In this chapter, we describe the entire process of designing, fabricating, and operating a microfluidic chemostat device. The chip we chose as an example is a revised and simplified version of the microchemostat presented in Niederholtmeyer et al. 2013 [134], and is shown in Figure 3.1. The operation of the device first involves selecting an input solution using the multiplexer unit, which is directed to one of eight separate reactor rings. Each reactor contains four output ports, located at specific positions around the ring. Opening these ports exchanges a fixed fraction of the reactor volume, with the exact fraction depending on the position of the port. The placement of these ports allows the reactor to be loaded with a reaction of fixed composition, and importantly also allows a dilution step to occur which preserves this composition. In between dilution steps, the reaction is mixed using a peristaltic pump.

We describe the photolithographic steps required to print the chip design on a chrome mask, and subsequently transfer it onto silicon wafers. Once fabricated, these silicon molds can be used for multiple rounds of soft lithography where they are used to cast PDMS devices. Finally, the hardware required for operating the chip is described, and a standard experiment outlined. Related protocols are available in the literature.

3.3 Materials

The photolithography steps were carried out in a Class 100 clean room at EPFL. Soft lithography was done in a dedicated space in a standard wet lab. Specialised machines, consumables, and chemicals are listed below.

- **Photolithography machines**

- VPG200 photoresist laser writer (Heidelberg Instruments Mikrotechnik GmbH)
- HMR900 mask processor (Hamatech APE GmbH)
- Optispin SB20 spin coater and VB20 hotplate (ATMsse GmbH)
- MJB4 mask aligner (Süss MicroTec AG)
- Tepla 300 plasma stripper (PVA Tepla AG)
- LSM250 spin coater and HP200 hotplate (Sawatec AG)
- AccuPlate thermal accumulator and hot plate system (Detlef Gestigkeit)

- **Photolithography consumables**

- AZ 9260 positive photoresist (MicroChemicals GmbH)
- GM1070-SU8 negative photoresist (Gersteltec)
- 1-methoxy-2-propyl-acetate (PGMEA) developer (Sigma)
- AZ 400K developer (Merck)
- AZ 351B developer (Merck)
- Cr01 chrome etchant (Technic)
- Hexa-methyl-disilazane (HMDS) primer (Technic)
- Silicon wafers, diameter 100 ± 0.5 mm, thickness 525 ± 25 μm , P-type (boron-doped), resistivity 0.1-100 Ω/cm (Siegert)
- SLM5 5" blank chrome mask (Nanofilm)

- **Soft lithography machines**

- ARE-250 centrifugal mixer (Thinky)
- SCS G3P-8 spin coater (Specialty Coating Systems Inc.)
- Schmidt Press manual hole puncher and 21-gauge (OD 0.04") pins (Technical Innovations, Inc.)
- Diener Femto 40 kHz low pressure plasma oven with O₂ supply (Diener electronic GmbH + Co. KG)
- Universal Oven UF110, 108L (Memmert)
- SZX10 dissection microscope with DF PLANO 1.25x objective and KL 1500 LCD light source (Olympus)

- **Soft lithography consumables**

- Trimethylchlorosilane (Sigma)
- Sylgard 184 polydimethylsiloxane (PDMS) elastomer and curing agent (Dow Corning)
- Glass slides 76x26x1 mm 631-1550 (VWR)

- **Microfluidic hardware**

- 12-station aluminium pneumatic manifold with 24V 3-way normally-open solenoid valves (S10MM-31-24-2/A Pneumadyne)
- Polycarbonate manual luer manifold (Cole-Parmer)
- Custom relay circuit board (*see* Note 1)
- Type 10, 2-60 psi and 2-25 psi pressure regulators (Marsh Bellofram)
- 0.1-3 bar pressure gauge (Riegler & Co. KG)

- **Microfluidic connectors**

- Synflex 1201-M06 polyethylene (PE) tubing, OD 6 mm ID 4mm (Eaton)
- PE-LD tubing OD 1/8" ID 1/16" (Tuyau)
- Tygon tubing, OD 0.06" ID 0.02" (Cole-Parmer)
- FEP tubing, OD 1/16" ID 1/32" (Upchurch)
- PEEK tubing, OD 1/32" ID 0.18 mm (Vici)
- Luer stubs 12 mm, 23 and 20 ga
- Male-to-male and 1/16" barb to male luer adaptors
- Stainless steel connecting pins OD 0.65 mm ID 0.35 mm, 8 mm (Unimed)
- Brass Series G pneumatic fittings (Serto AG)
- Blue Series pneumatic fittings (Riegler & Co. KG)

- **Microscope hardware**

- Ti2 Eclipse Inverted Microscope (Nikon)
- Objectives: CFI Achrom 4x NA 0.1 (Nikon); CFI S Plan Fluor 20x NA 0.45 ELWD DIC N1 (Nikon)
- Filters: F36-504 mCherry HC filter set (Semrock); FITC (Nikon)
- Microscope enclosure and heater (Okolab)
- Sola SM II Light Engine (Lumencor)
- Orca-Flash 4.0 V3 Digital CMOS Camera (Hamamatsu)

- **Software**

- AutoCAD2019 (Autodesk)

- CleWin (WieWeb)
- LabView 2018 (National Instruments)
- Matlab 2019 (Mathworks)

- **Experimental reagents**

- TX-TL cell-free extract, ribosomes and energy solution, prepared as in (13)
- DNA template, prepared as in (14)

3.4 Methods

3.4.1 Design of microfluidic devices

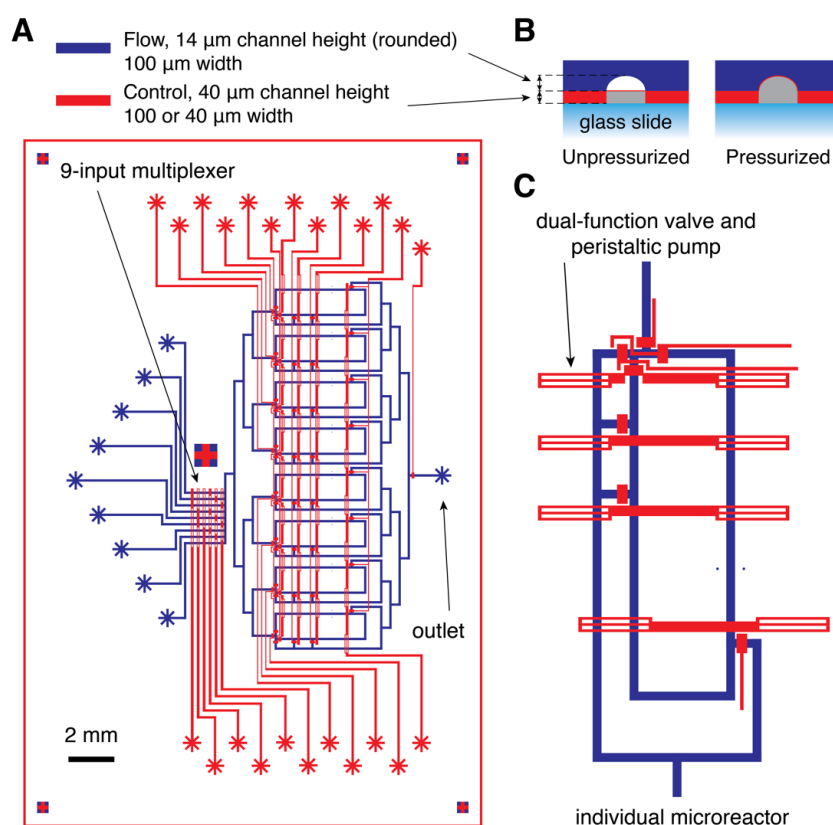


Figure 3.1: **(A)** A two-layer microchemostat design consists of a thin control layer sandwiched between a glass slide and a thicker flow layer. **(B)** Applying pressure to channels in the control layer pushes up valves which close off channels in the flow layer. **(C)** The chip contains eight individual chemostat reactors. Four control lines serve as dual-function valves and peristaltic pump. Actuating these lines sequentially mixes the liquid inside the reactors.

1. Design the device (*see Note 2*) on AutoCAD 2019 or other software with similar functionality.

A specific example is shown in Figure 3.1, and other designs are available on our webpage (*see Note 3*). Export the final design as a .dxf file.

2. Using CleWin, convert the designs to a machine-compatible .cif file ready for photomask fabrication.
3. During curing, the PDMS layers will differentially shrink, with the thicker flow layer shrinking more than the thinner control layer, which remains attached to the rigid mold. Thus, it is crucial to enlarge the entire flow layer design by 1.5% . This can be done in CleWin during the conversion.

3.4.2 Photolithography for mask and wafer fabrication

- **Mask fabrication**

1. Expose chrome masks with the VPG200 laser writer, using a 20 mm write lens (*see Note 4*) and 48% intensity. Make sure the polarity and mirroring of the mask is correct (*see Note 5*).
2. Next, process the exposed masks using the HMR900 mask processor. This involves the following automated steps:
3. First purge the machine with DI water.
4. Then develop for 100 s with a diluted developer mixture (AZ 351B:DI water in the ratio 1:3.75), and rinse with DI water.
5. Etch through the chrome layer for 60 s using the Cr01 etchant, and rinse.
6. Finally strip the photoresist using the AZ 400K developer for 35 s, followed by a final rinse and drying with CO₂. The completed masks should be completely dry before use.

- **Flow mold fabrication**

1. Prime a clean Si wafer with HMDS (*see Note 6*) for 10 s in vacuum, using the VB20 hotplate.
2. Transfer the wafer onto the Optispin SB20 spin coater and dispense a few ml of positive resist AZ9260 onto the centre of the wafer, taking care to avoid bubbles (*see Notes 7, 8*).
3. Spin coat at 920 rpm for 100 s, followed by 60 s relaxation at 0 rpm. This deposits a 14- μ m layer of photoresist on the surface of the wafer.
4. When the spin coating has finished, immediately transfer the wafer to a preheated hotplate, and 'softbake' for 6 minutes exactly at 115 °C.
5. Transfer the wafer to an opaque storage box and allow it to rehydrate for a minimum of 1 hour (*see Note 9*).
6. Load the appropriate chrome mask onto the MJB4 mask aligner, and expose for 2 cycles at 18 s per cycle, with a waiting time of 10-15 s between each cycle, using the Hg-i line (365 nm) at 20 mW/cm² (*see Notes 10, 11*). Use the following parameters: expose type = hard, alignment gap = 30, WEC type = cont, N2 purge = NO, WEC-offset = OFF.

7. Develop immediately (maximal waiting time is 1 hour) by transferring the wafer to a bath of diluted AZ 400K developer (1:3 developer:DI water). Develop face-up, and gently agitate the wafer in the bath for 10 minutes (*see Note 12*).
8. Rinse with DI water, then carefully but rapidly dry the wafer with N₂, and inspect features under a microscope. If photoresist residues remain, develop further until all the residues are removed and repeat the cleaning and drying.
9. Finally transfer the wafer to the AccuPlate hotplate, and carry out a 'reflow' bake using the following program to round off features (*see Note 13*): 1 hr ramp up to 170 °C, 2 hrs at 170 °C, 1 hr ramp down to room temperature

• **Control mold fabrication**

1. Clean an Si wafer with 2.45 GHz O₂ plasma in the Tepla 300 Plasma Stripper, using 500 W for 7 min and 400 ml/min of O₂.
2. Transfer the wafer onto the LSM250 spin coater, and dispense a few ml of negative resist GM1070-SU8 onto the centre of the wafer, taking care to avoid bubbles.
3. Spin coat a 40- μ m layer of photoresist onto the wafer using the following program: 5s/0-500 rpm, 5s/500rpm, 21s/500-1933rpm, 40s/1933rpm, 1s/1933-2933rpm, 1s/2933-1933rpm, 5s/1933rpm, 26s/1933-0rpm.
4. When the spin coating has finished, immediately transfer the wafer to the hotplate, and carry out an initial relaxation followed by a softbake using the following program (*see Note 14*): 30 minutes at 30 °C, then 3000 s ramp 30 °C to 130 °C, 300 s at 130 °C, then 3000 s ramp 130 °C to 30 °C.
5. Load the appropriate chrome mask onto the MJB4 mask aligner, and expose for 1 cycle at 16 s, using the Hg-i line (365 nm) at 20 mW/cm². Use the following parameters: expose type = soft, alignment gap = 30, WEC type = cont, N₂ purge = NO, WEC-offset = OFF.
6. Transfer the wafer to the HP200 hotplate for a post-exposure bake using the following program: 2400 s ramp 30 °C to 90 °C, 2400 s at 90 °C, 2700 s at 60 °C, 2700 s at 30 °C.
7. Transfer the wafer to an opaque storage box and wait from 1 hour to overnight before development.
8. Develop by transferring the wafer to a bath of PGMEA developer (*see Note 15*). Gently agitate the wafer in the bath for 2 minutes before transferring to a bath of new developer for a further 1 minute.
9. Rinse with isopropanol. If a reaction is visible (white residues appear) then return wafer to PGMEA for 30 s to 60 s before rinsing with isopropanol again. Let dry naturally.
10. Inspect features under a microscope and carefully develop further if needed. Avoid overdevelopment, which can lead to breaking of features.
11. Finally transfer to hotplate and carry out a 'hardbake' using the following program: 30 min ramp to 135 °C, 2 hrs at 135 °C, then 30 min ramp down to room temperature.

3.4.3 Soft lithography for device fabrication

- **Silanization of wafers**

1. Before first use, place wafers inside a sealed box with few drops (0.5 mL) of trimethylchlorosilane and incubate for at least 12 hours. Repeat the silanization before each use for 10 min.

- **Casting and curing of PDMS devices**

1. In two plastic cups, weigh out and add PDMS elastomer and curing agent in a ratio 5:1 (50 g : 10 g) for the flow layer, and 20:1 (20 g : 1 g) for the control layer.
2. Defoam the mixture using the ARE-250 centrifugal mixer, by mixing at 2000 rpm for 1 min followed by defoaming at 2200 rpm for 2 min.
3. Clean both flow and control wafers using pressurised N₂.
4. Put the flow layer wafer on aluminium foil inside a glass petri dish. Make sure the foil covers the dish and contains the PDMS fully. Pour all of the 5:1 PDMS mixture on top of the wafer, and place the dish inside a vacuum desiccator for 40 min to degas the mixture.
5. Put the control layer wafer in the SCS G3P-8 spin coater, and carefully pour a few ml of the 20:1 PDMS onto the centre of the wafer. To coat the wafer, run the following program: Step 0, rpm = 0, disp = 2, ramp = 0.0, dwell = 0; Step 1, rpm = 1420, disp = none, ramp = 20.0, dwell = 35; Step 2, rpm = 100, disp = none, ramp = 20.0, dwell = 1; Step 3, rpm = 100, disp = none, ramp = 1.0, dwell = 0.
6. After coating, the PDMS layer will be uneven due to the high 40- μ m features. Place the wafer on aluminium foil in a second petri dish, cover to protect from dust, and set aside on the bench for 40 minutes.
7. Then bake both flow and control wafers in an oven at 80 °C. The flow layer is baked for 20 minutes, and the control layer for 25 minutes. Timings for this step must be exact (*see Note 16*).
8. Remove the wafers from the oven. Using a sharp scalpel, cut out each design from the flow layer, and immediately place on top of the corresponding control layer region, roughly aligning the two layers.
9. Once all the devices have been roughly aligned in this way, transfer the control wafer to a stereo dissection microscope, and align the two layers by manually lifting off and carefully placing the top layer in its precise position (*see Note 17*).
10. Put the aligned devices back into the oven at 80 °C and bake for a minimum of 1 hour 30 minutes.
11. Cut the multilayer devices off the wafer using a scalpel.
12. Using the hole puncher, punch through all the channel inlets.

13. Protect the PDMS surfaces from dust using Scotch tape. The completed PDMS devices can now be stored in a clean petri dish until the next step.

- **Bonding of PDMS devices to a glass slide**

1. Clean glass slides using pressurised N₂.
2. Remove any residual dust from the slide and feature surface of the PDMS device using Scotch tape (*see Note 18*).
3. Switch on the Femto plasma oven and place the slide and PDMS device bonding-side-up.
4. Pump out the chamber for at least 15 minutes to ensure a clean vacuum environment.
5. Switch on the O₂ for 2 minutes at a flow rate of 25 sccm and 0.1 bar, then apply 30 s of plasma at 100 % power (which corresponds to a plasma of 40 kHz and 100 W (*see Note 19*)).
6. Immediately ventilate the plasma by-products before opening the chamber. Put the PDMS and glass together and manually apply even, moderate pressure for a few seconds (*see Note 20*). Then, put the bonded device into an oven at 80 °C for 1 hour to overnight.
7. The completed devices can finally be stored at room temperature until use (*see Note 21*).

3.4.4 Hardware setup

Air pressure is supplied to the setup using polyethylene (PE) tubing connected directly to the laboratory compressed air supply. A schematic of the setup's pneumatic connections is shown in Figure 3.2.

- **Regulation of control layer pressure**

1. Connect one branch of the input air supply to a regulator, and direct the regulated output supply to the aluminium electric manifold.
2. The electric manifold directs air pressure to the chip's control lines. Attach Tygon tubing (ID 0.02") to the manifold using appropriate adaptors as shown in Figure 3.2. The tubing contains a 23 ga luer stub on one end (used for filling and connecting to the manifold) and a stainless steel connector pin on the other (used for connecting to the chip).
3. Plug the electric manifold into the relay board, which links via USB to a PC running control software written in LabVIEW. An example of the code and full documentation can be found online (*see Note 22*).

- **Regulation of flow layer pressure**

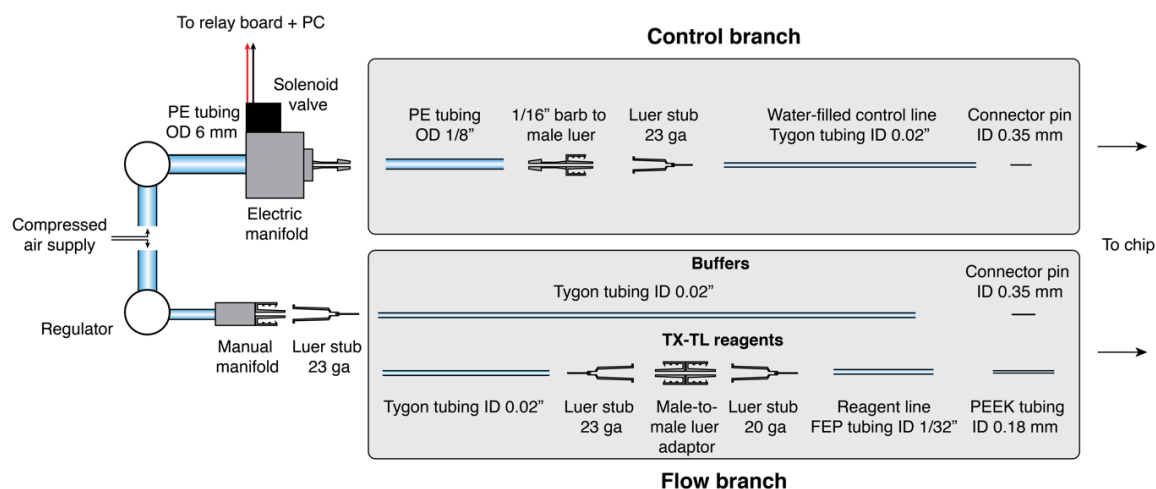


Figure 3.2: Pneumatic connections for the setup. The compressed air supply is split into two independently regulated branches. Pressure in the control branch is switched using electric valves while the flow branch is controlled manually. Buffers and other input solutions are stored in Tygon tubing, while cell-free (TX-TL) reagents are stored in FEP-PEEK tubing.

1. Connect the other branch of the input air supply to a regulator, and connect the regulated supply to the manual luer manifold.
2. Adjust the pressure as required (typically ~ 0.3 bar).

3.4.5 Device operation

• Filling control lines

1. Lower the control manifold pressure to around ~ 10 psi.
2. Using the PC software, close all the control line valves.
3. Fill each Tygon line with deionised water (*see Note 23*) through the connecting pin, using a syringe attached to a luer stub.
4. Connect each line to the appropriate control channel inlet.
5. Once all the lines are connected, open all valves. This pressurises the control channels, pushing air into the PDMS and allowing them to fill with water. Wait until the channels are completely filled with water, which can take up to 20 minutes. Slowly raise the pressure up to ~ 20 -30 psi.
6. Visually inspect all the valves to check that they actuate fully.

• Filling flow lines

1. Make sure the appropriate manual manifold valve is closed.

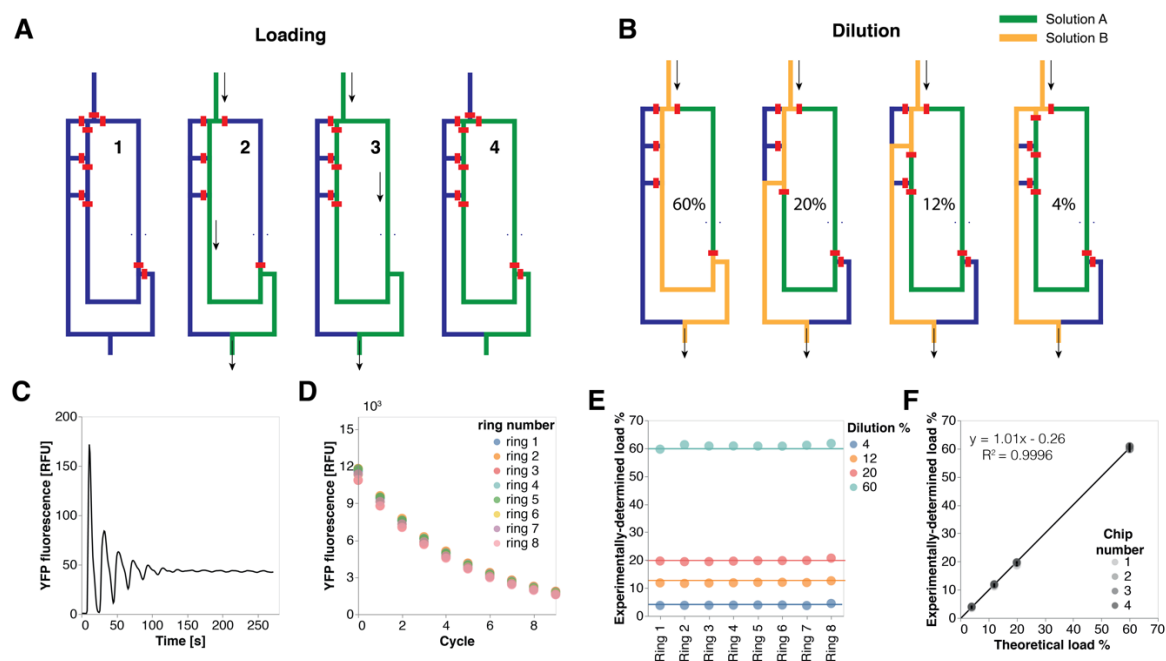


Figure 3.3: **Basic operations and characterisation of the chip:** (A) Initial loading is achieved by flowing an input solution (solution A, green) first through one side of the reactor, then the other. (B) Dilution takes place by flushing an input solution (solution B, yellow) through different outlets. The dilution fraction is controlled by the geometric positioning of the outlets and is fixed for a given design. (C) After loading 20% of a reactor with YFP, actuating the peristaltic pump at 20 Hz mixes the solution in ~ 100 s. (D) This shows the fluorescence from all eight reactor rings, initially loaded with 20% YFP, and repeatedly diluted with buffer. (E) Experimentally determined dilution fraction for each of the eight reactors. (F) Experimentally determined load fraction vs theoretical load fraction for four different chips.

2. Basic reagents such as buffers and chemicals are held in ID 0.02" Tygon tubing. First assemble the tubing which consists of a length of Tygon, a 23 ga luer stub on one end, and a connector pin on the other.
3. Attach a syringe to the luer stub, and carefully draw up the required reagent into the tubing. Make sure there are no bubbles.
4. Attach the connector pin to the appropriate flow inlet, before removing the syringe and attaching the luer stub to the manual manifold.
5. Make sure valves are in the appropriate configuration on the chip before opening the flow manifold valve, and allowing the reagent to fill into the device. Typically, a pressure of ~ 0.3 bar is ideal for the flow lines.
6. For the cell-free extract, follow the previous steps, but instead draw up the solution into the FEP coil through the PEEK tubing. Attach the PEEK tubing directly into the chip.
7. An important requirement for long-term steady-state reactions is that the cell-free

extract is separated from energy and DNA solutions. If required, cooling elements can be supplemented to further prevent degradation of the solutions [131, 134].

- **Cell-free expression**

1. The device can be characterised as shown in Figure 3.3.
2. A typical experimental program is shown in Figure 3.4. First switch on the environmental chamber to 29 °C.
3. Load each reactor with cell-free extract, energy solution, and DNA in the ratio 40% , 40% , 20% .
4. The reactor contents are mixed by actuating the four multi-function valves sequentially at a frequency of 20 Hz.
5. Dilution involves flowing cell-free extract, energy solution, and DNA into the reactors in the ratio 8% , 8% , 4% . This corresponds to a 20% dilution of the reactor which preserves the original reaction composition.
6. The dilution rate can be varied by adjusting the interval between dilution steps.
7. Image the resulting fluorescence using the microscope setup. Software for the analysis, example images, and full documentation can be found online (*see* **Note 24**).

3.4.6 Notes

1. A custom relay board is used to control the electric manifold actuation; any appropriate controller can be used in its place, for instance the 24-channel USB24PRMx (EasyDAQ).
2. Excellent guidance is available e.g. [156]
3. Designs for microfluidic devices are available online at http://lbnc.epfl.ch/microfluidic_designs.html.
4. The 20 mm lens provides the highest write speed, taking ~ 4 minutes to write a 100x100 mm mask with 2 μ m edge resolution, and 1 mm stripe width. Higher resolutions are possible but not necessary for soft lithography.
5. This is the step most often done incorrectly. The flow layer uses positive-resist AZ, and requires a DARK-mode mask. The control layer uses negative-resist SU8 and requires a CLEAR-mode mask. Finally as the exposure is chrome-side-down, the masks must be MIRRORED AT Y.
6. HMDS priming enhances photoresist adhesion. Alternatively the wafer can also be treated with O₂ plasma or thermally dehydrated.
7. Pouring directly from the bottle introduces fewer bubbles than using a plastic pipettor.

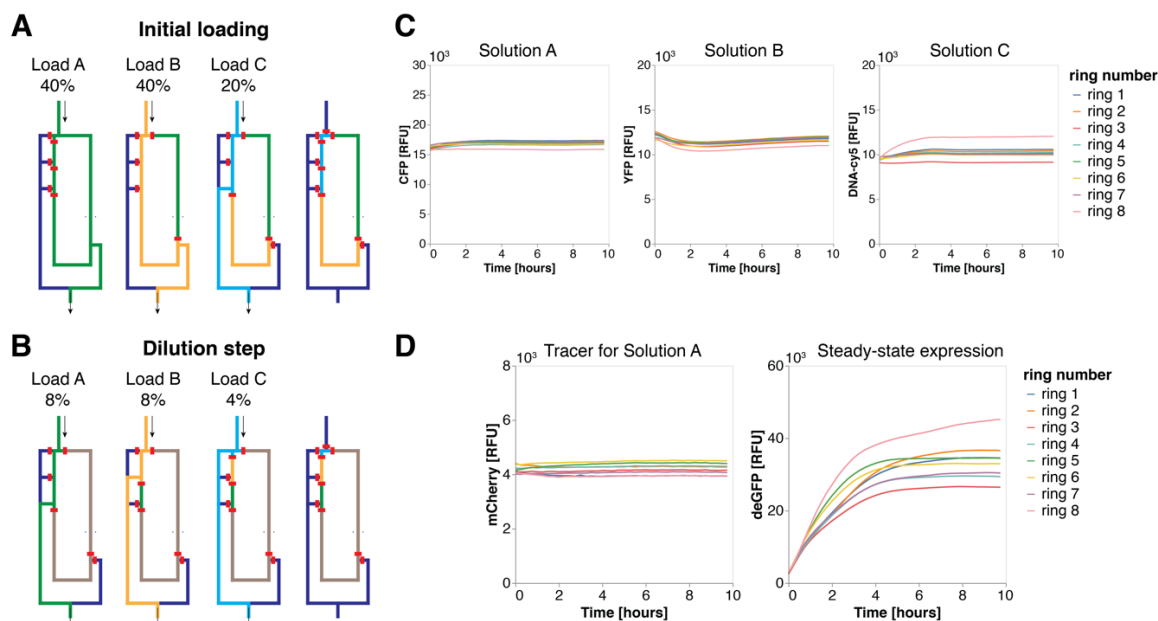


Figure 3.4: Typical experimental operation of the chip: Typical experimental operation of the chip. **(A)** The chip is initially loaded with three solutions A-C (green, yellow, blue) in the ratio 40%, 40%, 20%, and **(B)** subsequently diluted with the same solutions in the ratio 8%, 8%, 4%. **(C)** Carrying out this process using aqueous solutions of three different fluorescent tracers demonstrates that steady-state concentrations are maintained over many hours. **(D)** Steady-state cell-free expression can be achieved by adding as the three solutions cell-free lysate (solution A), energy solution (solution B), and DNA template (solution C). The lysate is labelled with an mCherry tracer to assess its concentration (left), while the reaction produces deGFP, which reaches a steady-state concentration when production and dilution rates are equal (right). Here, a dilution step was carried out every 15 minutes.

8. Opening the cap to the AZ9260 bottle to allow the release of air bubbles a few minutes before use can also help minimise bubbles.
9. Homogenous rehydration is important for efficient exposure, and the minimum rehydration time is a function of the photoresist thickness ($5\ \mu\text{m}$, 8 min; $20\ \mu\text{m}$, 2 hrs).
10. The mercury lamp contains spectral lines at 365, 405, and 436 nm. On the MJB4 machine the i-line filter is installed which passes only the 365 nm line. Without the filter, the exposure is broadband. The exposure mode must be taken into account during exposure time calculations.
11. For $15\ \mu\text{m}$ AZ9260, the recommended dose is $580\ \text{mJ}/\text{cm}^2$ for i-line exposure and $660\ \text{mJ}/\text{cm}^2$ for broadband.
12. The recommended development time is around 45 s per μm of AZ9260.

13. Rounded features are crucial for the flow layer as it allows valves to close completely.
14. The variable here is the ramp time, which depends on the specific type of SU8 used
15. It is highly recommended to develop the wafer upside down. Prepare two baths of PGMEA.
16. The precise timing here is important. The PDMS should set sufficiently so that it is not too sticky, but not so much that the resulting multilayer device does not bond together.
17. This step requires the most practice. Alignment should be completed as quickly and precisely as possible to ensure optimal bonding. Air bubbles are typically caused by buckling of the PDMS layers, and can be removed by first ensuring the top layer is completely flat, and then with gentle application of pressure. Putting weights on top of the PDMS during subsequent baking can also help.
18. This step is important as the presence of dust between the glass and PDMS can compromise bonding or render the device non-functional.
19. Plasma treatment converts methylsiloxane to siloxyl groups on the PDMS surface, enabling its covalent cross-linking to silica-containing glass. There is however an optimum amount of treatment, as over-treating increases the surface roughness of the PDMS and decreases the effective contact area [22].
20. The binding can be checked by putting the chip against a black piece of paper. Regions which are not bound will show up as bubble-like features.
21. In our experience, devices can still be functional after 6 months' storage.
22. <https://github.com/nadanai263/lbnc-cellfree2>
23. Ideally all Tygon control lines should have the same length and the same amount of water. The larger the volume of water in the line, the faster the pressure transfer and valve actuation, due to the incompressibility of water; in practice care must be taken so the water does not get into the electric manifold, so do not fill the lines fully. Finally, make certain that there are no air bubbles where the line connects to the chip.
24. <https://github.com/nadanai263/lbnc-cellfreeview>

4 A partially self-regenerating synthetic cell

This work has been published in Nature communications, 2020.

Authors: Barbora Lavickova and Sebastian J. Maerkl

Contribution: B.L. performed experiments designed experiments, analyzed data, and wrote the manuscript.

Reference: Lavickova, Barbora, Nadanai Laohakunakorn, and Sebastian J. Maerkl. "A partially self-regenerating synthetic cell." Nature communications 11.1 (2020): 1-11.

Permission to reproduce the article is granted by Springer Nature.

4.1 Abstract

Self-regeneration is a fundamental function of all living systems. Here we demonstrate partial molecular self-regeneration in a synthetic cell. By implementing a minimal transcription-translation system within microfluidic reactors, the system is able to regenerate essential protein components from DNA templates and sustain synthesis activity for over a day. By quantitating genotype-phenotype relationships combined with computational modeling we find that minimizing resource competition and optimizing resource allocation are both critically important for achieving robust system function. With this understanding, we achieve simultaneous regeneration of multiple proteins by determining the required DNA ratios necessary for sustained self-regeneration. This work introduces a conceptual and experimental framework for the development of a self-replicating synthetic cell.

4.2 Introduction

Bottom-up construction of a self-replicating synthetic cell that exhibits all the hallmarks of a natural living system is an outstanding challenge in synthetic biology [1, 14, 24]. While this goal is ambitious, progress is rapidly accelerating, and key structures and functions required for constructing a synthetic cell, including compartmentalization [10, 11, 157], mobility and shape [25, 158, 159], metabolism [160, 161], communication [12, 162], and DNA replication [51, 137, 163], have recently been demonstrated, suggesting that integration of these subsystems into a functional synthetic cell may be an attainable goal.

A biochemical system able to fully self-regenerate or self-replicate, is a crucial requirement for construction of a synthetic cell. A self-replicating artificial system has been first proposed by von Neumann in the 1940s [42]. Von Neumann developed the concept of a universal constructor, which is an abstract machine capable of self-replication using a set of instructions, external building blocks, and energy. So far, universal constructors have only been implemented *in silico* in the form of cellular automata [43]. Similar concepts have been explored experimentally with auto-catalytic chemical systems [164] and self-replicating ribozymes [165]. A self-replicating biochemical system is strictly analogous to the universal constructor in that it would be capable of self-replication using instructions encoded in DNA while being supplied with building blocks and energy (Figure 4.1A). A physical implementation of a universal constructor could therefore be theoretically achieved by a minimal recombinant transcription-translation system capable of regenerating all of its components including proteins, ribosomes, tRNAs, and DNA [81]. DNA replication has recently been demonstrated *in vitro* [51, 137, 163] and progress is being made in reconstituting ribosomes [62–64] and tRNAs [69]. Here we demonstrate the principle steps towards constructing a universal biochemical constructor by creating a system capable of sustained self-regeneration of proteins essential for transcription and translation.

Development of a transcription-translation system capable of self-regeneration faces several challenges. First, synthesis capacity of the system in terms of its protein synthesis rate must be

sufficient to regenerate the necessary components. This problem is exacerbated by the fact that protein synthesis capacity drastically decreases in a non-optimal system [93, 94, 141]. Second, the components being regenerated must be functionally synthesized which may require chaperones, and modifying enzymes. And third, the reaction must take place in an environment that allows continuous and sustained regeneration.

The PURE (protein synthesis using recombinant elements) system [88] as a viable starting point for achieving self-regeneration because of its minimal nature as well as its defined and adjustable composition [23]. Batch expression experiments combined with polyacrylamide gel electrophoresis (PAGE) and mass-spectrometric (MS) analysis indicated that the PURE system should be able to synthesize around 70% of all *E. coli* proteins [55]. Moreover, it was recently shown that co-expression of multiple PURE components in a single batch reaction yielded the required concentrations for self-replication [51]. However, these experiments didn't determine whether proteins were functionally synthesized, which varies largely for proteins expressed in the PURE system [56, 58]. Other studies showed that the 30S ribosomal subunit [63, 64], and nineteen of twenty aaRSs, can be functionally synthesized in the PURE system [59]. All of those experiments were performed in batch or continuous-exchange formats and self-regeneration of any component has yet to be demonstrated.

Here, we employ continuous transcription-translation reactions operating inside microfluidic reactors [134] to demonstrate self-regeneration of essential protein components. Our approach using the PURE system, microfluidic chemostats, and monitoring fluorescent protein production, allows activity and performance of self-regeneration to be assessed in real-time. We implemented a 'kick-start' method to 'boot-up' regeneration of essential PURE proteins from DNA templates. We demonstrate the concept and feasibility of this approach by regenerating different aminoacyl-tRNA synthetases (aaRSs). We also regenerated T7 RNA polymerase (RNAP) and mapped system optimality by varying T7 RNAP DNA concentration and were able to explain the observed genotype-phenotype relationships with a biophysical resource limitation model. We go on to show that several proteins can be regenerated simultaneously by regenerating up to seven aaRSs. This proof-of-principle work demonstrates the first steps towards constructing a self-replicating transcription-translation system and provides a viable approach for developing and optimizing other critical sub-systems including DNA replication, ribosome synthesis, and tRNA synthesis, with the goal of achieving a self-replicating biochemical constructor in the near term and ultimately a viable synthetic cell.

4.3 Results

4.3.1 Experimental design

To maintain continuous cell-free reactions we improved a microfluidic chemostat previously used for implementing and forward engineering genetic networks *in vitro* [134, 153]. The device consists of 8 independent, 15 nL reactors, with fluidically hard-coded dilution fractions defined by reactor geometry, as opposed to the original device which used peristaltic pumps for metering (Figure 4.1B, Supplementary Figure 4.5, Supplementary Movie 1) [166]. During experiments 20% of the reactor volume was replaced every 15 min with a ratio of 2:2:1 for energy, protein/ribosome, and DNA solution, respectively, resulting in an effective dilution time of ~ 47 min (Figure 4.1A, Supplementary Table 4.1, 4.2). Another key improvement was the supply of multiple solutions without the need for cooling. This was achieved by storing the energy and protein components separately, which when stored pre-mixed and without cooling resulted in non-productive resource consumption [83]. Secondly, reaction temperature was set to 34°C, which decreased PURE degradation with only a minor decrease in protein synthesis rate (Supplementary Figure 4.6). Lastly, as the redox reagent used in the PURE system is known to degrade rapidly, we eliminated 1,4-dithiothreitol (DTT) in the energy solution and instead added tris(2 carboxyethyl)phosphine (TCEP) to the energy and protein solutions. To allow PURE system modification and omission of protein components we produced our own PURE system based on the original formulation [89, 93]. For each protein regenerated, we produced a Δ PURE system lacking that particular protein or proteins. This allowed us to validate that the omitted protein is essential for system function. We furthermore adjusted PURE protein composition by reducing the concentration of several aaRSs (Supplementary Table 4.3, 4.4).

In all experiments we expressed a fluorescent protein (eGFP) as an indicator of functional self-regeneration and to provide a quantitative readout of protein synthesis capacity. We developed a 'kick-start' method to enable the system to self-regenerate proteins from DNA templates (Figure 4.1C). The experimental design involves three distinct phases: kick-start, self-regeneration, and wash-out. The kick-start phase is required to allow a productive switch from a complete to a Δ PURE system to occur. The self-regeneration phase tests whether the system functionally regenerated the omitted protein component or components, and the washout phase serves as a control to prove that the omitted component or components were indeed essential for system function. In the kick-start phase, which lasts for the first 4h, linear DNA templates coding for eGFP and the protein to be regenerated are added to a complete PURE system. This leads to the expression of eGFP and the protein to be regenerated. In the self-regeneration phase, the full PURE is gradually replaced with a Δ PURE solution lacking the particular protein that is to be regenerated. Thus at steady state, the system will remain functional only through self-regeneration of the omitted protein. Finally, in the wash-out phase, DNA encoding the protein being regenerated is no longer added to the system leading to dilution of the protein being regenerated. Once a critical concentration for the regenerated protein is reached overall protein synthesis falls and ultimately ceases.

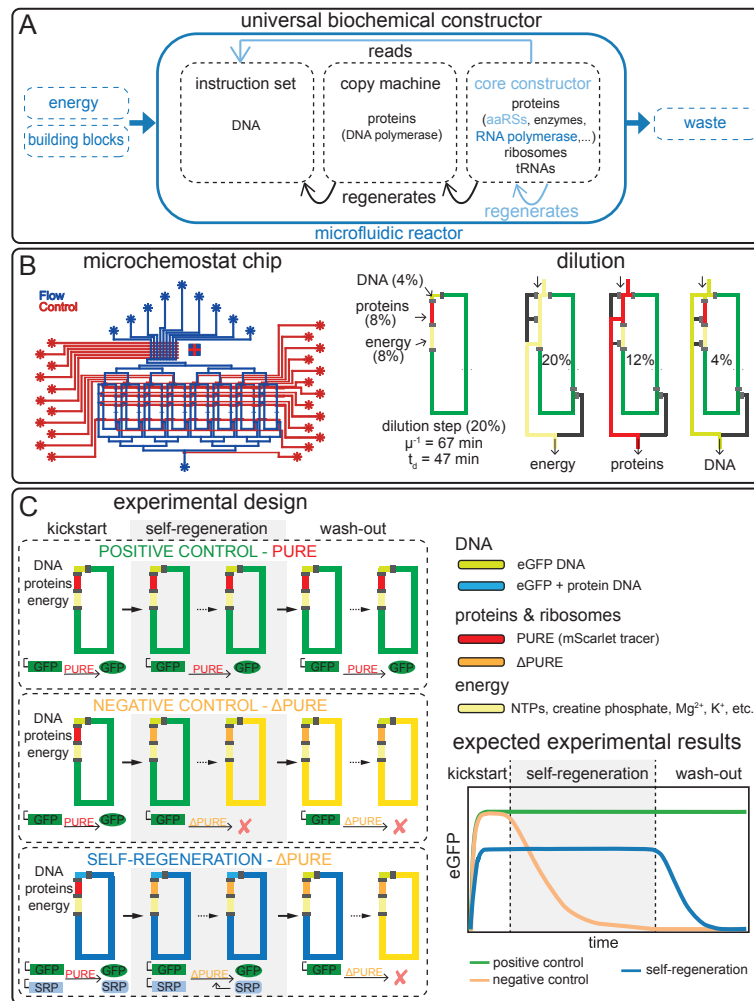


Figure 4.1: Experimental design for a self-regenerating synthetic cell: (A) Diagram of the universal biochemical constructor concept. Systems, components, and functions colored in blue and light-blue were fully or partially implemented in this work, respectively. (B) Design schematic of the microfluidic device with eight individual chemostat reactors. Flow layer is shown in blue and control layer in red. Design and functional details are provided in Supplementary Fig. 4.5. A schematic representation of one dilution cycle where 20% reaction volume is replaced every 15 min. Dilution rate $\mu = -\ln(C_t/C_0) \cdot t^{-1}$, residence time μ^{-1} and dilution time $t_d = \ln(2) \cdot \mu^{-1}$. One dilution cycle consists of three steps: energy solution (yellow) is loaded via the 20% segment, protein and ribosome solution (red) is flushed through the 12% segment, and DNA solution (green) through the 4% segment, resulting in the desired composition of 8%, 8%, and 4 %, respectively. (C) Experimental design, including the three experiment phases: kickstart, self-regeneration, and wash-out. Solutions are loaded in the rings at different time points: energy solution (yellow), full PURE (red), Δ PURE (orange), eGFP DNA (green), and eGFP + protein DNA (blue). A schematic showing the expected results for the different experimental phases indicating early cessation of synthesis activity for the negative control (yellow), continuous synthesis activity in the positive control (green), and continuous synthesis for self-regeneration (blue) during the self-regeneration phase followed by cessation of synthesis activity during the wash-out phase.

We implemented two additional control reactions in most experiments. Positive controls use full PURE and express only eGFP during all three phases and serve as a validation of steady-state chemostat function and a reference point for maximal protein synthesis capacity of an unloaded and optimal PURE reaction. Negative controls switch between complete and Δ PURE, but don't contain DNA template for the omitted protein component. This confirms that without self-regeneration, protein synthesis activity is indeed rapidly lost. We spiked the full PURE protein fraction with an mScarlet tracer to confirm that all fluid exchanges take place and the device functioned correctly.

4.3.2 Aminoacyl-tRNA synthetase regeneration

As a proof-of-concept and validation of the experimental design, we tested regeneration of two aaRSs: Asparaginyl-tRNA synthetase (AsnRS) and Leucyl-tRNA synthetase (LeuRS) (Figure 4.2A). We first carried out batch experiments to ascertain synthesis of the synthetases in our PURE system (Supplementary Figure 4.7). We also validated that both synthetases are essential by omitting them individually from a PURE reaction (Figure 4.2B). When we used the original PURE system's aaRS concentrations, decreases in protein synthesis activity were observed only after extended washout periods because the critical aaRS concentrations were reached only after numerous dilution cycles (data not shown). We therefore reduced the concentrations of the aaRSs being regenerated so that fast activity declines during wash-out occurred, while preserving high protein synthesis rates (Supplementary Figure 4.8, Table 4.3).

We achieved successful self-regeneration for both AsnRS and LeuRS and complete loss of protein synthesis activity during wash-out (Figure 4.2C, D). We tested four DNA concentrations for each aaRSs. AsnRS and LeuRS regeneration at DNA concentrations of 0.1 nM and 0.05 nM, respectively, resulted in high system activity comparable to the positive control throughout the self-regeneration phase. If an insufficient DNA template concentration of 0.05 nM was provided for AsnRS, a decrease in eGFP fluorescence was observed identical to the negative control but with a slight delay. A two-fold difference in DNA template concentration thus resulted in either optimal self-regeneration or complete system failure. For LeuRS a similar two-fold change was less consequential with either concentration resulting in self-regeneration, but with slightly lower expression obtained for the higher concentration of 0.1 nM. Higher DNA concentrations resulted in robust but markedly lower system activity for both aaRSs. These studies showed that our experimental design enables self-regeneration and that self-regeneration can be achieved with two different aaRSs.

DNA input concentration is critically important for system function. When higher than optimal DNA concentrations were used, we observed successful and robust self-regeneration, as indicated by the maintenance of synthesis activity above negative control levels, but considerably lower eGFP expression levels as compared to the positive control. Because no negative effects were observed in batch reactions for high aaRS protein concentrations in the PURE system (Supplementary Figure 4.8) [96], we attribute this effect to a resource competition or loading effect between the protein being regenerated and eGFP [71]. The onset of this loading effect can be estimated by

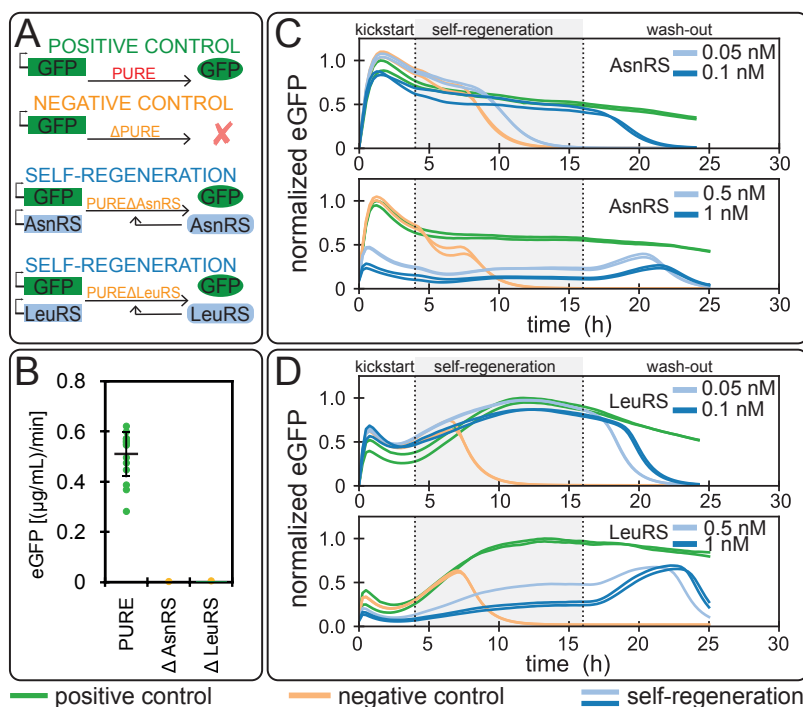


Figure 4.2: **Aminoacyl-tRNA synthetase regeneration:** (A) overview of the different aaRSs regeneration experiments. (B) eGFP batch synthesis rates for the full PURE system and AsnRS or LeuRS Δ PURE systems (mean \pm s.d. for PURE system (green, $n=16$ technical replicates), and mean for Δ PURE systems (yellow, $n=2$ technical replicates)). Self-regeneration experiments for (C) AsnRS (D) LeuRS at different DNA concentrations (positive control: green, negative control: yellow, self-regeneration: blue). Results for all DNA concentrations tested and corresponding mScarlet traces can be found in Supplementary Figure 4.10. The level of eGFP is normalised to the maximum level attained in the positive control. The composition of PURE systems used are given in Supplementary Table 4.3, 2 nM of eGFP template was used for all experiments, aaRS DNA template concentrations are indicated.

measuring the DNA concentration for which system output saturates, which is ~ 1 nM for the PURE system (Supplementary Figure 4.9). eGFP DNA template is present at a concentration of 2 nM in all experiments and is thus fully loading the system. Any additional DNA added to the system will thus give rise to resource competition effects.

A simple resource competition model gives rise to a couple of specific predictions. First, the level of eGFP synthesized during self-regeneration should never rise above the positive control, assuming that the concentration of the self-regenerated protein is at an optimal level in the positive control. This is because synthesis of an additional protein leads to resource competition and lower eGFP levels. Low concentrations of aaRS DNA has a minimal loading effect since the ratio of aaRS to eGFP DNA is small. As the concentration of aaRS DNA is increased the loading effect becomes stronger, leading to a noticeable decrease in eGFP levels. The second prediction is that eGFP levels can exhibit a transient peak during washout phase. This occurs because loading decreases before

the regenerated protein is diluted below critical levels. This is evident in our experiments with high load levels (high aaRS input DNA concentrations), where a transient spike in eGFP expression occurred during wash-out before a decrease was observed (Figure 4.2C-D, Supplementary Figure 4.10).

To approximate the optimal DNA input concentrations for self-regeneration, we estimated aaRS protein synthesis rates for different DNA concentrations by using the ratio of aaRS to eGFP DNA, while assuming the same synthesis rate for all proteins, and comparing them to the estimated synthesis rate required to reach the minimum concentration needed for each aaRS (Supplementary Figure 4.11A, Supplementary Table 4.4). In agreement with the observed data, we estimated 0.1 and 0.05 nM of DNA for AsnRS and LeuRS, respectively. Moreover, we confirmed these estimates based on the drop in eGFP synthesis rate for different DNA input concentrations (Supplementary Figure 4.11B).

4.3.3 T7 RNAP regeneration

After testing two proteins essential for translation, we tested self-regeneration of an essential protein for transcription (Figure 4.3A). For transcription the PURE system utilises T7 RNA polymerase (RNAP), a single 99 kDa protein. As before, we carried out batch experiments to validate T7 RNAP synthesis in the PURE system (Supplementary Figure 4.7), and essentiality of T7 RNAP (Figure 4.3B). T7 RNAP could be successfully regenerated in the system and we carried out extensive DNA template titrations with concentrations varying over three orders of magnitude (Figure 4.3C, Supplementary Figure 4.12). By omitting the wash-out phase and extending the self-regeneration phase to 26 hours, we showed that T7 RNAP can be regenerated at steady-state for over 25 hours with a DNA input concentration of 0.5 nM (Figure 4.3D).

To summarize the DNA titration results, we plotted eGFP expression levels as a function of T7 RNAP DNA template concentration at 11 hours of regeneration (corresponding to 15 hours after the start of the experiment), normalised to the positive control expression levels (Figure 4.3E). For lower DNA concentrations (<0.05 nM) we observe little or no eGFP expression, which we attribute to insufficient synthesis of T7 RNAP, similar to the results obtained for aaRSs. For high T7 RNAP DNA template concentrations (≥ 1 nM) resource competition similar to what was observed for AsnRS and LeuRS was taking place. This is also supported by the observed peak during the wash-out phase for high input DNA template concentrations. Near optimal system performance within 80% of the control reaction occurred in a narrow DNA template concentration range of 0.65 nM to 0.125 nM. The curve is asymmetric, with higher sensitivity to low concentrations than to higher concentrations, providing insights into how system robustness can be engineered. Surprisingly, and unlike the aaRS experiments, we observed an expression maximum that rises to a level of 1.3 above the positive control reactions, indicating that a simple resource competition model cannot account for the observed behaviour.

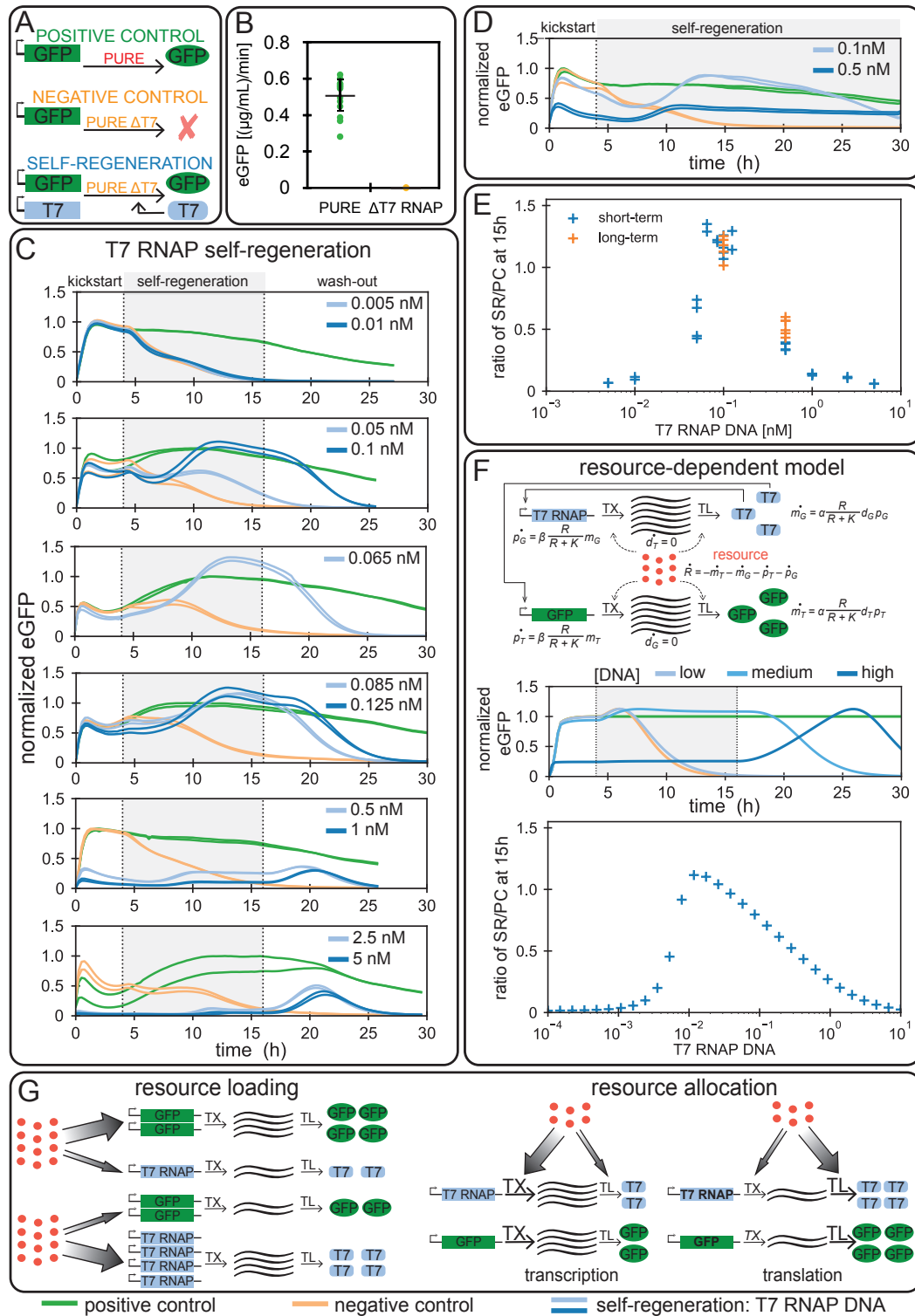


Figure 4.3: Caption on next page

Figure 4.3: **T7 RNAP regeneration:** (A) Overview of the T7 RNAP regeneration experiment. (B) eGFP batch synthesis rates for the full PURE and T7 RNAP Δ PURE systems (mean \pm s.d. for PURE system (green, $n=16$ technical replicates), and mean for Δ PURE systems (yellow, $n=2$ technical replicates)). (C) T7 RNAP regeneration at different DNA template concentrations. (D) Long-term regeneration experiment: the self-regeneration phase was extended by omitting the wash-out phase. The results for all DNA concentrations tested and the appropriate mScarlet traces can be found in Supplementary Fig. 4.12. The level of eGFP is normalised to the maximum level attained in the positive control experiments (positive control: green, negative control: yellow, self-regeneration: blue). The composition of the PURE system used for the self-regeneration experiments is given in Supplementary Table 4.3, 2 nM of eGFP template was used for all experiments, T7 RNAP DNA template concentrations are indicated. (E) Ratio of eGFP levels of the self-regeneration experiments and the positive control at 15 hours as a function of T7 RNAP DNA template concentration. Each data point represents a single measurement. (F) Our resource-dependent model consists of seven ODEs and three parameters. DNA, mRNA, and protein concentrations are denoted by d , m , and p , and the subscripts T and G refer to T7 RNAP and eGFP, respectively. Simulation of a self-regeneration experiment: the switch between stages occurs at 4 and 16 hours. DNA for T7 RNAP was present at three qualitatively different concentrations, indicated as ‘low’, ‘medium’, and ‘high’. All concentrations are non-dimensional. The level of GFP is normalised by the maximum level attained in the positive control experiment. The negative control corresponds to $d_T = 0$. (G) Schematic description of the concepts of resource loading and resource allocation. Resource loading is the distribution of a limited resource between two genes. Resource allocation is the distribution of a limited resource (red) between transcription (TX) and translation (TL). A detailed description of the different concepts can be found in Supplementary Fig. 4.23.

To investigate whether our hypothesis of resource competition could be extended to explain the T7 RNAP observations, we created a minimal model of the transcription-translation system. While transcription-translation systems can be described at varying levels of granularity e.g. [54, 100, 167, 168], we chose to model the processes at the most coarse-grained level using coupled ordinary differential equations (ODEs) (Figure 4.3F, Supplementary Figure 4.13-4.22, Supplementary Table 4.5).

The model consists of transcription and translation of eGFP and T7 RNAP, which consumes a single resource species R . This species is a lumped representation of CTP, UTP, ATP, GTP, and aminoacyl-tRNAs, which are consumed during transcription and/or translation. We model the transcription rate by a parameter α , linearly dependent on DNA and T7 RNAP concentration, and modulated by the availability of resources using a Hill function $R/(R + K)$. Likewise, translation proceeds at a rate β , is linearly dependent on mRNA concentration, and is modulated by the same Hill function. The rate of consumption of R is equal to the summed transcription and translation rates. The complete model consists of seven ODEs and three parameters, and is solved between discrete dilution steps to simulate chemostat operation.

This minimal model successfully captures the observed qualitative behaviour including: 1) eGFP washout at low T7 RNAP DNA concentrations (d_T) in the self-regeneration phase, 2) low eGFP production followed by a peak in the washout stage at high d_T , and importantly 3) eGFP production in excess of the positive control at medium d_T in the self-regeneration phase (Figure 4.3F). At low

d_T , mRNA concentration is low, while resources are abundant; translation rate is thus limited by mRNA concentration. High d_T leads to increased resource consumption, so despite the presence of large amounts of mRNA, translation is limited by resources. Further analysis reveals that at intermediate d_T concentrations, eGFP production can increase above the positive control during the self-regeneration phase. The model predicts that this is due to a reallocation of resources from transcription to translation, once self-regeneration of T7 RNAP begins. This effect requires a resource-limited condition (Figure 4.3G, Supplementary Figure 4.23).

We developed an alternative resource-independent model which only takes into account translational loading through a shared translational enzyme, which can also capture the observed optimum in the SR/PC ratio (Supplementary Figure 4.20). In this case, the optimum is due to a trade-off between mRNA concentration and enzyme availability. However it fails to predict the increase in eGFP production above the positive control during self-regeneration.

The modeling studies indicate that the requirement for an optimum in the SR/PC ratio is a coupling between eGFP and T7 RNAP expression, whether through a shared resource or a shared enzyme. However, the increase of eGFP above the positive control during the self-regeneration phase requires a resource-limited condition, and resource reallocation from transcription to translation (Figure 4.3G, Supplementary Figure 4.23). While both models can be combined, or extended to incorporate more realistic effects, such as saturation of transcription rates with substrate concentration, time delays in the various processes, and more intricate mechanisms of resource usage, none of these are required to explain our observations, apart from the essential feature of gene expression coupled through a shared resource.

4.3.4 Regeneration of multiple components

Having demonstrated that proteins essential for translation or transcription could be regenerated individually, we explored whether multiple proteins could be regenerated simultaneously. We first tested if T7 RNAP, AsnRS, and LeuRS could be regenerated together. Initial DNA concentrations tested were $1\times$ and $2\times$ the minimal DNA concentrations which led to successful self-regeneration of individual proteins, but these concentrations were not sufficient for sustained self-regeneration of multiple proteins (Supplementary Figure 4.24). Increasing DNA concentrations and maintaining 1:1 DNA template concentration ratios ultimately led to successful regeneration lasting 20-25 hours (Figure 4.4A, Supplementary Figure 4.24). Despite successfully regenerating for many hours, protein synthesis ultimately ceased under these conditions. Based on the T7 RNAP results and our computational modeling we hypothesized that a more optimal DNA ratio between T7 RNAP and the aaRSs needed to be established, as we previously observed strong resource loading effects by T7 RNAP and an apparent insensitivity of optimal T7 RNAP DNA concentration in respect to overall loading. Consequently, we decided to retain a relatively high DNA concentration of 0.5 nM for both aaRSs, and titrated T7 RNAP DNA template (Figure 4.4A). This had the desired effect and resulted in sustained regeneration at a T7 RNAP DNA concentration of 0.2 nM.

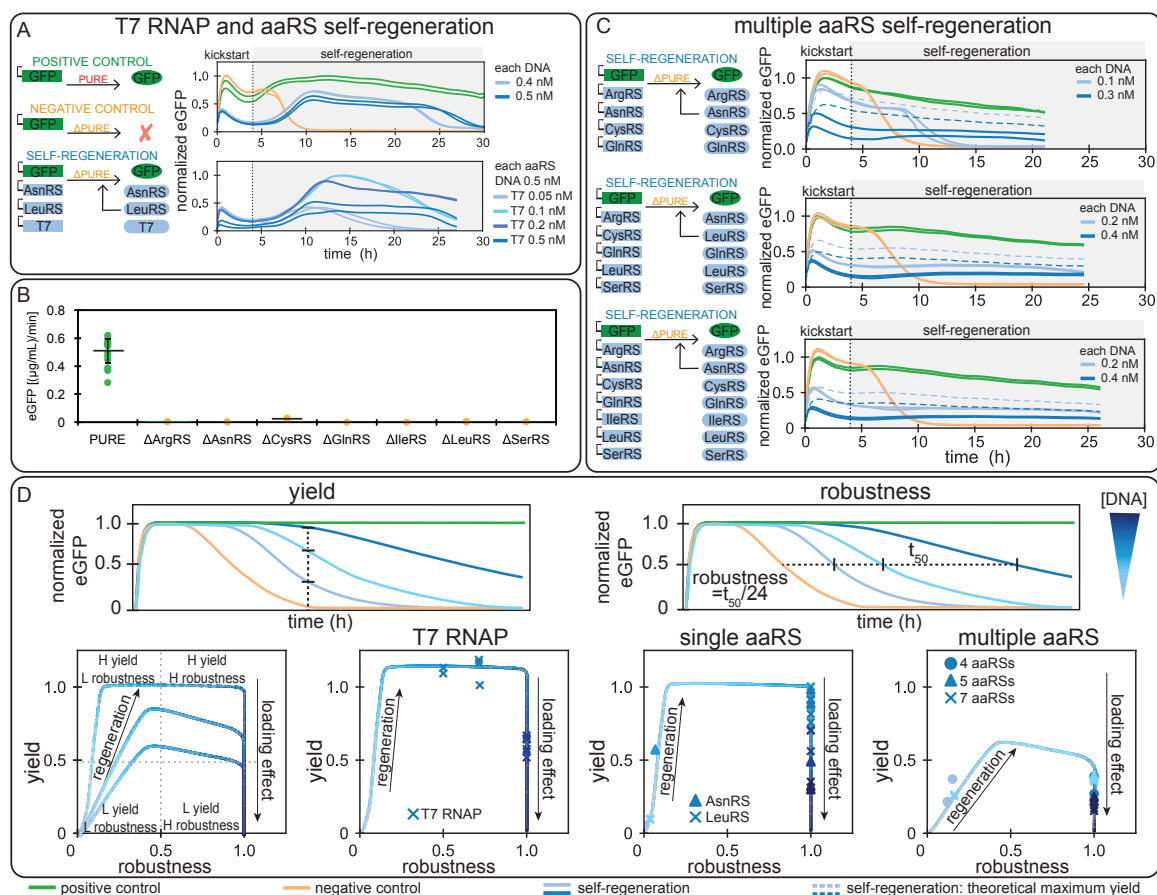


Figure 4.4: Multi-component regeneration: (A) Combined T7 RNAP, AsnRS, and LeuRS regeneration. Overview of the experiments on the left, with experimental results shown on the right. The top graph shows results for all DNA templates at concentrations of 0.4 or 0.5 nM. The bottom graph shows results for a titration of T7 RNAP DNA template with both aaRS DNA templates held constant at 0.5 nM. (B) eGFP batch synthesis rates for the PURE system and ΔPURE systems lacking additional aaRSs (mean ± s.d. for PURE system (green, n=16 technical replicates), and mean for ΔPURE systems (yellow, n=2 technical replicates)). (C) Simultaneously regeneration of 4, 5, and 7 aaRSs. Overview of self-regeneration experiments on the left, with experimental results shown on the right. Results for all DNA concentrations tested and the corresponding mScarlet traces can be found in Supplementary Figure 4.24. All eGFP traces were normalised to the maximum eGFP fluorescence output in the positive control, with exception of the T7 RNAP titration in panel (A) for which eGFP traces were normalised to the maximum eGFP fluorescence (positive control: green, negative control: yellow, self-regeneration: blue). PURE system compositions are given in Supplementary Table 4.3. 2 nM of eGFP DNA template was used in all experiments, other DNA template concentrations are indicated. (D) Schematic description of the definition of yield and robustness. Using these two terms we plotted theoretical curves for the relationship between DNA input concentration, yield, and robustness and superposed experimental values obtained from T7 RNAP, single aaRS, and multiple aaRS self-regeneration experiments. All three systems follow a similar trajectory and can be described in terms of Pareto optimality.

To explore the limits of the PURE transcription-translation system for self-regeneration, we tested whether several aaRSs could be regenerated simultaneously. We first carried out batch experiments to ensure efficient expression of the chosen aaRSs (Supplementary Figure 4.7), as well as lack of expression if a given aaRS was omitted from the PURE system (Figure 4.4B). As for the single aaRS experiments, we adjusted the concentrations of the various aaRS proteins (Supplementary Table 4.3) in the PURE system to ensure efficient wash-out. We gradually increased the number of aaRSs being regenerated from four to seven (Figure 4.4C, Supplementary Figure 4.25).

Based on eGFP synthesis rate and DNA ratios for the different conditions, we estimated that DNA inputs above 0.2 nM would be required for successful regeneration (Supplementary Figure 4.26A). This was in agreement with the observed data and decreases in eGFP synthesis rate due to loading (Supplementary Figure 4.26B). We observed successful self-regeneration of up to 22h for experiments with input DNA concentrations of 0.2 nM or above. DNA concentrations of 0.1 nM on the other hand led to rapid cessation of protein synthesis activity 10 hours into the experiment. Furthermore, when DNA input concentrations of 0.2 nM were used we saw variations in the length of self-regeneration amongst experiments (Supplementary Figure 4.25). The estimated synthesis levels are much higher than the concentrations of most aaRS diluted out of the reactor each cycle, with exception of ArgRS, where 0.027 ($\mu\text{g/mL}$)/min is diluted out, suggesting that optimization of DNA input for individual aaRSs could allow for better resource allocation and higher robustness.

eGFP levels are low when compared to the positive control. The positive control represents the maximum achievable eGFP steady-state levels in an otherwise unloaded system. Expression of 4-7 additional aaRS presents a considerable load on the system. When taking this load into account, self-regeneration of 4-7 aaRSs in addition to expressing eGFP reaches roughly 50% of the theoretically achievable yield (Figure 4.4C), indicating that the total synthesis capacity of the system remained quite high.

These experimental results suggest that achieving successful self-regeneration depends on an interplay of several factors. To more quantitatively describe the system we defined the terms yield and robustness (Figure 4.4D). We define yield as the level of non-essential protein such as eGFP that the system can synthesize during self-regeneration. In the case where an essential protein, for instance an aaRS, is missing, yield is zero. Expressing the aaRS will increase the yield, up to a point where the system's resources are preferentially directed towards aaRS production. At that point system yield begins to decrease again due to loading. A second important parameter is system robustness. We consider a robust system to be able to sustain self-regeneration for at least 24 hours. A non-robust system may temporarily reach steady-state self-regeneration, but changes in synthesis rates, DNA concentrations, or environmental conditions, can cause it to cease functioning. We therefore define robustness as the time the system self-regenerates beyond the negative control, normalized by 24 hours. A system that self-regenerates for 24 hours or longer receives a robustness score of 1 while systems that cease regeneration before 24 hours receive a score between 0 and 1.

Given these two parameters: yield and robustness, one can now describe the system in terms of

Pareto optimality and determine whether there exists a trade-off between yield and robustness. In Figure 4.4D we show the calculated values of yield against robustness for our experimental observations, as well as the theoretically expected relationship of yield, robustness, and DNA concentration. For an essential protein, increasing its expression constrains the yield of the system onto a Pareto front [169]. This is because low expression of that protein leads to large increases in yield as the protein begins to confer its advantage on the system. Above a critical concentration, the system is able to continuously regenerate, corresponding to a robustness of 1. Expressing the protein at higher levels than the critical value incurs a cost on the system, which is exhibited by decreasing yield due to loading.

For single protein self-regeneration it is indeed possible to reach maximal yield and robustness. However, whether that situation can be attained or not depends on the activity of the essential protein. Proteins with low activity require higher concentrations, and hence more resources, to produce. This thus limits the attainable yield of the system, and shifts the yield-robustness curve downwards. In severe cases (which we do not observe), yield may never reach 1. Regeneration of multiple proteins falls into this category: when several essential proteins are being regenerated, the available capacity to express other proteins becomes less. Nonetheless, it is possible to attain high robustness with a corresponding trade-off in yield. And finally, the range of DNA concentrations that give rise to high yield and high robustness are often quite narrow indicating that feedback regulation may become a necessary design requirement [170].

4.4 Discussion

We demonstrate how a biochemical constructor could be created by implementing a transcription-translation system running at steady-state on a micro-chemostat that supplies the reaction with resources and energy. We showed that the system is capable of self-regenerating components of its core constructor by synthesizing proteins required for transcription and translation. We regenerated up to seven components simultaneously and show that system optimality is surprisingly similar to fitness landscapes observed in living systems [171], requires both minimizing resource loading and optimizing resource allocation, and can be described in terms of Pareto optimality.

Just like the universal constructor envisioned by von Neumann ~80 years ago, a biochemical universal constructor will consist of 3 components: i) an instruction set (DNA), ii) a core constructor (RNA and proteins), iii) and a copy machine (proteins). The core constructor consists of RNAs and proteins that read and implement the information contained in the instruction set. The core constructor is capable of constructing copies of itself and of the copy machine. The copy machine consists of the protein components necessary for DNA replication which copy the instruction set [137]. Similar to von Neumann's universal constructor, the biochemical constructor requires supply of resources and energy, which is also a necessary requirement for all living systems.

Although we show that creation of a biochemical constructor is feasible, a number of considerable challenges remain. It will be critical to develop a transcription-translation system with a high enough synthesis rate to self-regenerate all of its components. The PURE system is currently orders

of magnitude away from this target. We estimate that around 50% of all PURE proteins could be regenerated by the current PURE system, and that the total synthesis rate required is 25 fold above the current rate (Supplementary Figure 4.27). These estimates do not yet include ribosome or tRNA synthesis. Current approaches to optimizing transcription-translation systems mainly focus on increasing component concentrations or adding components to the system which can give rise to overall higher synthesis yields but consequently also require higher synthesis rates to achieve self-regeneration [58, 94, 141]. Instead, optimizing protein synthesis rates and the ratio of protein synthesis rate to total amount of protein contained in the system will be important for development of a biochemical universal constructor. A second major challenge lies in achieving functional *in vitro* ribosome biogenesis [62, 64, 172]. The most promising near-term goal will be demonstration of steady-state self-replication of DNA. Several promising advances have recently been demonstrated in this area [51, 137], although *in vitro* DNA replication efficiency likely needs to be improved in order to reach sustained steady-state DNA replication.

Achieving high yield and robustness will be as well important for the development of a universal biochemical constructor. These concepts are tightly connected to resource usage and loading effects recently described in cell-free systems [71] and living cells [173]. We showed that several components could be regenerated at the same time. However, finding optimal DNA concentrations for several components is critical to achieving sustained regeneration without unnecessarily loading the system. Moreover, our results and corresponding modeling suggest that specific components might have to be tightly regulated, and could benefit from active feedback regulation [170], especially once system complexity increases. Currently, self-regenerating systems can be optimized by varying individual DNA input concentrations in order to adjust protein synthesis rates for each component being regenerated. In the future, all genes will be encoded on a single 'genome' [47, 51], requiring expression strengths to be tuned by the use of synthetic transcription factors [113], promoters [22], terminators [72], and ribosome binding sites [174]. Work on a biochemical universal constructor thus provides ample challenges and opportunities for synthetic biology in the areas of protein biochemistry, tRNA synthesis, ribosome biogenesis, metabolism, regulatory systems, genome design, and system engineering.

The development of a universal biochemical constructor and the creation of synthetic life are exciting prospects and recent progress in technology and biochemistry are making these seemingly plausible goals. Many challenges remain, but pieces to the puzzle are being added at an increasing rate. It is thus not far-fetched to consider that synthetic life, engineered by humans from basic building blocks, may be a possibility.

4.5 Methods

4.5.1 Materials

E. coli BL21(DE3) and M15 strains were used for protein expression. *E. coli* RB1 strain [91] originally obtained from G. Church (Wyss Institute, Harvard University, USA) was used for His-tag ribosome purification. All plasmids encoding PURE proteins used in this work were originally obtained from Y. Shimizu (RIKEN Quantitative Biology Center, Japan). Plasmid encoding mScarlet was a gift from P. Freemont (Imperial College London, UK).

Linear template DNA for *in vitro* eGFP synthesis (Supplementary Table 4.6) was initially prepared by extension PCR from a pKT127 plasmid as described previously [134] and cloned into a pSBlue-1 plasmid. The DNA fragment used for PURE system characterization and self-replication experiments was amplified from this plasmid by PCR. Linear DNA fragments encoding different proteins used for self-regeneration experiments were prepared by extension PCR from their respective plasmids. Primer sequences are listed in Supplementary Table 4.7. All DNA fragments were purified using DNA Clean and Concentrator-25 (Zymo Research). DNA was eluted in nuclease-free water instead of elution buffer, and its concentration was quantified by absorbance (NanoDrop, ThermoFisher). Double stranded Chi DNA [175] was prepared by annealing to primers listed in Supplementary Table 4.6.

4.5.2 Ribosome purification

All buffers used in this work are listed in Supplementary Table 4.8. All buffers were filtered (Flow Bottle Top Filters, 0.45 μ m aPES membrane) and stored at 4°C. 2-mercaptoethanol was added immediately before use. Ribosomes were prepared from *E. coli* RB1 strain by His-tag purification [91]. *E. coli* RB1 strain was grown overnight in 3 mL LB media at 37°C. 4 \times 3 mL of the overnight culture was used to inoculate 4 \times 500 mL of LB in a 1 L baffled flask. Cells were grown at 37°C, 260 RPM to exponential phase (3-4 h), pooled together and harvested by centrifugation (3220 RCF, 20 min, at 4°C), and stored at -80°C. The cells were then resuspended in 15 mL suspension buffer and lysed by sonication on ice (Vibra cell 75186, probe tip diameter: 6 mm, 11 \times 20s:20s pulse, 70% amplitude). Cell debris was removed by centrifugation (21130 RCF, 20 min, at 4°C). The recovered fraction was filtered with a GD/X syringe filter membrane (0.45 μ m, PVDF, Whatman).

Ribosomes were purified using 5 mL IMAC Sepharose 6 FF (GE Healthcare) by Ni-NTA gravity-flow chromatography. The corresponding buffers were prepared by mixing buffer C and buffer D at the required ratios. After the column was equilibrated with 30 mL of lysis buffer (100% buffer C), the prepared lysate solution was loaded onto the column. The column was washed with 30 mL of lysis buffer (100% buffer C), followed by 30 mL of wash buffer 1 (5 mM imidazole), 60 mL of wash buffer 2 (25 mM imidazole), 30 mL wash buffer 3 (40 mM imidazole), 30 mL wash buffer 4 (60 mM imidazole) and eluted with 7.5 mL elution buffer (150 mM imidazole). Ribosomes from two purifications were pooled together (around 15 mL) and subjected to buffer exchange using a 15 mL Amicon Ultra filter unit with a 3 kDa molecular weight cutoff (Merck). All centrifugation steps

were performed at 3220 RCF and 4°C. The elution fraction was concentrated to 1 mL (60 min). The concentrated sample was then diluted with 15 mL of ribosome buffer and re-concentrated to 1 mL (60-70 min); this step was repeated three times. The recovered ribosomes (1 mL) were further concentrated using a 0.5 mL Amicon Ultra filter unit with a 3 kDa molecular weight cutoff (Merck) by centrifugation (14,000 RCF, at 4°C). Ribosome concentration was determined by measuring absorbance at 260 nm of a 1:100 dilution. An absorbance of 10 for the diluted solution corresponds to a 23 μ M concentration of undiluted ribosome solution. Final ribosome solution used for *in vitro* protein synthesis was prepared by diluting to 3.45 μ M. The usual yield is around 0.75 mL of 3.45 μ M ribosome solution.

4.5.3 PURE system preparation

All buffers used in this work are listed in Supplementary Table 4.8. All buffers were filtered (Flow Bottle Top Filters, 0.45 μ m aPES membrane) and stored at 4°C. 2-mercaptoethanol was added immediately before use. Proteins were purified by Ni-NTA gravity-flow chromatography as described previously [93]. All cultures were grown at 37 °C, 250 rpm. Overnight cultures were grown in 3 mL of LB supplemented with 100 μ g/mL of ampicillin and/or 50 μ g/mL of kanamycin. Each strain was inoculated in a flask with 2 L of LB. Cells were grown 2 h before induction with 0.1 mM of IPTG for 3 h, then harvested by centrifugation and stored at -80°C. The cells were resuspended in 30 mL of buffer A and lysed by sonication on ice (Vibra cell 75186; probe tip diameter: 6 mm; 8 \times 20 s:20 s pulse; 70% amplitude). Cell debris was removed by centrifugation (25 000 RCF, 20 min, 4°C). The supernatant was mixed with 2-3 mL of equilibrated resin (described below), and incubated for up to 2 h, at 4°C. After the incubation, lysate was allowed to flow through the column. The column was washed with 30 mL of a wash buffer (95% buffer A, 5% buffer B) and eluted with 15 mL of an elution buffer (10% buffer A, 90% buffer B). The elution fraction was dialyzed against HT buffer (2 \times) and stock buffer and stored at -80 °C. Protein concentrations were estimated by absorbance at 280 nm and calculated protein extinction coefficients. When a higher protein concentration was required, the protein solution was concentrated using a 0.5 mL Amicon Ultra filter unit (Merck). Different PURE protein formulations are summarised in Supplementary Table 4.3. Different PURE or Δ PURE systems were prepared by supplying the corresponding Δ PURE systems with the omitted protein or buffer solution, respectively.

4.5.4 Ni-NTA resin preparation and regeneration for ribosome purification

5 mL IMAC Sepharose 6 FF (GE Healthcare) was pipetted into Econo-Pac chromatography columns (Bio-Rad), and charged with 15 mL of 100 mM nickel sulfate solution. The charged column was washed with 50 mL of demineralized water. After protein purification, columns were regenerated with 10 mL of buffer containing 0.2 M EDTA and 0.5 M NaCl, and washed with 30 mL of 0.5 M NaCl, followed by 30 mL of demineralized water, and stored in 20% ethanol at 4°C.

4.5.5 Energy solution preparation

Energy solution was prepared as described previously with slight modifications [93]. 2.5× energy solution contained 0.75 mM of each amino acid, 29.5 mM magnesium acetate, 250 mM potassium glutamate, 5 mM ATP and GTP, 2.5 mM CTP, UTP and TCEP (tris(2-carboxyethyl)phosphine hydrochloride), 130 U_{A260}/mL tRNA, 50 mM creatine phosphate, 0.05 mM folinic acid, 5 mM spermidine, and 125 mM HEPES.

4.5.6 Batch *in vitro* protein expression experiments

Batch PURE reactions (5 μ L) were established by mixing 2 μ L of 2.5× energy solution, 0.9 μ L of 3.45 μ M ribosomes (final concentration: 0.6 μ M), 0.65 μ L of PURE proteins (Supplementary Table 4.3), DNA template, and brought to a final volume of 5 μ L with addition of water. All reactions measuring eGFP expression were prepared as described above with eGFP linear template at a final concentration of 4 nM and incubated at 37°C at constant shaking for 3 h, and measured (excitation: 488 nm, emission: 507 nm) on a SynergyMX platereader (BioTek). The eGFP production rate was calculated between 20-50 min based on an eGFP calibration curve (Supplementary Figure 4.28A). Reactions expressing other proteins were prepared as described above and supplemented with 0.2 μ L FluoroTect GreenLys (Promega). DNA templates were used at a final concentration of 2 nM and the reactions were incubated at 37°C for 3 h.

4.5.7 SDS-PAGE gels

PURE reactions (5 μ L) labeled with FluoroTect GreenLys (Promega) were incubated with 0.8 μ g or 0.2 μ L of RNase A solution (Promega) and incubated for 30 min at 37°C and subsequently analyzed by SDS-PAGE using 10-well 4-20% Mini-PROTEAN TGX Precast Protein Gels (Bio-Rad). Gels were scanned (AlexaFluor 488 settings, excitation: Spectra blue 470nm, emission: F-535 Y2 filter) with a Fusion FX7 Imaging System (Vilber) and analyzed with ImageJ. Protein sizes were calculated based on a BenchMark™ Fluorescent Protein Standard (Invitrogen).

4.5.8 Fabrication and design of the microfluidic device

The microfluidic device was fabricated by standard multilayer soft lithography [176], detailed device preparation, operation, and characterisation are described previously [166]. The device with 8 reactors and 9 fluid inputs (Figure 4.5) is based on a previous design [134]. Molds for the control and the flow layer were fabricated on separate wafers by standard photolithography techniques and patterned with photoresist to produce channels with the heights stated (Supplementary Figure 4.5C). For the control layer, a silicon wafer was primed in an oxygen plasma processor for 7 minutes (TePla 300), and SU-8 photoresist (GM 1070, Gersteltec Sarl) was spin-coated onto the wafer yielding a height of 40 μ m. After relaxation and soft bake, the wafer was illuminated using a chrome mask for 18.2 s (365 nm illumination, 20 mW/cm² light intensity) on a Süss MJB4 mask aligner, followed by a post-exposure bake, the wafer development with PGMEA (propylene

glycol monomethyl ether acetate) and a hard bake. For the flow layer, a silicon wafer treated with HMDS (hexamethyldisilazane) vapor (YesIII primer oven) was spin-coated with AZ 9260 photoresist (Microchemicals GmbH) to a height of 15 μm . After baking and relaxation time, the coated wafer was exposed two times 18 s with a 10 s wait period between (20 mW/cm² light intensity) on a Süss MJB4 mask aligner. The wafer was developed with AZ 400K developer and baked at 175 °C for two hours. The microfluidic chips were fabricated from PDMS by standard multilayer soft lithography. Each of the wafers was treated with TMCS (trimethylchlorosilane). For the flow layer PDMS with an elastomer to crosslinker ratio of 5:1 was prepared and poured over the wafer and place to a desiccator for 40 min. For the control layer, PDMS with a 20:1 elastomer to crosslinker ratio was spin coated at 1400 rpm on to the wafer, and let sit for 40 min before baking. Both PDMS coated wafers were baked in the oven at 80 °C for 20 minutes. After the layers were aligned by hand and the aligned devices were placed in the oven for 90 minutes. The bonded chip was punched using a 900 mm pin and plasma bonded to a glass slide.

4.5.9 Device setup

To prime the chip, control lines were filled with phosphate buffered saline (PBS) and pressurized at 1.38 bar. The flow layer was primed with a solution of 2% bovine serum albumin (BSA) in 0.5× PBS. For washes between loading steps, 10 mM TRIS buffer (pH = 8) was used. For the experiments energy, PURE, and DNA solutions were mixed in the microfluidic reactors on the microfluidic chip in a 2:2:1 ratio. The peristaltic pump was actuated at 20 Hz to mix the solutions. Every 15 min, the reactor was imaged and a 20% fraction of the reactor volume was replaced with fresh components with the same 2:2:1 ratio. Details on the operation of the microfluidic chip can be found in Supplementary Tables 4.1 and 4.2. 2.5× energy solution was prepared as described above. 2.5× PURE or Δ PURE solutions were prepared by mixing the desired protein solutions (Supplementary Table 4.3) with ribosomes (final concentration: 0.6 μM) and supplied with 10 μM TCEP (final concentration: 4 μM). The PURE solution was supplemented with mScarlet protein to allow visualization, and the solutions were brought to final volume with the addition of water. The DNA solution at five times its final concentration was prepared by mixing the desired linear templates and Chi DNA. The final concentration of eGFP reporter in the reaction was 2 nM, the Chi DNA was used at a final concentration 1.25 μM . The Chi decoys were added to help mitigate potential DNA absorption and degradation, while the DNA solution is stored in the FEP tubing before it is added to the chip.

4.5.10 Data acquisition and analysis

Solenoid valves, microscope, and camera were controlled by a custom Matlab and LabVIEW program. The chip and microscope stage were enclosed in an environmental chamber at 34°C. Green and red fluorescence was monitored over time on an automated inverted fluorescence microscope (Nikon), using 20x magnification and FITC / mCherry filters. The microscope hardware details are described in [166].

The fluorescence images were analyzed and corrected in Python, by subtracting the background fluorescence of a position next to the fluidic channel. The fluorescence signal was normalized in respect to maximal positive control signal intensity in a given experiment, or to the overall maximal intensity if a positive control was not included. The eGFP synthesis rate was calculated based on an eGFP calibration curve (Supplementary Figure 4.28B) and dilution rate.

4.6 Modeling

4.6.1 Minimal resource-dependent TX-TL model

While cell-free transcription and translation can be described at varying levels of granularity [54, 83, 97, 100, 167, 168, 177, 178], here we chose to model the processes at the most coarse-grained level using coupled ordinary differential equations (ODEs). This model can be easily extended to incorporate more complex effects, but the aim here was to show a minimal mechanism which qualitatively captures the observed experimental effects.

The model consists of simultaneous transcription and translation of GFP and T7 RNAP, which consumes a single resource species R . This species is a lumped representation of NTPs which are consumed during transcription, and ATP, GTP, and aminoacyl tRNAs which are consumed during translation. We model the transcription rate by a parameter α , linearly dependent on DNA and T7 RNAP concentration, and modulated by the availability of resources using a Hill function $R/(R + K)$. Likewise, translation proceeds at a rate β , which is linearly dependent on mRNA concentration, and is modulated by the same Hill function for resource dependence. The rate of consumption of R is equal to the summed transcription and translation rates. The complete model consisting of seven ODEs and three parameters, is shown below.

$$\dot{R} = -\dot{m}_T - \dot{m}_G - \dot{p}_T - \dot{p}_G \quad (4.1)$$

$$\dot{d}_T = 0 \quad (4.2)$$

$$\dot{d}_G = 0 \quad (4.3)$$

$$\dot{m}_T = \alpha \frac{R}{R + K} d_T p_T \quad (4.4)$$

$$\dot{m}_G = \alpha \frac{R}{R + K} d_G p_T \quad (4.5)$$

$$\dot{p}_T = \beta \frac{R}{R + K} m_T \quad (4.6)$$

$$\dot{p}_G = \beta \frac{R}{R + K} m_G \quad (4.7)$$

DNA, mRNA, and protein concentrations are denoted by d , m , and p , and the subscripts T and G refer to T7 RNAP and eGFP respectively. The model was implemented in Julia 1.4.2 and solved using the `DifferentialEquations.jl` package. All code is available on github.

4.6.2 Chemostat simulation

During chemostat operation, concentrations of species in the cell-free reaction are periodically adjusted. All components are diluted at a specific dilution fraction, while certain components (proteins, ribosomes, energy solution, and DNA) are replenished. This can be captured in the model by explicitly including the dilution steps. In Julia this is achieved by implementing callbacks which modify the concentrations at specified time points while solving the ODEs. More detail can be found in the documentation for the code.

Simulating the chemostat leads to a sawtooth-like behaviour as eGFP is diluted, and subsequently produced between dilution steps, as shown by the green curve in Supplementary Figure 4.13. In the real experiment, images are taken immediately before each dilution step, and thus the data appear smooth: this is shown by the dashed black curve in Supplementary Figure 4.13.

At each dilution step in the model, all species' concentrations are reduced by a fixed dilution fraction, while the concentrations of certain species are refreshed by addition of a fraction of those species at their initial concentrations:

$$c_{i+1} = c_i(1 - \gamma) + \gamma c_0 \quad (4.8)$$

The dilution fraction γ was set to 20%, and the periodicity of dilution to 15 minutes, corresponding to experimental values. Each *in silico* experiment contained three stages: 1.) kick-start, 2.) self-regeneration, and 3.) washout. The species were replenished as indicated in Supplementary Table 4.5. The negative control corresponded to a self-regeneration experiment with $d_T = 0$.

4.6.3 Model design and parameters

Since our overall goal was to capture qualitative rather than quantitative behaviour, we used effective parameters and arbitrary units to describe system dynamics, which were combined with physical time values and experimental chemostat operation parameters. Nevertheless, initial parameter selection was guided by relative magnitudes of various parameters. In particular, the resource saturation term K is typically several orders of magnitude less than the initial resource concentration [179], and cell-free translation rates are typically an order of magnitude slower than transcription [180]. The initial parameter set was manually chosen to reflect experimentally-observed behaviour; parameter scans were then conducted to test the robustness of model behaviour on parameter variations, as discussed below.

We have assumed equal resource consumption for transcription and translation, which is motivated by the fact that translation consumes $2N$ GTP and N ATP to synthesise a polypeptide of length N (accounting for aminoacylation), while transcription consumes on average $3N/4$ ATP and $3N/4$ GTP (as well as UTP and CTP), which is the same as translation to within an order of magnitude.

4.6.4 Elucidation of model behaviour

In order to elucidate the origins of the observed behaviour, we can inspect protein, mRNA, and resource levels, as shown in Supplementary Figure 4.14. Because translation rate is the product of mRNA concentration and the resource dependence term $R/(R + K)$, high levels of translation require both to be present. Let us consider the self-regeneration phase (4–16h). At low concentrations of d_T , resource levels are high; however mRNA concentrations are low, and thus overall the translation rate of eGFP is low. In the converse situation at high d_T , mRNA levels are high, but resources are low, leading once again to low eGFP production. It is only at intermediate concentrations of d_T where eGFP production is high when there is a small but nonzero amount of resource availability, as well as an intermediate level of mRNA present. The model thus predicts that the production of eGFP is determined by a trade-off between resource availability and mRNA concentration.

In order to further interrogate the model, we can look at transcription and translation rates. These can be determined from the model by evaluating the derivatives directly from the ODEs. As the system is periodically diluted, the rates are also periodically modulated. An example is shown in Supplementary Figure 4.15A (grey line), from which we can calculate the average rate (green line). Here we observe that the translation rate of GFP in the positive control experiment varies from a high value to zero in every cycle. This is due to resources being completely depleted in each cycle, as shown in Supplementary Figure 4.15B. The average rates of transcription and translation of GFP and T7 RNAP are shown in Supplementary Figure 4.16, where we again observe that increasing d_T increases average transcription rates (Supplementary Figure 4.16B), but decreases translation rates (Supplementary Figure 4.16A).

In our model the consumption of resources is directly equal to the summed transcription and translation rates. Thus we can determine the allocation of resources between different model processes, as shown in Supplementary Figure 4.17. We observe that at the onset of the self-regeneration phase, transcriptional resource consumption decreases while translational consumption increases (Figure 4.17A and B), which forms one part of our hypothesis to explain the increase in eGFP production over the positive control. Supplementary Figure 4.17E and F show that as T7 RNAP is washed out at late times, resource allocation tends to 100% translation, and this accounts for the ‘bump’ in eGFP production in the washout phase.

We can also carry out parameter variations, shown in Supplementary Figure 4.18 as a contour map of the variation of the parameter of interest against a T7 DNA titration. Here we show the model predictions for two quantities: the ratio of self-regeneration to positive control (SR/PC) at 15h, as shown in the main text, and the overall eGFP production at 15h, which is a measure of the productivity of the self-regeneration process. These results yield further insights into the mechanisms of the model; of relevance is the observation that both eGFP production and the ratio SR/PC exhibits an optimum with respect to T7 RNAP DNA, and the position of the optimum is only significantly affected by transcription and translation rates: increasing these rates shifts the optimum to lower values. The optimum is otherwise relatively robust; in particular, the position

of the SR/PC optimum is insensitive to d_G (shown in more detail in Supplementary Figure 4.19). An important observation is that the the ratio SR/PC contains an optimum for high values of T7 DNA and small values of the initial resource concentration R_0 . The interpretation of this is that the model predicts that high SR/PC ratios are achieved when the resources become scarce.

In summary, analysis of the single resource-dependent model behaviour leads to two main conclusions:

1. eGFP production depends on a trade-off between resource availability and mRNA concentration. As d_T is increased, eGFP production therefore exhibits a maximum.
2. For intermediate concentrations, eGFP production is higher than the positive control during the self-regeneration phase. This is accounted for by a reallocation of resources from transcription to translation during the transition between kick-start and self-regeneration, and by an overall resource-limited condition.

4.6.5 Sufficiency of model mechanism

We would like to understand whether the resource-dependent model is necessary and sufficient to explain our observations. Therefore we developed a second model, whose transcriptional and translational activities do not depend on any resource. This ‘resource-independent’ model instead contains TX and TL rates which decrease exponentially over time, with a fixed decay constant λ , which represents a resource-independent inactivation of cell-free protein synthesis. Such effects are also observed experimentally [167]. This model can be written as follows:

$$\dot{d}_T = 0 \quad (4.9)$$

$$\dot{d}_G = 0 \quad (4.10)$$

$$\dot{m}_T = \alpha \exp(-\lambda t) d_T p_T \quad (4.11)$$

$$\dot{m}_G = \alpha \exp(-\lambda t) d_G p_T \quad (4.12)$$

$$\dot{p}_T = \beta \exp(-\lambda t) \frac{m_T}{m_T + m_G + K_{TL}} \quad (4.13)$$

$$\dot{p}_G = \beta \exp(-\lambda t) \frac{m_G}{m_T + m_G + K_{TL}} \quad (4.14)$$

Here, we model translation as saturating at high total mRNA concentrations, with a Hill function and a saturation constant K_{TL} . This is a typical way of taking into account translational loading effects [71]. We observe that this model can also qualitatively capture some of the experimental observations. Supplementary Figure 4.20A shows the time courses and SR/PC ratio plot of the single-resource model. Supplementary Figure 4.20B shows the same for the resource-independent model, which again captures the optimum in SR/PC ratio as a function of T7 RNAP DNA. The model exhibits the three features of decaying eGFP production at low d_T , high eGFP (potentially above the positive control level) at intermediate d_T , and low eGFP production followed by a peak during washout at high d_T .

The explanation of a maximum in eGFP production as a function of T7 RNAP DNA, is different from in the single-resource model. Here, at low d_T , the concentration of m_G is low, leading to low translation rates. At high d_T , the concentration of m_T is high, loading the translational machinery and again leading to low translation rates. At intermediate concentrations, where mRNA concentrations are high but before translational loading effects set in, we observe a maximum eGFP production.

Despite the different mechanism, there is a crucial similarity between this and the resource-dependent model: both involve coupling of the expression of eGFP and T7 RNAP. In the resource-dependent model, this is through a shared resource term, and in the resource-independent model, this is through a shared translational term. To demonstrate this, the coupling term can be artificially removed in the resource-independent model, allowing each protein to be translated independently. This leads to Supplementary Figure 4.20C, where the ratio SR/PC monotonically increases with increasing T7 RNAP template, and no maximum is observed.

A second feature of both models is the striking increase of GFP above positive control levels (SR/PC > 1), for intermediate T7 RNAP template concentrations. These again result from two different mechanisms. In the resource-dependent model, analysis from the previous section shows that this is due to release of resources, under resource-limited conditions.

In the resource-independent model, T7 RNAP concentration is low in the kick-start phase. Thus any increase in T7 RNAP DNA template will increase T7 RNAP concentration, leading to greater transcription and translation, with no incurred costs. As long as translational capacity is not loaded, this effect can increase GFP over the positive control level. The increase of GFP is thus due to the activity of extra T7 RNAP in the system. However, the increase begins immediately in the kick-start phase, and is maintained throughout self-regeneration.

The explanation for these mechanisms can be tested *in silico*: in the first case, increasing the availability of resources should alleviate the resource constraint, and decrease the SR/PC ratio. This is observed in the parameter study shown in Supplementary Figure 4.18. In the second case, increasing the initial T7 RNAP concentration should decrease the effect of any additional T7 RNAP produced. This is also observed in a similar parameter exploration, shown in Supplementary Figure 4.21.

In reality, it is likely that both mechanisms are at play. While the PURE system is known to be resource-limited under certain conditions [58], some lysate-based systems exhibit resource-independent deactivation [134]. Since a model which simultaneously takes both effects into account is likely to be more general, we tested a combined model, whose results are shown in Supplementary Figure 4.20D and 4.22. While this model also successfully captures experimental observations, it is less robust than the simpler models, requiring fine-tuning of parameters. Experimentally, since we observe an increase in GFP after self-regeneration begins, and not immediately from the beginning of the kick-start phase, it is likely that under our experimental conditions, the resource limitation is a more dominant effect.

4.7 Supplementary information

4.7.1 Supplementary figures

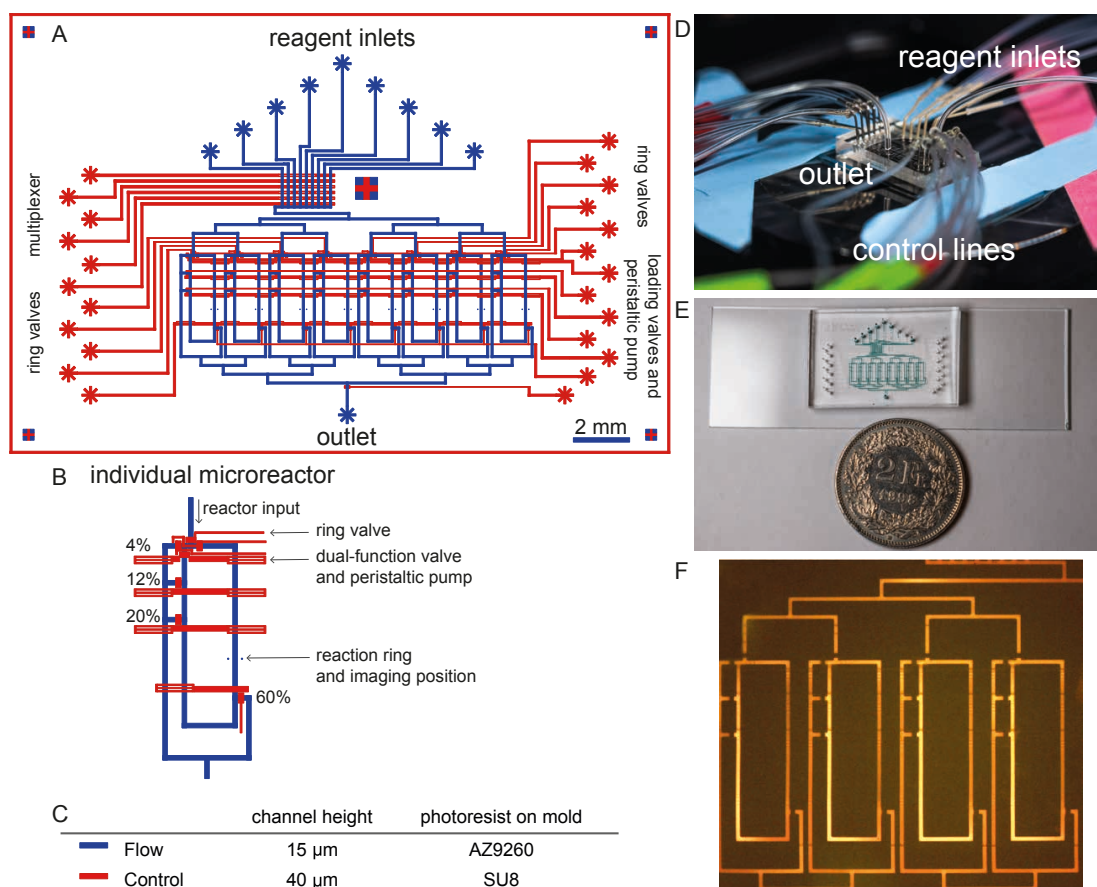


Figure 4.5: **Microfluidic device design:**

(A) Design schematic of the microfluidic device. The control layer is shown in red and the flow layer in blue. The device contains eight individually addressable chemostat reactors. (B) Close-up of a microfluidic reactor. Each reactor has four outlets corresponding to four different dilution fractions. Four control lines serve dual-functions as valves and peristaltic pump. The width of a flow channel is $100\mu\text{m}$. (C) Table of channel heights and corresponding photoresists used in mold fabrication. (D) Image of microfluidic chip connected to the control lines, reagent inputs and outlet. (E) Image of microfluidic chip, flow channels are filled with blue dye for visualization. (F) Microscope images of four microreactors. Control channels are filled with fluorescence dye for visualization.

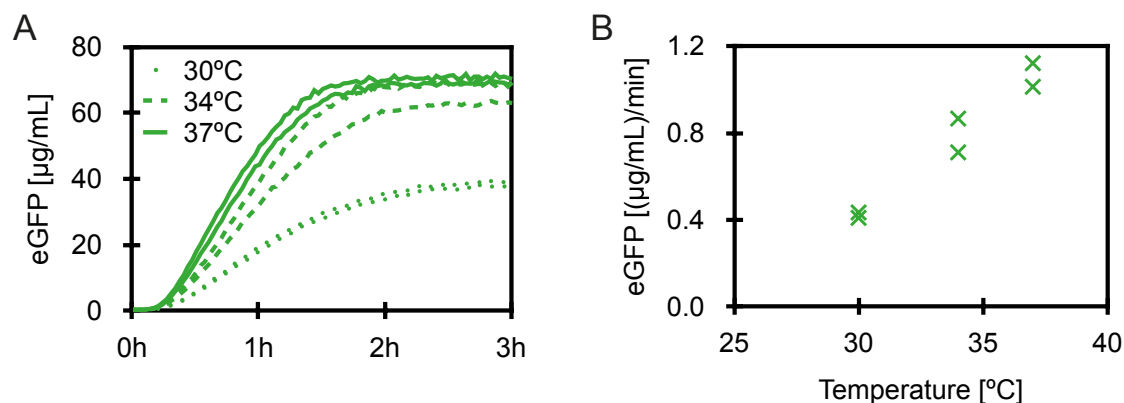


Figure 4.6: **Comparison of eGFP expression at different temperatures in batch reactions:** (A) eGFP expression over time, (B) eGFP expression rates. Each data point represents technical replicate.

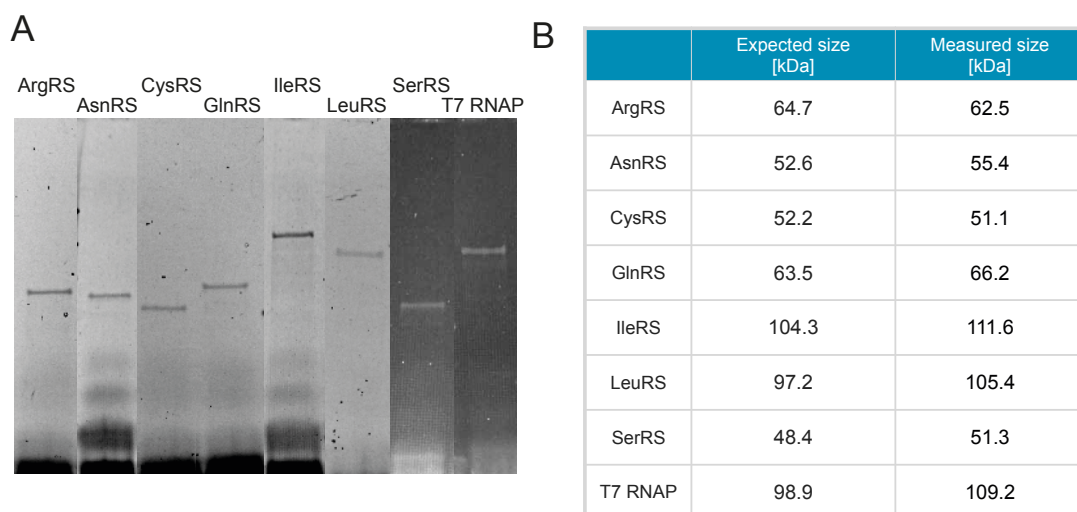


Figure 4.7: ***In vitro* expression of different self-regenerated proteins:** (A) SDS-PAGE gel of *in vitro* synthesized proteins labeled with FluoroTect GreenLys. Full protein gels are provided in a Source data file. (B) Mass analysis of the expressed proteins. Proteins ArgRS, AsnRS, CysRS, GlnRS and LeuRS were expressed analyzed by PAGE gel twice, SerRS, IleRS and T7 RNAP were expressed analyzed by PAGE gel once with similar results.

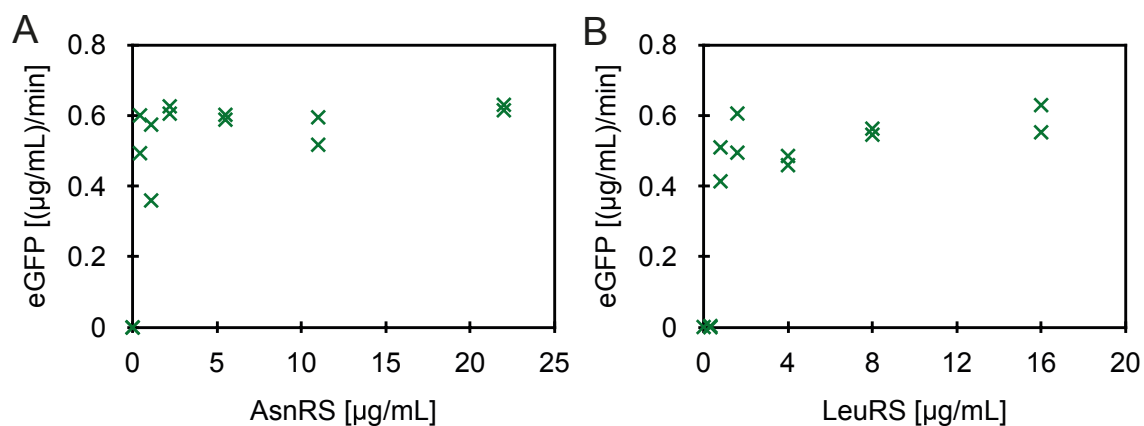


Figure 4.8: **Comparison of eGFP expression rates in batch reactions at different components concentrations:**

(A) AsnRS, (B) LeuRS. Each data point represents a technical replicate.

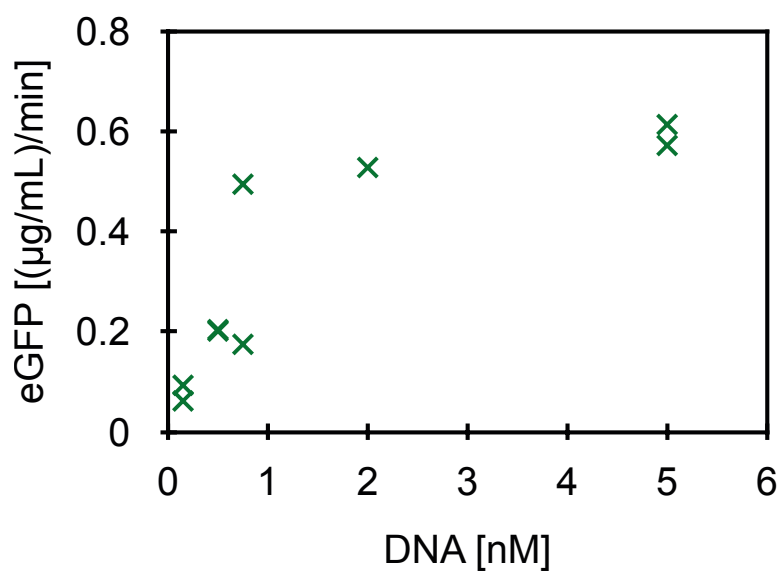


Figure 4.9: **Comparison of eGFP expression rates in batch reactions at different DNA template concentrations.** Each data point represents a technical replicate.

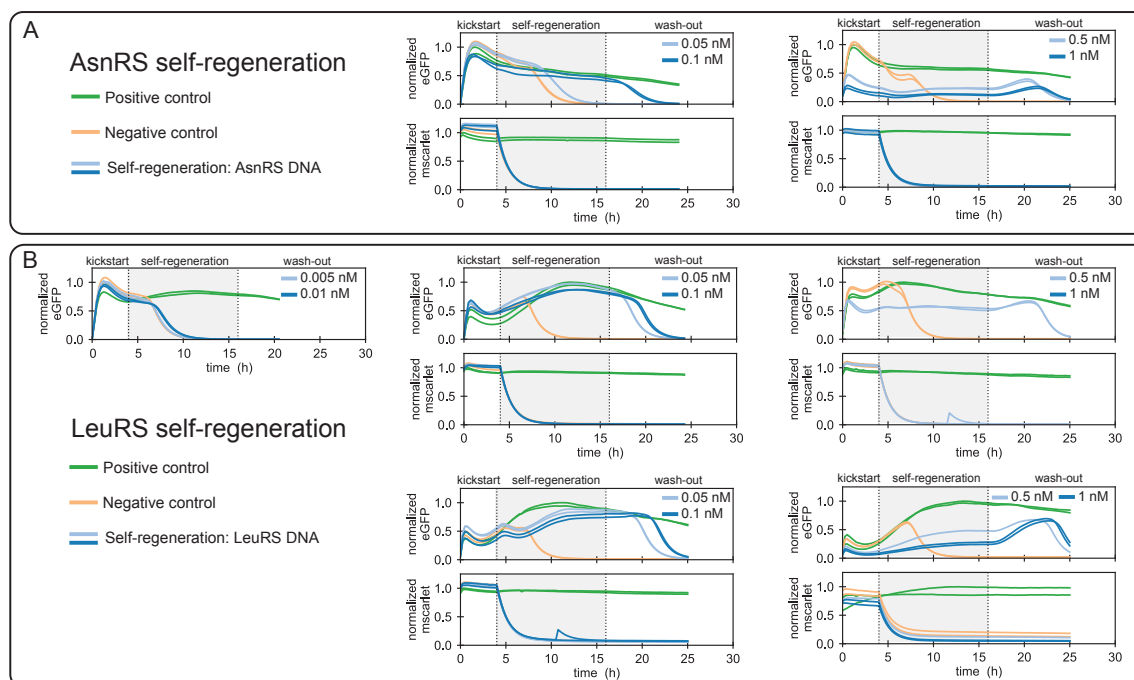


Figure 4.10: Aminoacyl-tRNA synthetase regeneration:

Summary of all (A) AsnRS and (B) LeuRS regeneration experiments and their corresponding mScarlet traces. The level of eGFP intensity is normalised to the maximum intensity obtained in the positive control (positive control: green, negative control: yellow, self-regeneration: blue). PURE system compositions used for the different experiments are given in Supplementary Table 4.3. 2 nM eGFP DNA template was used, and aaRS DNA template concentrations are indicated in the corresponding graphs.

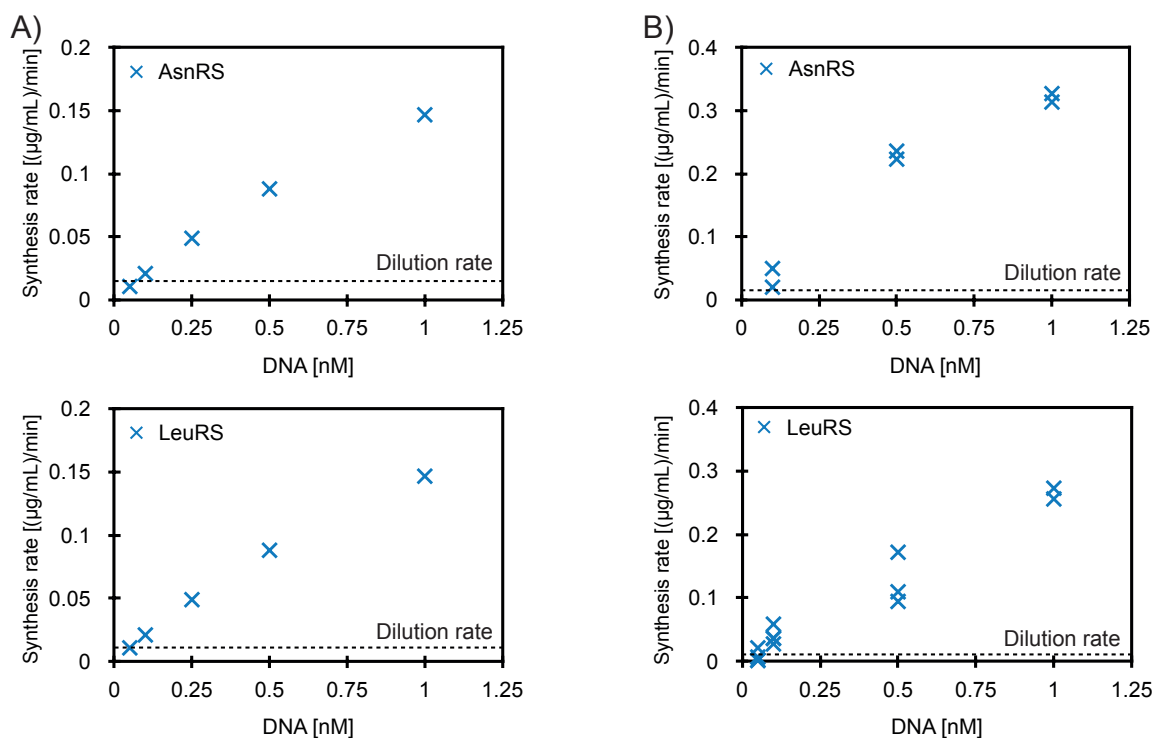


Figure 4.11: **Synthesis rate for single component expression:**

(A) Theoretical synthesis rate for single components expression, calculated based on eGFP synthesis rate in a microfluidic chemostat ($0.44 \mu\text{g/mL/min}$) and DNA loading in DNA saturated system. (B) Estimated synthesis for AsnRS and LeuRS at different DNA concentrations based on the difference in eGFP synthesis rate for positive control and self-regeneration experiment at 15 hours. The eGFP synthesis rate was calculated based on an eGFP calibration curve (Supplementary Fig. 4.28B) and dilution rate. Dashed line represents the dilution rate of the given components based on the input component concentration (Supplementary Table 4.4).

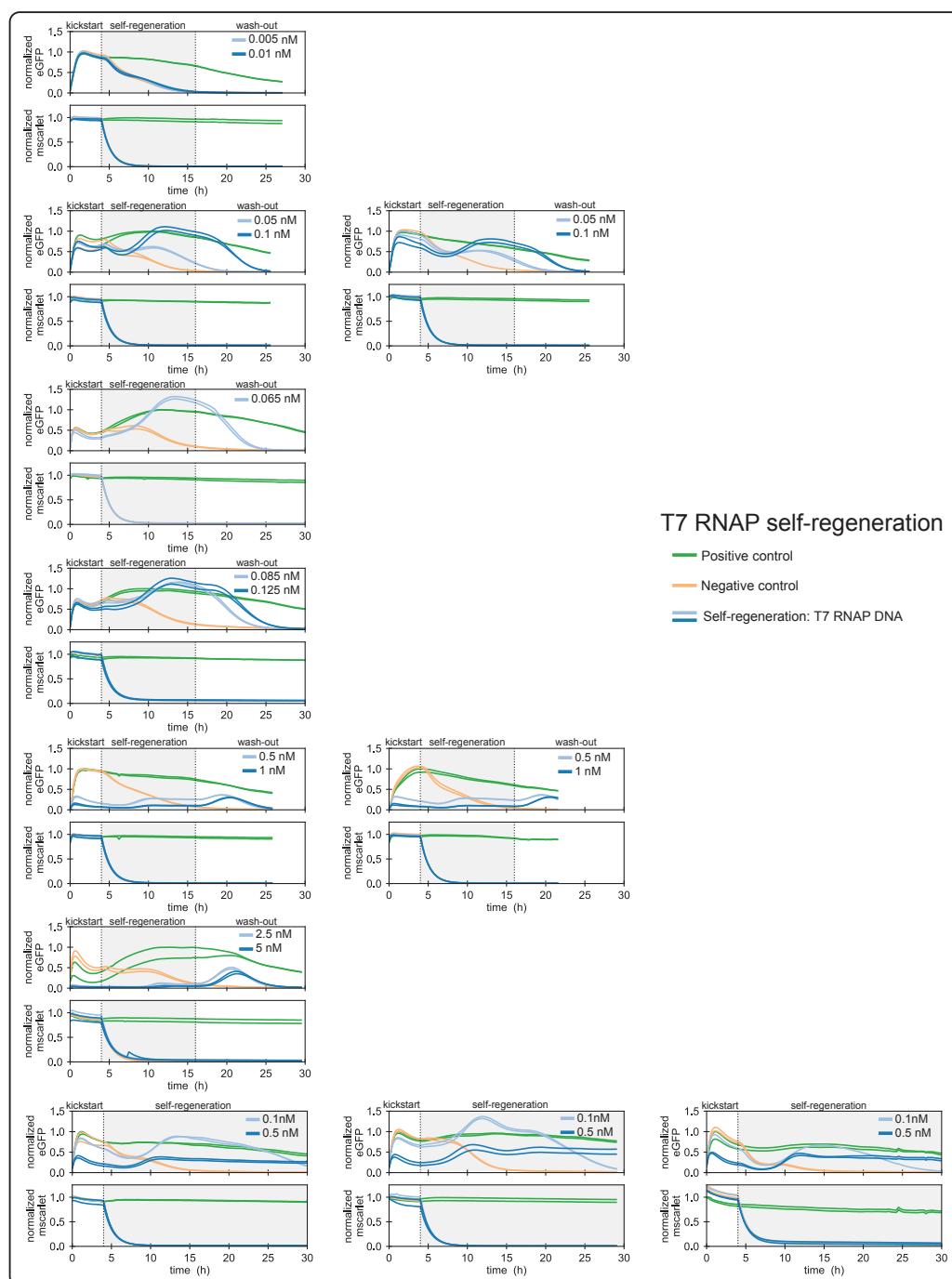


Figure 4.12: T7 RNAP regeneration:

Results of regeneration experiments for all T7 RNAP DNA concentrations shown in Figure 4.3E, together with their corresponding mScarlet traces. The level of eGFP intensity is normalised to the maximum intensity obtained in the positive control (positive control: green, negative control: yellow, self-regeneration: blue). PURE system compositions used for different experiments are given in Supplementary Table 4.3. 2 nM of eGFP DNA template was used, and T7 RNAP DNA template concentrations are indicated in the corresponding graphs.

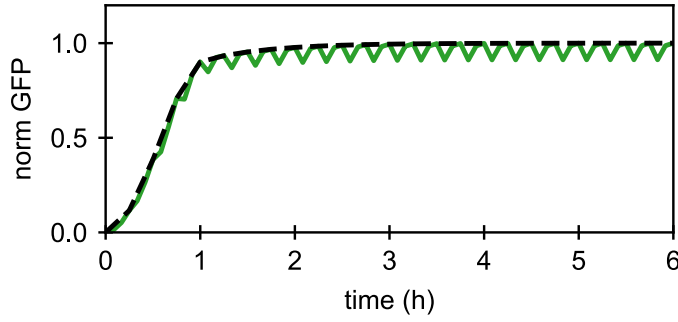


Figure 4.13: **Chemostat simulations:** The chemostat is simulated by periodically diluting and replenishing species, and solving ODEs between the dilution steps. This leads to a sawtooth curve (green). Experimental measurements are taken immediately before each dilution step, which results in a smooth observation (dashed black line).

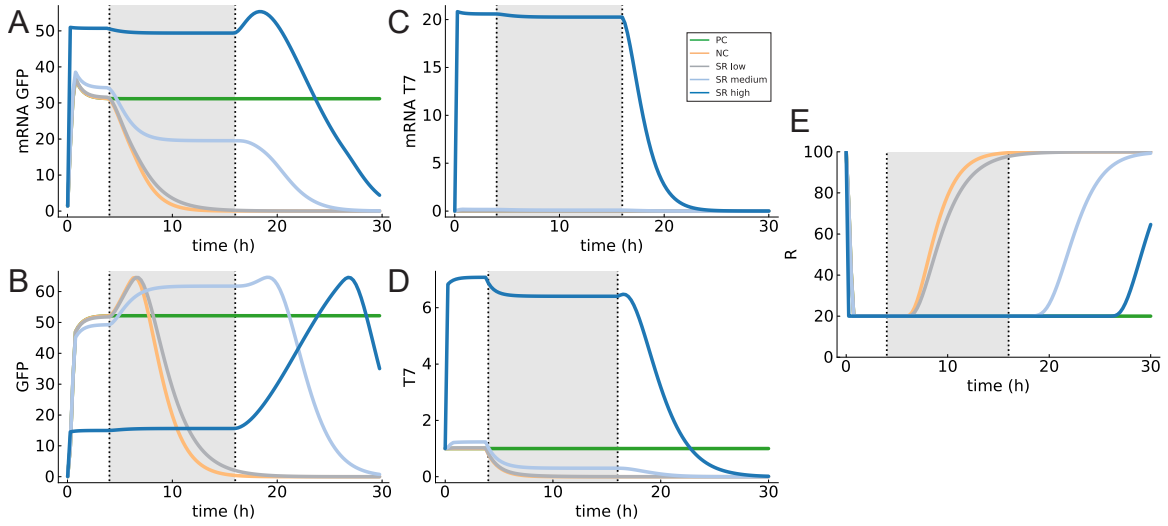


Figure 4.14: **Simulation results for mRNA, protein and resource concentration:**

(A,B) Simulation results showing eGFP and (C,D) T7 RNAP mRNA and protein concentrations, as well as concentration of resource R (E). Parameter values were $\alpha = 0.7$, $\beta = 0.07$, $K = 1$ and initial conditions $R_0 = 100$, $p_T = 1$, $d_G = 2$, with all other species set to zero. The three concentrations of d_T are 0.001, 0.01, and 1, corresponding to the labels ‘low’, ‘medium’, and ‘high’, respectively.

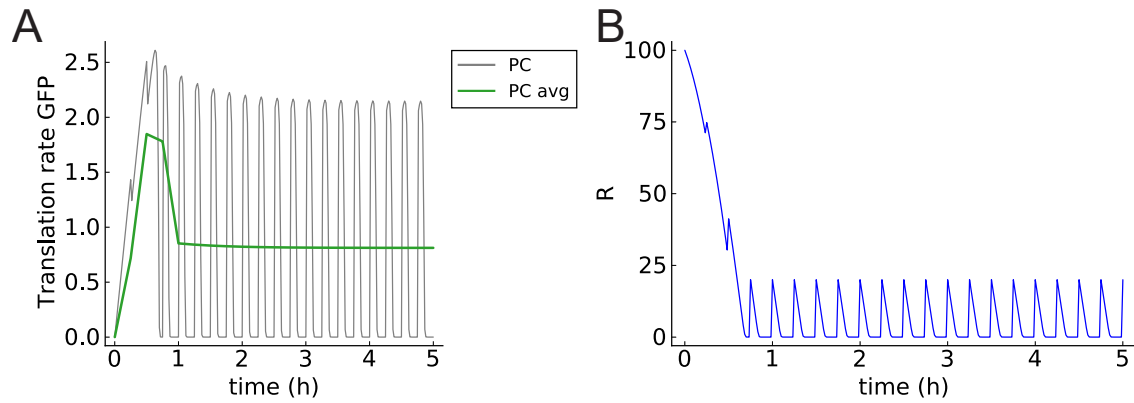


Figure 4.15: **Derivatives can be directly calculated in the model, yielding rates of transcription and translation:**

(A) Periodic dilution of the chemostat leads to variations in rates, so we report the rates averaged over every period. (B) Translation of GFP occurs in a resource-limited regime, as resources are fully depleted over the course of each period.

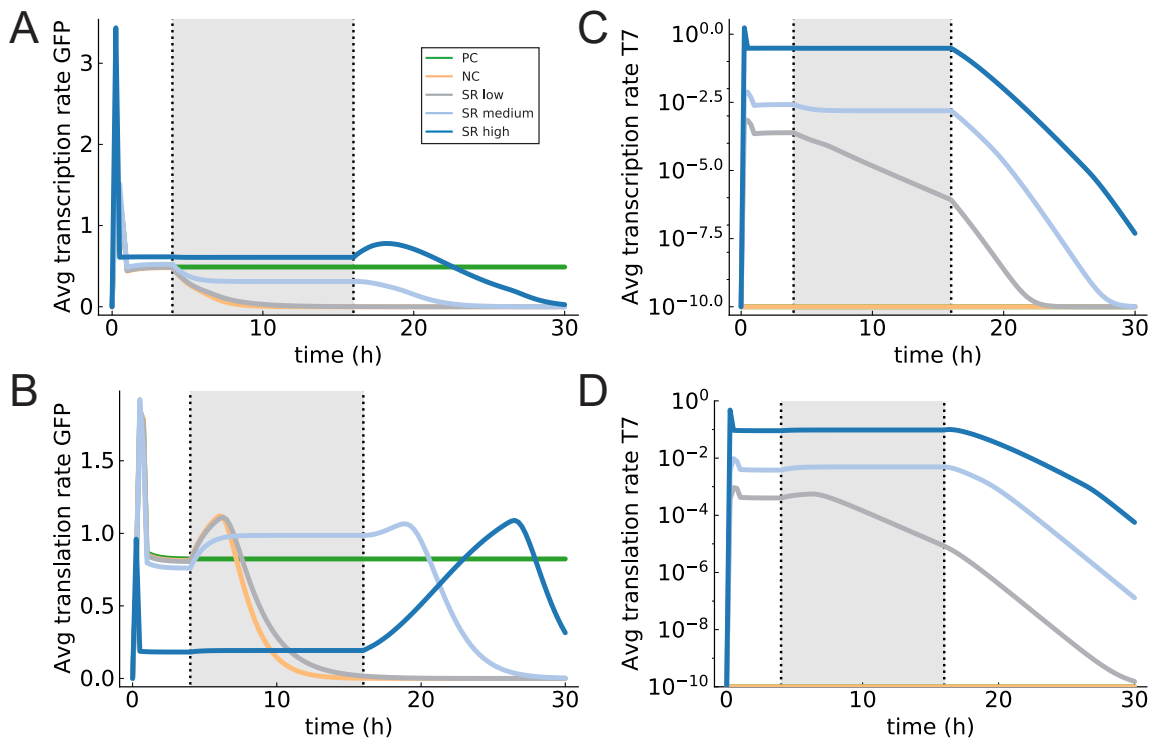


Figure 4.16: **Parameter variations for the resource-dependent model:**

(A,B) Averaged transcription and translation rates for GFP and (C,D) T7 RNAP, for the same parameters as in Figure 4.14. To make the T7 rates more clear we plotted them on a log scale, with all values smaller than 10^{-10} set to 10^{-10} .

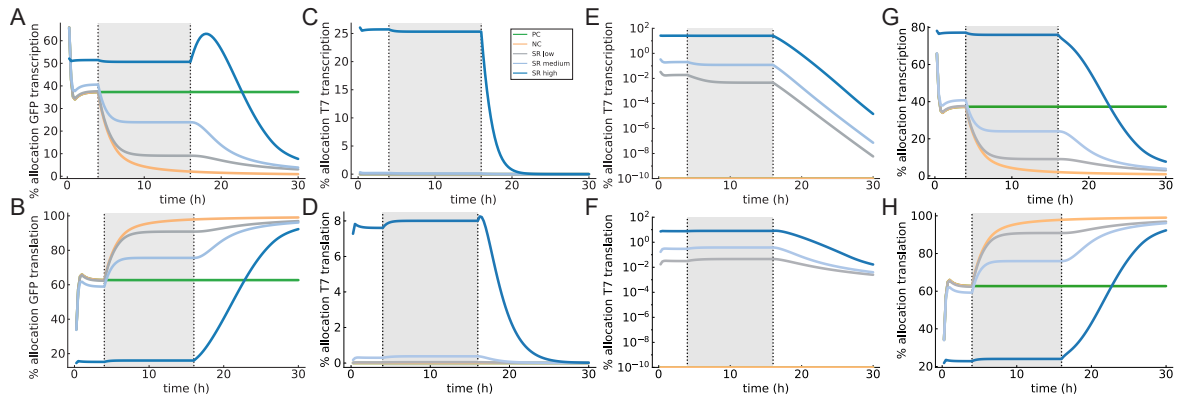


Figure 4.17: **Varying resource allocation over the course of the simulation:**

(A,B) We observe reallocation of resources from transcription to translation at the beginning of the self-regeneration phase. (C,D) Resources consumed by T7 transcription and translation are shown on linear and (E,F) log scales for clarity. (G,H) The division of resources between total transcription and total translation. As T7 RNAP is washed out after 16 hours, resource allocation tends to 100% translation.

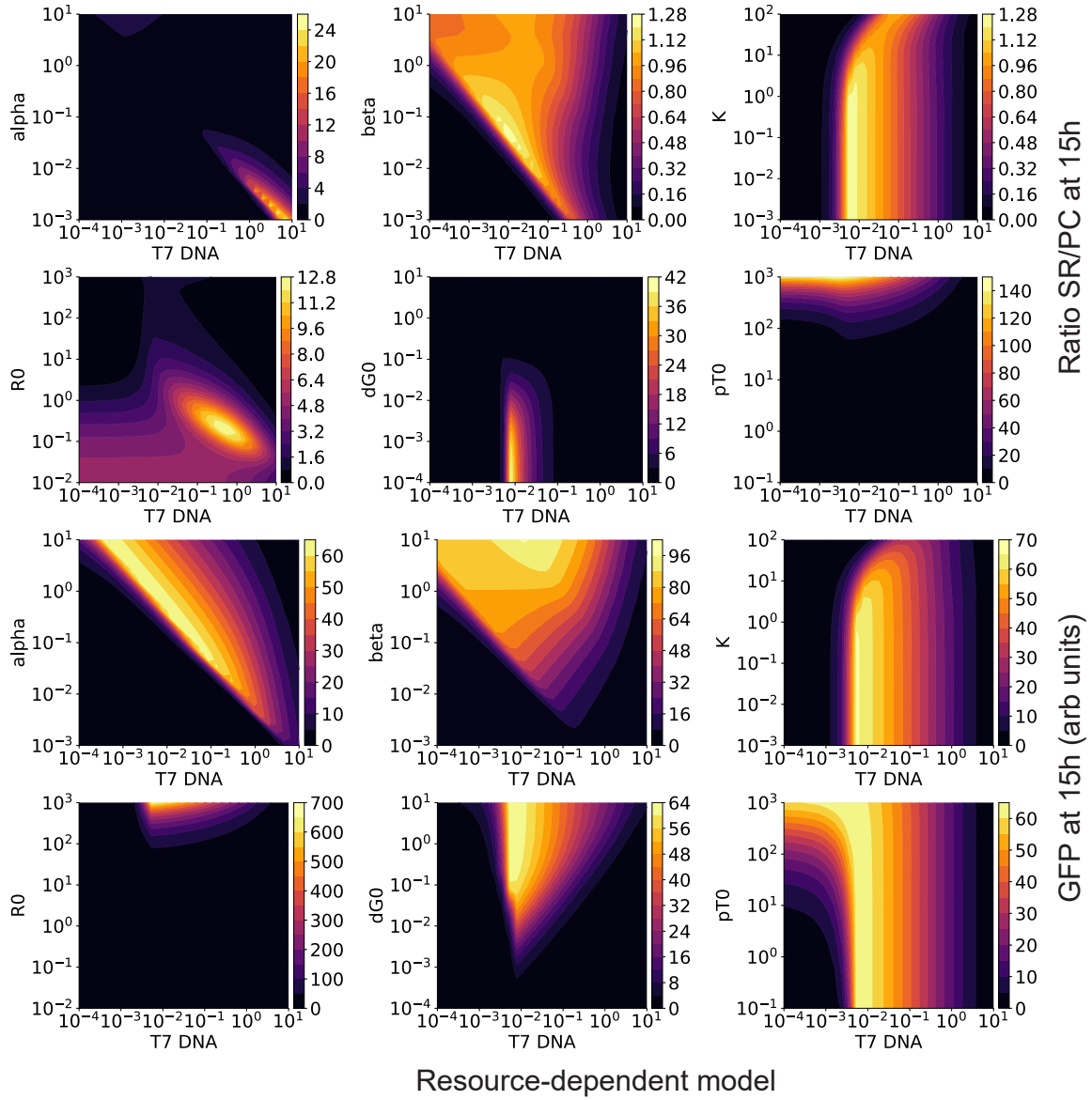


Figure 4.18: **Parameter variations for the resource-dependent model:**

The effects of parameter variations on SR/PC ratio (top) and total GFP yield (bottom) for the resource-dependent model. We observe that SR/PC ratios are high for small values of R_0 , or for very high T7 DNA concentrations combined with low transcription rates; both these cases correspond to a resource-constrained situation.

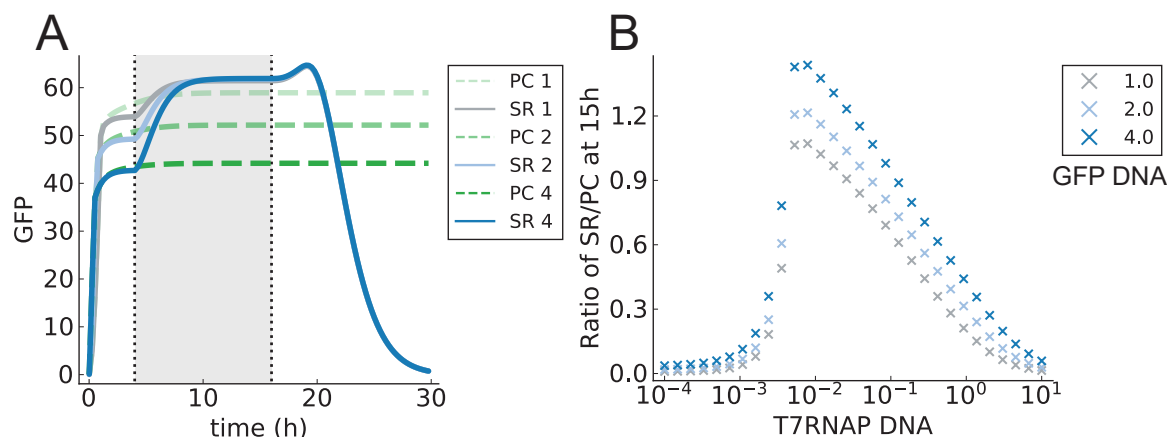


Figure 4.19: **The effect of varying eGFP DNA (for values of 1, 2, and 4 nondimensional units) on the SR/PC ratio:**

(A) The resource-dependent model predicts that increasing eGFP DNA concentration lowers the positive control, as the reaction reaches steady state sooner due to faster consumption of resources. (B) This results in an increased SR/PC ratio during the self-regeneration phase.

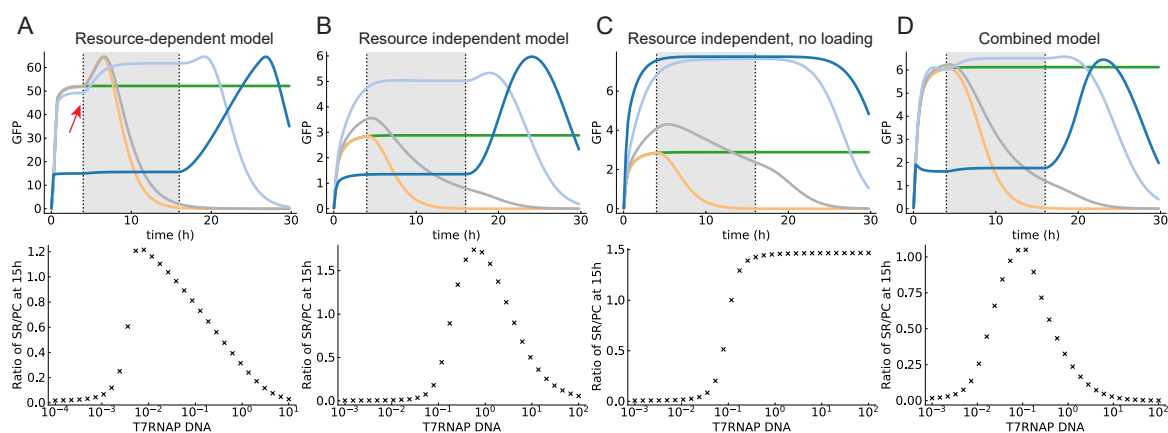


Figure 4.20: **Comparison of different models:**

A resource-independent model (B) can also capture qualitatively similar results as the resource-dependent model (A), showing a peak in eGFP production over a titration of T7 RNAP DNA. The major difference between the predicted behaviours is the rise in eGFP production after the beginning of the self-regeneration phase for the resource-dependent model (indicated by the red arrow), compared with the immediate rise at the beginning of the kick-start for the resource-independent model. Both models rely on coupling of eGFP and T7 RNAP production, through either a shared resource or enzyme. Removing the coupling eliminates the experimentally-observed optimum (C). In reality both effects are likely to be present, and a combined model (D) can also capture experimental results, at the expense of increased complexity.

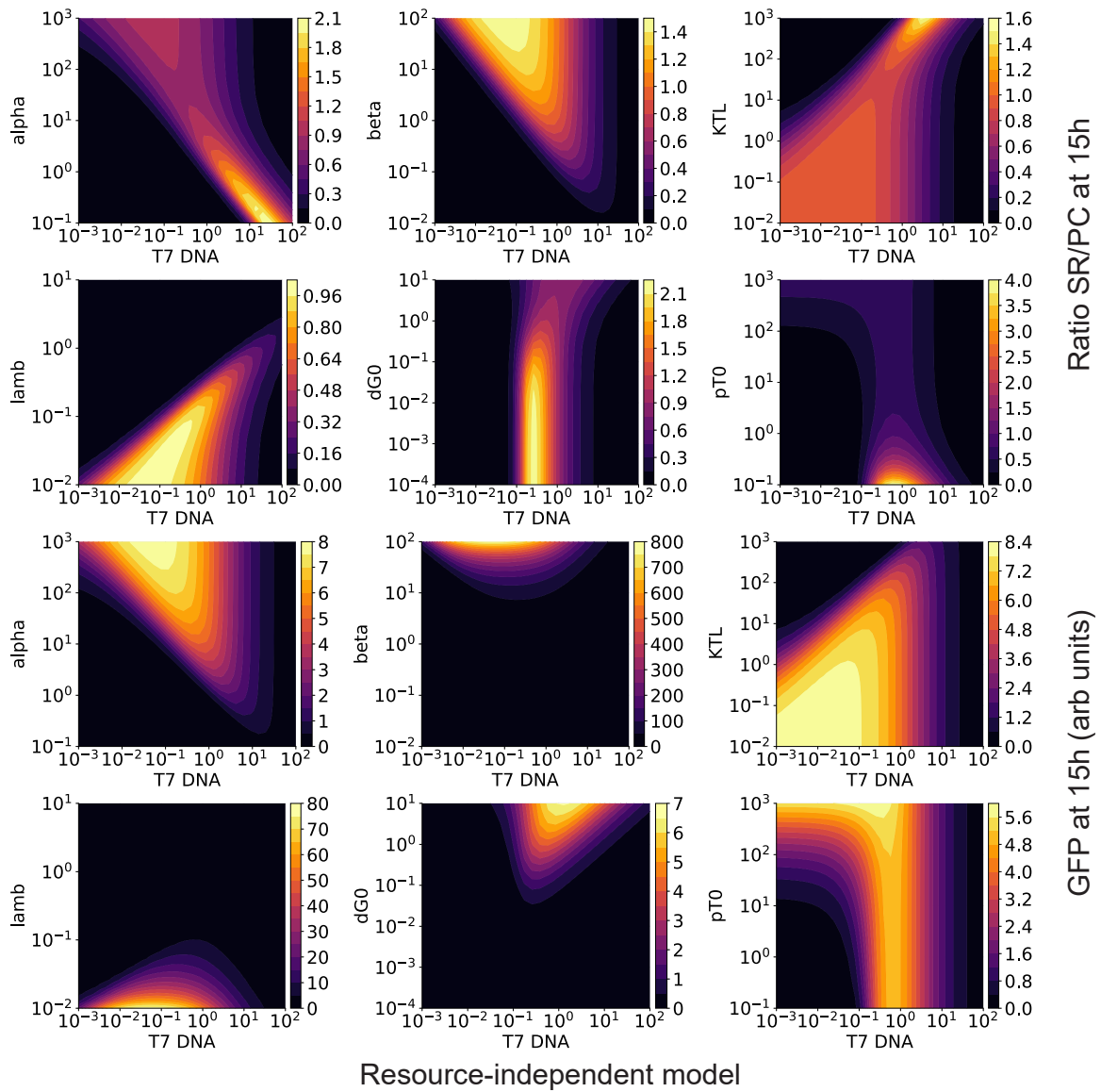


Figure 4.21: **Parameter variations for the resource-independent model:**

The effects of parameter variations on SR/PC ratio (top) and total GFP yield (bottom) for the resource-independent model. The variations are broadly similar to the resource-dependent model for the shared parameters α , β , dG_0 , and pT_0 . The behaviour of λ , the activity decay constant, is opposite to that of R_0 for the single resource model, as both parameters qualitatively limit the reaction lifetime. Finally, the model is sensitive to variations in the translation saturation constant K_{TL} .

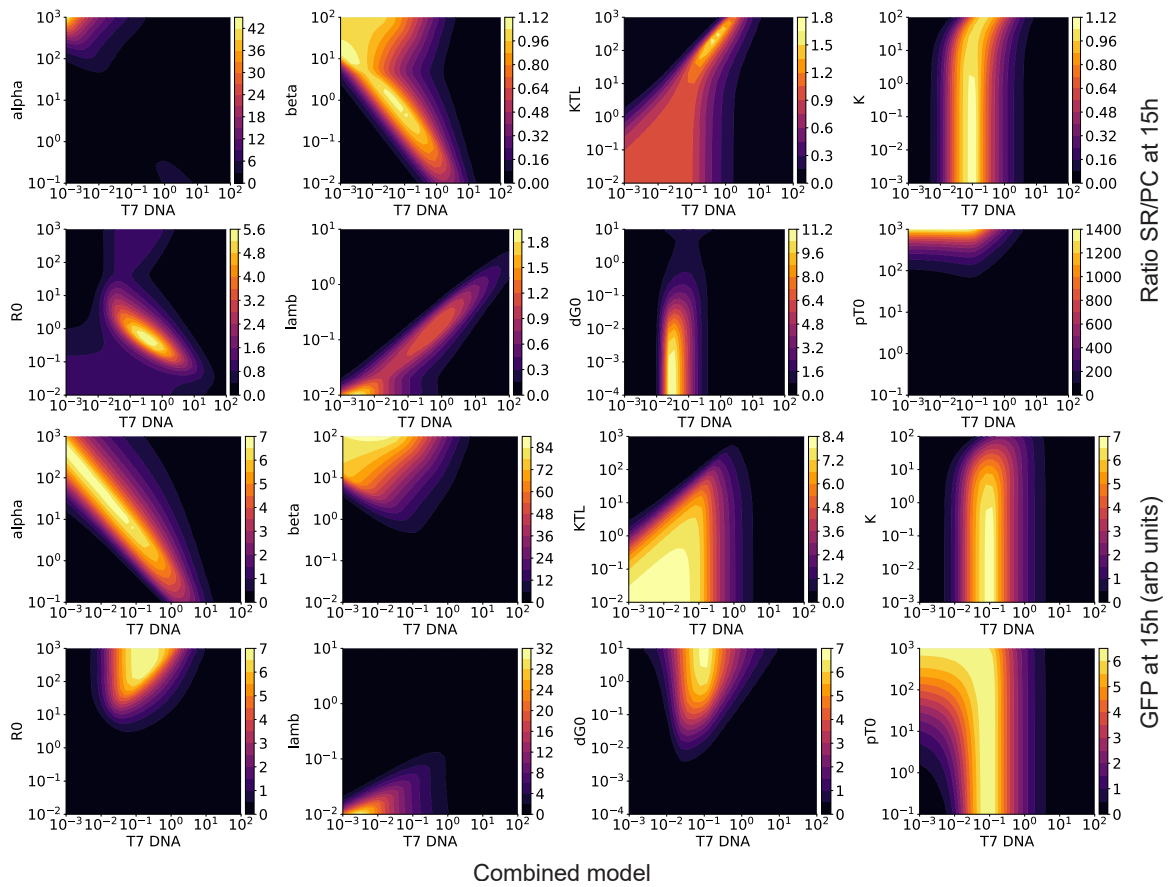


Figure 4.22: **Parameter variations for the combined model:**

The effects of parameter variations on SR/PC ratio (top) and total eGFP yield (bottom) for the combined model. The more complex model is sensitive to parameter variations, requiring fine-tuning to recapitulate experimental results.

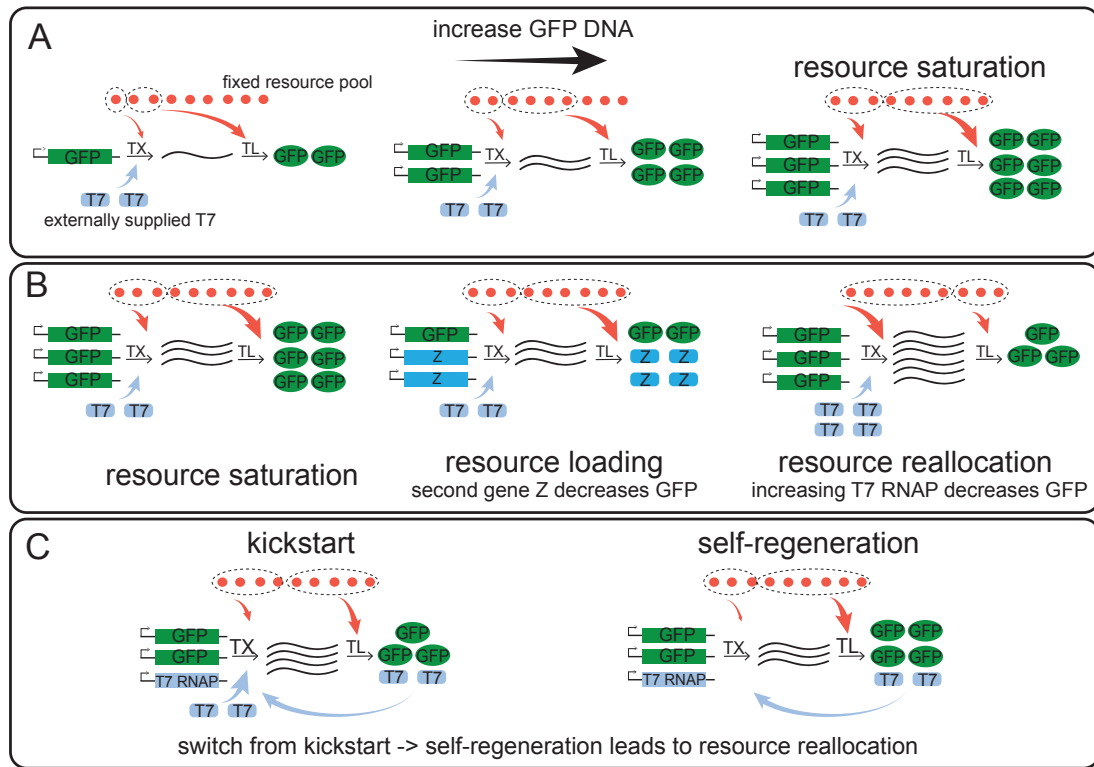


Figure 4.23: **Schematic description of the concepts of resource loading and resource allocation depicted in Figure 4.3G:**

(A) With increasing DNA concentration, the fixed resource pool gets saturated. (B) Resource loading is the distribution of a limited resource between two genes. Addition of different gene Z to GFP DNA leads to a decrease in the production of GFP. Resource allocation is the distribution of a limited resource between transcription (TX) and translation (TL). Increase in T7 RNAP concentration leads to redistribution of the resources from translation to transcription, and therefore decrease in GFP production. (C) Difference between resource distribution in the kickstart and self-regeneration phase. In the kickstart phase, T7 RNAP is both synthesised and supplied in the PURE system pushing the resources to transcription. In the self-regeneration phase, no T7 RNAP is provided in the Δ PURE leading to release of resources from transcription and an increase in GFP production.

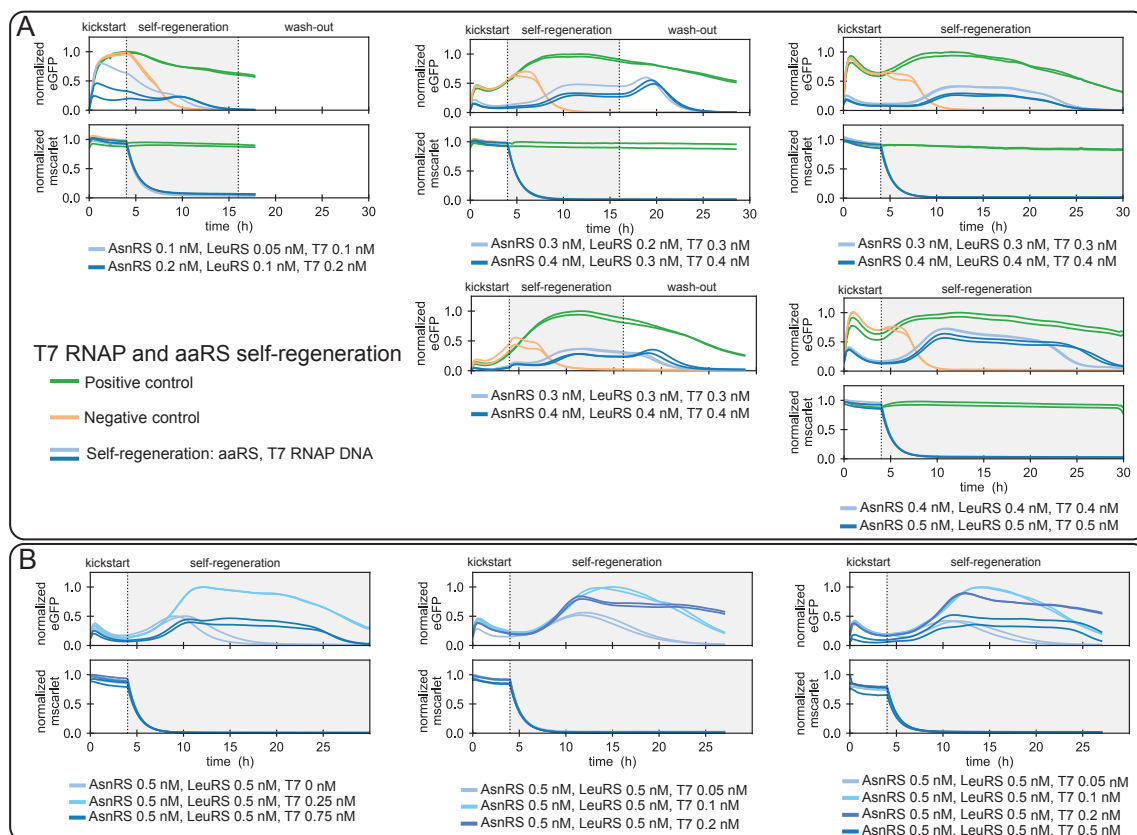


Figure 4.24: Multi-component regeneration:

Result summary of regeneration experiments with multiple components being regenerated. Regeneration of AsnRS, LeuRS and T7 RNAP is shown in (A). Titration of T7 RNAP DNA template is depicted in (B). The corresponding mScarlet traces for the given experiments are shown. The level of eGFP intensity is normalised to the maximum intensity obtained in the positive control or to the overall maximum intensity if no positive control was included (positive control: green, negative control: yellow, self-regeneration: blue). PURE composition used for the regeneration experiments are given in Supplementary Table 4.3. 2 nM of eGFP DNA template was used, and other DNA template concentrations are indicated in the corresponding graphs.

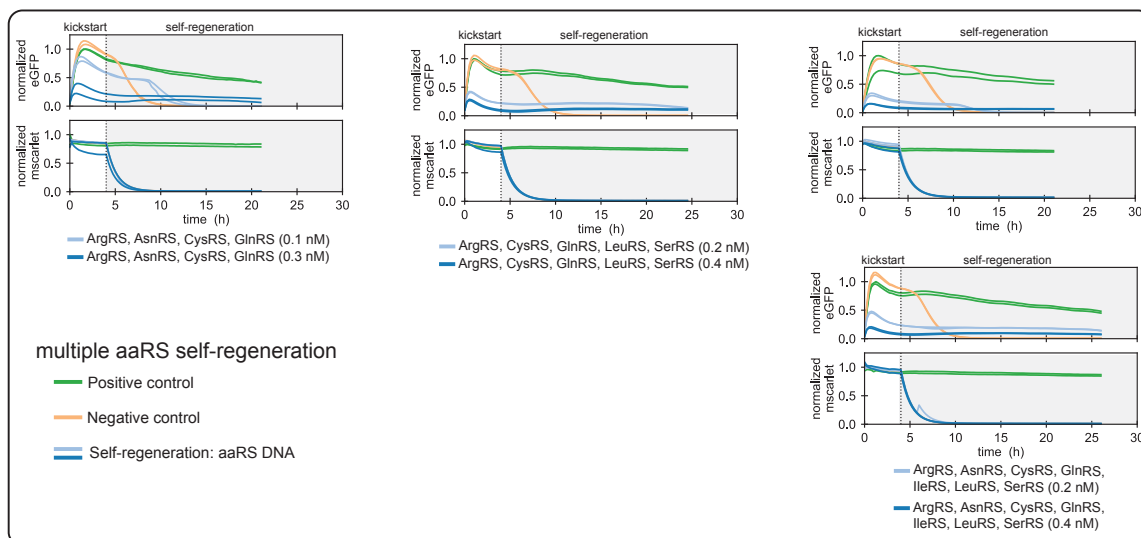


Figure 4.25: **Multiple aaRSs protein regeneration:**

Result summary of multiple aaRSs protein regeneration experiments. The corresponding mScarlet traces for the given experiments are shown. The level of eGFP intensity is normalised to the maximum intensity obtained in the positive control (positive control: green, negative control: yellow, self-regeneration: blue). PURE composition used for the regeneration experiments are given in Supplementary Table 4.3. 2 nM of eGFP DNA template was used, and other DNA template concentrations are indicated in the corresponding graphs.

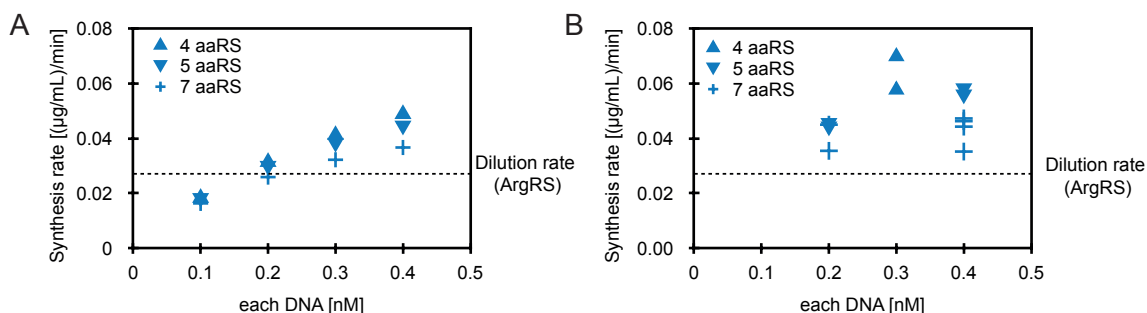


Figure 4.26: **Synthesis rate for single components in multi-component expression:**

(A) Theoretical synthesis rate for single component in multiple components expression, calculated based on eGFP synthesis rate in a microfluidic chemostat (0.44 μg/mL/min) and DNA loading in DNA saturated system. **(B)** Estimated synthesis for each component at different DNA concentrations based on the difference in eGFP synthesis rate for positive control and self-regeneration experiment at 15 hours. The eGFP synthesis rate was calculated based on an eGFP calibration curve (Supplementary Fig. 4.28B) and dilution rate. Dashed line represents the dilution rate of the highest concentrated component (ArgRS), based on the input component concentrations (Supplementary Table 4.4).

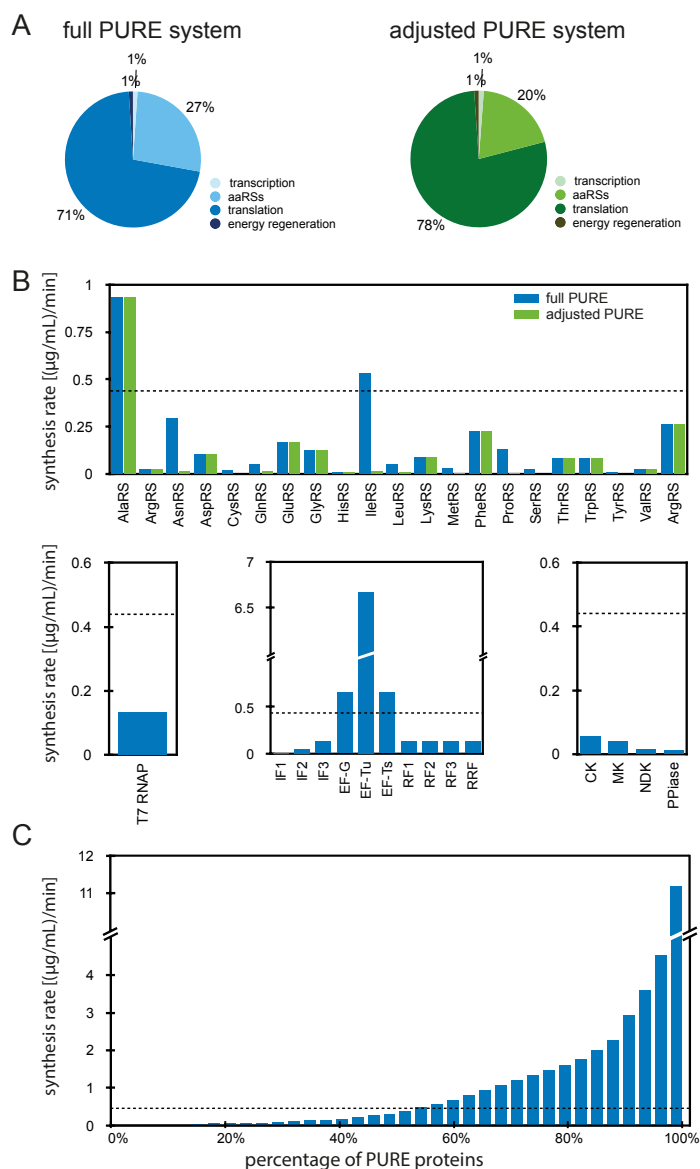


Figure 4.27: PURE system composition and synthesis rates:

(A) Schematic representation of the composition of the full PURE system (blue) and adjusted PURE system (green) used for multiple components regeneration. Detailed compositions are given in Supplementary Table 4.3. (B) Estimated minimal required synthesis rate of each PURE component based on dilution rate of each component (Supplementary Table 4.4) in comparison to the PURE synthesis rate (dashed line). (C) Estimated required cumulative synthesis rate for the regeneration of different PURE protein percentage in comparison to the PURE synthesis rate (dashed line). The PURE synthesis rate was calculated based on eGFP expression in a microfluidic chemostat.

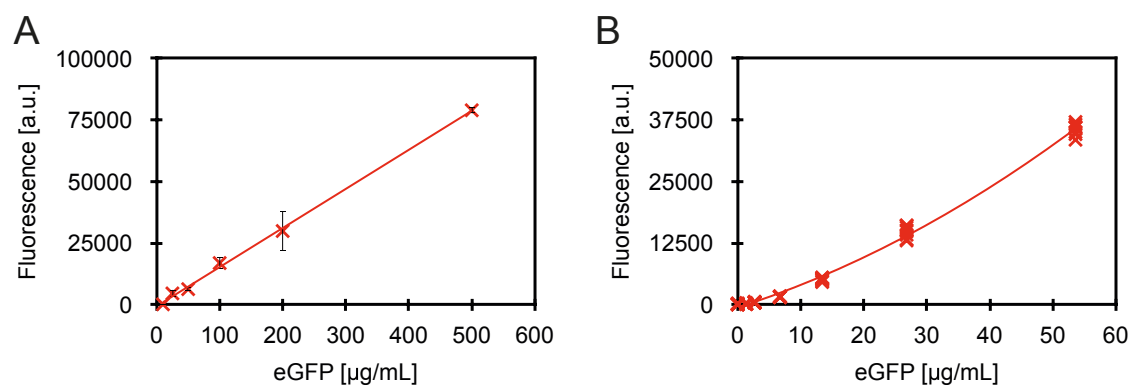


Figure 4.28: **Calibration curve for different eGFP (TP790050, AMS Biotechnology) concentrations in PBS:**

(A) Plate-reader: the standard curve was produced by measuring fluorescence over 60 min with the same settings as for *in vitro* expression. Excitation and emission wavelengths were 488 nm and 507 nm, respectively. Experiments were performed in triplicates. Fluorescence measurements in the first 20 min were not considered. Values are mean \pm s.d. ($n = 3$ technical replicates). (B) Microfluidic device: the standard curve was produced by measuring fluorescence over 10 min with the same settings as for *in vitro* expression. Each point represents individual reactor. The fit errors were not propagated as they were negligible compared to experimental errors.

4.7.2 Supplementary tables

Table 4.1: Microfluidic chip operations for self-regeneration experiments, including positive, and negative controls

Initial fill			
Step	Operation	Solution	Ring number
Repeat the following steps every 15 min			
0B	Energy solution addition		
	Flush rings	Buffer	1-8
	Flush rings	Energy solution	1-8
0C	PURE solution addition		
	Load 40% (Flush through outlet 60%)	PURE	1-8
0D	DNA solution addition		
	Load 20% (Flush through outlet 20%)	GFP DNA	1-4
	Load 20% (Flush through outlet 20%)	GFP DNA & protein DNA 1	5-6
	Load 20% (Flush through outlet 20%)	GFP DNA & protein DNA 2	7-8
0E	Mix		
Follow with dilution steps after 15 min			

kickstart			
Step	Operation	Solution	Ring number
Repeat the following steps every 15 min			
1A	Image each reactor		
Replace 20% of the ring content			
1B	Energy solution addition		
	Flush through outlet 20%	Buffer	1-8
	Load 8% (Flush through outlet 20%)	Energy solution	1-8
1C	PURE solution addition		
	Flush through outlet 12%	Buffer	1-8
	Load 8% (Flush through outlet 12%)	PURE	1-8
1D	DNA solution addition		
	Flush through outlet 4%	Buffer	1-8
	Load 4% (Flush through outlet 4%)	GFP DNA	1-4
	Load 4% (Flush through outlet 4%)	GFP DNA & protein DNA 1	5-6
	Load 4% (Flush through outlet 4%)	GFP DNA & protein DNA 2	7-8
1E	Mix		
Repeat from the step 1A-E			

self-regeneration			
Step	Operation	Solution	Ring number
Repeat the following steps every 15 min			
2A	Image each reactor		
Replace 20% of the ring content			
2B	Energy solution addition		
	Flush through outlet 20%	Buffer	1-8
	Load 8% (Flush through outlet 20%)	Energy solution	1-8
2C	PURE solution addition		
	Flush through outlet 12%	Buffer	1-8
	Load 8% (Flush through outlet 12%)	PURE	1-2
	Load 8% (Flush through outlet 12%)	Δ PURE	3-8
2D	DNA solution addition		
	Flush through outlet 4%	Buffer	1-8
	Load 4% (Flush through outlet 4%)	GFP DNA	1-4
	Load 4% (Flush through outlet 4%)	GFP DNA & protein DNA 1	5-6
	Load 4% (Flush through outlet 4%)	GFP DNA & protein DNA 2	7-8
2E	Mix		
Repeat from the step 2A-E			

wash-out			
Step	Operation	Solution	Ring number
Repeat the following steps every 15 min			
3A	Image each reactor		
Replace 20% of the ring content			
3B	Energy solution addition		
	Flush through outlet 20%	Buffer	1-8
	Load 8% (Flush through outlet 20%)	Energy solution	1-8
3C	PURE solution addition		
	Flush through outlet 12%	Buffer	1-8
	Load 8% (Flush through outlet 12%)	PURE	1-2
	Load 8% (Flush through outlet 12%)	Δ PURE	3-8
3D	DNA solution addition		
	Flush through outlet 4%	Buffer	1-8
	Load 4% (Flush through outlet 4%)	GFP DNA	1-8
3E	Mix		
Repeat from the step 3A-E			

Table 4.2: Microfluidic chip operations with four self-regeneration experiments

Initial fill			
Step	Operation	Solution	Ring number
Repeat the following steps every 15 min			
0B	Energy solution addition		
	Flush rings	Buffer	1-8
	Flush rings	Energy solution	1-8
0C	PURE solution addition		
	Load 40% (Flush through outlet 60%)	PURE	1-8
0D	DNA solution addition		
	Load 4% (Flush through outlet 4%)	GFP DNA & protein DNA 1	1-2
	Load 4% (Flush through outlet 4%)	GFP DNA & protein DNA 2	3-4
	Load 4% (Flush through outlet 4%)	GFP DNA & protein DNA 3	5-6
	Load 4% (Flush through outlet 4%)	GFP DNA & protein DNA 4	7-8
0E	Mix		
Follow with dilution steps after 15 min			

kickstart			
Step	Operation	Solution	Ring number
Repeat the following steps every 15 min			
1A	Image each reactor		
Replace 20% of the ring content			
1B	Energy solution addition		
	Flush through outlet 20%	Buffer	1-8
	Load 8% (Flush through outlet 20%)	Energy solution	1-8
1C	PURE solution addition		
	Flush through outlet 12%	Buffer	1-8
	Load 8% (Flush through outlet 12%)	PURE	1-8
1D	DNA solution addition		
	Flush through outlet 4%	Buffer	1-8
	Load 4% (Flush through outlet 4%)	GFP DNA & protein DNA 1	1-2
	Load 4% (Flush through outlet 4%)	GFP DNA & protein DNA 2	3-4
	Load 4% (Flush through outlet 4%)	GFP DNA & protein DNA 3	5-6
	Load 4% (Flush through outlet 4%)	GFP DNA & protein DNA 4	7-8
1E	Mix		
Repeat from the step 1A-E			

self-regeneration			
Step	Operation	Solution	Ring number
Repeat the following steps every 15 min			
2A	Image each reactor		
Replace 20% of the ring content			
2B	Energy solution addition		
	Flush through outlet 20%	Buffer	1-8
	Load 8% (Flush through outlet 20%)	Energy solution	1-8
2C	PURE solution addition		
	Flush through outlet 12%	Buffer	1-8
	Load 8% (Flush through outlet 12%)	Δ PURE	1-2
2D	DNA solution addition		
	Flush through outlet 4%	Buffer	1-8
	Load 4% (Flush through outlet 4%)	GFP DNA & protein DNA 1	1-2
	Load 4% (Flush through outlet 4%)	GFP DNA & protein DNA 2	3-4
	Load 4% (Flush through outlet 4%)	GFP DNA & protein DNA 3	5-6
	Load 4% (Flush through outlet 4%)	GFP DNA & protein DNA 4	7-8
2E	Mix		
Repeat from the step 2A-E			

Table 4.3: PURE system formulations used

SR experiment		PURE system	T7 RNAP	AsnRS	LeuRS	aaRSs + T7 RNAP	aaRSs
Protein		Concentration [µg/ml]					
AlaRS	Alanyl-tRNA synthetase	70.0	70.0	70.0	70.0	70.0	70.0
ArgRS	Arginyl-tRNA synthetase	2.0	2.0	2.0	2.0	2.0	2.0
AsnRS	Asparaginyl-tRNA synthetase	22.0	22.0	1.1	22.0	1.1	1.1
AspRS	Aspartate-tRNA synthetase	8.0	8.0	8.0	8.0	8.0	8.0
CysRS	Cysteinyl-tRNA synthetase	1.2	1.2	1.2	1.2	1.2	0.1
GlnRS	Glutaminyl-tRNA synthetase	3.8	3.8	3.8	3.8	3.8	1.0
GluRS	Glutamyl-tRNA synthetase	12.6	12.6	12.6	12.6	12.6	12.6
GlyRS	Glycyl-tRNA synthetase	9.6	9.6	9.6	9.6	9.6	9.6
HisRS	Histidyl-tRNA synthetase	0.8	0.8	0.8	0.8	0.8	0.8
IleRS	Isoleucyl-tRNA synthetase	40.0	40.0	40.0	40.0	40.0	1.0
LeuRS	Leucyl-tRNA synthetase	4.0	4.0	4.0	0.8	0.8	0.8
LysRS	Lysyl-tRNA synthetase	6.4	6.4	6.4	6.4	6.4	6.4
MetRS	Methionine-tRNA ligase	2.3	2.3	2.3	2.3	2.3	0.4
PheRS	Phenylalanyl-tRNA synthetase	17.0	17.0	17.0	17.0	17.0	17.0
ProRS	Prolyl-tRNA synthetase	10.0	10.0	10.0	10.0	10.0	0.4
SerRS	Seryl-tRNA synthetase	1.9	1.9	1.9	1.9	1.9	0.2
ThrRS	Threonyl-tRNA synthetase	6.2	6.2	6.2	6.2	6.2	6.2
TrpRS	Tryptophanyl-tRNA synthetase	6.3	6.3	6.3	6.3	6.3	6.3
TyrRS	Tyrosyl-tRNA synthetase	0.6	0.6	0.6	0.6	0.6	0.1
ValRS	Valyl-tRNA synthetase	1.8	1.8	1.8	1.8	1.8	1.8
IF1	Initiation factor 1	1.0	1.0	1.0	1.0	1.0	1.0
IF2	Initiation factor 2	4.0	4.0	4.0	4.0	4.0	4.0
IF3	Initiation factor 3	10.0	10.0	10.0	10.0	10.0	10.0
EF-G	Elongation factor G	50.0	50.0	50.0	50.0	50.0	50.0
EF-Tu	Elongation factor Tu	500.0	500.0	500.0	500.0	500.0	500.0
EF-Ts	Elongation factor Ts	50.0	50.0	50.0	50.0	50.0	50.0
RF1	Release factor 1	10.0	10.0	10.0	10.0	10.0	10.0
RF2	Release factor 2	10.0	10.0	10.0	10.0	10.0	10.0
RF3	Release factor 3	10.0	10.0	10.0	10.0	10.0	10.0
RRF	Ribosome recycling factor	10.0	10.0	10.0	10.0	10.0	10.0
MTF	Methionyl-tRNA formyltransferase	20.0	20.0	20.0	20.0	20.0	20.0
CK	Creatine kinase	4.0	4.0	4.0	4.0	4.0	4.0
MK	Adenylate kinase (Myokinase)	3.0	3.0	3.0	3.0	3.0	3.0
NDK	Nucleotide diphosphate kinase	1.1	1.1	1.1	1.1	1.1	1.1
PPiase	Inorganic pyrophosphatase	1.0	1.0	1.0	1.0	1.0	1.0
T7 RNAP	T7 RNA polymerase	10.0	10.0	10.0	10.0	10.0	10.0

Table 4.4: Calculated dilution rates based on concentrations in Table 4.3

SR experiment		PURE system	T7 RNAP	AsnRS	LeuRS	aaRSs + T7 RNAP	aaRSs
Protein		Dilution rate $[(\mu\text{g/mL})/\text{min}]$					
AlaRS	Alanyl-tRNA synthetase	0.93	0.93	0.93	0.93	0.93	0.93
ArgRS	Arginyl-tRNA synthetase	0.03	0.03	0.03	0.03	0.03	0.027
AsnRS	Asparaginyl-tRNA synthetase	0.29	0.29	0.015	0.29	0.015	0.015
AspRS	Aspartate-tRNA synthetase	0.11	0.11	0.11	0.11	0.11	0.11
CysRS	Cysteinyl-tRNA synthetase	0.02	0.02	0.02	0.02	0.02	0.001
GlnRS	Glutaminyl-tRNA synthetase	0.05	0.05	0.05	0.05	0.05	0.013
GluRS	Glutamyl-tRNA synthetase	0.17	0.17	0.17	0.17	0.17	0.17
GlyRS	Glycyl-tRNA synthetase	0.13	0.13	0.13	0.13	0.13	0.13
HisRS	Histidyl-tRNA synthetase	0.01	0.01	0.01	0.01	0.01	0.01
IleRS	Isoleucyl-tRNA synthetase	0.53	0.53	0.53	0.53	0.53	0.013
LeuRS	Leucyl-tRNA synthetase	0.05	0.05	0.05	0.011	0.011	0.011
LysRS	Lysyl-tRNA synthetase	0.09	0.09	0.09	0.09	0.09	0.09
MetRS	Methionine-tRNA ligase	0.03	0.03	0.03	0.03	0.03	0.005
PheRS	Phenylalanyl-tRNA synthetase	0.23	0.23	0.23	0.23	0.23	0.23
ProRS	Prolyl-tRNA synthetase	0.13	0.13	0.13	0.13	0.13	0.005
SerRS	Seryl-tRNA synthetase	0.03	0.03	0.03	0.03	0.03	0.003
ThrRS	Threonyl-tRNA synthetase	0.08	0.08	0.08	0.08	0.08	0.08
TrpRS	Tryptophanyl-tRNA synthetase	0.08	0.08	0.08	0.08	0.08	0.08
TyrRS	Tyrosyl-tRNA synthetase	0.01	0.01	0.01	0.01	0.01	0.001
ValRS	Valyl-tRNA synthetase	0.02	0.02	0.02	0.02	0.02	0.02
IF1	Initiation factor 1	0.01	0.01	0.01	0.01	0.01	0.01
IF2	Initiation factor 2	0.05	0.05	0.05	0.05	0.05	0.05
IF3	Initiation factor 3	0.13	0.13	0.13	0.13	0.13	0.13
EF-G	Elongation factor G	0.67	0.67	0.67	0.67	0.67	0.67
EF-Tu	Elongation factor Tu	6.67	6.67	6.67	6.67	6.67	6.67
EF-Ts	Elongation factor Ts	0.67	0.67	0.67	0.67	0.67	0.67
RF1	Release factor 1	0.13	0.13	0.13	0.13	0.13	0.13
RF2	Release factor 2	0.13	0.13	0.13	0.13	0.13	0.13
RF3	Release factor 3	0.13	0.13	0.13	0.13	0.13	0.13
RRF	Ribosome recycling factor	0.13	0.13	0.13	0.13	0.13	0.13
MTF	Methionyl-tRNA formyltransferase	0.27	0.27	0.27	0.27	0.27	0.27
CK	Creatine kinase	0.05	0.05	0.05	0.05	0.05	0.05
MK	Adenylate kinase (Myokinase)	0.04	0.04	0.04	0.04	0.04	0.04
NDK	Nucleotide diphosphate kinase	0.01	0.01	0.01	0.01	0.01	0.01
PPiase	Inorganic pyrophosphatase	0.01	0.01	0.01	0.01	0.01	0.01
eGFP	T7 RNA polymerase	0.13	0.13	0.13	0.13	0.13	0.13

Table 4.5: Replenishing schedule for modeling the three-stage experiment

Self-regeneration	Species replenished
Stage 1	R, d_T, d_G, p_T
Stage 2	R, d_T, d_G
Stage 3	R, d_G
Positive control	Species replenished
Stage 1	R, d_G, p_T
Stage 2	R, d_G, p_T
Stage 3	R, d_G, p_T

Table 4.6: DNA sequences

[illegible]

Table 4.7: Primer sequences

	Amplification Primers	Extension primers		
ArgRS	5'CCTCTAGAATAATTTTGTTAACTTAA GAAGGAGGAAAAAAAATGCAATATCA GGCTCTTCTCGAGAAAAAGTCC 3'	5'GTAGCAGCCTGAGTCGTTATTACATC GCTCTACAGTCTCAATACCCGAGC 3'	5'GATCTTAAGGCTAGAGTACTAATACGA CTCAGCTATAGGAGACCCAAACGGTTT CCCTCTAGAAATAATTTTGTTTAAC 3'	5'CAAAAAACCCCTCAAGACCCGGTTA GAGGCCCAAGGGGTATGCTAGTTT TTTTTTTTTTTTTTTTTTTTTTTGTAC CAGCCTGAGTCG 3'
AsnRS	5'CCTCTAGAATAATTTTGTTAACTTAA GAAGGAGGAAAAAAAATGAGCGTGT GCCTGTGACCG 3'	5'GTAGCAGCCTGAGTCGTTATTAGAAG CTGGCGTTACGCGGAGTAC 3'	5'GATCTTAAGGCTAGAGTACTAATACGA CTCAGCTATAGGAGACCCAAACGGTTT CCCTCTAGAAATAATTTTGTTTAAC 3'	5'CAAAAAACCCCTCAAGACCCGGTTA GAGGCCCAAGGGGTATGCTAGTTT TTTTTTTTTTTTTTTTTTTTTTTGTAC CAGCCTGAGTCG 3'
CysRS	5'CCTCTAGAATAATTTTGTTAACTTAA GAAGGAGGAAAAAAAATGCTAAAT CTTCAATACGCTACGACGC 3'	5'GTAGCAGCCTGAGTCGTTATTACTAC GACGCGAGTGGTCCC 3'	5'GATCTTAAGGCTAGAGTACTAATACGA CTCAGCTATAGGAGACCCAAACGGTTT CCCTCTAGAAATAATTTTGTTTAAC 3'	5'CAAAAAACCCCTCAAGACCCGGTTA GAGGCCCAAGGGGTATGCTAGTTT TTTTTTTTTTTTTTTTTTTTTTTGTAC CAGCCTGAGTCG 3'
GlnRS	5'CCTCTAGAATAATTTTGTTAACTTAA GAAGGAGGAAAAAAAATGAGTGAAG CAGAAGCCGC 3'	5'GTAGCAGCCTGAGTCGTTATTACTCG CCTACTTTGCCCGAGTATC 3'	5'GATCTTAAGGCTAGAGTACTAATACGA CTCAGCTATAGGAGACCCAAACGGTTT CCCTCTAGAAATAATTTTGTTTAAC 3'	5'CAAAAAACCCCTCAAGACCCGGTTA GAGGCCCAAGGGGTATGCTAGTTT TTTTTTTTTTTTTTTTTTTTTTTGTAC CAGCCTGAGTCG 3'
IleRS	5'CCTCTAGAATAATTTTGTTAACTTAA GAAGGAGGAAAAAAAATGCTGACTA TAATACACCTCGAATTTGCC 3'	5'GTAGCAGCCTGAGTCGTTATTAGCCA AACTAGCTGTTTCCACGCTCAC 3'	5'GATCTTAAGGCTAGAGTACTAATACGA CTCAGCTATAGGAGACCCAAACGGTTT CCCTCTAGAAATAATTTTGTTTAAC 3'	5'CAAAAAACCCCTCAAGACCCGGTTA GAGGCCCAAGGGGTATGCTAGTTT TTTTTTTTTTTTTTTTTTTTTTTGTAC CAGCCTGAGTCG 3'
LeuRS	5'CCTCTAGAATAATTTTGTTAACTTAA GAAGGAGGAAAAAAAATGCAAGAGCA ATACCCGCC 3'	5'GTAGCAGCCTGAGTCGTTATTAGCCA ACGACCAAGTATGAGGAGTTTAC 3'	5'GATCTTAAGGCTAGAGTACTAATACGA CTCAGCTATAGGAGACCCAAACGGTTT CCCTCTAGAAATAATTTTGTTTAAC 3'	5'CAAAAAACCCCTCAAGACCCGGTTA GAGGCCCAAGGGGTATGCTAGTTT TTTTTTTTTTTTTTTTTTTTTTTGTAC CAGCCTGAGTCG 3'
SerRS	5'CCTCTAGAATAATTTTGTTAACTTAA GAAGGAGGAAAAAAAATGCTCGATCC CAATCTGCTGC 3'	5'GTAGCAGCCTGAGTCGTTATTAGCCAA TATATCCAGTCGCTTCATATAGC 3'	5'GATCTTAAGGCTAGAGTACTAATACGA CTCAGCTATAGGAGACCCAAACGGTTT CCCTCTAGAAATAATTTTGTTTAAC 3'	5'CAAAAAACCCCTCAAGACCCGGTTA GAGGCCCAAGGGGTATGCTAGTTT TTTTTTTTTTTTTTTTTTTTTTTGTAC CAGCCTGAGTCG 3'
T7 RNAP	5'CCTCTAGAATAATTTTGTTAACTTAA GAAGGAGGAAAAAAAATGCAACAGT TAACATCGCTAGAGCAAGCTTC 3'	5'GTAGCAGCCTGAGTCGTTATTACGCG AAGCGGAAGTCG 3'	5'GATCTTAAGGCTAGAGTACTAATACGA CTCAGCTATAGGAGACCCAAACGGTTT CCCTCTAGAAATAATTTTGTTTAAC 3'	5'CAAAAAACCCCTCAAGACCCGGTTA GAGGCCCAAGGGGTATGCTAGTTT TTTTTTTTTTTTTTTTTTTTTTTGTAC CAGCCTGAGTCG 3'
DNA sequence				
Linear DNA fragment	gattcttaaggctagagctcaatcagctcactataggagaccacaagcttcctctagaasatttggtaacttaagaggagggaaaaaaATG—protein— taatacagctaggctgcacaaaasaaaaasaaaaasaaaaaaatacagctacacccctgggctgggctcgaaggtcttgagggtttttg			
Blue	T7 promoter			
Red	RBS			
Bold	T7 terminator			

Table 4.8: Buffers and energy solution

PURE buffer

Compound	Catalog number	Company	Buffer A	Buffer B	HT buffer	Stock buffer	Note
			mM	mM	mM	mM	
HEPES	H0887-100ML	Sigma-Aldrich	50	50	50	50	pH = 7.6
Ammonium chloride	09718-250G	Sigma-Aldrich	1000				
Magnesium chloride	63020-1L	Honeywell Fluka	10	10	10	10	
Potassium chloride	P5405-1KG	Sigma-Aldrich		100	100	100	
Imidasol	I2399	Sigma-Aldrich		500			pH = 7
Glycerol	G7757-1L	Sigma-Aldrich				30%	
β-mercaptoethanol	M6250-100ML	Sigma-Aldrich	7	7	7	7	

Ribosome purification buffers

Compound	Catalog number	Company	Buffer C	Buffer D	Ribosome buffer	Note
			mM	mM	mM	
HEPES	H0887-100ML	Sigma-Aldrich			20	pH = 7.6
Tris-HCl	BP152-500	Fisher	20	20		
Magnesium acetate	M0631	Sigma-Aldrich			6	
Magnesium chloride	63020-1L	Honeywell Fluka	10	10		
Potassium chloride	P5405-1KG	Sigma-Aldrich	150	150	30	
Ammonium chloride	09718-250G	Sigma-Aldrich	30	30		
Imidasol	I2399	Sigma-Aldrich		150		pH = 7
β-mercaptoethanol	M6250-100ML	Sigma-Aldrich	7	7	7	

Energy solution

Compound	Catalog number	Company	Concentration in reaction	Concentration in subset (2.5x)	Units
Amino acids	LAA21-1KT	Sigma-Aldrich	0.3	0.75	mM
Magnesium acetate	M0631	Sigma-Aldrich	11.8	29.5	mM
Potassium glutamate	49601	Sigma-Aldrich	100	250	mM
TCEP	646547	SantaCruz Biotech	1	2.5	mM
ATP	R0481	ThermoFisher	2	5	mM
GTP	R0481	ThermoFisher	2	5	mM
CTP	R0481	ThermoFisher	1	2.5	mM
UTP	R0481	ThermoFisher	1	2.5	mM
tRNA	10109541001	Roche	52	130	U _{A260} /mL
Creatine phosphate	27920	Sigma-Aldrich	20	50	mM
Folinic acid	PHR1541	Sigma-Aldrich	0.02	0.05	mM
Spermidine	S2626	Sigma-Aldrich	2	5	mM
HEPES	H0887-100ML	Sigma-Aldrich	50	125	mM

5 Continuous-exchange cell-free expression in microfluidic chemostats with hydrogel membranes

5.1 Introduction

A reconstituted cell-free transcription-translation (TX-TL) system is a viable chassis for constructing a synthetic cell. However, one of the critical requirements of a synthetic cell in terms of its protein synthesis rate is sufficient synthesis rate to regenerate all of its components. We recently demonstrated that components of the PURE system could be regenerated in a microfluidic-based synthetic cell (Chapter 4) [181]. However, the synthesis rate and yield in the recombinant cell-free system are currently orders of magnitude away from being able to regenerate all of its components.

A standard cell-free protein synthesis system in batch configuration ceases mainly due to the rapid depletion of the key components, i.e., NTPs. This rapid approach to chemical equilibrium can be overcome by providing replenishment of substrates and the enzymatic machinery while at the same time diluting away reaction products [132, 134, 166]. This approach allows for an efficient protein turnover but does not lead to a sufficient increase in production rate. A protein synthesis yield can successfully be increased in a continuous-exchange reaction format [23]. These passive diffusion exchange systems based on dialysis allow for the exchange of small molecules with the environment while retaining the TX-TL machinery within a defined reaction compartment [182]. The continuous-exchange reaction formats mostly rely on separating a large volume of feeding solution from in comparison small TX-TL reaction, either by carrying out standard tube-based dialysis [95] or by implementing dialysis membrane to a micro-well plate [124, 127] or a passive PDMS microreactor [128]. By enabling the protein synthesis to last for up to several days, synthesis yields in the range of mg/mL of protein can be achieved [95]. Although the time of the synthesis is extended, the reaction reaches chemical equilibrium eventually. Therefore, integration of replenishment of the small molecules, together with the replenishment of the enzymatic machinery, is crucial to achieving adequate synthesis rates in dynamical systems such as oscillators or self-replicating systems.

Integration of a dialysis membrane into a microfluidic reactor requires a complex assembly, limiting the complexity of the system. Recently, poly(ethylene glycol) diacrylate (PEG-DA) membranes were implemented in a simple PDMS microfluidic chip via direct UV writing and utilized for protein crystallization [183]. The membrane fabrication by photo-patterning directly inside a microfluidic channel offers many advantages, as simple membrane integration and the ability to form hydrogels at varying levels of permeability [184]. However, it holds challenges, such as anchoring of hydrogel to the PDMS walls and complex hydrogel patterning.

In this work, we designed a microfluidic chemostat with integrated PEG-DA membranes, which should allow for simultaneous implementation of continuous-exchange and steady-state reactions. Moreover, we report a simple way to avoid water evaporation from PDMS at low humidity and elevated temperature. Furthermore, we describe a simple silanization protocol, which does not require the use of plasma and solvents, and a technique allowing simple PEG-DA hydrogel membranes patterning in an oxygen-free environment with pneumatic valves. Additionally, we report on how to vary the permeability of the membranes to achieve an ideal membrane cut-off for continuous-exchange TX-TL reaction and show that the protein synthesis in the chemostat reactor

can be extended when the continuous-exchange reaction is implemented.

5.2 Results

To overcome the limits in the protein synthesis yield while preserving the advantage of protein turnover, we designed a microfluidic chip (Figure 5.1a, b) enabling continuous protein synthesis and continuous-exchange reaction format simultaneously. A previous microfluidic reactor design with fluidically hard-coded dilution fractions defined by the reactor geometry [166] was utilized to maintain the protein turnover, and a feeding channel to allow for a continuous supply of small molecules was included on the bottom of the reactor. PEG-DA hydrogel membranes were patterned between the reactor and the feeding channel to enable small molecule exchange with the feeding channel without dilution of the TX-TL machinery.

5.2.1 Prevention of evaporation in microfluidic chip

A common challenge with PDMS-based microfluidic chips is evaporation through PDMS due to its porosity. This challenge is heightened at elevated temperatures required for cell culturing, thermocycling, and cell-free protein synthesis. Salts concentrations have a crucial role in cell-free systems, and are essential to achieving good synthesis yields. Therefore, any changes in the concentrations of the components due to evaporation limit the ability to extend the reaction. There are many different approaches to prevent evaporation from PDMS: submerging the whole chip in water [185], placement of water-filled reservoirs on-chip [186, 187], polyethylene [188], or parylene C film water-proof layer [189, 190]. However, most of these methods are not compatible with cell-free expression or pneumatic valve-based microfluidic chips. An anti-evaporation water chamber is an appalling choice for implementation in a microfluidic chip with pneumatic valves. However, so far, an anti-evaporation water chamber was not successfully implemented in a microfluidic chip while pneumatic valves were in use. In addition, water chambers often require challenging assembly and fluid filling [191–193].

As seen in Figure 5.1c, without any evaporation prevention, severe evaporation can be seen after only 2 hours. Although, the evaporation was lower when the chamber humidity was increased, a significant evaporation (data not shown) was still observed. Therefore, we implemented a third (anti-evaporation) PDMS layer to the classical double-layer microfluidic setup to prevent the evaporation (Figure 5.1d). The flow layer PDMS thickness was decreased to around 0.3 cm; this thickness ensures sufficient space for connector pin attachment while keeping the anti-evaporation layer in close adjacency to the flow layer. The anti-evaporation layer, composed of a dead-end serpentine channel, was aligned above the reactors and attached by oxygen plasma on top of the flow layer (Figure 5.1e, f). During the experiment, the channel was connected to water-filled tubing, which was pressurized to maintain a constant water supply to the water-chamber channel (Figure 5.1g). This design is easy to fabricate, assemble, and can be applied to most standard double layer microfluidic designs without additional hardware. As shown in Figure 5.1c, with the anti-evaporation layer, no discernable evaporation was observed even after 16 hours.

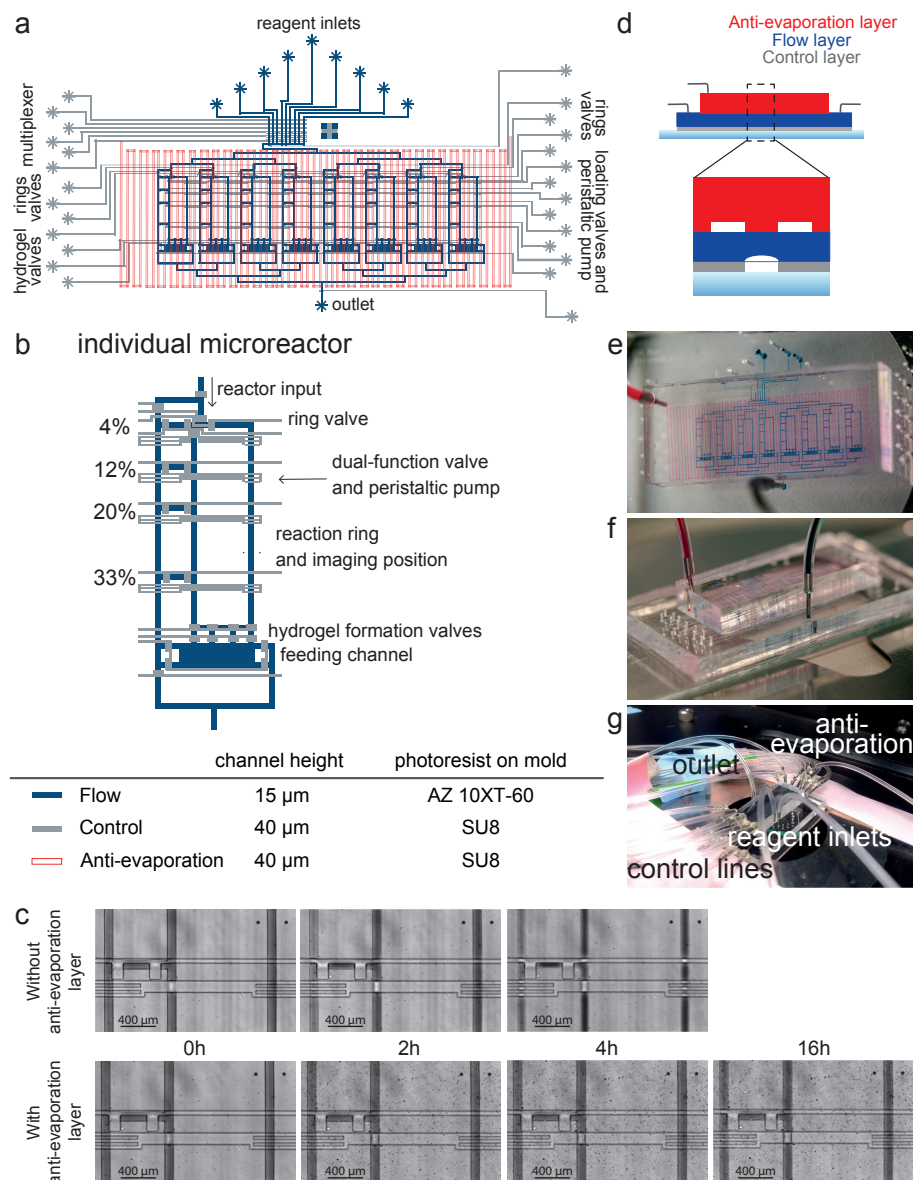


Figure 5.1: **Design of microfluidic device with hydrogel membranes:**

(a) Design schematic of the microfluidic device. The control layer is shown in grey, the flow layer in blue, and anti-evaporation layer in red. The device contains eight chemostat reactors. (b) Close-up of a microfluidic reactor and table of channel heights and corresponding photoresists used in mold fabrication. Each reactor has four outlets corresponding to four different dilution fractions. Four control lines serve dual-functions as valves and peristaltic pump. The width of a flow channel is 100 μm . (c) Comparison of the water evaporation in the chip with and without the anti-evaporation layer at different times at 34 $^{\circ}\text{C}$. The flow channels were filled with blue dye for better visualization. (d) Schematic depiction (not to scale) of microfluidic chip cross-section. Image of microfluidic chip from top (e) and from side (f), for visualization the flow channels and the anti-evaporation channel are filled with blue and red dye, respectively. (g) Image of microfluidic chip connected to the control lines, reagent inputs and outlet.

5.2.2 Formation of PEG-DA hydrogel

Though PEG-DA hydrogel membrane can be formed inside a PDMS chip with direct UV writing [183], its requirements limits the design complexity. Hence, we decided to pattern the membranes using pneumatic valves. Moreover, thinner ($25\ \mu\text{m}$) and longer membranes ($9.1\ \text{mm}$) showed to be able to withstand much less trans-membrane pressure drops than shorter ($500\ \mu\text{m}$) membranes. In the chemostat, the pressure on the membranes is not only imposed during the pressure-driven loading phase but also due to a volume displacement from pneumatic valve actuation. As the mixing inside of the microfluidic reactor is driven by peristaltic pumps, the membranes are under constant pressure over extended periods. Moreover, the difference in the composition of the buffers generated osmotic pressures. Therefore, to ensure long-term hydrogels adherence to the PDMS, we decided to form four shorter ($100\ \mu\text{m}$) and thicker ($100\ \mu\text{m}$) membranes, rather than one longer membrane.

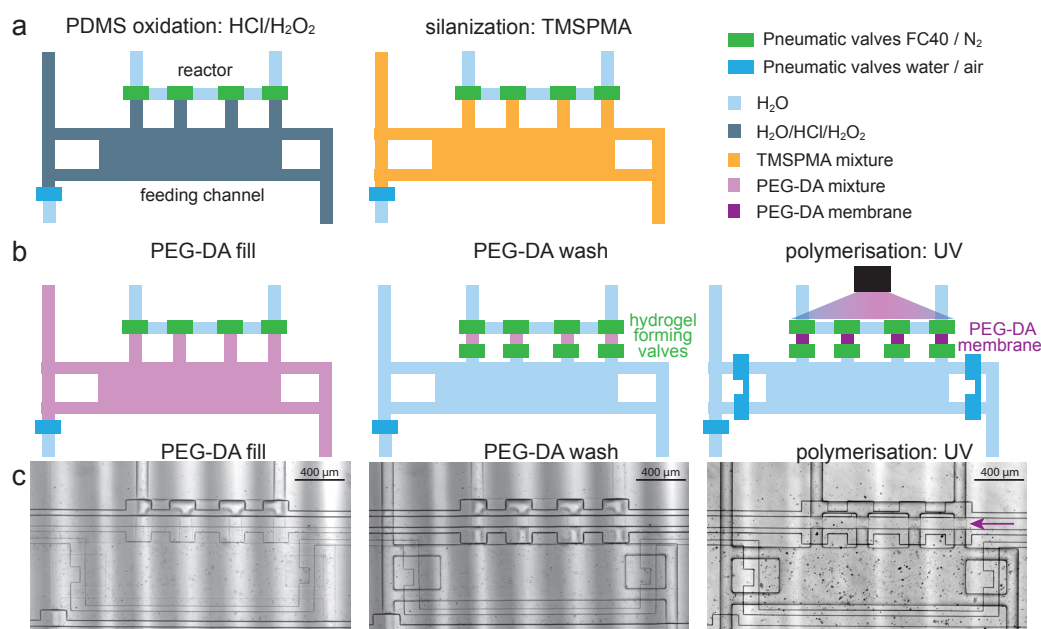


Figure 5.2: **Hydrogel membranes formation:**

(a) Schematic depiction of protocol for making hydrogel membranes. The feeding channel is first oxidized with hydrochloric acid and hydrogen peroxide mixture, followed by silanization with TMSPMA. (b) In the second step, PEG-DA polymer solution is injected into the feeding channel after the hydrogel-forming valves are closed, and the PEG-DA solution from the feeding channel is flushed out with water before the remaining PEG-DA is polymerized. The hydrogel-forming valves are filled with Fluorinert FC-40 and pressurized by nitrogen instead of water and air used for the remaining valves. (c) Microscope images of the different steps involved in hydrogel membranes formation corresponding to the steps in panel (b), scale bar $400\ \mu\text{m}$.

The formation of PEG-DA membranes was initially tested in a non-silanized chip. Though the polymerization of the membranes was successful, the adherence of membranes varied with water content in the PEG-DA mixture and with the types of buffers used in subsequent reactions. There-

fore, the PDMS walls were silanized to strongly anchor the hydrogels to withstand the imposed trans-membrane pressure drops. The control over the fluid in different parts of the chip is the main advantage of pneumatic valves. Therefore, silanization (Figure 5.2a) was performed only in the feeding channel and not in the reactor. The plasma treatment is often utilized to oxidize the PDMS walls before silanization [183]. However, due to the design of the flow layer above the control layer, a plasma treatment could not be implemented. Accordingly, the channels walls were oxidized by hydrochloric acid / hydrogen peroxide treatment [194, 195]. After oxidation, TMSPMA hydrolyzed in acidic conditions was injected into the channels and followed by thorough rinsed with water [196].

In the presence of oxygen, the hydrogel does not adhere to the PDMS due to the formation of a thin uncrosslinked layer [183]. Therefore, the polymerization of membranes has to be performed in an oxygen-free environment. Accordingly, the hydrogel-forming valves and the anti-evaporation layer were pressurized with nitrogen instead of air. Moreover, the PEG-DA polymerization solution, composed of the PEG-DA polymer, photo-initiator, and water, was purged with nitrogen. The oxygen-free solution was then injected into the feeding channel, before the hydrogel-forming valves were closed, the excess solution was washed away, and the remaining solution was polymerized (Figure 5.2b,c). The hydrogel membranes were highly stable against rupture and could withstand the imposed trans-membrane pressure over several days.

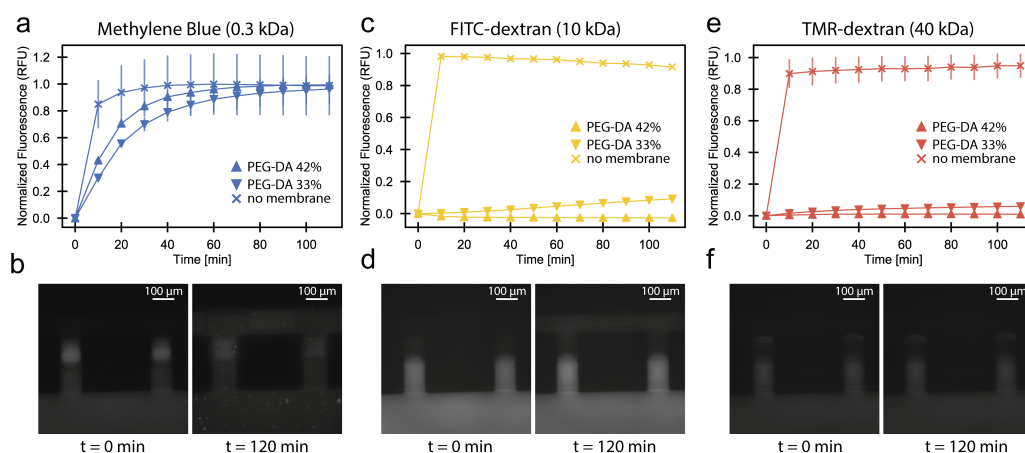


Figure 5.3: Solute diffusion through the membrane:

Diffusion of (a, b) methylene blue, (c, d) 10 kDa FITC-dextran, (e, f) 40 kDa TMR-dextran, from the enclosed feeding channel to the reactor chamber through the membrane over time. The methylene blue fluorescence was normalized to the maximum level attained in each experiment, for 10 kDa FITC-dextran and 40 kDa TMR-dextran fluorescence was normalized to the maximum level attained in reactors with no membrane.

To form hydrogel membranes of varying permeability, water at various ratios was added into the polymer mixture. Water acts as a porogen during polymerization. The higher the content of water, the larger the size of the pores in the formed membrane. In order to determine the permeability of the hydrogel membranes, diffusion of different molecular weight solutes from feeding channels

to the chemostat reactor was tested (Figure 5.3). While small molecular weight methylene blue diffused rapidly to the ring for both PEG-DA formulations, 10 kDa and 40 kDa dextran diffused into the rings at a much slower rate and only for the 33% PEG-DA formulation, showing that the membranes permeability can be adjusted with the amount of water added to the polymer mixture. The membranes are particularly suitable for any dialysis application with a molecular cut-off in the 10–40 kDa range, which is in agreement with previously reported values [183]. This makes the formed membrane ideal candidates for continuous-exchange protein synthesis format.

5.2.3 Cell-free expression

The PURE system batch reaction terminates on chip after only one hour (Figure 5.4a), due to the lack of an energy source, such as ATP, and accumulation of by-products, which hinders long-term protein synthesis in cell-free system. Continuous-exchange or dialysis mode showed to improve the protein yield in this system.

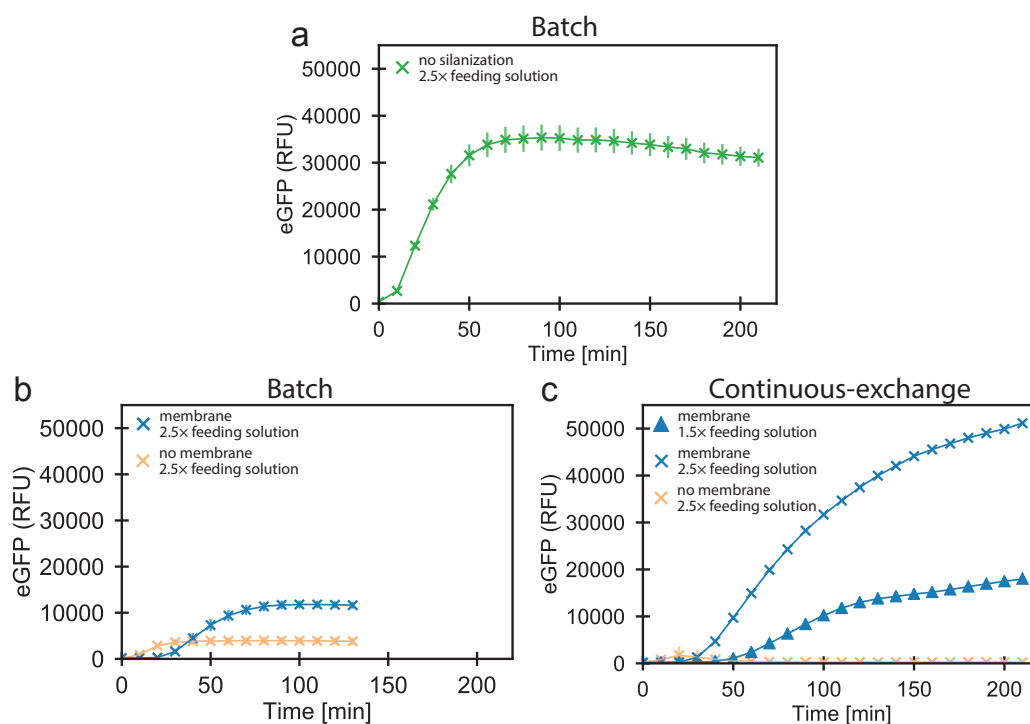


Figure 5.4: **Cell-free expression in microfluidic device with hydrogel membranes:**

Batch eGFP expression over time in non-silanzed microfluidic chip (a) and the silanzed chip with and without membrane hydrogel (b). The TX-TL machinery and DNA was loaded to the reactor, and 2.5× energy solution was loaded to the feeding channels. (c) Continuous-exchange cell-free expression in the silanzed chip with and without membrane hydrogel. The TX-TL machinery and DNA was loaded to the reactor. Energy solutions at two different concentrations were supplied to the feeding channel every 10 minutes.

To ensure that small molecules can diffuse to the ring from the feeding channel, the chemostat ring

was filled with PURE system and DNA, while energy solution was loaded into the feeding channel (Figure 5.4b). As the small molecules first have to diffuse into the reactor before the expression initiates, a slightly delayed expression was observed in rings with membranes. However, a higher yield was observed for those rings compare to rings without membranes, probably due to higher proteins and ribosome concentration in the reactors as the machinery is not diluted when mixed with the energy solution from the feeding channel. Nevertheless, a lower synthesis was observed in silanized chip compare to non-silanized.

To prolong the reaction and, therefore, the protein synthesis, a continuous-exchange mode was tested (Figure 5.4c). Two different energy solution concentrations were supplied to the feeding channel every 10 minutes. For both concentrations, the reaction lifespan was significantly extended to a minimum of 3 hours. Moreover, the $2.5\times$ energy solution concentration resulted in a higher expression yield compare to $1.5\times$ energy solution concentration and the batch reaction in a non silanized chip.

5.3 Conclusion

We demonstrated that it is possible to produce PEG-DA hydrogel membranes with an adjustable permeability, able to withstand trans-membrane pressures in microfluidic PDMS chip with integrated pneumatic valves. Our microfluidic design allows for simple membrane patterning with valves pressurized with nitrogen, ensuring an oxygen-free environment for polymerization, further improving the anchoring of the membranes to PDMS. This enables the creation of complex designs without the need for direct UV writing or masks. Moreover, we showed that the peristaltic valves can be integrated into the chip design to mix the components inside of the reactor without the hydrogel membrane rupturing. The diffusion of solutes of different weights through the membranes shows that the PEG-DA membranes are suitable for dialysis application with a molecular cut-off in the 10–40 kDa range, required for continuous-exchange protein synthesis format. Lastly, to avoid evaporation through the PDMS during the reaction, we implemented a third anti-evaporation layer to the chip, which prevented evaporation for up to 16 hours. This allowed us to extend the protein synthesis to several hours through the continuous-exchange reaction format.

5.4 Methods

5.4.1 Microfluidic chip fabrication

The device with 8 reactors and 9 fluid inputs (Figure 5.1) is based on a previous design [166, 181]. Molds for the control, the flow layer, and the anti-evaporation layer were fabricated on separate wafers by standard photolithography techniques. The positive photoresist AZ 10XT-60 (Merck) at the height of 14 μm was used to generate the flow channels features. For the control layer and the anti-evaporation layer, a negative photoresist SU-8 photoresist (Microchem 3025, Kayaku Advanced Materials) was used to generate the channels features at the height of 40 μm . Afterward, each of the wafers was treated with trimethylchlorosilane. For the flow and the anti-evaporation layers PDMS with an elastomer to crosslinker at 5:1 ratio was prepared and poured over the wafers to a height ~ 0.3 cm or 0.6 cm, respectively. The wafers with PDMS were placed in a desiccator for 40 min before baking. For the control layer, PDMS with a 20:1 elastomer to crosslinker ratio was spin-coated at 1400 rpm onto the wafer and let sit for 40 min before baking. The anti-evaporation layer was cured at 80 $^{\circ}\text{C}$ for 90 minutes, after which each layer was cut out. The flow and control layers were partially cured at 80 $^{\circ}\text{C}$ for 20 minutes. The flow layer was then cut out and aligned onto the control layer by hand using a Nikon stereo microscope. The aligned devices were placed back in the oven at 80 $^{\circ}\text{C}$ for 90 minutes before they were cut and removed from the wafer. The aligned devices and the anti-evaporation layer were punched using a 900 μm pin. Afterward, the devices were plasma bonded to a glass slide before the anti-evaporation layer was plasma bonded on top.

5.4.2 Chip silanisation and formation of PEG-DA hydro-gel membrane

To prime the chip, control lines were filled with water, except for hydrogel-forming valves, which were filled FluorinertTM FC-40 (Sigma) and pressurized with air or nitrogen, respectively, at 1.38 bar. The inner walls of the flow channels, except for the reactors, were oxidized by flowing fresh $\text{H}_2\text{O}:\text{H}_2\text{O}_2$ (30% (w/w)): HCl (36% (w/w)) solution in ratio 5:1:1 for 10 minutes, followed by rinsing MiliQ with water for 2-4 min. The silanization solution was prepared by mixing deionized water with 0.4% (v/v) 3-(Trimethoxysilyl)propylmethacrylate (TMSPMA, Sigma) and 0.4% (v/v) glacial acetic acid. The freshly prepared silanization solution was flowed for 20 min to the oxidized channels. Finally, the channels were washed with MiliQ water for 15 min.

Meanwhile, an aqueous solution for polymerization of the hydrogel membrane was prepared. First, the PEG-DA (M_n 700 g/mol, Sigma) was mixed with photo-initiator 2-hydroxy-2-methylpropionophenone (Sigma) (90/10% v/v). Subsequently, different volumes of UltraPure water (Invitrogen) were added to the mixture. The oxygen was removed from the mixture by perfusion of nitrogen gas through the solution for 10-20 minutes. The PEG-DA formulation was injected into the feeding chamber for 10 min, after which the hydrogel-forming valves were closed, and the remaining PEG-DA was flushed away with water. The remaining PEG-DA was polymerized for 2×30 s with an Omnicure S1500 200W UV curing lamp with a standard filter (320nm-500nm). The formed

membranes were first washed with UltraPure water for 20 hours and then with a wash buffer (50 mM HEPES, 100 mM potassium chloride, 11.8 mM magnesium acetate) for 2 hours. The anti-evaporation layer was primed with water 1-2 hours before the experiment start.

5.4.3 Solute diffusion through the membrane

After the formation of the hydrogel membrane, the flow layer was primed with a solution of 2% bovine serum albumin (BSA) in 0.5× PBS and washes with a wash buffer (50 mM HEPES, 100 mM potassium chloride, 11.8 mM magnesium acetate). The reactors were thoroughly washes and filled with the wash buffer, while the feeding channel was loaded with either 10 $\mu\text{g}/\text{mL}$ of methylene blue, Fluoresceinisoithiocyanat-dextran (FITC-dextran, 10 kDa) or Tetramethylrhodamine-dextran (TMR-dextran, 40 kDa) solutes. The peristaltic pump was actuated at 20 Hz to mix the solutions inside of the reactor. The reactor was imaged every 10 min.

5.4.4 PURE system and energy solution preparation

The PURE system and energy solution were prepared as described previously [181]. Proteins and ribosomes were purified by Ni-NTA gravity-flow chromatography. Energy solution was prepared as described previously [181]. 2.5× energy solution contained 0.75 mM of each amino acid, 29.5 mM magnesium acetate, 250 mM potassium glutamate, 5 mM ATP and GTP, 2.5 mM CTP, UTP and TCEP (tris(2-carboxyethyl)phosphine hydrochloride), 130 $\text{U}_{A260}/\text{mL}$ tRNA, 50 mM creatine phosphate, 0.05 mM folinic acid, 5 mM spermidine, and 125 mM HEPES.

5.4.5 Device setup for cell-free expression

After the formation of the hydrogel membrane. The flow layer was primed with a solution of 2% bovine serum albumin (BSA) in 0.5× PBS. For washes between loading steps a wash buffer (50 mM HEPES, 100 mM potassium chloride, 11.8 mM magnesium acetate) was used. For the experiments PURE, and DNA solutions were mixed in the microfluidic reactors on the microfluidic chip in a 4:1 ratio. The energy solution was loaded into the feeding channel. The peristaltic pump was actuated at 20 Hz to mix the solutions. Every 10 minutes, the reactor was imaged and for continuous-exchange the feeding channel solution was replenish. 2.5× energy solution was prepared as described above. The PURE solutions were prepared by mixing the desired protein solutions (Table 5.1) with ribosomes and supplied with tRNA and 10 μM TCEP. The PURE solution was supplemented with mScarlet protein to allow for visualization. The DNA solution at five times its final concentration was prepared by mixing 10 nM of eGFP linear templates and 6.25 μM Chi DNA. The Chi decoys were added to help mitigate potential DNA absorption and degradation, while the DNA solution is stored in the FEP tubing before it is added to the chip.

5.4.6 Data acquisition and analysis

Solenoid valves, microscope, and camera were controlled by a custom Matlab and LabVIEW program. The chip and microscope stage were enclosed in an environmental chamber at 37°C. The fluorescence was monitored over time on an automated inverted fluorescence microscope (Nikon), using 20× magnification and FITC / Cy5 / mCherry filters. The microscope hardware details are described in [166]. The fluorescence images were analyzed and corrected in Python, by subtracting the background fluorescence of a position next to the fluidic channel.

Table 5.1: PURE system formulations used

PURE system					
Protein	Concentration		Protein	Concentration	
AlaRS	204.4	μg/mL	IF1	2.9	μg/mL
ArgRS	5.9	μg/mL	IF2	11.7	μg/mL
AsnRS	64.2	μg/mL	IF3	29.2	μg/mL
AspRS	23.4	μg/mL	EF-G	146.0	μg/mL
CysRS	3.5	μg/mL	EF-Tu	1460.0	μg/mL
GlnRS	11.1	μg/mL	EF-Ts	146.0	μg/mL
GluRS	36.8	μg/mL	RF1	29.2	μg/mL
GlyRS	28.0	μg/mL	RF2	29.2	μg/mL
HisRS	2.3	μg/mL	RF3	29.2	μg/mL
IleRS	116.8	μg/mL	RRF	29.2	μg/mL
LeuRS	11.6	μg/mL	MTF	58.4	μg/mL
LysRS	18.7	μg/mL	CK	11.7	μg/mL
MetRS	6.7	μg/mL	MK	8.8	μg/mL
PheRS	49.6	μg/mL	NDK	3.2	μg/mL
ProRS	29.2	μg/mL	PPiase	2.9	μg/mL
SerRS	5.5	μg/mL	T7 RNAP	29.2	μg/mL
ThrRS	18.2	μg/mL	tRNA	11.7	mg/mL
TrpRS	18.4	μg/mL	Ribosome	1.8	μM
TyrRS	1.8	μg/mL			
ValRS	5.4	μg/mL			

6 Conclusion and outlook

The construction of a synthetic cell is the holy grail of synthetic biology with many potential applications. However, one of the crucial elements of a synthetic cell, i.e., self-reproduction, remains to be established. The work presented in this thesis shows that cell-free environments and microfluidic compartments are powerful technologies to engineer and prototype self-regeneration systems. This section will briefly summarize the results and discuss limitations and future steps.

In chapter 2 we describe a novel "OnePot" method to produce the PURE system based on coculturing and co-purification, without extensive cloning steps. We showed that the inoculation ratios of the coculture can control the protein composition of the OnePot PURE system. Moreover, we demonstrated that the concentration of EF-Tu is of fundamental importance for the expression yields. In contrast, changes in the concentrations of the other protein components have a relatively low impact on the robustness of the PURE system. By adjusting the inoculation ratio of EF-Tu with regard to all the other components, we achieved a comparable composition to the standard PURE composition and generated similar yields. However, this preparation streamlining limits the flexibility of the PURE system, as the proteins cannot be adjusted individually after the preparation. Moreover, as the concentration of the components is determined based on the inoculation ratio of the coculture, the exact composition of the system is unknown and somewhat varies for different preparations. Additional analyses such as mass-spectrometry measurements bring details on the system composition. The full protocol for the method presented here was also recently published [197].

For the successful implementation of self-regeneration, it is critical to maintain non-equilibrium conditions. Chapter 3 summarised in detail the protocol to fabricate a microfluidic chemostat device with hard-coded dilution fractions defined by reactor geometry. This improved microfluidic nano-reactor device allows us to run continuous TX-TL reactions at constant steady-state levels. Furthermore, the dilution by reactor geometry allows loading different viscosity solutions as well as high chip-to-chip reproducibility and therefore does not require calibrations. However, the hard-coded dilution somewhat limits the device flexibility as the fixed dilution fractions determine the dilution rates.

In chapter 4 we demonstrate that the microfluidic device in combination with cell-free systems can be used for prototyping protein-based self-regenerating systems. We show that essential PURE system components can be regenerated for several generations and that fine-tuning the amounts of added DNA template is a critical factor to achieve robust protein regeneration of multiple proteins. Moreover, our results and corresponding modeling suggest that due to resource loading and allocation, specific components might have to be tightly regulated, for example, by feedback regulation. The current setup only allows interrogation of the translation activity of the system and regenerated components by fluorescent readouts. One of our experimental design limitations is that we could not directly observe the expression of the regenerated components and their concentrations. Therefore, it would be exciting to couple the system with electrophoresis, western blot, or mass spectrometry. Moreover, it would be valuable to implement a quantitative model of mRNA dynamics to help determine mRNA concentrations during TX-TL reactions via integration of binary probes [130], molecular beacons [198], spinach aptamers [199], or malachite

green aptamers [71]. Since the PURE system is free of DNAase, linear DNA templates can be utilized without extensive cloning steps. By varying individual DNA input concentrations, we were able to adjust protein synthesis rates for each component. However, in the future, expression strengths will need to be tuned using synthetic transcription factors [113], promoters [22], terminators [72], and ribosome binding sites [174].

In chapter 5 we demonstrate that PEG-DA gels implemented in PDMS can be used in place of dialysis membranes. We then engineered the membrane's permeability for different molecular weight solutes to match the requirements for a continuous-exchange cell-free format, where small molecules can freely diffuse to the reactor and byproducts can diffuse out, while the TX-TL machinery remains in the reactor. Using this microfluidic device, we were able to show that cell-free batch reactions can be extended when a continuous-exchange cell-free format is implemented. However, it remains to be seen for how long the reaction can be extended and if the continuous-exchange can be combined with steady-state reactions.

Many challenges remain to be overcome to achieve a fully sustainable self-replication system and eventually autonomous synthetic cell. As stated in the chapters above, it remains to be determined if the PURE system can regenerate all of its components. In its current composition, it is unlikely that the system will be able to regenerate all of its components. There are two main reasons for this. The first concern is related to protein folding and post-translational modifications. Albeit specific protein modifications and chaperones are presumed to be essential to the system, it will be of utmost importance to determine their actual essentiality or benefit to the regeneration process because any additional system component will need to be regenerated, increasing the system complexity and requiring a higher synthesis rate. The synthesis rate is the second difficulty for the regeneration, as the PURE synthesis rate is significantly lower than the total synthesis rate needed. Current approaches mainly focus on increasing component concentrations or adding components to the system instead of optimizing protein synthesis rates and the ratio of protein synthesis rate to the total amount of protein contained in the system. Fundamental non-genetic properties such as molecular self-organization, molecular crowding, non-equilibrium conditions will be of fundamental importance for self-replicating cells [13] and are expected to increase the production rates of the system. For example, as mentioned in chapter 5, a continuous-exchange based system might be beneficial to improve the system synthesis yields and achieve self-regeneration. As we have shown in chapter 4, the implementation of the computation model helps to understand the underlying self-regeneration processes. Furthermore, it would be exciting to implement artificial intelligence with data from the experiments to optimize the self-reconstitution.

To conclude, we showed that continuous TX-TL reactions are potent for synthetic cell research because they allow the prototyping of separate fundamental sub-processes.

Bibliography

1. Szostak, J. W., Bartel, D. P. & Luisi, P. L. Synthesizing life. *Nature* **409**. Number: 6818 Publisher: Nature Publishing Group, 387–390 (2001).
2. Xavier, J. C., Patil, K. R. & Rocha, I. Systems Biology Perspectives on Minimal and Simpler Cells. *Microbiology and Molecular Biology Reviews* **78**, 487–509 (2014).
3. Stano, P. Is Research on “Synthetic Cells” Moving to the Next Level? *Life* **9** (2018).
4. Jewett, M. C. & Forster, A. C. Update on designing and building minimal cells. *Current Opinion in Biotechnology* **21**, 697–703 (2010).
5. Gibson, D. G. *et al.* Creation of a Bacterial Cell Controlled by a Chemically Synthesized Genome. *Science* **329**, 52–56 (2010).
6. Hutchison, C. A. *et al.* Design and synthesis of a minimal bacterial genome. *Science* **351**, aad6253 (2016).
7. Henry, C., Overbeek, R. & Stevens, R. L. Building the blueprint of life. *Biotechnology Journal* **5**, 695–704 (2010).
8. Glass, J. I., Merryman, C., Wise, K. S., Hutchison, C. A. & Smith, H. O. Minimal Cells—Real and Imagined. *Cold Spring Harbor Perspectives in Biology*, a023861 (2017).
9. Ichihashi, N. What can we learn from the construction of in vitro replication systems? *Annals of the New York Academy of Sciences* **1447**, 144–156 (2019).
10. Izri, Z., Garenne, D., Noireaux, V. & Maeda, Y. T. Gene Expression in on-Chip Membrane-Bound Artificial Cells. *ACS Synthetic Biology* **8**, 1705–1712 (2019).
11. Aufinger, L. & Simmel, F. C. Artificial Gel-Based Organelles for Spatial Organization of Cell-Free Gene Expression Reactions. *Angewandte Chemie International Edition* **57**, 17245–17248 (2018).
12. Niederholtmeyer, H., Chaggar, C. & Devaraj, N. K. Communication and quorum sensing in non-living mimics of eukaryotic cells. *Nature Communications* **9**, 1–8 (2018).
13. Noireaux, V., Maeda, Y. T. & Libchaber, A. Development of an artificial cell, from self-organization to computation and self-reproduction. *Proceedings of the National Academy of Sciences* **108**, 3473–3480 (2011).
14. Schwille, P. *et al.* MaxSynBio: Avenues Towards Creating Cells from the Bottom Up. *Angewandte Chemie-International Edition* **57**, 13382–13392 (2018).

Bibliography

15. Jia, H., Heymann, M., Bernhard, F., Schwille, P. & Kai, L. Cell-free protein synthesis in micro compartments: building a minimal cell from biobricks. *New Biotechnology. European Congress of Biotechnology - ECB 2016* **39**, 199–205 (2017).
16. Solé, R. V., Munteanu, A., Rodriguez-Caso, C. & Macía, J. Synthetic protocell biology: from reproduction to computation. *Philosophical Transactions of the Royal Society B: Biological Sciences* **362**, 1727–1739 (2007).
17. Rasmussen, S. *et al.* Transitions from Nonliving to Living Matter. *Science* **303**. Publisher: American Association for the Advancement of Science Section: Perspective, 963–965 (2004).
18. Damiano, L. & Stano, P. On the “Life-Likeness” of Synthetic Cells. *Frontiers in Bioengineering and Biotechnology* **8**. Publisher: Frontiers (2020).
19. Salehi-Reyhani, A., Ces, O. & Elani, Y. Artificial cell mimics as simplified models for the study of cell biology. *Experimental Biology and Medicine* **242**, 1309–1317 (2017).
20. Gil, R. & Peretó, J. Small genomes and the difficulty to define minimal translation and metabolic machineries. *Frontiers in Ecology and Evolution* **3** (2015).
21. Stano, P. Synthetic biology of minimal living cells: primitive cell models and semi-synthetic cells. *Systems and Synthetic Biology* **4**, 149–156 (2010).
22. Swank, Z., Laohakunakorn, N. & Maerkl, S. J. Cell-free gene-regulatory network engineering with synthetic transcription factors. *Proceedings of the National Academy of Sciences* **116**, 5892–5901 (2019).
23. Laohakunakorn, N. *et al.* Bottom-Up Construction of Complex Biomolecular Systems With Cell-Free Synthetic Biology. *Frontiers in Bioengineering and Biotechnology* **8** (2020).
24. Forster, A. C. & Church, G. M. Towards synthesis of a minimal cell. *Molecular Systems Biology* **2**, 45 (2006).
25. Fanalista, F. *et al.* Shape and Size Control of Artificial Cells for Bottom-Up Biology. *ACS Nano* **13**, 5439–5450 (2019).
26. Yewdall, N. A., Mason, A. F. & van Hest, J. C. M. The hallmarks of living systems: towards creating artificial cells. *Interface Focus* **8**, 20180023–15 (2018).
27. Lentini, R., Yeh Martín, N. & Mansy, S. S. Communicating artificial cells. *Current Opinion in Chemical Biology. Synthetic Biology * Synthetic Biomolecules* **34**, 53–61 (2016).
28. Hennig, S., Rödel, G. & Ostermann, K. Artificial cell-cell communication as an emerging tool in synthetic biology applications. *Journal of Biological Engineering* **9**, 13 (2015).
29. Powell, K. How biologists are creating life-like cells from scratch. *Nature* **563**. Number: 7730 Publisher: Nature Publishing Group, 172–175 (2018).
30. Xu, C., Hu, S. & Chen, X. Artificial cells: from basic science to applications. *Materials Today* **19**, 516–532 (2016).
31. Elani, Y. Construction of membrane-bound artificial cells using microfluidics: a new frontier in bottom-up synthetic biology. *Biochemical Society Transactions* **44**, 723–730 (2016).

32. Buddingh', B. C. & van Hest, J. C. M. Artificial Cells: Synthetic Compartments with Life-like Functionality and Adaptivity. *Accounts of Chemical Research* **50**. Publisher: American Chemical Society, 769–777 (2017).
33. Abil, Z. & Danelon, C. Roadmap to Building a Cell: An Evolutionary Approach. *Frontiers in Bioengineering and Biotechnology* **8**. Publisher: Frontiers (2020).
34. Breuer, M. *et al.* Essential metabolism for a minimal cell. *eLife* **8** (eds Nikoloski, Z. & Barkai, N.) Publisher: eLife Sciences Publications, Ltd, e36842 (2019).
35. Gil, R., Silva, F. J., Peretó, J. & Moya, A. Determination of the core of a minimal bacterial gene set. *Microbiology and molecular biology reviews: MMBR* **68**, 518–537, table of contents (2004).
36. Yue, K., Zhu, Y. & Kai, L. Cell-Free Protein Synthesis: Chassis toward the Minimal Cell. *Cells* **8**. Number: 4 Publisher: Multidisciplinary Digital Publishing Institute, 315 (2019).
37. Bersini, H. Software Replica of Minimal Living Processes. *Origins of Life and Evolution of Biospheres* **40**, 121–130 (2010).
38. Purcell, O., Jain, B., Karr, J. R., Covert, M. W. & Lu, T. K. Towards a whole-cell modeling approach for synthetic biology. *Chaos: An Interdisciplinary Journal of Nonlinear Science* **23**. Publisher: American Institute of Physics, 025112 (2013).
39. Ugrinic, M., deMello, A. & Tang, T.-Y. D. Microfluidic Tools for Bottom-Up Synthetic Cellularity. *Chem* **5**, 1727–1742 (2019).
40. Supramaniam, P., Ces, O. & Salehi-Reyhani, A. Microfluidics for Artificial Life: Techniques for Bottom-Up Synthetic Biology. *Micromachines* **10**, 299 (2019).
41. Mutschler, H., Robinson, T., Tang, T.-Y. D. & Wegner, S. Special Issue on Bottom-Up Synthetic Biology. *ChemBioChem* **20**, 2533–2534 (2019).
42. Neumann, J., Burks, A. W., *et al.* *Theory of self-reproducing automata* (University of Illinois press Urbana, 1966).
43. Pesavento, U. An Implementation of von Neumann's Self-Reproducing Machine. *Artificial Life* **2**, 337–354 (1995).
44. Gibson, D. G. *et al.* Enzymatic assembly of DNA molecules up to several hundred kilobases. *Nature Methods* **6**, 343–345 (2009).
45. Quan, J. & Tian, J. Circular Polymerase Extension Cloning of Complex Gene Libraries and Pathways. *PLOS ONE* **4**, e6441 (2009).
46. Engler, C., Kandzia, R. & Marillonnet, S. A One Pot, One Step, Precision Cloning Method with High Throughput Capability. *PLOS ONE* **3**. Publisher: Public Library of Science, e3647 (2008).
47. Shepherd, T. R. *et al.* De novo design and synthesis of a 30-cistron translation-factor module. *Nucleic Acids Research* **45**, 10895–10905 (2017).
48. Gibson, D. G. *et al.* Complete chemical synthesis, assembly, and cloning of a *Mycoplasma genitalium* genome. *Science (New York, NY)* **319**, 1215–1220 (2008).

Bibliography

49. Fujiwara, K., Katayama, T. & Nomura, S.-i. M. Cooperative working of bacterial chromosome replication proteins generated by a reconstituted protein expression system. *Nucleic Acids Research* **41**, 7176–7183 (2013).
50. Sakatani, Y., Ichihashi, N., Kazuta, Y. & Yomo, T. A transcription and translation-coupled DNA replication system using rolling-circle replication. *Scientific Reports* **5**. Number: 1 Publisher: Nature Publishing Group, 10404 (2015).
51. Libicher, K., Hornberger, R., Heymann, M. & Mutschler, H. In vitro self-replication and multicistronic expression of large synthetic genomes. *Nature Communications* **11**, 904 (2020).
52. Okauchi, H., Sakatani, Y., Otsuka, K. & Ichihashi, N. Minimization of Elements for Isothermal DNA Replication by an Evolutionary Approach. *ACS Synthetic Biology* **9**. Publisher: American Chemical Society, 1771–1780 (2020).
53. Sakatani, Y., Yomo, T. & Ichihashi, N. Self-replication of circular DNA by a self-encoded DNA polymerase through rolling-circle replication and recombination. *Scientific Reports* **8**, 13089 (2018).
54. Nieß, A., Failmezger, J., Kuschel, M., Siemann-Herzberg, M. & Takors, R. Experimentally Validated Model Enables Debottlenecking of in Vitro Protein Synthesis and Identifies a Control Shift under in Vivo Conditions. *ACS Synthetic Biology* **6**, 1913–1921 (2017).
55. Niwa, T. *et al.* Bimodal protein solubility distribution revealed by an aggregation analysis of the entire ensemble of Escherichia coli proteins. *Proceedings of the National Academy of Sciences* **106**, 4201–4206 (2009).
56. Niwa, T., Kanamori, T., Ueda, T. & Taguchi, H. Global analysis of chaperone effects using a reconstituted cell-free translation system. *Proceedings of the National Academy of Sciences* **109**, 8937–8942 (2012).
57. Doerr, A., Foschepoth, D., Forster, A. C. & Danelon, C. In vitro synthesis of 32 translation-factor proteins from a single template reveals impaired ribosomal processivity. *Scientific Reports* **11**, 1898 (2021).
58. Li, J. *et al.* Dissecting limiting factors of the Protein synthesis Using Recombinant Elements (PURE) system. *Translation* **5**, e1327006 (2017).
59. Awai, T., Ichihashi, N. & Yomo, T. Activities of 20 aminoacyl-tRNA synthetases expressed in a reconstituted translation system in Escherichia coli. *Biochemistry and Biophysics Reports* **3**, 140–143 (2015).
60. Wei, E. & Endy, D. Experimental tests of functional molecular regeneration via a standard framework for coordinating synthetic cell building. *bioRxiv*. Publisher: Cold Spring Harbor Laboratory Section: New Results, 2021.03.03.433818 (2021).
61. Libicher, K. & Mutschler, H. Probing self-regeneration of essential protein factors required for *in vitro* translation activity by serial transfer. *Chemical Communications* **56**, 15426–15429 (2020).

62. Jewett, M. C., Fritz, B. R., Timmerman, L. E. & Church, G. M. In vitro integration of ribosomal RNA synthesis, ribosome assembly, and translation. *Molecular Systems Biology* **9**, 678 (2013).
63. Li, J. *et al.* Cogenerating Synthetic Parts toward a Self-Replicating System. *ACS Synthetic Biology* **6**, 1327–1336 (2017).
64. Shimojo, M. *et al.* In vitro reconstitution of functional small ribosomal subunit assembly for comprehensive analysis of ribosomal elements in *E. coli*. *Communications Biology* **3**, Number: 1 Publisher: Nature Publishing Group, 1–10 (2020).
65. Levy, M., Falkovich, R., Daube, S. S. & Bar-Ziv, R. H. Autonomous synthesis and assembly of a ribosomal subunit on a chip. *Science Advances* **6**. Publisher: American Association for the Advancement of Science Section: Research Article, eaaz6020 (2020).
66. Iwane, Y. *et al.* Expanding the amino acid repertoire of ribosomal polypeptide synthesis via the artificial division of codon boxes. *Nature Chemistry* **8**, Number: 4 Publisher: Nature Publishing Group, 317–325 (2016).
67. Cui, Z., Stein, V., Tnimov, Z., Mureev, S. & Alexandrov, K. Semisynthetic tRNA Complement Mediates in Vitro Protein Synthesis. *Journal of the American Chemical Society* **137**, 4404–4413 (2015).
68. Calles, J., Justice, I., Brinkley, D., Garcia, A. & Endy, D. Fail-safe genetic codes designed to intrinsically contain engineered organisms. *Nucleic Acids Research* **47**, 10439–10451 (2019).
69. Hibi, K. *et al.* Reconstituted cell-free protein synthesis using in vitro transcribed tRNAs. *Communications Biology* **3**, 350 (2020).
70. Belliveau, N. M. *et al.* Systematic approach for dissecting the molecular mechanisms of transcriptional regulation in bacteria. *Proceedings of the National Academy of Sciences* **115**. Publisher: National Academy of Sciences Section: PNAS Plus, E4796–E4805 (2018).
71. Siegal-Gaskins, D., Tuza, Z. A., Kim, J., Noireaux, V. & Murray, R. M. Gene circuit performance characterization and resource usage in a cell-free "breadboard". *ACS Synthetic Biology* **3**, 416–425 (2014).
72. Chen, Y.-J. *et al.* Characterization of 582 natural and synthetic terminators and quantification of their design constraints. *Nature Methods*, 1–8 (2013).
73. Niederholtmeyer, H. *et al.* *A cell-free framework for biological systems engineering* (2015).
74. Chizzolini, F. *et al.* Cell-Free Translation Is More Variable than Transcription. *ACS Synthetic Biology* **6**, 638–647 (2017).
75. Chizzolini, F., Forlin, M., Cecchi, D. & Mansy, S. S. Gene Position More Strongly Influences Cell-Free Protein Expression from Operons than T7 Transcriptional Promoter Strength. *ACS Synthetic Biology* **3**, 363–371 (2014).
76. Greiss, F., Daube, S. S., Noireaux, V. & Bar-Ziv, R. From deterministic to fuzzy decision-making in artificial cells. *Nature Communications* **11**, Number: 1 Publisher: Nature Publishing Group, 5648 (2020).

Bibliography

77. Gregorio, N. E., Levine, M. Z. & Oza, J. P. A User's Guide to Cell-Free Protein Synthesis. *Methods and Protocols* **2** (2019).
78. Zemella, A., Thoring, L., Hoffmeister, C. & Kubick, S. Cell-Free Protein Synthesis: Pros and Cons of Prokaryotic and Eukaryotic Systems. *ChemBioChem* **16**, 2420–2431 (2015).
79. Perez, J. G., Stark, J. C. & Jewett, M. C. Cell-Free Synthetic Biology: Engineering Beyond the Cell. *Cold Spring Harbor Perspectives in Biology* **8**. Company: Cold Spring Harbor Laboratory Press Distributor: Cold Spring Harbor Laboratory Press Institution: Cold Spring Harbor Laboratory Press Label: Cold Spring Harbor Laboratory Press Publisher: Cold Spring Harbor Lab, a023853 (2016).
80. Kung, H. F. *et al.* DNA-directed in vitro synthesis of beta-galactosidase. Studies with purified factors. *Journal of Biological Chemistry* **252**, 6889–6894 (1977).
81. Shimizu, Y. *et al.* Cell-free translation reconstituted with purified components. *Nature Biotechnology* **19**, 751–755 (2001).
82. Tuckey, C., Asahara, H., Zhou, Y. & Chong, S. Protein Synthesis Using A Reconstituted Cell-Free System. *Current protocols in molecular biology / edited by Frederick M. Ausubel ... [et al.]* **108**, 16.31.1–16.31.22 (2014).
83. Doerr, A. *et al.* Modelling cell-free RNA and protein synthesis with minimal systems. *Physical Biology* **16**, 025001 (2019).
84. Maddalena, L. L. d. *et al.* GreA and GreB Enhance Expression of Escherichia coli RNA Polymerase Promoters in a Reconstituted Transcription–Translation System. *ACS Synthetic Biology* **5**, 929–935 (2016).
85. Kuruma, Y. & Ueda, T. The PURE system for the cell-free synthesis of membrane proteins. *Nature Protocols* **10**, 1328–1344 (2015).
86. Niwa, T. *et al.* Comprehensive study of liposome-assisted synthesis of membrane proteins using a reconstituted cell-free translation system. *Scientific reports* **5**, 18025–18025 (2015).
87. Jacobs, M. L., Boyd, M. A. & Kamat, N. P. Diblock copolymers enhance folding of a mechanosensitive membrane protein during cell-free expression. *Proceedings of the National Academy of Sciences* **116**, 4031–4036 (2019).
88. Shimizu, Y., Kanamori, T. & Ueda, T. Protein synthesis by pure translation systems. *Methods. Engineering Translation* **36**, 299–304 (2005).
89. Shimizu, Y. & Ueda, T. in *Cell-Free Protein Production* (eds Endo, Y., Takai, K. & Ueda, T.) 11–21 (2010).
90. Horiya, S., Bailey, J. K. & Krauss, I. J. in *Methods in Enzymology* (ed Imperiali, B.) Supplement C vols., 83–141 (Academic Press, 2017).
91. Wang, H. H. *et al.* Multiplexed *in Vivo* His-Tagging of Enzyme Pathways for *in Vitro* Single-Pot Multienzyme Catalysis. *ACS Synthetic Biology* **1**, 43–52 (2012).
92. Villarreal, F. *et al.* Synthetic microbial consortia enable rapid assembly of pure translation machinery. *Nature Chemical Biology* **14**, 29–35 (2018).

93. Lavickova, B. & Maerkl, S. J. A Simple, Robust, and Low-Cost Method To Produce the PURE Cell-Free System. *ACS Synthetic Biology* **8**, 455–462 (2019).
94. Li, J., Gu, L., Aach, J. & Church, G. M. Improved Cell-Free RNA and Protein Synthesis System. *PLOS ONE* **9**, e106232 (2014).
95. Kazuta, Y., Matsuura, T., Ichihashi, N. & Yomo, T. Synthesis of milligram quantities of proteins using a reconstituted in vitro protein synthesis system. *Journal of Bioscience and Bioengineering* **118**, 554–557 (2014).
96. Matsuura, T., Kazuta, Y., Aita, T., Adachi, J. & Yomo, T. Quantifying epistatic interactions among the components constituting the protein translation system. *Molecular Systems Biology* **5**, 297 (2009).
97. Mavelli, F., Marangoni, R. & Stano, P. A Simple Protein Synthesis Model for the PURE System Operation. *Bulletin of Mathematical Biology* **77**, 1185–1212 (2015).
98. Carrara, P., Altamura, E., D'Angelo, E., Mavelli, F. & Stano, P. Measurement and Numerical Modeling of Cell-Free Protein Synthesis: Combinatorial Block-Variants of the PURE System. *Data* **3**, 41 (2018).
99. Matsuura, T., Hosoda, K. & Shimizu, Y. Robustness of a Reconstituted Escherichia coli Protein Translation System Analyzed by Computational Modeling. *ACS Synthetic Biology* **7**, 1964–1972 (2018).
100. Matsuura, T., Tanimura, N., Hosoda, K., Yomo, T. & Shimizu, Y. Reaction dynamics analysis of a reconstituted Escherichia coli protein translation system by computational modeling. *Proceedings of the National Academy of Sciences* **114**, E1336–E1344 (2017).
101. Kempf, N. *et al.* A Novel Method to Evaluate Ribosomal Performance in Cell-Free Protein Synthesis Systems. *Scientific Reports* **7**, 46753 (2017).
102. Kazuta, Y. *et al.* Comprehensive Analysis of the Effects of Escherichia coli ORFs on Protein Translation Reaction. *Molecular & Cellular Proteomics : MCP* **7**, 1530–1540 (2008).
103. Wang, P. *et al.* A Single Polyphosphate Kinase-Based NTP Regeneration System Driving Cell-Free Protein Synthesis (2019).
104. Ge, X., Luo, D. & Xu, J. Cell-Free Protein Expression under Macromolecular Crowding Conditions. *PLOS ONE* **6**, e28707 (2011).
105. Moriizumi, Y., Tabata, K. V., Miyoshi, D. & Noji, H. Osmolyte-Enhanced Protein Synthesis Activity of a Reconstituted Translation System. *ACS Synthetic Biology* **8**, 557–567 (2019).
106. Norred, S. E. *et al.* Macromolecular Crowding Induces Spatial Correlations That Control Gene Expression Bursting Patterns. *ACS Synthetic Biology* **7**, 1251–1258 (2018).
107. Niwa, T. *et al.* Large-scale analysis of macromolecular crowding effects on protein aggregation using a reconstituted cell-free translation system. *Frontiers in Microbiology* **6** (2015).
108. Damiani, S., Mhanna, R., Kodzius, R. & Ehmoser, E.-K. Cell-Free Approaches in Synthetic Biology Utilizing Microfluidics. *Genes* **9**. Number: 3 Publisher: Multidisciplinary Digital Publishing Institute, 144 (2018).

Bibliography

109. Dubuc, E. *et al.* Cell-free microcompartmentalised transcription–translation for the prototyping of synthetic communication networks. *Current Opinion in Biotechnology* **58**, 72–80 (2019).
110. Maerkl, S. J. & Quake, S. R. A systems approach to measuring the binding energy landscapes of transcription factors. *Science (New York, NY)* **315**, 233–237 (2007).
111. Martin, L. L. *et al.* Systematic reconstruction of RNA functional motifs with high-throughput microfluidics. *Nature Methods* **9**, 1192–1194 (2012).
112. Rockel, S., Geertz, M., Hens, K., Deplancke, B. & Maerkl, S. J. iSLIM: a comprehensive approach to mapping and characterizing gene regulatory networks. *Nucleic acids research* **41**, e52 (2013).
113. Blackburn, M. C., Petrova, E., Correia, B. E. & Maerkl, S. J. Integrating gene synthesis and microfluidic protein analysis for rapid protein engineering. *Nucleic Acids Research* **44**, e68–e68 (2015).
114. Hori, Y., Kantak, C., Murray, R. M. & Abate, A. R. Cell-free extract based optimization of biomolecular circuits with droplet microfluidics. *Lab on a Chip* **17**, 3037–3042 (2017).
115. Georgi, V. *et al.* On-chip automation of cell-free protein synthesis: new opportunities due to a novel reaction mode. *Lab on a Chip* **16**. Publisher: The Royal Society of Chemistry, 269–281 (2016).
116. Elani, Y., Law, R. V. & Ces, O. Vesicle-based artificial cells as chemical microreactors with spatially segregated reaction pathways. *Nature Communications* **5**. Number: 1 Publisher: Nature Publishing Group, 5305 (2014).
117. Jiao, Y., Liu, Y., Luo, D., Huck, W. T. S. & Yang, D. Microfluidic-Assisted Fabrication of Clay Microgels for Cell-Free Protein Synthesis. *ACS Applied Materials & Interfaces* **10**. Publisher: American Chemical Society, 29308–29313 (2018).
118. Lee, K.-H., Lee, K.-Y., Byun, J.-Y., Kim, B.-G. & Kim, D.-M. On-bead expression of recombinant proteins in an agarose gel matrix coated on a glass slide. *Lab on a Chip* **12**. Publisher: The Royal Society of Chemistry, 1605–1610 (2012).
119. Byun, J.-Y., Lee, K.-H., Lee, K.-Y., Kim, M.-G. & Kim, D.-M. In-gel expression and in situ immobilization of proteins for generation of three dimensional protein arrays in a hydrogel matrix. *Lab on a Chip* **13**. Publisher: The Royal Society of Chemistry, 886–891 (2013).
120. Spirin, A. S., Baranov, V. I., Ryabova, L. A., Ovodov, S. Y. & Alakhov, Y. B. A continuous cell-free translation system capable of producing polypeptides in high yield. *Science (New York, N.Y.)* **242**, 1162–1164 (1988).
121. Kim, D.-M. & Choi, C.-Y. A Semicontinuous Prokaryotic Coupled Transcription/Translation System Using a Dialysis Membrane. *Biotechnology Progress* **12**, 645–649 (1996).
122. Madin, K., Sawasaki, T., Ogasawara, T. & Endo, Y. A highly efficient and robust cell-free protein synthesis system prepared from wheat embryos: plants apparently contain a suicide system directed at ribosomes. *Proc Natl Acad Sci U S A* **97**, 559–564 (2000).

123. Mei, Q., Fredrickson, C. K., Lian, W., Jin, S. & Fan, Z. H. Ricin Detection by Biological Signal Amplification in a Well-in-a-Well Device. *Analytical Chemistry* **78**. Publisher: American Chemical Society, 7659–7664 (2006).
124. Mei, Q., Fredrickson, C. K., Simon, A., Khnouf, R. & Fan, Z. H. Cell-free protein synthesis in microfluidic array devices. *Biotechnology progress* **23**, 1305–1311 (2007).
125. Khnouf, R., Beebe, D. J. & Fan, Z. H. Cell-free protein expression in a microchannel array with passive pumping. *Lab on a Chip* **9**, 56–61 (2009).
126. Khnouf, R., Olivero, D., Jin, S. & Fan, Z. H. Miniaturized fluid array for high-throughput protein expression. *Biotechnology Progress* **26**, 1590–1596 (2010).
127. Jackson, K., Kanamori, T., Ueda, T. & Fan, Z. H. Protein synthesis yield increased 72 times in the cell-free PURE system. *Integrative Biology* **6**, 781–788 (2014).
128. Hahn, G.-H., Asthana, A., Kim, D.-M. & Kim, D.-P. A continuous-exchange cell-free protein synthesis system fabricated on a chip. *Analytical Biochemistry* **365**, 280–282 (2007).
129. Siuti, P., Retterer, S. T. & Doktycz, M. J. Continuous protein production in nanoporous, picolitre volume containers. *Lab on a Chip* **11**. Publisher: The Royal Society of Chemistry, 3523–3529 (2011).
130. Niederholtmeyer, H., Xu, L. & Maerkl, S. J. Real-Time mRNA Measurement during an in Vitro Transcription and Translation Reaction Using Binary Probes. *ACS Synthetic Biology* **2**, 411–417 (2013).
131. Linden, A. J. v. d. *et al.* A Multilayer Microfluidic Platform for the Conduction of Prolonged Cell-Free Gene Expression. *JoVE (Journal of Visualized Experiments)*, e59655 (2019).
132. Karzbrun, E., Tayar, A. M., Noireaux, V. & Bar-Ziv, R. H. Programmable on-chip DNA compartments as artificial cells. *Science* **345**, 829–832 (2014).
133. Noireaux, V., Bar-Ziv, R. & Libchaber, A. Principles of cell-free genetic circuit assembly. *Proceedings of the National Academy of Sciences* **100**, 12672–12677 (2003).
134. Niederholtmeyer, H., Stepanova, V. & Maerkl, S. J. Implementation of cell-free biological networks at steady state. *Proceedings of the National Academy of Sciences* **110**, 15985–15990 (2013).
135. Goering, A. W. *et al.* In vitro reconstruction of nonribosomal peptide biosynthesis directly from DNA using cell-free protein synthesis. *ACS Synthetic Biology* **6**, 39–44 (2017).
136. Nguyen, P. H. B., Wu, Y., Guo, S. & Murray, R. M. Design Space Exploration of the Violatein Pathway in Escherichia coli Based Transcription Translation Cell-Free System (TX-TL). *bioRxiv*, 027656 (2016).
137. Van Nies, P. *et al.* Self-replication of DNA by its encoded proteins in liposome-based synthetic cells. *Nature Communications* **9**, 1583 (2018).
138. Pardee, K. *et al.* Rapid, Low-Cost Detection of Zika Virus Using Programmable Biomolecular Components. *Cell* **165**, 1255–1266 (2016).

Bibliography

139. Pardee, K. *et al.* Portable, On-Demand Biomolecular Manufacturing. *Cell* **167**, 248–254 (2016).
140. Huang, A. *et al.* BioBits™ Explorer: A modular synthetic biology education kit. *Science Advances* **4**, eaat5105 (2018).
141. Zhang, Y., Huang, Q., Deng, Z., Xu, Y. & Liu, T. Enhancing the efficiency of cell-free protein synthesis system by systematic titration of transcription and translation components. *Biochemical Engineering Journal* **138**, 1–26 (2018).
142. Goers, L., Freemont, P. & Polizzi, K. M. Co-culture systems and technologies: taking synthetic biology to the next level. *Journal of The Royal Society Interface* **11**, 20140065–20140065 (2014).
143. Li, G.-W., Burkhardt, D., Gross, C. & Weissman, J. S. Quantifying absolute protein synthesis rates reveals principles underlying allocation of cellular resources. *Cell* **157**, 624–635 (2014).
144. Bolanos-Garcia, V. M. & Davies, O. R. Structural analysis and classification of native proteins from *E. coli* commonly co-purified by immobilised metal affinity chromatography. *Biochim Biophys Acta* **1760**, 1304–1313 (2006).
145. Ederth, J., Mandava, C. S., Dasgupta, S. & Sanyal, S. A single-step method for purification of active His-tagged ribosomes from a genetically engineered *Escherichia coli*. *Nucleic Acids Research* **37**, e15 (2009).
146. Horiya, S., Bailey, J. K. & Krauss, I. J. *Directed Evolution of Glycopeptides Using mRNA Display* Published: Elsevier (2017).
147. Purnick, P. E. M. & Weiss, R. The second wave of synthetic biology: from modules to systems. *Nature Reviews. Molecular Cell Biology* **10**, 410–422 (2009).
148. Garenne, D. & Noireaux, V. Cell-free transcription–translation: engineering biology from the nanometer to the millimeter scale. *Current Opinion in Biotechnology. Systems Biology • Nanobiotechnology* **58**, 19–27 (2019).
149. Takahashi, M. K. *et al.* Characterizing and prototyping genetic networks with cell-free transcription–translation reactions. *Methods. Bacterial and Archaeal Transcription* **86**, 60–72 (2015).
150. Wick, S. *et al.* PERSIA for Direct Fluorescence Measurements of Transcription, Translation, and Enzyme Activity in Cell-Free Systems. *ACS Synthetic Biology* **8**. Publisher: American Chemical Society, 1010–1025 (2019).
151. Kwon, Y.-C. & Jewett, M. C. High-throughput preparation methods of crude extract for robust cell-free protein synthesis. *Scientific Reports* **5**, 8663 (2015).
152. Sun, Z. Z. *et al.* Protocols for Implementing an *Escherichia coli* Based TX-TL Cell-Free Expression System for Synthetic Biology. *Journal of Visualized Experiments : JoVE* (2013).
153. Niederholtmeyer, H. *et al.* Rapid cell-free forward engineering of novel genetic ring oscillators. *eLife* **4**, e09771 (2015).

154. Chang, J.-C., Swank, Z., Keiser, O., Maerkl, S. J. & Amstad, E. Microfluidic device for real-time formulation of reagents and their subsequent encapsulation into double emulsions. *Scientific Reports* **8** (2018).
155. Tayar, A. M., Karzbrun, E., Noireaux, V. & Bar-Ziv, R. H. Synchrony and pattern formation of coupled genetic oscillators on a chip of artificial cells. *Proceedings of the National Academy of Sciences of the United States of America* **114**, 11609–11614 (2017).
156. Chau, K. *et al.* Dependence of the quality of adhesion between poly(dimethylsiloxane) and glass surfaces on the composition of the oxidizing plasma. *Microfluidics and Nanofluidics* **10**, 907–917 (2011).
157. Voglele, K. *et al.* Towards synthetic cells using peptide-based reaction compartments. *Nature Communications* **9**, 3862 (2018).
158. Crowe, C. D. & Keating, C. D. Liquid–liquid phase separation in artificial cells. *Interface Focus* **8**, 20180032 (2018).
159. Cheng, X. & Ferrell, J. E. Spontaneous emergence of cell-like organization in *Xenopus* egg extracts. *Science* **366**. Publisher: American Association for the Advancement of Science Section: Report, 631–637 (2019).
160. Miller, T. E. *et al.* Light-powered CO₂ fixation in a chloroplast mimic with natural and synthetic parts. *Science* **368**, 649–654 (2020).
161. Berhanu, S., Ueda, T. & Kuruma, Y. Artificial photosynthetic cell producing energy for protein synthesis. *Nature Communications* **10**, 1325 (2019).
162. Tayar, A. M., Karzbrun, E., Noireaux, V. & Bar-Ziv, R. H. Propagating gene expression fronts in a one-dimensional coupled system of artificial cells. *Nature Physics* **11**, 1037–1041 (2015).
163. Su’etsugu, M., Takada, H., Katayama, T. & Tsujimoto, H. Exponential propagation of large circular DNA by reconstitution of a chromosome-replication cycle. *Nucleic Acids Research* **45**. Publisher: Oxford Academic, 11525–11534 (2017).
164. Bissette, A. J. & Fletcher, S. P. Mechanisms of Autocatalysis. *Angewandte Chemie International Edition* **52**, 12800–12826 (2013).
165. Lincoln, T. A. & Joyce, G. F. Self-Sustained Replication of an RNA Enzyme. *Science* **323**. Publisher: American Association for the Advancement of Science Section: Report, 1229–1232 (2009).
166. Laohakunakorn, N., Lavickova, B., Swank, Z., Laurent, J. & Maerkl, S. J. in *Synthetic Gene Circuits* (ed Menolascina, F.) 1st ed. (Springer US, 2021).
167. Stögbauer, T., Windhager, L., Zimmer, R. & O. Rädler, J. Experiment and mathematical modeling of gene expression dynamics in a cell-free system. *Integrative Biology* **4**, 494–501 (2012).
168. Horvath, N. *et al.* Toward a genome scale sequence specific dynamic model of cell-free protein synthesis in *Escherichia coli*. *Metabolic Engineering Communications* **10**, e00113 (2020).

Bibliography

169. Shoval, O. *et al.* Evolutionary Trade-Offs, Pareto Optimality, and the Geometry of Phenotype Space. *Science* **336**. Publisher: American Association for the Advancement of Science Section: Report, 1157–1160 (2012).
170. Aoki, S. K. *et al.* A universal biomolecular integral feedback controller for robust perfect adaptation. *Nature* **570**. Number: 7762 Publisher: Nature Publishing Group, 533–537 (2019).
171. Keren, L. *et al.* Massively Parallel Interrogation of the Effects of Gene Expression Levels on Fitness. *Cell*, 1–32 (2016).
172. Mulder, A. M. *et al.* Visualizing Ribosome Biogenesis: Parallel Assembly Pathways for the 30S Subunit. *Science* **330**. Publisher: American Association for the Advancement of Science Section: Report, 673–677 (2010).
173. Ceroni, F. *et al.* Burden-driven feedback control of gene expression. *Nature Methods* **15**. Number: 5 Publisher: Nature Publishing Group, 387–393 (2018).
174. Eppinger, M. *et al.* Genome Sequences of the Biotechnologically Important *Bacillus megaterium* Strains QM B1551 and DSM319. *Journal of Bacteriology* **193**. Publisher: American Society for Microbiology Journals Section: Genomics and Proteomics, 4199–4213 (2011).
175. Marshall, R., Maxwell, C. S., Collins, S. P., Beisel, C. L. & Noireaux, V. Short DNA containing Chi sites enhances DNA stability and gene expression in *E. coli* cell-free transcription–translation systems. *Biotechnology and Bioengineering* **114**, 2137–2141 (2017).
176. Thorsen, T., Maerkl, S. J. & Quake, S. R. Microfluidic large-scale integration. *Science (New York, NY)* **298**, 580–584 (2002).
177. Karzbrun, E., Shin, J., Bar-Ziv, R. H. & Noireaux, V. Coarse-grained dynamics of protein synthesis in a cell-free system. *Physical Review Letters* **106**, 048104 (2011).
178. Tuza, Z. A., Singhal, V., Kim, J. & Murray, R. M. An in silico modeling toolbox for rapid prototyping of circuits in a biomolecular “breadboard” system. *52nd IEEE Conference on Decision and Control* (2013).
179. Weiße, A. Y., Oyarzún, D. A., Danos, V. & Swain, P. S. Mechanistic links between cellular trade-offs, gene expression, and growth. *Proceedings of the National Academy of Sciences* **112**, E1038–E1047 (2015).
180. Underwood, K. A., Swartz, J. R. & Puglisi, J. D. Quantitative polysome analysis identifies limitations in bacterial cell-free protein synthesis. *Biotechnology and Bioengineering* **91**, 425–435 (2005).
181. Lavickova, B., Laohakunakorn, N. & Maerkl, S. J. *A partially self-regenerating synthetic cell; lbnc-epfl/2020_Lavickova_model*. DOI: 10.5281/zenodo.4160156. 2020.
182. Spirin, A. S. in *Cell-Free Translation Systems* (ed Spirin, A. S.) 3–20 (Springer Berlin Heidelberg, Berlin, Heidelberg, 2002).
183. Nguyen, H.-T., Massino, M., Keita, C. & Salmon, J.-B. Microfluidic dialysis using photo-patterned hydrogel membranes in PDMS chips. *Lab on a Chip* **20**, 2383–2393 (2020).

184. Decock, J., Schlenk, M. & Salmon, J.-B. In situ photo-patterning of pressure-resistant hydrogel membranes with controlled permeabilities in PEGDA microfluidic channels. *Lab on a Chip* **18**. Publisher: Royal Society of Chemistry, 1075–1083 (2018).
185. Zheng, B., Roach, L. S. & Ismagilov, R. F. Screening of protein crystallization conditions on a microfluidic chip using nanoliter-size droplets. *Journal of the American Chemical Society* **125**, 11170–11171 (2003).
186. Urbanski, J., Thies, W., Rhodes, C., Amarasinghe, S. & Thorsen, T. Digital microfluidics using soft lithography. *Lab on a Chip* **6**, 96–104 (2006).
187. Song, J. W. *et al.* Computer-Controlled Microcirculatory Support System for Endothelial Cell Culture and Shearing. *Analytical Chemistry* **77**. Publisher: American Chemical Society, 3993–3999 (2005).
188. Lee, S. H. *et al.* Bubble-free rapid microfluidic PCR. *Biosensors and Bioelectronics* **126**, 725–733 (2019).
189. Heyries, K. A. *et al.* Megapixel digital PCR. *Nature Methods* **8**, 649–651 (2011).
190. Heo, Y. S. *et al.* Characterization and Resolution of Evaporation-Mediated Osmolality Shifts That Constrain Microfluidic Cell Culture in Poly(dimethylsiloxane) Devices. *Analytical Chemistry* **79**. Publisher: American Chemical Society, 1126–1134 (2007).
191. Ning, Y. *et al.* A self-digitization chip integrated with hydration layer for low-cost and robust digital PCR. *Analytica Chimica Acta* **1055**, 65–73 (2019).
192. Zhou, X., Ravichandran, G. C., Zhang, P., Yang, Y. & Zeng, Y. A microfluidic alternating-pull–push active digitization method for sample-loss-free digital PCR. *Lab on a Chip* **19**. Publisher: The Royal Society of Chemistry, 4104–4116 (2019).
193. Zambrano, A., Zadorin, A. S., Rondelez, Y., Estévez-Torres, A. & Galas, J.-C. Pursuit-and-Evasion Reaction-Diffusion Waves in Microreactors with Tailored Geometry. *The Journal of Physical Chemistry B* **119**. Publisher: American Chemical Society, 5349–5355 (2015).
194. Yu, L. *et al.* Flow-through functionalized PDMS microfluidic channels with dextran derivative for ELISAs, 5 (2009).
195. Sui, G. *et al.* Solution-Phase Surface Modification in Intact Poly(dimethylsiloxane) Microfluidic Channels. *Analytical Chemistry* **78**. Publisher: American Chemical Society, 5543–5551 (2006).
196. Park, B. & Song, S. Investigation on Coating Methods of a Self-Assembled Monolayer on PDMS (Poly (dimethylsiloxane)) Surface. *BIOCHIP JOURNAL* **1**, 2 (2007).
197. Grasmann, L., Lavickova, B., Elizondo-Cantú, M. C. & Maerkl, S. J. OnePot PURE Cell-Free System. *JoVE (Journal of Visualized Experiments)*, e62625 (2021).
198. Sokolova, E. *et al.* Enhanced transcription rates in membrane-free protocells formed by coacervation of cell lysate. *Proceedings of the National Academy of Sciences* **110**, 11692–11697 (2013).

Bibliography

199. Nies, P. v. *et al.* Unbiased Tracking of the Progression of mRNA and Protein Synthesis in Bulk and in Liposome-Confined Reactions. *ChemBioChem* **14**, 1963–1966 (2013).

BARBORA LAVIČKOVÁ



Epesses, CH



barbora.lavickova@gmail.com



+41 77 981 30 43



1992



Czech, Swiss residence permit B



[linkedin.com/in/barboralavickova](https://www.linkedin.com/in/barboralavickova)



EDUCATION

2016–2021

Swiss Federal Institute of Technology (EPFL), CH

Ph.D. in Biotechnology and Bioengineering

2014–2016

KU Leuven & University Grenoble Alpes, BE & FR

Erasmus Mundus Master of Nanoscience and Nanotechnology, *Greatest distinction*

2011–2014

Technical University of Liberec, CZ

Bachelor studies in Nanotechnology, *Graduated with honors*

WORK EXPERIENCE

2016
–
current

DOCTORAL RESEARCHER *Laboratory of Biological Network Characterization, EPFL, CH*

Towards an artificial cell: Development of a system which self-reconstitutes the protein components of the PURE system in microfluidic reactors

- Development and integration of an autonomous microfluidic platform for cell-free steady-state reactions
- Development of a protocol for preparation of recombinant cell-free expression system
- Collaboration on DNA delivery by laser-based jet injection and DNA detection using a pH-sensing system
- Supervision of master and bachelor students in the laboratory and during exercise sessions

2016
(4 months)

MASTER THESIS *G2ELab, FR*

Design and characterisation of an electrochemical detection system coupled to a magnetic immunoassay

- Development of a protocol for magnetic bead-based electrochemical immunoassay
- Preparation of electrodes integrated with micromagnets array prepared by magnetic particles grafting
- Preparation of antibody functionalized magnetic nanoparticles

2014
(4 months)

TECHNICIAN R&D *Contipro Biotech Ltd., CZ*

Development of non-woven fabrics from hyaluronic acid containing antiseptic drugs

- Development of a bath precipitation method for production of hyaluronic acid-based non-woven fabrics containing antiseptic drugs
- Analysis of the fabric structure (SEM) and release of antiseptic drugs (UV-VIS)

2013
–
2014

BACHELOR THESIS *The Institute for Nanomaterials, TUL, CZ*

Modification of plastics through antibacterial nanolayers for medical applications

- Synthesis of antibacterial nanolayers using the sol-gel method
- Analysis of the synthesised layers by Zetasizer, IR spectroscopy, SEM, and ICP
- Analysis of antibacterial and antimicrobial properties against pathogenic bacteria and yeast

2013
(2 months)

INTERNSHIP *Contipro Biotech Ltd., CZ*

Development of ZnO nanoparticles

- Chemical synthesis of ZnO quantum dots functionalized by hyaluronic acid
- Development of a protocol for quantum yield analysis

SKILLS

LABORATORY:

BIOLOGICAL TECHNIQUES

PCR, DNA/RNA extraction, gel electrophoresis, protein purification, molecular cloning, bacterial cultures, cell-free TX-TL

MICROFLUIDICS

Design and fabrication of double-layer microfluidic devices (photolithography - clean room, soft lithography), fluorescence microscopy, image processing and analysis

SOFTWARE:

Python, LabVIEW, ImageJ, MATLAB, CAD software, MS Office, Adobe Illustrator, InDesign, LaTeX, Clewin, KLayout

PROJECT MANAGEMENT & TEACHING:

Laboratory safety management, exercise session supervision, interdisciplinary/multicultural collaborations, training and mentoring students working on research projects, direction of a team of students in the iGEM competition

COMMUNICATION SKILLS:

Poster presentations, oral presentations, and scientific writing

PUBLICATIONS

Lavickova, B., and Maerkl, S. "A simple, robust, and low-cost method to produce the PURE cell-free system." ACS synthetic biology (2019)

Lavickova, B., Laohakunakorn, N. and Sebastian J. Maerkl. "A partially self-regenerating synthetic cell." Nature communications (2020).

Laohakunakorn, N. et al. "Steady-state cell-free gene expression with microfluidic chemostats." Synthetic Gene Circuits. (2021)

Laohakunakorn, N., et al. "Bottom-up construction of complex biomolecular systems with cell-free synthetic biology." Frontiers in bioengineering and biotechnology (2020)

Grasemann, L., Lavickova, B., Elizondo-Cantú, C. and Sebastian J. Maerkl. "OnePot PURE cell-free system." Jove (2021).

Krizek, J., Lavickova, B. and Moser, Ch. "Degradation study on molecules released from laser-based jet injector." International Journal of Pharmaceutics (2021)

LANGUAGES

CZECH (native)

ENGLISH (full professional working proficiency)

ADDITIONAL EXPERIENCE

COSEC (UNIT SAFETY COORDINATOR)

Unit Safety Coordinator, EPFL (2018-current)
(CONCURRENT WITH RESEARCH ASSISTANT)

- Communication with Safety, Prevention and Health Domain Management (DSPS) of laboratory safety
- Chemical storage and waste management
- Laboratory supplies organisation

YOGA INSTRUCTOR

YTT 200 certified (2019)

Private practice

Yoga Instructor at TOTEM rock climbing gyms, CH

AWARDS & HONORS

Scholarship - Merit scholarship (2011-2014)

Award - Award of the Rector of the University for Bachelor thesis (2014)

Scholarship - LANEF PreDoc program (2015)

Conference Proceedings - SEED (Synthetic Evolution, Engineering and Design) (2021)

EXTRACURRICULAR COURSES

2013

SUMMER SCHOOL

Tissue engineering

Technical University of Liberec, CZ

2013

BIOMEDICAL RESEARCH SERIES

- Basics in receptor neurophysiology
- Tissue engineering
- The function and structure of cell membranes

Institute of Physiology, Academy of Science, CZ (3 x 1 week)

HOBBIES



References

Professor S. Maerkl, EPFL, sebastian.maerkl@epfl.ch

Dr. N. Laohakunakorn, University of Edinburgh, nadanai.laohakunakorn@ed.ac.uk

Professor C. Guiducci, EPFL, carlotta.guiducci@epfl.ch